MORPHOGENESIS IN INORGANIC PRECIPITATES IN GELS

A Thesis submitted to the

UNIVERSITY OF GLASGOW

for the degree of

DOCTOR OF PHILOSOPHY

in the Faculty of Science

by

ALLEN WILLIAM REID

Department of Chemistry

University of Glasgow

May 1992

CONTENTS

INTRODUCTION

1 THE IMPORTANCE OF PRECIPITATION 1

2 BACKGROUND ON PRECIPITATION 42

EXPERIMENTAL

3 PRECIPITATION TECHNIQUES AND SAMPLE PREPARATION 61

4 TECHNIQUES OF ANALYSIS 74

RESULTS

5 $BaCO_3$ PRECIPITATED BY A DIFFUSION MECHANISM IN SILICA GEL ON GLASS MICROSCOPE SLIDES AND BY HOMOGENEOUS METHODS 102

6 $BaCO_3$ PRECIPITATED BY A DIFFUSION MECHANISM IN SILICA GEL IN GLASS CASSETTES 113

7 $BaSO_4$ PRECIPITATED BY A DIFFUSION MECHANISM IN SILICA GEL IN GLASS CASSETTES 135

8 PRECIPITATION OF FERROUS MATERIALS BY A DIFFUSION MECHANISM IN SILICA GEL 149

DISCUSSION

9 DISCUSSION 158

REFERENCES 183

ACKNOWLEDGEMENTS

I would like to thank my supervisors, Dr T. Baird, Dr P.S. Braterman and Dr R.D. Peacock for their valuable advice and encouragement throughout the course of this work. I am also indebted to Prof. J. M. Garcia Ruiz, Dr A.G. Cairns-Smith, Dr J. R. Fryer and Prof. M. Russell for useful discussions during the course of this work and to P. Chen for carrying out XPS and Rutherford backscattered image analysis.

I would also like to thank Mr. D. Thom, Mr E. Robertson, Mrs M. Mullin and Mr D. Turner for technical assistance.

Finally I would like to thank my family, friends and colleagues for their help and patience.

I acknowledge financial support from the Science and Engineering Research Council and British and Spanish Councils, and (for equipment used in Texas) I thank the University of North Texas faculty research fund and the Robert A. Welch foundation.

For my parents

SUMMARY

This thesis is concerned with the precipitation of inorganic materials and in particular Induced Morphology Crystal Aggregates (IMCA's). This strange phenomenon occurs when an akaline earth metal carbonate and an alkaline earth metal silicate precipitate simultaneously in basic silica gel. The metal silicate precipitates as a sheath which acts to control the crystal-to-crystal relations of the metal carbonate aggregate and therefore the overall morphology of the precipitate. Very strange morphologies result such as sheet-like and spiral structures in the case of $BaCO_3$.

$BaCO_3$ was studied extensively in this project. A glass cassette reaction vessel was developed in collaboration with J. M. Garcia Ruiz which enabled in-situ light microscopical analysis of morphology. Precipitates were then removed from their gels and subjected to chemical analysis and further morphological observation by scanning electron microscopy (SEM). The surface analysis techniques of energy dispersive spectroscopy (EDS) and X-ray photoelectron spectroscopy (XPS) were utilised to determine the chemical composition of the sheath or membrane which controls morphology.

Some key factors which affect $BaCO_3$ IMCA formation were established. A very clear morphogenetical transition from dendrites (normal crystal growth) through to fully

induced morphologies was observed. This transition depends on the amount of soluble silicate in the gel and its ability to react with the metal and form a membrane. The main factors which affect this are pH and the presence of NaCl in the gel. High pH values promote IMCA growth. This is attributed to increased silicate ion concentrations at higher pH values. The presence of NaCl also promotes the formation of IMCA's. This may be due to charge effects stabilising the precipitating membrane. Growth mechanisms are proposed which have similarities to cement chemistry and the silica garden effect.

Experiments carried out on the nature of the membrane have shown it to be a barium silicate carbonate in the region of one micron thick.

Other insoluble barium precipitates such as $BaSO_4$ (studied extensively), $BaCrO_4$ and $BaHPO_4$ have been found to form IMCA's suggesting that the effect may be quite widespread and experiments on iron carbonate and iron sulphide suggested that silica may influence morphology. In the case of iron sulphide, precipitates were obtained which were remarkably similar to naturally occurring iron sulphide framboids, unusual spherical aggregates recently implicated in origin of life studies.

INTRODUCTION.

1 THE IMPORTANCE OF PRECIPITATION

1.1 MATERIALS IN GENERAL

1.2 CERAMICS

1.2.1 Crystalline Ceramics

1.2.2 Non-crystalline Ceramics

1.2.3 Glass-bonded Ceramics

1.2.4 Chemically Bonded Ceramics

1.2.5 Cements

1.3 INDUCED MORPHOLOGY CRYSTAL AGGREGATES (IMCA's)

1.3.1 Introduction

1.3.2 Growth Procedures and Characterisation

1.3.3 On the Nature of the Phenomenon

1.3.4 On the Nature of the Membrane

1.3.5 On the Morphogenesis of IMCA's

1.3.6 Summary

1.4 BIOMINERALISATION

1.4.1 Organic Matrix-mediated Biomineralisation

1.4.2 Chemical Control of Biomineralisation

1.4.3 Spatial Control of Biomineralisation

1.4.4 Structural Control of Biomineralisation

1.4.5 The Function of Organic Matrices in Oriented Mineral Overgrowth

1.4.6 Mimicking Biomineralisation

1.5 SELF-ORGANISATION AND THE ORIGINS OF LIFE

1 THE IMPORTANCE OF PRECIPITATION

1.1 MATERIALS IN GENERAL

The importance of materials technology was recently summerized by J.D. Birchall (in Mann et al 1989). He wrote "It is no exaggeration to state that the progress of technology depends on the discovery and refinement of new materials that are harder, stiffer, stronger, tougher, lighter, resistant to chemical attack and to high temperatures or that display magnetic, electronic or optical "effects". Our ability to travel by plane and car, to communicate, to generate energy, to replace worn out bone joints, to "drip dry" shirts, to explore space etc. depends on new materials".

Controlled precipitation of highly insoluble inorganic materials is involved in the production of a wide range of materials of major importance in the progress of this technology, including cements, conventional and high performance ceramics, pigments, recording media, heterogeneous catalysts and their supports, finely divided metals and special glasses. The study of precipitation and factors which affect it are of both fundamental and practical significance in relation to these processes. Models of the nucleation and development of these particles as a function of surface free energy could be tested as well as the effects of adding particular additives. The results would be of

significance to the controlled production of both simple and composite materials at several levels. The relationships between particle size and shape, and chemical bonding of surface additives, will be of quite general importance in the understanding of product size and shape, and the development of texture, in any process involving the formation of small solid particles. Additive effects will be exceedingly important in processes that lead to the production of intermeshed solid particles. Thus they are relevant to the rational choice of chemical bonding additives for composites of all levels of sophistication, from bulk cements to the precursors of special performance ceramics and even to the control of grain structure in metals. There is also secondary relevance to naturally occurring precipitation processes, as in diagenesis, and hence to the interpretation of sediments. The use of polymeric additives is a first step towards mimicking the biological control of mineral deposition, (Williams, 1984) with the longer term goal of using organised polymers as templates.

The following sections describe in more detail some of the materials and processes mentioned above, which have a direct relevance to the work described in this thesis. There is also a short section on the possible relevance of precipitation and the origins of life.

1.2 CERAMICS

Ceramic materials consist of phases containing compounds of metallic and non-metallic elements. They are often classified according to their functions and properties into groups such as pure oxide ceramics, refractories, abrasives and cementing materials. As noted by Schlenker (1969) few of these groups are mutually exclusive, eg alumina, Al_2O_3 is a pure oxide ceramic, a refractory and an abrasive of considerable importance. Schlenker offers a more useful classification which is based on structure. The main groups are: crystalline ceramics, non-crystalline ceramics including glasses, glass-bonded ceramics and cements. A detailed account of this group is given by Brostow (1979). Recent advances in ceramic processing technology leads one to include another group in this classification, namely "chemically bonded ceramics" in which modern cements are included. The name was coined by Rustum Roy and an excellent account given by Birchall (1983).

1.2.1 Crystalline Ceramics

Crystalline ceramics are either single compounds (eg MgO) or mixtures (eg MgO & Al_2O_3). Two important ceramics are hafnium carbide, with the highest melting point of any known material, 4420K, and boron carbide, which is the hardest known material. As suggested by the high melting points of some ceramics, chemical bonds in ceramic

compounds are highly stable. These bonds can be purely ionic as in NaCl or purely covalent as in SiC or intermediate as in SiO_2. A group of ceramic oxides with important magnetic properties are spinels, with the general formula AB_2O_4, where A and B are different metals or the same metal at two different oxidation states. Examples are magnesium aluminate spinel $MgAl_2O_4$ and zinc ferrospinel $ZnFe_2O_4$.

Growing good crystals of many ceramic materials is difficult. For instance Roy and White (1972) studied a large number of phases in the Ti:O system and found high melting oxides with complicated defect character, intermediate oxides with very restricted stability in terms of temperature and oxygen partial pressure, as well as lower oxides stable only in an extremely reducing environment. After working on this project for eight years they concluded that "by utilising a variety of methods which provide controlled oxygen fugacities varying from roughly 10^2 to 10^{-30} one can prepare all the higher titanium oxides with at least the stoichiometry controlled".

A large and important class of crystalline ceramic is the silicates. The fundamental unit of structure in all silicates is the silicon-oxygen tetrahedron, with 0 atoms in the four corners and a Si atom in the centre of the tetrahedron. Infinite three dimensional networks may be formed from such tetrahedra with different structures

being produced by different arrangements of the tetrahedra; the most common arrangements are shown in fig 1.2.1a.

Most silicates are complex, formed by substituting various metal ions into the network. Very important are feldspars, alkali alumina silicates, which are rock forming materials. Several silicates are known as gems, such as garnets and olivines. There are also zeolites which are used as water softners and as molecular sieves. Coloured silicates known as ultramarines are used for paint pigments. Another important class of crystalline ceramics are the sialons. Their name comes from the combination of symbols Si-Al-O-N. Two important sialons are silicon nitride and silicon oxynitride. Both are good engineering materials with high strength, good wear resistance, high decomposition temperatures, excellent thermal shock properties, resistance to oxidation and to corrosive environments and have also a low coefficient of friction.

1.2.2 Non-crystalline Ceramics

The most important non-crystalline ceramics are glasses. A glass is essentially a liquid phase which has failed to crystallise on cooling and is therefore metastable. There are many glasses of various compositions. The most common type of glass is called soda-lime glass and contains 70-75% SiO_2, 12-18% Na_2O, 0-1% K_2O, 5-14% CaO, 0.5-2.5%

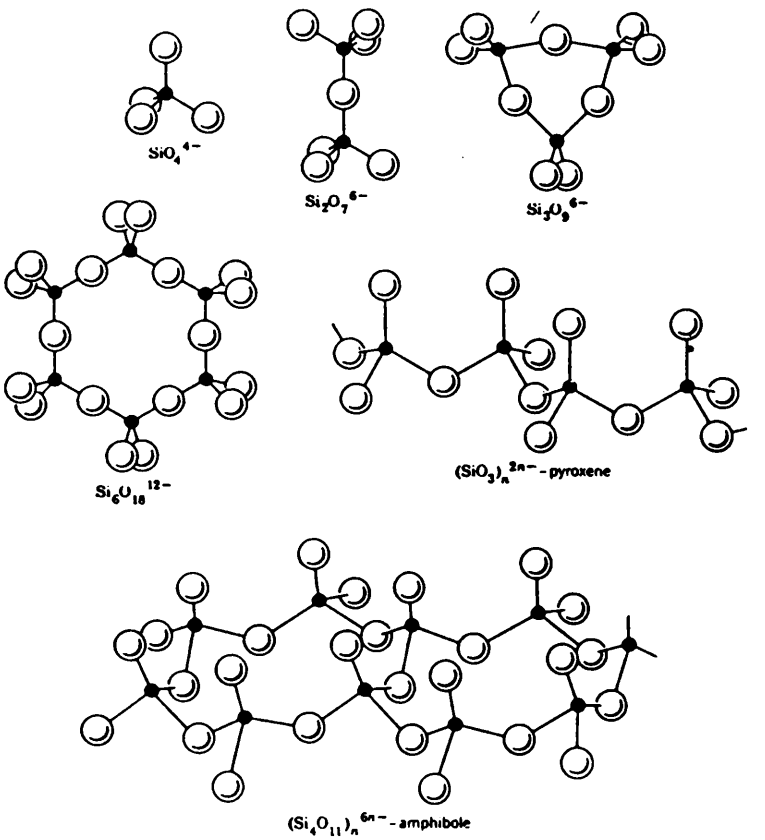

Some common silicate structures obtained from the basic SiO_4^{4-} tetrahedron

fig 1.2.1a (from Brostow, 1979)

Al_2O_3 and 0-4% MgO. Most glasses contain oxides and the oxide components can be classified on the basis of functions they perform. Glass formers are the main components which form the basis of the random three dimensional network, eg SiO_2. Then there are intermediates which cannot form the network themselves but can link it once it exists, eg Al_2O_3. And finally there are modifiers which fill voids in the network and modify properties such as density, viscosity, colour and electrical properties, eg CaO.

A variety of methods are involved in the preparation of glasses (Roy, 1973). One method is from a gel. Mukherjee et al (1976) added various oxides in desired proportions to silica gel, fused the mixture in a furnace, and obtained glasses in the system SiO_2 + Ca_2O_3, SiO_2 + Ca_2O_3 + Al_2O_3 and SiO_2 + Ca_2O_3 + ZrO_2. Gel glasses have more uniform microstructures than glasses produced by fusion of mixtures of oxides. Controlled precipitation of densely packed small oxide particles in silica gel could then lead to the production of high performance glasses.

1.2.3 Glass-Bonded Ceramics

This group of ceramics contain crystalline phases held in a glassy matrix, of which fired clay minerals are an example. Natural clays are sheet silicate structures, believed to be the weathered remains of various types of rock. Clays are characterised by strong intralayer

bonding but weak interlayer bonding. Polar molecules such as water can be easily absorbed between the layers, producing plasticity, swelling and slippiness. These properties are lost when the clay is dry as the moistening process may be reversible. Natural clay composition varies considerably. Important clay minerals are Kaolinite ($Al_2O_3.2SiO_2.2H_2O$), montmorillonite ($Al_2O_3.4SiO_2.nH_2O$) and muscovite ($K_2O.3Al_2O_3.6SiO_2.2H_2O$). These formulas do not indicate how a sheet structure is formed, eg Kaolinite has a double layer structure in which a ($-Si_2O_5^{2-}-$) layer is ionically bound to a ($-Al_2(OH)_4^{2+}-$) layer. Fired clay ceramics are made from three components: clay, flint and feldspar. Feldspar is a low melting point component which forms a glass during firing and binds together the refractory crystalline components. This is why they are called glass bonded ceramics. They are classified according to porosity with the main classes being Earthenware, Fine China, Stoneware and Porcelain.

1.2.4 Chemically Bonded Ceramics CBC's

The name Chemically Bonded Ceramics was coined by Rustum Roy and a definition by J D Birchall is "densely packed assemblies of ceramic particles free from macroscopic voids and in which union between grains is produced at temperatures far lower than those required in conventional ceramic technology". The key to this technology is the use of organic polymers to control

precipitate size and morphology and allow the assembly, packing and binding of particles with the elimination of macroscopic voids and defects. In other words CBC's are high technology composites with the volume fraction of solid at least equal to that of hexagonal close packing (0.74). The main problems to be overcome in the production of CBC's are (i) to break down aggregates; (ii) to disperse and prevent re-aggregation; (iii) to adjust the relevant positions of the particles so as to attain maximum packing. Spherical particles are desired since they have a great packing efficiency and small particles are desired since they sinter more easily than large particles. The final assembly of particles should be malleable under modest pressure to give complex shapes and finally the assembly of particles should be mechanically strong enough to withstand pre-firing manipulation. To some extent (Raistrick, 1983) this technology has been applied to particles such as Al_2O_3, SiO_2 and Fe_3O_4 and it has been shown that they can be packed and moulded into complex shapes with high flexural strength (100MPa) and with particle/polymer interfaces such that bonding is strong and irreversible. The properties of the composite, apart from its thermal properties, are dominated by the solid phase which has a volume fraction greater than 0.8. Thermal performance is dominated by the organic phase but not all ceramics are used at high temperatures.

1.2.5 Cements

Cements consist of several compounds of lime, alumina and silica. When mixed with water they form a paste which sets and hardens. There are two main types of cement; hydraulic cement which set and harden under water and non-hydraulic cements which set in air. Portland cement which is hydraulic, is the most important of all. It is the principal component of concrete and is made from a mixture of four minerals; tricalcium silicate ($3CaO.SiO_2$), dicalcium silicate ($2CaO.SiO_2$), tricalcium aluminate ($3CaO.Al_2O_3$) and tetracalcium aluminoferrite ($4CaO.Al_2O_3.Fe_2O_3$). A typical composition is 65% Ca, 20% SiO_2, 5% Al_2O_3 and 10% Fe_2O_3 plus other mixtures. Portland cement is obtained by mixing materials which supply lime (usually limestone or chalk) with materials which supply silica (usually clay), grinding and firing at 1800K. The cooled melt is then ground to a powder and a little gypsum is added to prevent too rapid a hydration of tricalcium aluminate known as "flash setting". The hydration reactions of cements are complex and long with the setting of pastes taking between thirty minutes and ten hours. Subsequent hardening is normally measured up to 28 days but in reality it continues for years. Since the hydration reactions involve thermal effects microcalorimetry has been used extensively to study the long term processes, the early experimental techniques being developed notably by Swietoslawski (1947). Results have shown that the rates of heat evolution over periods

of 10^2-10^3 hours can be interpreted as resulting from a diffusion controlled phase reaction proceeding by nucleation and growth. A high voltage electron microscope (HVEM) study of the hydration of Portland cement carried out by Double and Hellawell (1976) achieved results compatible with the calorimetric studies. They suggest a possible mechanism analogous to the "silica garden" effect. Figs 1.2.5a (i-iv) are time lapse optical micrographs of the "silica garden" effect. A crystal of $Co(NO_3)$, an aqueously soluble salt, has been placed in dilute sodium silicate solution and begins to dissolve. A gelatinous coating forms around the crystal and acts as a semi-permeable membrane through which osmosis occurs. The salt continues to dissolve within the membrane until the pressure rises enough to cause a rupture. The jet of salt solution which erupts into the silicate solution precipitates a continuous solid tube of material. Salt solution continues to be pumped through this tube (from the primary envelope) and almost steady state growth proceeds for considerable distances. Fig 1.2.5b is a diagram illustrating this mechanism. Figs 1.2.5c (i-iii) show how the tubes grow until falling pressure and viscous drag cause necking down and closing of the tubes. These tubes can be of variable cross-section, they are strong and brittle when dry, they do not yield coherent X-Ray diffraction patterns and can be formed from almost any water soluble salts of metal cations except those from group 1A of the Periodic Table. The similarity of this process to the hydration of Portland cement is clear

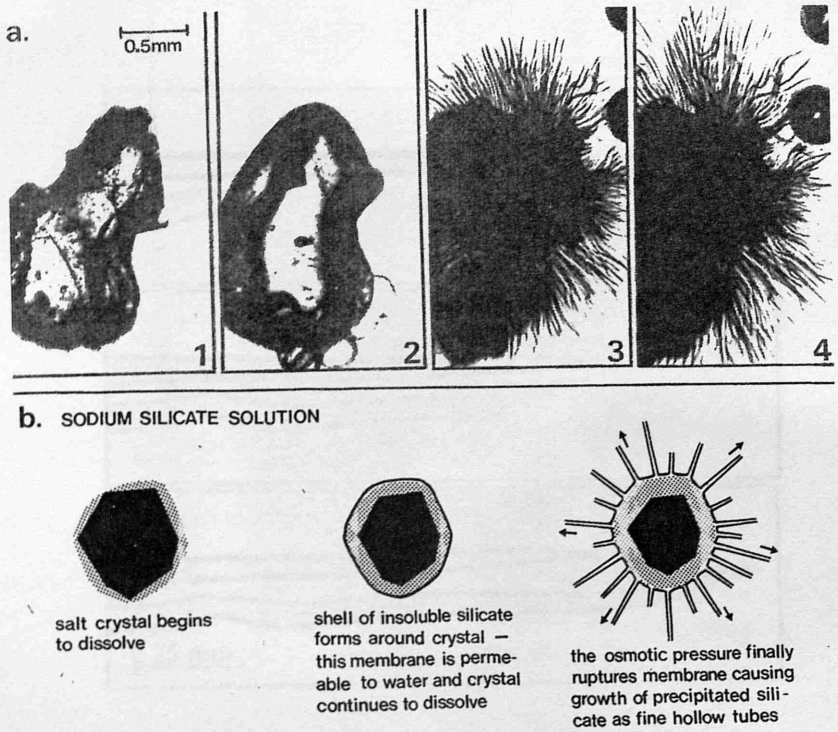

(a) Sequence of light micrographs showing the development of a silicate garden from a crystal of $Co(NO_3)_2$ immersed in dilute sodium silicate solution. Total time interval ~30 s. (b) Schematic illustrating mode of growth of silicate garden.

figs 1.2.5a (1 - 4) and 1.2.5b (from Brostow, 1979)

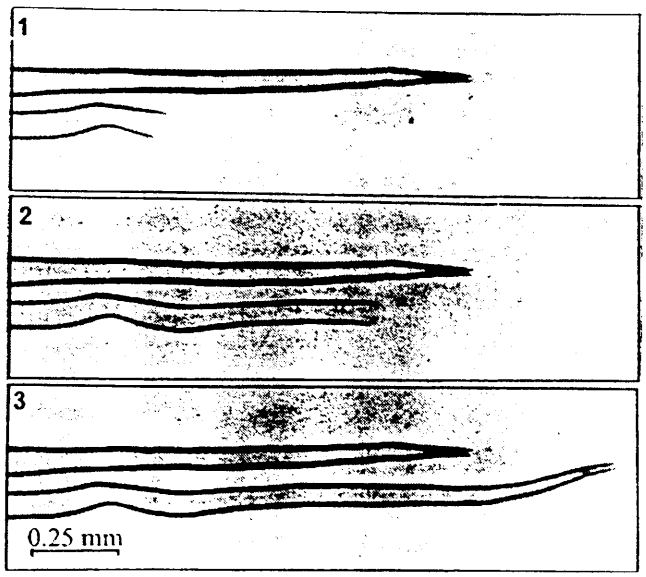

10 second time lapse sequence of light micrographs showing growth of two cobalt silicate tubes.

fig 1.2.5c (from Double & Hellawell, 1976)

(i)

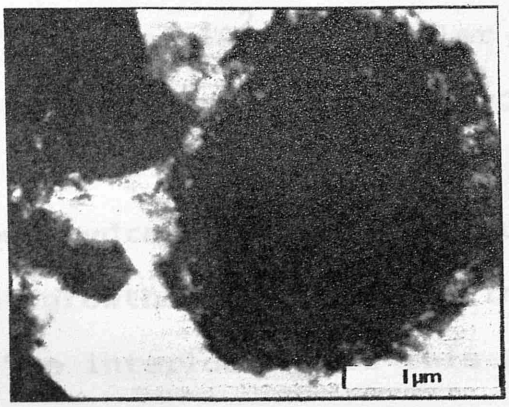

(ii)

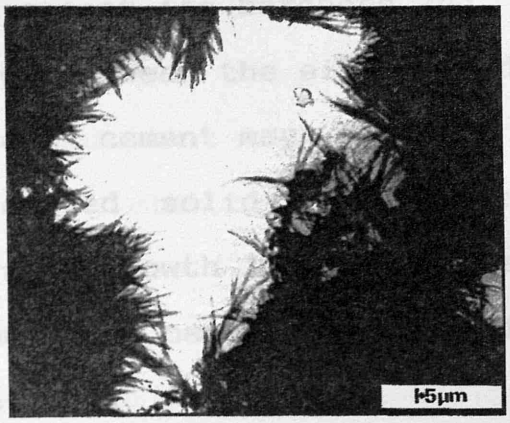

(iii)

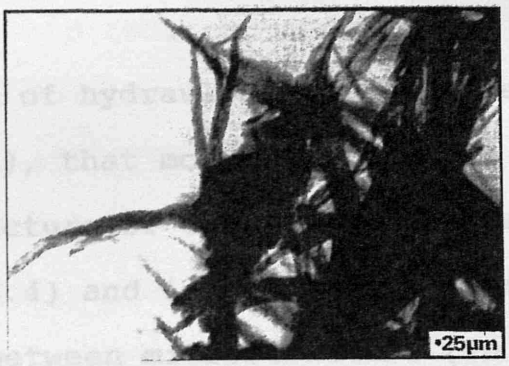

Cement and water samples viewed in the environmental stage of a HVEM: (i) showing the initial gel coating around a cement grain; (ii) after one day, showing fibrillar development of gel around the cement grains and illustrated in detail in (iii).

figs 1.2.5d (i - iii) (from Brostow, 1979)

as shown in figs 1.2.5d (i-iii) although the rates of formation and scale are some 10^2-10^3 smaller than those described for the silica garden. There are two stages in the reaction involving (i) the formation of an initial coating of gelatinous hydrate on the anhydrous crystals and (ii) subsequent growth from this coating of fine fibrillar material. The interlocking of this material is thought to give the cement its hardness and compressive strength. This analogy between the silica garden and the hydration of Portland cement may explain why cement fibrils are not faceted solid crystals as normally obtained through crystal growth from aqueous solution and suggests a mechanism where osmosis is the driving force for secondary growth.

It is in the area of hydraulic cements, eg ordinary Portland Cement (OPC), that most progress has been made, both in the manufacture of chemically bonded ceramics (CBC's) (section 1.2.4) and in the basic understanding of the relationships between microstructure (in particular porosity) and mechanical properties. Hydraulic cements can be considered to be CBC's since ceramic particles (calcium silicates and aluminates) react with water to produce hydrated phases which bond grain residues and added filler particles together. As discussed earlier the interlocking of the hydrated material is thought to give the cement its compressive strength but it appears not to be important from the viewpoint of tensile strength since this is very low (5-15MPa). It is conventional to relate

cement strength (usually compressive, since tensile is expected to be low) to total porosity volume of the hardened cement. Reducing total porosity volume should increase cement strength dramatically. When cement and water are mixed only a proportion of the water is used in the hydration processes. Some of it will be lost through evaporation and the hardened solid will contain 25-35% total volume porosity, with pore sizes ranging from nanometres to millimetres. The small pores constitute the majority of the total porosity volume with a small number of the large pores dictating strength, with the additional problem that the large pores are not often detected since they can be closed or narrow necked. The theory that elimination of large pores would result in stronger (flexural and compressive) cements led to new techniques and the development of "macro-defect-free" (MDF) cements (Birchall, 1983). These materials contain close packed cement grains (>0.74) bonded by an intimate combination of organic polymer and inorganic hydrated material. There are no macroscopic flaws and the total volume porosity can be less than 1%. This is achieved when, for example, calcium aluminate cement (average particle size 10μm) is mixed with a thick gel instead of water, eg poly(vinylacetate/alcohol) in water , 15-20% by mass polymer. The gel acts as a lubricant and with intense mixing a particle volume fraction of 0.7 is obtained in sharp contrast to 0.56 obtained with water alone. The key to this lubrication is the strong attachment of polymer loops, through OH groups to the

aluminium ions. The insolubilisation of the polymer takes place as aluminium ions enter the aqueous phase and precipitate as hydroxide and form organic/inorganic co-polymers. Packing is then increased by the removal of bound water from the polymer by drying out or by inorganic hydrate formation. The un-adsorbed polymer chains contract while the loops remain adsorbed. The result is a 10% volume contraction giving a particle volume fraction of 0.8. The remaining space is filled by inorganic hydrates to give a final pore volume fraction of 0.01. MDF cements have flexural strength of 150-200MPa and a fracture toughness of $300Jm^{-2}$. Fracture toughness can be increased to $10^{4}Jm^{-2}$ when reinforced with nylon fibre. These properties compare very favourably with ordinary Portland cement with a flexural strength of 5-15MPa and fracture toughness of 20 Jm^{-2}.

1.3 INDUCED MORPHOLOGY CRYSTAL AGGREGATES (IMCA's)

In the late 1970's a Spanish PhD student, J.M. Garcia Ruiz and J.L. Amoros, (1981) discovered by accident, a new type of material which he called "Induced Morphology Crystal Aggregates" (IMCA's). These materials are alkaline earth metal (Ba,Ca,Sr) carbonates which are precipitated in basic silica gel, the morphologies of which are controlled by a silicon-rich membrane. The following is an account of the IMCA phenomonen drawn mainly from one of Garcia Ruiz' papers (1985) and references therein.

1.3.1 Introduction

IMCA's, like other crystal aggregates, are composed of an ill-defined number of crystallites, but by way of contrast to other crystal aggregates, the crystal-to-crystal relationships in IMCA's, and therefore their overall morphologies, are controlled by a silicon-rich membrane. The morphologies are highly ordered and visually astonishing with planar curved sheets and twisted ribbons being very characteristic for $BaCO_3$. The IMCA phenomenon is one which mimics biomineralisation (section 1.4). In nature organic membranes control the nucleation and growth of minerals in eg bones and shells. In a cuttlefish bone $CaCO_3$ (aragonite) is built in highly ordered stacks and columns (Birchall and Thomas 1983). The structure acts as a buoyancy tank and can withstand enormous compressive forces. Laboratory modelling of biomineralisation, as in IMCA's, may lead to a better understanding of biomineralisation mechanisms and could be developed as a means of preparing speciality orthopaedic implants. The chemistry of IMCA's is also closely related to the chemistry of the silica-garden and therefore cement (section 1.2.7). The IMCA phenomenon is not a simple one and cannot be treated in terms of classical crystal growth problems as several processes act simultaneously. The following sections deal with the growth procedure and characterisation of IMCA's and an in-depth discussion on the nature of the phenomenon, the membrane and morphogenesis.

1.3.2 Growth Procedures and Characterisation

IMCA's of alkaline earth metal carbonates can be obtained by either (i) diffusing a metal chloride solution through a silica gel of pH between 8.5 and 10.5 containing Na_2CO_3 in a test tube or (ii) counter-diffusing a metal chloride solution and a Na_2CO_3 solution through a silica gel of pH between 8.5 and 10.5 in a U-tube. Both arrangements are represented in fig 1.3.2a. The use of gels other than silica does not yield IMCA's. The gels were prepared by acidifying, to the desired pH, a sodium silicate solution of density 1.059 g cm^{-3} with 1M HCl (procedure 3.1.2). Before gelling the solutions were transferred to the test tube or U-tube, allowed to gel and the appropriate solution placed in contact with it. After several hours the first precipitates appear in the gel. Growth continues for up to two weeks depending on the conditions. A morphological evolution is observed from the first precipitate to the last. Fig 1.3.2b (i-iii) shows some light micrographs of typical IMCA's of Ba, Ca and Sr carbonate. Under cross-polarised light a pseudo-uniaxial dark cross is observed, being particularly clear with planar aggregates of $BaCO_3$. If the aggregate is rotated the cross remains stationary in the laboratory frame. This implies there are always crystallites orientated in the cross-polarised light. In other words there is an ordered arrangement of strings of crystallites radiating out from the point of nucleation. Fig 1.3.2c (i-ii) shows two SEM views of the twisted

ribbon morphology of $BaCO_3$. After removal of the aggregates from the gel by dissolution with NaOH (procedure 3.6.2), X-Ray diffraction (powder) analysis shows typical peaks belonging to $CaCO_3$ (calcite), $BaCO_3$ (analogous to $CaCO_3$ aragonite) and $SrCO_3$ with the addition of several broad bands, the positions of which are related to the metal used for the precipitation. Infra-red analysis shows the normal carbonate adsorptions as well as two extra peaks. Howevever the most convincing test for the presence of a membrane is the acid dissolution test. Under an optical microscope an intact aggregate is seen to undergo no change when subjected to a drop of 0.5M HCl placed on top of it. If the aggregate is, however, cracked in any way the acid penetrates and the carbonate crystals are dissolved leaving behind a sheath the same shape as that of the whole aggregate, fig 1.3.2d (unfortunately, this is a poor reproduction. A clearer example,generated as part of this study is shown in figs 6.2.3a b, & c). Thus, the existence of a membrane, and ordered arrangement of material and an overall morphology which cannot be described in terms of normal inorganic crystal symmetry led Garcia Ruiz to imply that the membrane controls the crystal-to-crystal relationships and therefore the overall morphology.

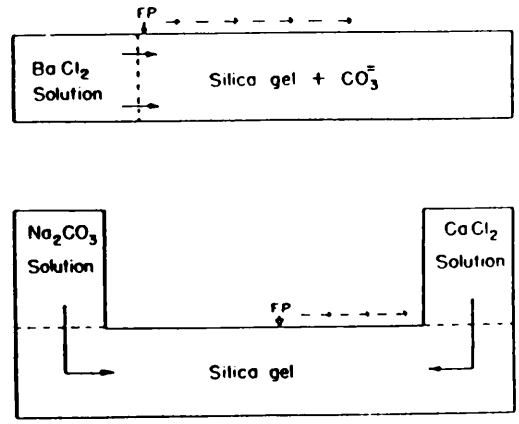

Two different arrangements for the growth of IMCA's. FP indicates the position of the first precipitates. Arrows indicate the advancement of the precipitation front.

fig 1.3.2a (from Garcia Ruiz, 1985)

fig 1.3.2b (i) $CaCO_3$ IMCA

(from Garcia Ruiz, 1985)

fig 1.3.2b (ii) $BaCO_3$ IMCA viewed under cross—polarized light microscopy and exhibiting uniaxial dark cross.

(from Garcia Ruiz, 1985)

fig1.3.2b (iii) $SrCO_3$ IMCA

(from Garcia Ruiz, 1985)

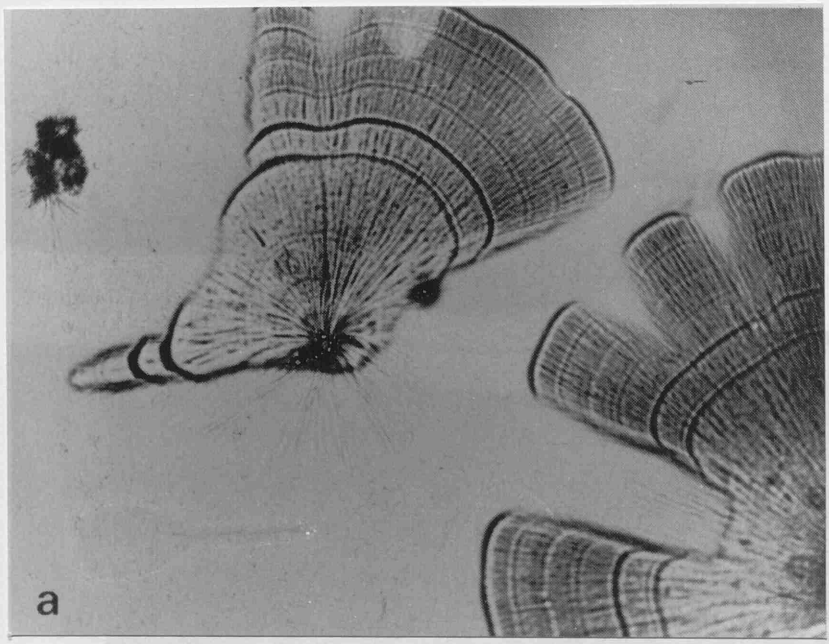
a

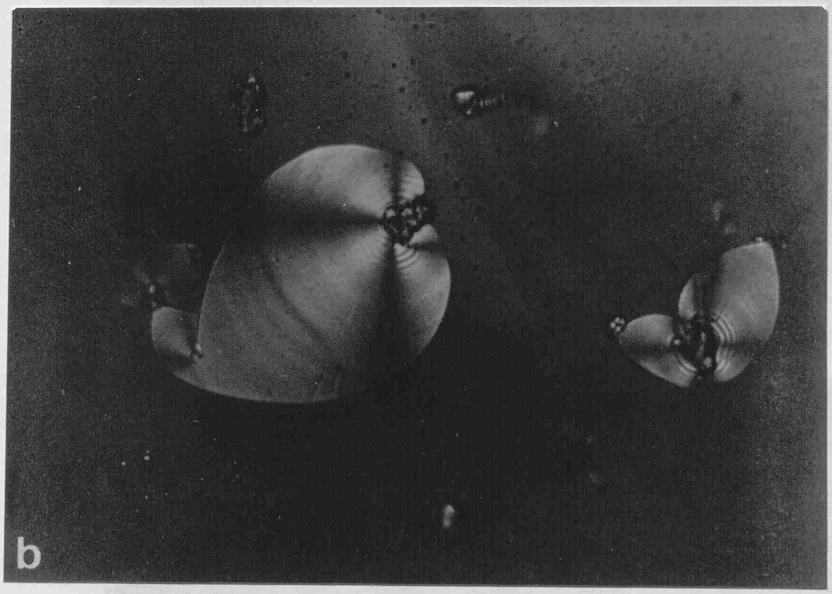
b

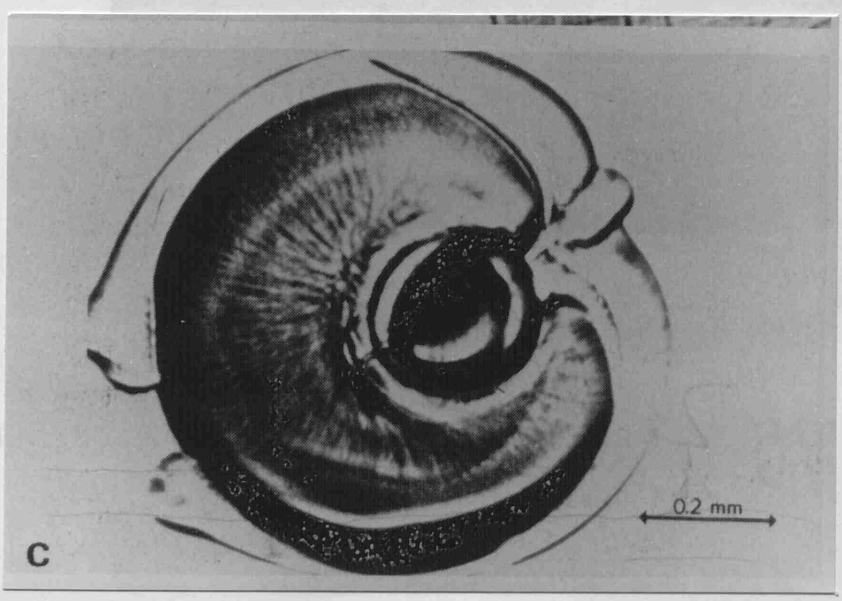
0.2 mm
c

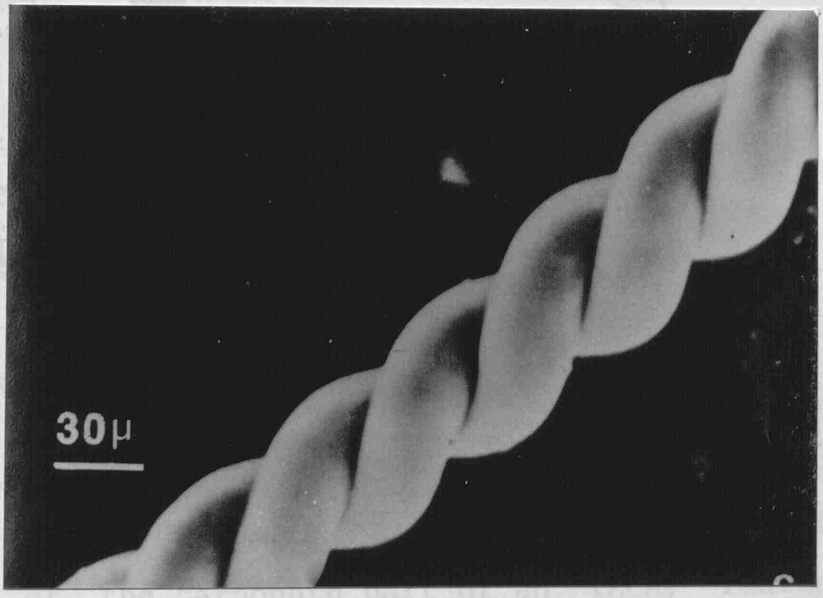

fig 1.3.2c (i - ii)

Two views of $BaCO_3$ IMCA twisted ribbon or spiral parts

(from Garcia Ruiz, 1985)

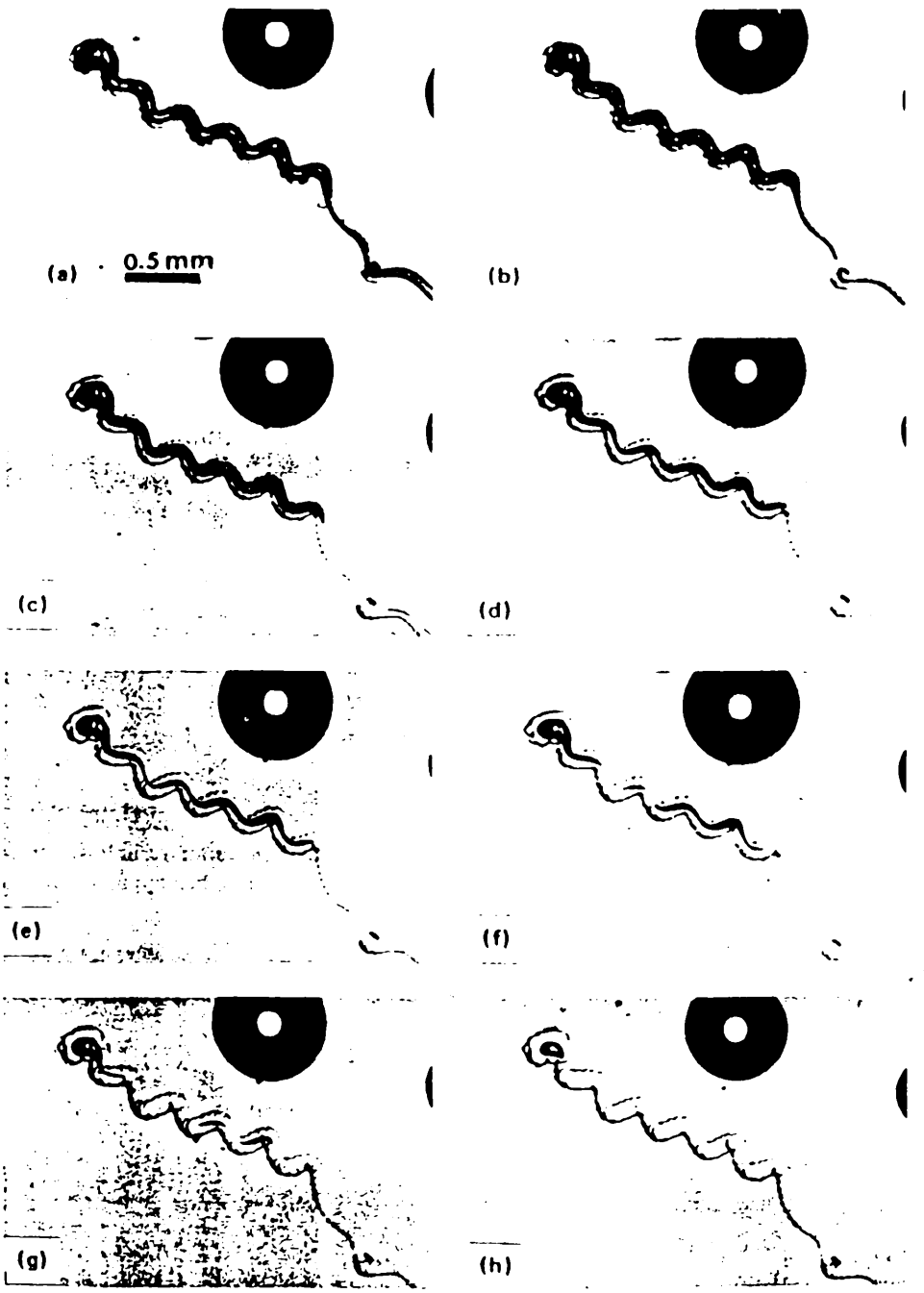

A series of micrographs showing progressive acid dissolution of the carbonate part of an IMCA, leaving behind an external sheath.

fig 1.3.2d (from Garcia Ruiz, 1981)

1.3.3 On The Nature of the Phenomenon

Garcia Ruiz explains the formation of IMCA's on the basis of two simultaneous processes :

(i) the nucleation and growth of alkaline earth carbonate crystals.

(ii) the formation of a silicate matrix, as a result of the hydration of silicic acid (with different degrees of condensation) and metal ions.

On the evidence described earlier it is clear there must be an effective interaction between (i) and (ii) in the form of some crystallographic relationship. To date the structure of the silicate membrane is not known and therefore no quantitative epitaxial relationships can be established. Nevertheless, Garcia Ruiz indirectly infers the existence of such epitaxial relationships. Figs 1.3.3a & b are scanning electron micrographs of $CaCO_3$. A number of calcite crystals can be seen all with the same orientation, parallel to the [0001] c-axis. This alignment or ordering of crystallites appears to take place even when no physical contact between the crystallites exists. Hence the existence of an epitaxial substrate is postulated. Similar observations can be made for $BaCO_3$ and $SrCO_3$. Fig 1.3.3c shows parallel crystallites of $BaCO_3$ sandwiched between two silicate membranes. These observations demonstrate the role of the membrane in controlling orientation and geometrical relationships between crystals which form the aggregate.

fig 1.3.3a

Calcite rhombohedral crystals on the outer part of an IMCA with whole morphology as in fig 1.3.2b (i).

Scale bar 5 μm.

(from Garcia Ruiz, 1985)

fig 1.3.3b

Enlarged view of above.

Scale bar 0.5 μm.

(from Garcia Ruiz, 1985)

fig 1.3.3c

A cracked $BaCO_3$ IMCA.

Arrows show $BaCO_3$ crystals

(from Garcia Ruiz, 1985)

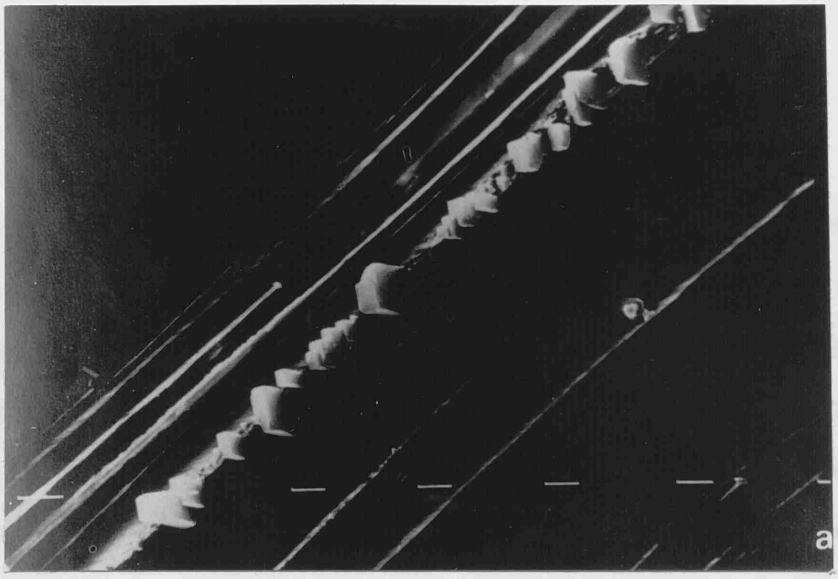
a

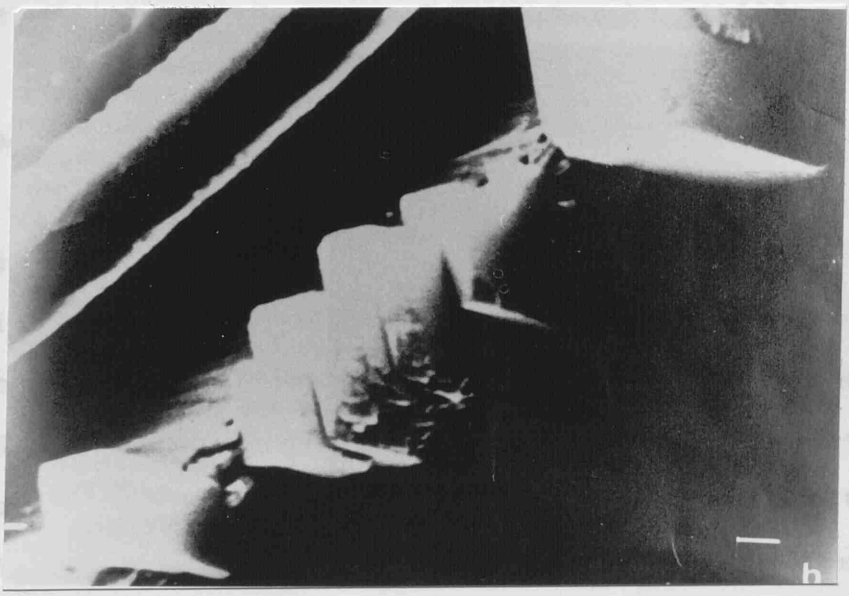
b

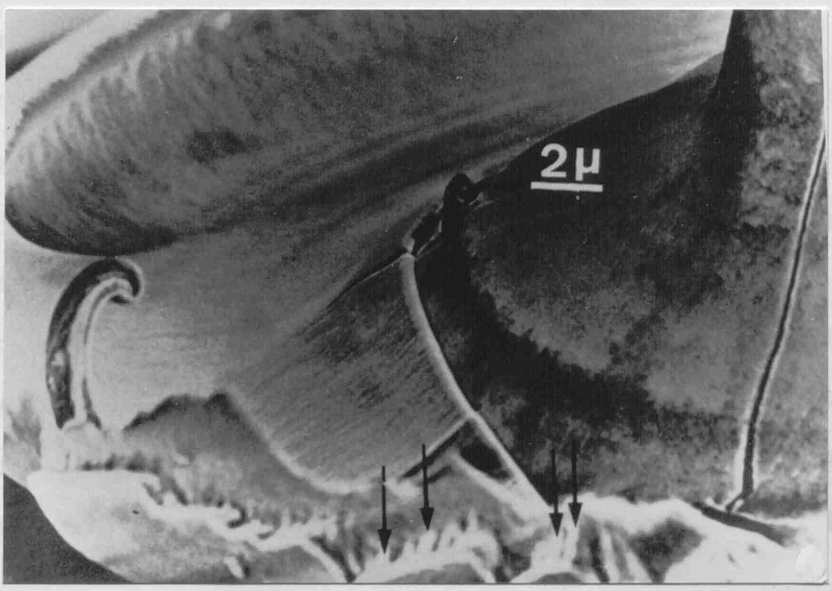
2µ

1.3.4 On The Nature of the Membrane

As can be seen from above, the experimental conditions for the growth of IMCA's bear a close relation to the conditions present in the silica garden (previously discussed for $Co(NO_3)_2$ in section 1.2.5). The process by which a calcium silicate hydrate (CSH) membrane forms during the silica garden effect for a soluble calcium salt is now discussed in more detail according to a model proposed by Birchall, Howard and Double (1980). The initial reaction is between the calcium solution (pH 6) from the surface dissolution of the calcium-containing-crystal and the sodium silicate solution (pH 12.6). At the interface of these two solutions a narrow zone is formed in which the pH changes to intermediate values at which calcium ions and silicate groups become rapidly hydrated. As a result, nucleation takes place at very high supersaturations and heterocoagulation of $Ca(OH)_2$ and polysilicic acid occurs, leading to a combined precipitate in the form of a membrane. However, there are some important differences between this system and the IMCA system. The pH of the gels in which IMCA's are formed are less than 10.5. The pK_a for monosilicic acid is 9.9 (Schwartz & Muller, 1958) and for higher polymers this decreases to 6.5 (Belyakov et al, 1974). It has been demonstrated that silicate solutions form precipitates with multivalent ions at pH values roughly two units below those at which metal hydroxides are precipitated (Falcone, 1982). Therefore, as a metal salt diffuses

through the gel an interaction between the metal ions and silicate ions present in the gel would be expected to take preference over the formation of metal hydroxides. Hence the formation of a metal silicate precipitate is possible in the pH ranges in which IMCA's are formed. Garcia Ruiz has also shown that IMCA formation is somewhat dependent on soluble carbonate concentration, with increased carbonate concentration producing more complicated morphologies and larger (twisted ribbons up to 50mm in length) IMCA's. If morphology is controlled by the growth mechanism of the membrane then Garcia Ruiz suggests that carbonate groups could be one of the components forming the matrix which enhances the hydration of the metal silicate particles in the gel. A similar process is known to exist in cement chemistry where carbon dioxide accelerates the hydration of calcium silicate cement pastes giving materials with compressive strengths greater than samples hydrated under normal conditions (Berger et al, 1972). The above arguments lead Garcia Ruiz to suggest that the IMCA forming membrane has a metal carbonate silicate structure. For the case of calcium, some structures of this composition are known, such as, $Ca_5Si_2O_7(CO_3)_2$ and $Ca_5(SiO_4)_2CO_3$ (powder diffraction files).

1.3.5 On The Morphogenesis of IMCA's

Garcia Ruiz describes morphogenesis as one of the most interesting problems related to IMCA growth. The growth

morphology and therefore morphogenesis of IMCA's is related to the silicate matrix growth conditions and analogies can be drawn between its formation and that of the precipitating membrane in the silica garden effect (section 1.2.5 & 1.3.4). In the silica garden osmosis causes the build-up of pressure within a membrane. The membrane eventually breaks and growth of a new membrane occurs. This is similar to the IMCA effect but there are some important differences, namely IMCA's are a precipitation phenomenon whereas the silica garden is dissolution phenomenon. It is also difficult to believe that the morphologies obtained for IMCA's are created exclusively by a breakage/growth process. However, Birchall et al (1980) have suggested that the membraneous character of the silica garden arises from the fact that it nucleates in the so-called non classical nucleation region, in which critical clusters are smaller than the unit cell of the growing compound, resulting in an amorphous phase. This will be true of the silicate matrix in IMCA's formed in conditions of high supersaturation and growth rate. Since the very structure of the silicate matrix prevents three-dimensional layer stacking (Williamson, 1968; Smith et al, 1972), this would lead to a two-dimensional disordered membrane. As supersaturation and growth rate decrease the membrane should become more ordered even to the point of a two-dimensional quasi-perfect crystal. Garcia Ruiz reports that this is in harmony with experimental results obtained. For the case of $BaCl_2$ diffusing through a silica gel, pH 9.5 and low

carbonate concentration, irregular aggregates are observed near the interface. As time passes the precipitation zone moves farther away from the interface to lower supersaturation and growth rate regions resulting in increasingly regular morphologies. This explanation suggests several mechanisms of growth which could be active. The existence of rotation defects in ordered membranes is known (Kleman, 1980) and could explain the existence of twisted ribbon morphologies. The IMCA system is a chemical reaction-transport system, one in which waves of chemical composition may propagate with a variety of structures. This could, perhaps, explain the banding observed in IMCA's (fig 1.3.2b). This is clearly not related to any periodicity imposed on the system and therefore can be described as a self-organisation process under conditions far from equilibrium. Also in this context, some of the morphologies observed (figs 1.3.5a & b) together with the very nature of the phenomenon suggest that IMCA growth could be analysed in terms of the development of unstable interfaces similar to the Mullins-Sekerka instability (1964) which occurs when a light fluid pushes a heavier fluid.

1.3.6 Summary

The essential condition for IMCA growth is the co-existence of two phases, a three-dimensional periodic crystalline one, and a two-dimensional membraneous one. The two phases must simultaneously grow during IMCA

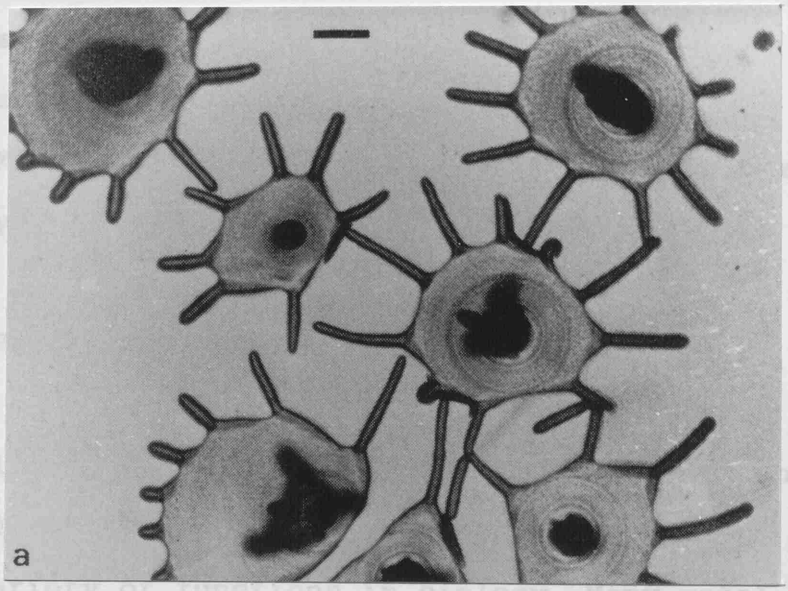

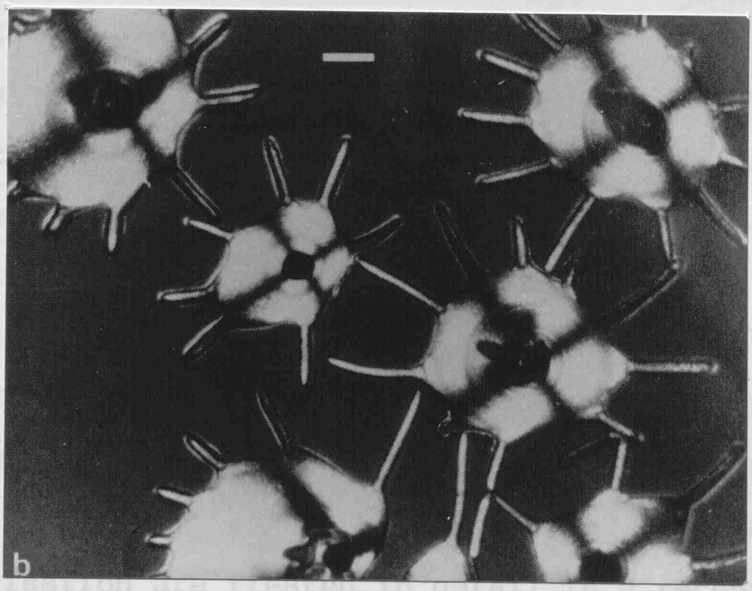

figs 1.3.5 a & b

Finger-like growths obtained in $CaCO_3$ IMCA's.

a. Ordinary light. b. Cross-polarized light

Scale bar 0.5mm

(from Garcia Ruiz, 1985)

formation. The existence of a previous membraneous substrate on which a crystalline phase is later grown, even when epitaxial relations exist between the components, will not necessarily lead to the morphogenetical behaviour observed in IMCA's. In other words IMCA's are composites with self-organised morphology.

1.4 BIOMINERALISATION

Biomineralisation is the process by which nature selectively controls the precipitation of minerals which serve a variety of functions in biology. Many metal salts undergo this biological manipulation, (table 1.4a). The end result is that a biomineral is obtained which may have a physical strength far in excess of the mineral precipitated under normal conditions, eg the enormous compressive strength of the cuttlefish bone (Birchall and Thomas, 1983), already discussed in section 1.3.1. Biominerals do not only provide construction materials though; they can act as sensors (table 1.4b) by interacting with gravitational and magnetic fields. The functional forms of biominerals and other aspects of biomineralisation are treated in detail in a recent book on the subject (Mann et al, 1989). In section 1.3 it was stated that the chemistry of IMCA's mimicked that of biomineralisation. This is because, in many cases, organic membranes control the nucleation and growth of minerals and therefore the overall morphology of the

Some Biominerals

Metal	Salt	Occurrence
Calcium	Carbonates	Very many species
	Oxalates	Especially plants
	Phosphates	Very many species
	Sulphate	Rare
Strontium	Sulphate	Especially Acantharia
Barium	Sulphate	Several unicellular species and some plants
Iron	Oxides Hydroxides	Many species
Silicon	Oxides (Hydroxides)	Many unicellular species and many plants
Aluminium	(Oxides)	Rare (some trees)

table 1.4a (from Williams, 1984)

Biomineral Sensors

Sensor	Comment on Crystallography
Calcite in Otoconia (Gravity)	Crystal size and morphology controlled (vesicles?)
Aragonite in Otoliths (Gravity)	Size grows with size of fish
Magnetic in Bacteria (Magnetic Field)	Normally cubic crystal grows as a rectangle. Crystals are organised morphologically
Barytes in Desmids (Gravity)	Conventional inorganic morphology

table 1.4b (from williams, 1984)

biomineral. The analogy of this process to the IMCA process where an inorganic membrane controls nucleation and growth of alkaline earth carbonates is clear. The following is an account of organic matrix mediated biomineralisation drawn mainly from a paper by S. Mann (1983). An understanding of these processes may lead to a better understanding of the IMCA phenomenon and to composite processes in general.

1.4.1 Organic Matrix-Mediated Biomineralisation

Organic matrix-mediated biomineralisation is a biologically-controlled process carried out under strict genetic control. The nucleation and growth of minerals is controlled by an organic matrix generated by cellular activity. Thus, unlike normal inorganic minerals, many biominerals are highly ordered composites. The role of the organic can be described in terms of three fundamental processes; structural, spatial and chemical control. These factors can be incorporated into a generalised scheme (fig 1.4.1a). Mineralisation can either occur within localised volumes such as lipid vesicles or at major extracellular sites. In both cases ion transport is controlled by cellular processes and there is much evidence for transport of minerals at various stages of their development.

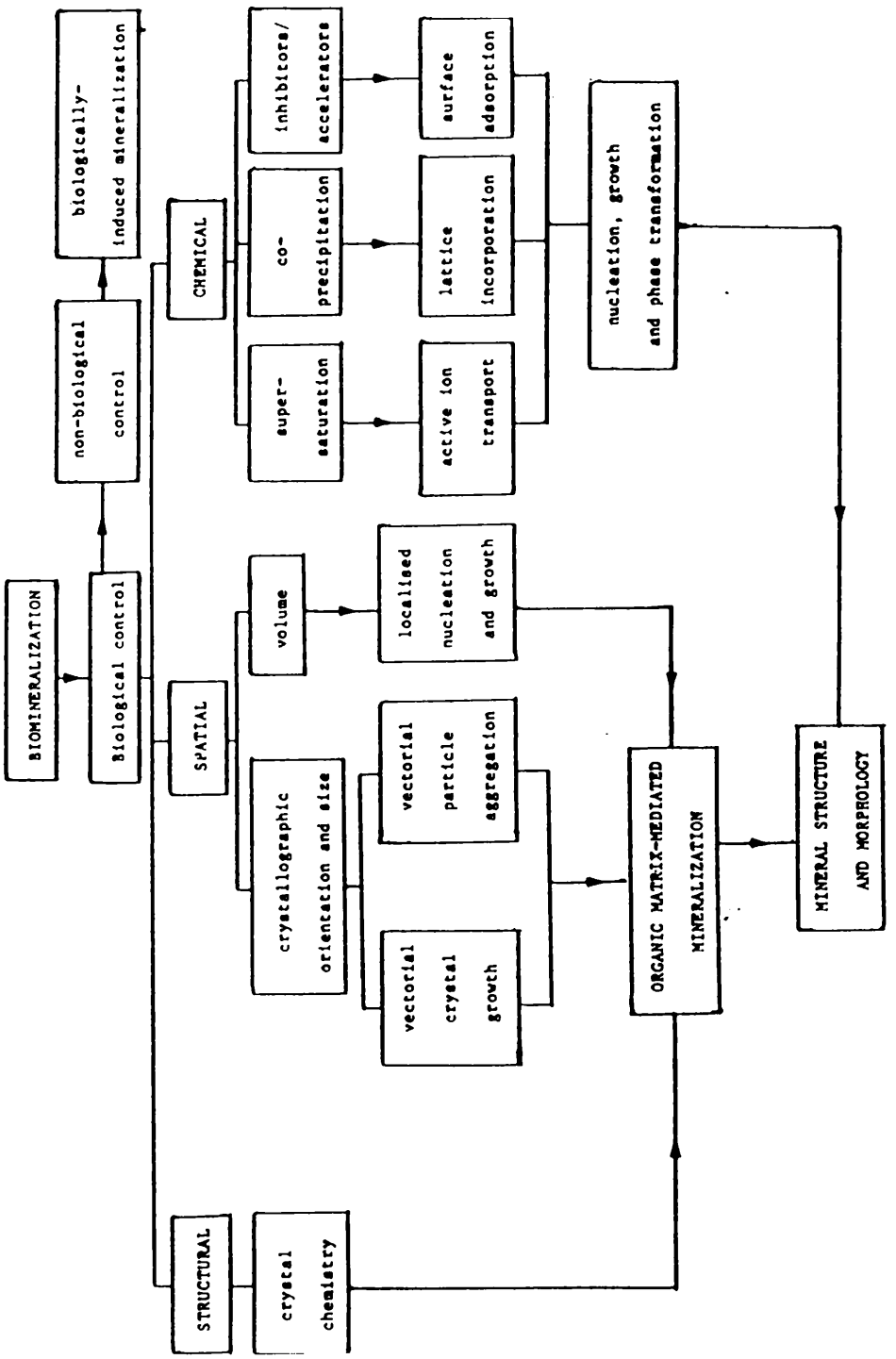

General scheme for biological control in mineralizing systems

fig 1.4.1a (from Mann, 1983)

1.4.2 Chemical Control of Biomineralisation

The chemical control of biomineralisation can be considered as the "normal" chemistry of precipitation where levels of supersaturation and co-precipitating ions at mineralisation sites control the nucleation and growth of minerals. This chemical control will be bio-energetically determined with ion concentrations at mineralisation sites being set by active transport across membranes. Further chemical control can be exerted through the interaction of the precipitating mineral with other molecules, organic or inorganic, which act as growth modifiers by accelerating or inhibiting mineral development. In principle, organic matrices may not be necessary in processes of chemically controlled biomineralisation since specificity can be determined solely by the physico-chemical properties of the mineralising environment such as accelerator/inhibitor design, concentration levels and temporal control over molecular transport of co-precipitating ions into the mineralising zone. However, in organic matrix-mediated processes chemical control of biomineralisation always plays an essential role. Theories of nucleation, crystal growth and habit modification will be discussed in chapter 2.

1.4.3 Spatial Control of Biomineralisation

An organic matrix is essential for the spatial control of biomineralisation. The matrix can exert its control in two ways; (i) as a limiting volume for mineralisation, and (ii) as a surface for controlling the vectorial properties of mineral formation, ie crystal size and orientation.

(i) Volume Control of Biomineralisation

In this type of control the mineralising zone is confined within a localised volume and there is no preferential alignment of the constituent mineral particles. Control of this type is achieved by two processes, either by spatial organic nets, usually extracellular, or by intra- and extracellular compartmentalisation through the formation of localised spherical membrane-bound vesicles. Since there is no control over crystal orientation no in depth discussion of this process is necessary.

(ii) Control of Vectorial Properties of Biomineralisation

Mineral size and orientation can be controlled by two possible mechanisms, either vectorial particle aggregation or vectorial crystal growth.

(a) Vectorial Particle Aggregation

Vectorial particle aggregation is the bulk orientation of mineral sub-units by an organic matrix. The size of the sub-units is pre-determined, possibly by precipitation in a limited volume such as the compartment of a vesicle. This could possibly be followed by transportation to the extracellular membrane and spatial ordering to form the biomineral. The spatial alignment of the crystallite sub-units will occur through chemical interactions between the charged crystallites and the oppositely charged side chains of the polymeric framework. Thus, orientation is obtained without the necessity of lattice matching (epitaxis) between mineral and substrate. Extension of this biomineral into three dimensions will require continuous synthesis of the membrane followed by the ordering of the mineral sub-units until a repeating sandwich structure is obtained such as that found in the leg tendon of a turkey, (fig 1.4.3a).

(b) Vectorial Crystal Growth of Biominerals

The growth of specific crystal faces of a crystallite through the deposition of ions on an active polymer surface can lead to biominerals of controlled size and orientation. The specific face at which growth occurs is dependent on the properties of the precipitating material and those of the organic matrix. Crystallographic orientations can occur with or without epitaxis. Where there is epitaxis between crystal and substrate, energetically favoured growth occurs at the face with the

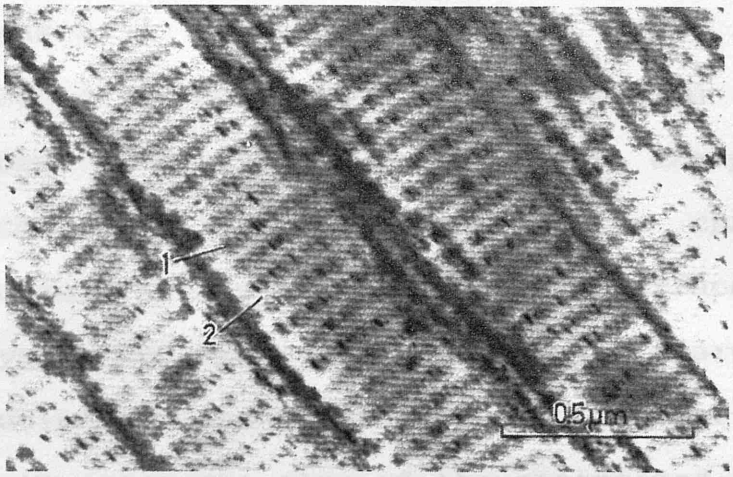

Electron micrograph of mineralized turkey leg tendon showing possible vectorial ordering of apatite crystallites on collagenous matrix; arrow 1, arrangement of crystallites in a line; arrow 2, zone free of crystallites.

fig 1.4.3a (from Mann, 1983)

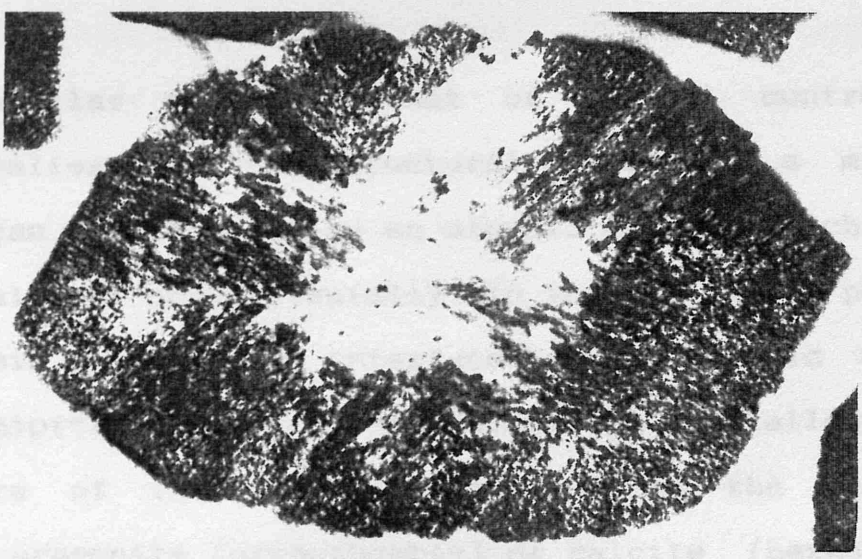

Sectioned mouse otoconium showing an iso-oriented mosaic of calcite sub-units within an organic matrix (x 40,000).

fig 1.4.3b (from Mann, 1983)

closest match. Where there is no epitaxis crystallographic orientations are determined by the surface geometry of the membrane. For example the molecular configuration of polypeptide side chains can result in surface irregularities at the interface between growing crystal and membrane resulting in energetically favoured nucleation and growth along particular crystal faces. In both cases the size of the orientated sub-units can be determined by temporal and spatial regulation of the synthesis of the organic matrix. The end result can be layers of orientated mineral sandwiched between lamellae of organic material. A probable example of this type of control over mineral growth is in the formation of calcite otoconia in mammals, (fig 1.4.3b)

1.4.4 Structural Control of Biominerals

In a similar process to that of spatial control of biomineralisation, the structural control of a mineral phase can be achieved by an organic matrix which acts epitaxially or non-epitaxially. In the epitaxial process the atomic match at the interface between organic matrix and precipitating mineral determines the crystallographic structure of the forming mineral, eg in the case of $CaCO_3$, aragonite (orthorhombic) or calcite (hexagonal). It should also be considered that any surface which exhibits structural control over a precipitating phase of a mineral will at the same time control cystallographic orientation. Thus, the molecular nature of the organic

matrix can be as important as the macroscopic spatial arrangement of the framework in determining spatial orientation of the mineral phase. In short, the function of an organic matrix in biomineralisation is to provide a surface which favours nucleation of specific crystal forms and growth of these crystals in a preferential direction to a determined size. Mann (1983) suggests that epitaxial processes may not be dominant in biomineralisation but several examples where it may be dominant have been suggested, eg the organic matrix from a mollusc shell consisting of an anti-parallel β-sheet protein and a polysaccharide phase of chitin has close structural relationships with the ab plane of aragonite, the morphology of which, it controls, (fig 1.4.4a).

The possibility of non-epitaxial structural control had not been generally considered until Mann addressed the problem, despite the fact that oriented overgrowth in inorganic systems (fig 1.4.4b) occurs where lattice matching appears to be unimportant. This may be because one of the major problems involved in the study of biomineralisation is the in-vivo study of the organic membrane.

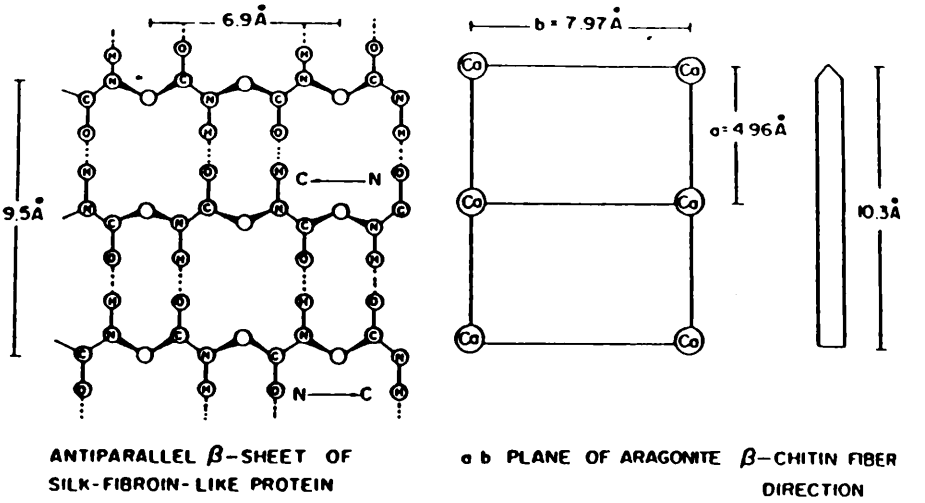

Schematic representation of the structural relationships between protein sheets, aragonite crystals and chitin fibres in the nacreous layer of N. repertus.

fig 1.4.4a (from Mann, 1983)

		Lattice	Orientation	
Substrate	Deposit	Misfit %	Substrate	Deposit
NaCl	NaI	15	(001)	(001)
	KCN	16		
	NH_4Cl	16		
	KBr	17		
	NH_4Br	23		
	KI	25		
	NH_4I	29		
	RbI	30		
PbS	RbBr	15	(001)	(001)
	KI	18		
CaF_2	KBr	21	(111)	(111)

Oriented overgrowth of inorganic crystals on insoluble substrates with large lattice misfits.

fig 1.4.4b (from Mann, 1983)

1.4.5 The Function of Organic Matrices in Oriented Mineral Growth

As discussed in the previous sections, oriented overgrowth in biomineralisation may result from three possible mechanisms:

(i) Epitaxis resulting from the deposition of ions at an organic net resulting in a lattice match between the organic net and the growing crystal faces.

(ii) Vectorial crystal growth resulting from the deposition of ions at an organic net according to an energy relationship between the organic net and the depositing nucleus.

(iii) Vectorial particle aggregation resulting from the deposition of pre-formed crystallites at an organic framework due to the interaction of opposite charges. Fig 1.4.5a illustrates these three mechanisms.

The question as to which of these mechanisms actually takes place in biomineralisation has been addressed by Mann. Of the three, vectorial aggregation of mineral particles is most likely to be recognised in practice since the presence of mineral particles in regions away from the bulk mineralising site can be observed by electron microscopy. However, it is difficult to discriminate between epitaxial and non-epitaxial

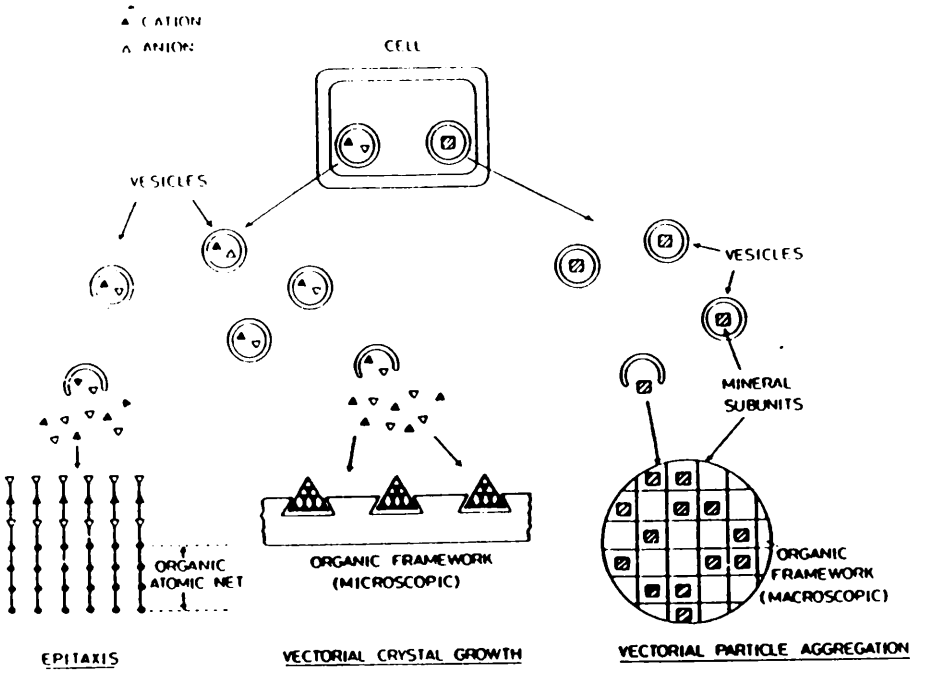

Generalised scheme showing the three possible mechanisms of oriented overgrowth in biomineralization.

fig 1.4.5a (from Mann, 1983)

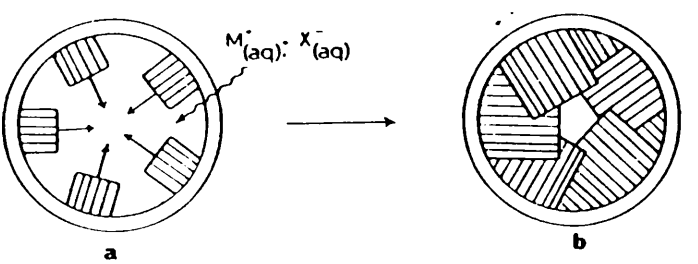

Epitaxial deposition of minerals within vesicles is limited by the spherical geometry of the compartments; a) aqueous ions are transported across a vesicle membrane and precipitated on an atomic net on the inner membrane surface; b) epitaxial growth from the membrane sites results in incoherent development of the mineral nuclei and the formation of a polycrystalline material.

fig 1.4.5b (from Mann, 1983)

mechanisms since investigation of the atomic structure at the interface is virtually impossible, although some a priori arguments are offered in the favour of non-epitaxial processes being the main mechanism of oriented overgrowth. Firstly epitaxis requires a rigid two-dimensional atomic net whereas non-epitaxial deposition can be achieved from a more flexible surface on which there are specific molecular cofigurations of polypeptide side chains. Secondly, many biominerals are observed to be formed within membrane bound vesicles (<100nm). Epitaxial growth in these vesicles would result in the incoherent development of a polycrystalline material as illustrated in fig 1.4.5b. The formation of a single crystal would be favoured by nucleation at one site in the vesicle. This has recently been synthetically demonstrated by the precipitation of single crystals of Ag_2O in 30nm phosphatidycholine vesicles (Mann & Williams, 1983) In summary Mann suggests the role of epitaxis in biomineralisation may be overestimated and that other factors such as surface structure and vectorial crystal aggregation may be responsible for biomineral orientation.

1.4.6 Mimicking Biomineralisation

Mann's interest in biomineralisation led him to try and model the process in the laboratory (Mann, 1990). He prepared synthetic vesicles (30-50nm in diameter) made of phospholipids. These are long chain molecules with a

hydrophobic body and hydrophilic tail. They form a membrane by lining up with the tails pointing in one direction. He found that the surrounding membrane influenced the structure, morphology and size of minerals formed in the vesicle, e.g. when experimenting with iron oxides, spherical crystals of magnetite were formed under the same conditions that produced needle like crystals of goethite in the absence of the membranes. The magnetite crystals were about 5nm in diameter. Crystals this size could be of considerable importance in the production of catalysts or ceramics.

Further work led to Mann using Langmuir-Blodgett films in an attempt to influence inorganic crystallisation. A Langmuir-Blodgett film is a one molecule thick soap film (hydrophobic body and hydrophilic tail) spread across the surface of water. The film can be of positive, negative or neutral charge. He found in the case of $CaCO_3$ that positive or negative charged films had an influence on crystal orientation, structure, morphology and size resulting in the deposition of floret shaped crystals of vaterite with each crystal orientated at the same angle to the surface of the monolayer. In contrast uncharged films produce calcite crystals that do not have any particular orientation and in the absence of any film a jumbled mass of rhombohedral crystals is obtained. Further experimentation showed that the shape of the molecules making up the film influences to what extent the crystals are oriented. So it would appear that Mann

has replicated the process of vectorial crystal growth, the same one that he argues may be the dominant one in biomineralisation.

1.5 SELF-ORGANISATION AND THE ORIGINS OF LIFE

There is the view held by some that the first organisms on earth had a biochemistry very different from ours, that they had a solid state biochemistry and that life on earth evolved through natural selection from inorganic crystals. This evolutionary process where an organism with one type of central control machinery is transformed into an organism with a completely different control machinery has been called Genetic Takeover by Graham Cairns-Smith (1982 & 1985). The main ideas and clues towards the solution of the problem of origin of life are summarised below:

(i) The only thing that can evolve through natural selection is genetic information as it is the only thing that passes between generations over the long-term. This genetic information is held in a genetic material but it is not substance, it is form, and can outlast substance as it is replicable. Evolution can only begin once this kind of form is established. (ii) Our genetic materials, DNA and RNA, are large complicated molecules. Chemically and biochemically they are very complicated to make; even to make the nucleotide sub-units takes many steps. This suggests these genetic materials were relatively late arrivers.

(iii) In evolution, things can be subtracted when there is no further use for them as in the construction industry where scaffolding is removed on the completion of a building. This suggests an earlier design of organism at the start of evolution which was based on a genetic material no longer present today.

(iv) Genetic material, contained in collections of genes, can be passed on between generations. This collection of genes can be likened to the fibres which make up a rope. New genes can be added and others subtracted. This will allow genetic information to be transferred without any disruption to the overall continuity. This analogy suggests how organisms based on one genetic material could evolve into organisms based on an entirely different genetic material.

(v) Primitive organisms would have been very different from today's organisms and most likely they would have been made from different materials also. An analogy would be the way primitive machinery is usually different, in design approach and materials of construction, from modern machinery. Primitive machines and organisms must work but more advanced ones have to work well and may contain a complex assembly of components working in collaboration.

(vi) Whatever the first genetic material was it must have been able to store information. An object can store

information if it can exist in one of a large number of alternative configurations. A book holds information because there are many ways of arranging letters and words. Similarly, a DNA molecule stores information through having one of a very large number of possible base sequences. In this sense, then, it would be possible for crystals to store information. Over and above its regularly repeating crystal structure any given crystal will contain defects such as vacancies, substitutions and dislocations. The positioning of these defects could represent specific information analogous to a DNA base sequence or to letters on a page. Alternatively information could be stored on a larger scale such as crystal domains and twinned crystals. As to what type of crystal could have been the first " naked genes " ; by considering bonding characteristics in organic and inorganic molecules and crystals, inorganic crystals with covalent bonds seem more likely than organic polymers which have little self control.

(vii) What would appear to be ideal naked genes are colloidal minerals that could crystallise from aqueous solutions at ordinary temperatures. In other words clays. Nature makes clays continually. Microcrystalline clay particles precipitate from aqueous solutions derived from the weathering of hard rocks. Very often these clays have a layer silicate structure. Defects will be present in these layers which could act to store information. Furthermore electron microscopy reveals that colloidal

minerals often have the forms of membranes and tubes which can be imagined as potential phenotypic apparatus for first life.

These seven points are all very well but they raise four important questions: assuming inorganic crystals were the first naked genes, how and why did organic molecules come in and how and why did they take over?

On the question of how organic molecules came in, there is the possibility that not much has changed over the billions of years of evolution. Then, as now, carbon dioxide could have been the source of carbon in the first biochemicals which would have been acquired by mineral organisms through photosynthesis in the same way as plants have the unique ability of using energy from sunlight to make complex organic molecules from carbon dioxide and water. The primitive fixation of carbon would certainly not have been as complicated a process as that of photosynthesis in plants today but there are minerals that mimic the effect to some extent. Photo-oxidation of aqueous Fe(II) solutions occurs at pH < 6.5 (Braterman et al, 1984) under u.v light to produce a solvated electron which can react with carbon dioxide and hydrogen to produce formaldehyde (Akermark et al 1980). Some crystalline minerals are also known to act in this way, such as in the oxidation of iron monosulphide to iron disulphide (pyrite) which Wachterschauser argues (1988) could have been the electron donating energy source for

an autotrophic origin of life. This argument is taken further by Russell et al (1981 & 1983) who have reported fossil hot spring structures formed below 150^{o}C at the vent sites of 360 million year old hydrothermal systems driven by the heat stored in the earth's crust. These fossil vents consist of pyrite tubes between 0.1 and 10mm in diameter. Similar iron monosulphide morphologies have been reproduced in the laboratory by passing Fe(II) and Fe(III) solutions through a small aperture into a sodium sulphide solution at room temperature. These iron monosulphide tubes crystallised to pyrite within six months. Pyrite is hydrophobic, thus, organic matter carried in hydrothermal solution may have adhered to and collected in porous iron sulphide traps. Organic reactions may have taken place, such as the polymerisation of amino acids, driven by the energy released through the convertion of iron monosulphide to iron disulphide. Russell et al suggest (1990) one more important role for iron sulphide, that of nucleating the membrane of the earliest cell walls. Spherical aggregates of pyrite about 5μm in diameter (known as framboids) are found within fossil hydrothermal chimneys. The internal crystallites are of a similar size (0.1 μm) to those found in magnetotactic bacteria. These framboids appear to be grown inorganically from a spherical shell of iron sulphide gel. During the precipitation of the framboids the sulphide shells, consisting of periodic arrays of iron monosulphide crystallites, would have provided a site for the concentration of polar organic species by

adsorption onto the iron sulphide surfaces. At a critical concentration of organics, iron sulphide precipitation would be inhibited and an organic layer would result, perhaps assisted by the periodic arrays of iron sulphide crystallites. Further adsorption of organics onto this ordered organic layer could then lead to a cell membrane precursor.

Nitrogen fixation, into ammonia, is also known to occur on wet crystals of titanium dioxide in the presence of sunlight. Ammonia is far more easily built into bigger molecules than nitogen alone.

Under an inert atmosphere of mainly carbon dioxide, nitrogen and water vapour, a kind generally favoured for the early earth, one can imagine the synthesis of small organic molecules taking place, not on a large scale but certainly in localised areas where damp minerals were exposed to sunlight. These molecules would be continually made and broken up as ultraviolet light destroys molecules too.

Returning to clay minerals, could organic molecules interact with clay minerals, and through natural selection, could evolved mineral organisms be imagined as creating conditions for the synthesis of more difficult molecules and how would this happen? Why it should happen will be addressed later. Clay minerals contain iron atoms which act as light catchers in the same way as

chlorophyll catches energy in photosynthesis. By analogy to photosynthesis the light package would generate an electron and a positive charge. This could lead to the fixation of carbon dioxide, if, the electron and positive hole were prevented from coming together again and cancelling the process out. The clay layers themselves could achieve this. Success would be dependent on having the appropriate arrangement of clay layers and iron atoms.

Going one stage further than the initial capturing of light energy, clay minerals seem like ideal apparatus for the synthesis of organic molecules. They can act as catalysts, the can form tubes or vessels, they can hold on to organic molecules at edges or stacked between layers and any number of defect structures are possible for more sophisticated synthetic needs. In this way, the problem of sequencing, inherent in long organic syntheses, may be solved through appropriate spatial organisation. The success of these syntheses would be the genetic control, through natural selection, which would put new clay particles together.

This now leads us to ask why organic molecules became involved and what use organic molecules are to evolving clay minerals?

A variety of uses can be imagined including mixtures which could act as glues and uv shields to elaborate self

locking polymer molecules for more sophisticated purposes. Organic molecules could also help in the processes of making clays. Formic acid and oxalic acid help clay synthesis by controlling acidity and acting as chelating agents. Molecules like amino acids could also help by chelating aluminium ions and holding them in solution and nucleotides are good at binding clay minerals together. Polysaccharides could help by forming slimes or gels which could soften or harden under appropriate conditions. This could find uses in preventing drying out in strong sunlight or preventing washing away. As the clay mineral apparatus became more sophisticated more complex organic molecules were synthesised including DNA and RNA. Originally, they would have been structural materials since different segments of chain can lock together. The fact that they can replicate information would have been discovered later and it would have been an accident. This replicating process, once established, must pass on information which benefits the whole inorganic/organic system, if there is to be evolution. Such benefits could have been better structural materials or better pieces of apparatus. The system would then evolve until the central control machinery was complete. Various sorts of enzymes and membranes had to evolve in order to replace the clay apparatus. Then there would be no need for minerals.

As to why the organic molecules won, they are held together far more securely. They may be more difficult to

assemble than inorganic ones but once assembled they will hold together indefinitely. By way of contrast crystalline structures are far more likely to fall apart, rearrange or dissolve.

Cairns-Smith concludes that the battle for supremacy is decided on scale. "Organic machinery can be made much smaller. Such clever things become possible as sockets which can recognise, hold and manipulate other molecules- and in any competition to do with molecular control the system with the smallest fingers will win."

2 BACKGROUND ON PRECIPITATION

2.1 NUCLEATION

2.2 CRYSTAL GROWTH

2.2.1 Crystal Growth from Pure Solution

2.2.2 Crystal Habit Modification

2.2.3 Pattern Formation in Non-Equilibrium Crystal Growth

2.3 THE GEL GROWTH METHOD

2.3.1 Introduction

2.3.2 Gel Structure and Properties

2.3.2.1 Silica Gel

2.3.2.2 Agarose Gel

2.4 AIM OF PRESENT WORK

2 BACKGROUND ON PRECIPITATION

2.1 NUCLEATION

Nucleation can occur in two different ways, heterogeneously and homogeneously. Homogeneous nucleation occurs by spontaneous formation of nuclei in the bulk of supersaturated solutions whereas heterogeneous nucleation involves the formation of nuclei on the surface of a substrate present in the aqueous medium. Homogeneous nucleation is a rarely observed phenomenon (although it can be achieved by controlled precipitation in gels) but the classical theory of homogeneous nucleation and crystal growth provides a basis for the understanding of all nucleation and growth processes. This classical theory relates the barrier to nucleation to the surface energy of the particle, hence the energy required for the formation of a nucleus and therefore the work done, w, to form a nucleus is equal to the work required to form a surface, $w_{surface}$, minus the work required to form a bulk particle, w_{bulk}:

$$w = w_{surface} - w_{bulk}$$

In other words when the energy released through the making of bonds in the bulk of the particle exceeds the energy required to make the surface of the particle nucleation becomes energetically favourable.

Using the analogy of a liquid drop in a supersaturated vapour, then:

$$w = a\sigma - v\Delta p$$

where: a is the surface area of a drop,

v is the volume of a drop,

σ is the surface energy of a drop per unit area,

Δp is the pressure difference between the vapour and interior of the drop.

Knowing:

$$a = 4\pi r^2$$

$$v = {}^4/_3\pi r^3$$

$$p = \frac{2\sigma}{r}$$

where r is the radius of the drop.

then by substitution:

$$w = 4\pi r^2\sigma - {}^4/_3\pi r^3 \cdot \frac{2\sigma}{r}$$

$$= {}^4/_3\pi r^2\sigma \qquad (1)$$

The smaller a drop is, the greater its internal pressure, ie:

$$\ln \frac{p_r}{p_\infty} = \frac{2M\sigma}{RT\rho r}$$

where: p_r is the vapour pressure of a drop,

p_l is the vapour pressure of a flat liquid surface, ie the equilibrium vapour pressure of the surroundings,

M is the molecular weight,

ρ is the density,

T is the temperature in Kelvin,

R is the gas constant.

The pressure can be replaced by supersaturation term S, the factor by which the actual activity of ions in solution (product) exceeds the ionic activity at equilibrium (product). When $p_r = p_l$ the supersaturation reaches the value of 1.

Hence:

$$\ln S = \frac{2M\sigma}{RT\rho r}$$

Therefore:

$$r = \frac{2M\sigma}{RT\rho \ln S} \qquad (2)$$

By substitution of (2) into the work expression,(1), the work to form a nucleus or the activation free energy of formation of a nucleus, ΔG_N^*, is given by:

$$w = \Delta G_N^* = \frac{16\pi\sigma^3 M^2}{3(RT\rho \ln S)^2} \qquad (3)$$

Fig 2.1a illustrates the relationship between cluster size and surface and bulk energy terms. The critical cluster radius, r_c, is the radius of a particle at the point at which nucleation becomes energetically feasible.

In the case of heterogeneous nucleation where there is the presence of additives such as organic membranes in biomineralisation, inorganic membranes in IMCA's or even particles of dust in any precipitation medium, the surface energy, σ, will decrease. Hence critical cluster size, r_c, will be smaller leading to a lower energy barrier to nucleation, w, and greater rate of nucleation.

From the thermodynamic relationships established the role of supersaturation, S, can be seen to be of great importance to precipitation, e.g. from the equation (3) if a system is only just saturated, ie S=1 then logS=0 and spontaneous nucleation cannot occur. By considering the kinetics, which in most cases are far more important, the role of supersaturation is seen more clearly. The rate of nucleation can be expressed by an Arrhenius-type equation:

$$N = A \exp\left[\frac{-\Delta G_N^*}{RT}\right]$$

therefore:

$$N = A \exp\left[\frac{-16\pi\sigma^3 M^2}{3R^3T^3\rho^2(\ln S)^2}\right] \qquad (4)$$

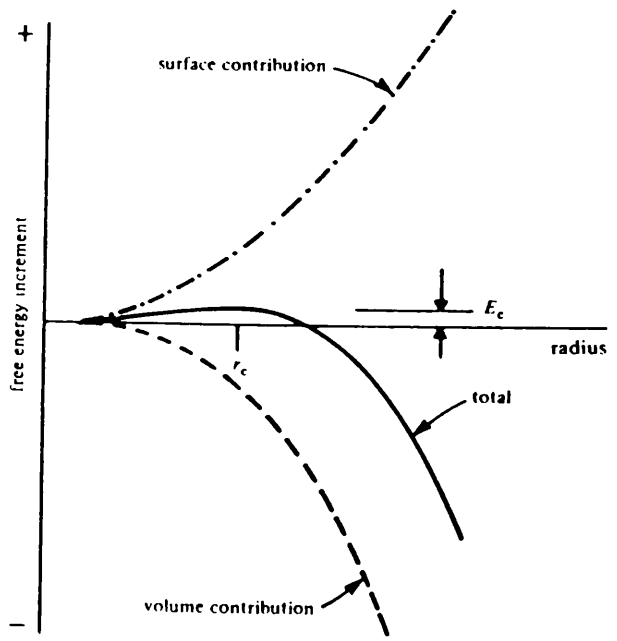

Role of volume and surface energies in the determination of the critical radius r_C. Classical picture, perfect spherical nucleus assumed.

fig 2.1a (from Henisch, 1973)

From this relationship it can be seen that the prominent factors affecting rate of nucleation are supersaturation, S, interfacial tension arising through surface energy, σ, and temperature, T, with the supersaturation dominating.

It can also be seen that if ΔG_N^* was lowered due to nucleation at a substrate then supersaturation, S, would decrease to keep N constant, hence heterogeneous nucleation occurs at lower supersaturation levels than those required for homogeneous nucleation.

Since N is a steep function of S it is usual to assume that there is a critical supersaturation corresponding to the sudden onset of nucleation; under conditions of smoothly increasing concentration, nucleation will take place in a narrow range of concentrations at or only just above this limit (homogeneous precipitation only).

Then since w and S are effectively fixed we have, from (1):

$$r \propto \sigma^{-1/2}$$

However, there will be constraints linking r to the amount, and rate of supply of the material being precipitated. If, for instance, nucleation proceeds until the fresh nuclei have achieved a certain total area (at which point the growth of existing nuclei takes precedence over the formation of new ones), the number of

particles nucleated is proportional to σ; if it proceeds until the nuclei have achieved a certain total volume (thereby removing enough material from solution to reduce S below a critical limit) the number varies as $\sigma^{3/2}$. While such assumptions may be far too simple, it is clear that any factor that affects σ will have major effects on the number of nuclei formed and, in the case of gel growth, their distribution.

The structure of the critical nucleus will influence to a large degree the structure of the precipitating phase. Two extreme possibilities can be envisaged. Firstly, the initiating nucleus resembles a piece of the bulk crystalline phase. There is a strong interaction between ions in the nucleus, and lattice solvation has been overcome. This situation will arise through low supersaturation levels resulting in a critical nucleus radius larger than the unit cell. The resultant precipitate will be a well ordered crystalline phase with crystal size dependent on supersaturation which will also determine the amount of nuclei formed. The second possibility is a critical cluster of low radius formed under high supersaturation levels. The possibility here is that the ions in the cluster will be weakly attracted to each other and heavily solvated. The resultant precipitate will be a disordered crystalline phase of low order or even an amorphous phase where critical cluster radius is actually smaller than the unit cell.

2.2 CRYSTAL GROWTH

2.2.1 Crystal Growth from Pure Solution

Early theoretical work on the growth of pure crystalline phases was carried out by Kossel (1934) and Stranski (1928) and later by Becker and Doring (1935 & 1949). These theories were a continuation of the classical nucleation theory and considered crystal growth to occur through surface nucleation of further ions or molecules at a crystal surface in a manner similar to that described for heterogeneous nucleation. Growing crystal surfaces contain sites of high binding energy such as steps and kinks at which further deposition can occur. Ions or molecules are adsorbed onto the crystal surface and diffuse to active sites such that the crystal grows in a step-wise manner. The theories predict that energy barriers have to be overcome in this process, hence, rapid crystal growth should occur at crystal faces with the most kinks or steps. However, at any one instant, there are very few kinks or steps at crystal faces (Mullin, 1972) and therefore theories which relate crystal morphology to surface energies of particular faces have fallen into disuse.

The classical nucleation theory predicts surface nucleation to occur at supersaturation values of 0.25-5. Thus, this model does not account for observations that many crystals grow at supersaturation levels as low as

0.01. However, this can be explained by the screw dislocation theory of crystal growth (Frank, 1949; Burton et al, 1951) which considers crystals to contain faces intersected by dislocation ledges which act as high energy binding sites of further crystal growth as illustrated in fig 2.2.1a. Growth takes place by the spreading of the ledge over the surface and since it is self-perpetuating there is no need for surface nucleation and the ledge winds itself up into a closed spiral during growth.

The kinetics of crystal growth are dependent on a series of factors. Where mechanisms such as ion transport, adsorption of ions at a surface and incorporation into the crystal structure are active, the slowest step is rate determining whereas if mechanisms involving screw dislocation steps are active, the fastest step is decisive. The rate control can alter from one mechanism to another due to changes in the system such as ion concentration and particle size.

At high supersaturations, where bulk diffusion is likely to be the limiting factor, first order kinetics are predicted whereas at low supersaturations second order kinetics are predicted for screw dislocation growth.

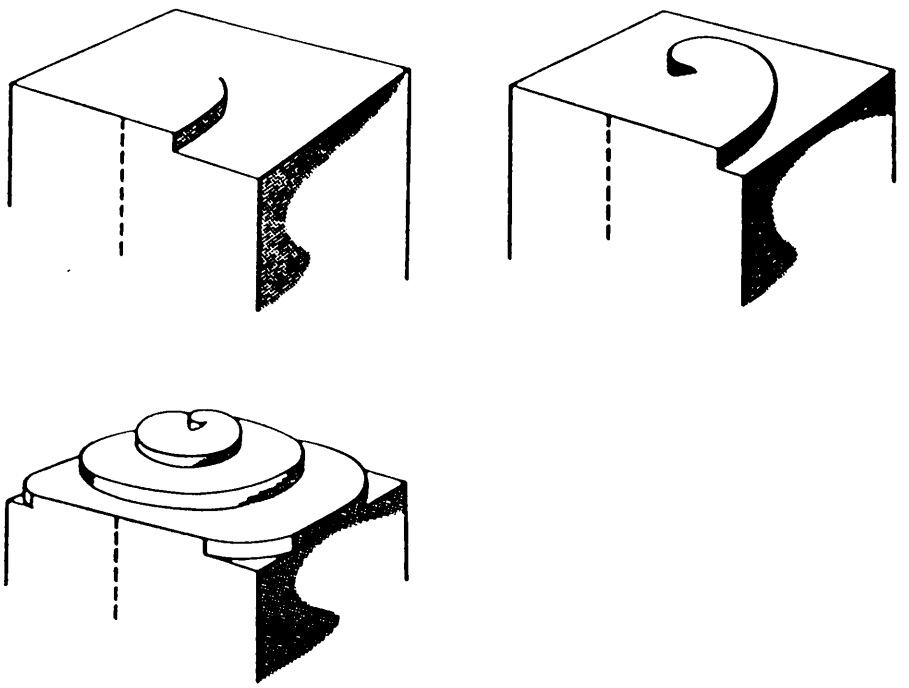

Schematic showing the growth of a crystal at a screw dislocation. Deposition of new material at the screw dislocation edge occurs at a uniform rate but the anchor dislocation centre causes the relative rate of "winding" to be larger at the origin. Consequently the screw dislocation winds into a growth spiral.

fig 2.2.1a (from Mann, 1983)

2.2.2 Crystal Habit Modifications

Impurities or additives in a precipitating system may have an effect on crystal growth, morphology and chemical properties. Incorporation of additive ions into a precipitate will depend on the relative ion sizes, charge and polarization. Ion mismatch is generally less than 15%. Many examples of additive incorporation into precipitating crystals are known such as the incorporation of CO_3^{2-} for PO_4^{3-} in hydroxyapaptite which causes lattice distortions (Posner, 1980). When $CaCO_3$ is precipitated in the presence of Mg^{2+}, the calcite phase is favoured, whereas Sr^{2+} incorporation favours formation of the aragonite phase. In this way rates of precipitation (and phase) may be selectively controlled, eg the presence of Mg^{2+} ions has no effect on the rate of crystal growth of aragonite although it retards the formation of calcite which is thought to be due to its non-equilibrium incorporation into the growing calcite crystal making them considerably more soluble than pure calcite (Berner, 1975; Kinsman & Holland, 1969). Many other examples of crystal habit modification are known such as the incorporation of organic materials into inorganic layer compounds (Lagaly, 1981) such as crystalline silicic acids, some niobates, titanates and layer silicates (see origins of life, section 1.5). Addadi et al (1983) have performed controlled modification of crystal habit and therefore changes in morphology in benzamides and benzoic acids by the

interaction of tailor-made impurities at specific crystal faces which inhibit growth relative to the other unaffected faces.

2.2.3 Pattern Formation in Non-equilibrium Crystal Growth

Crystal growth under non-equilibrium conditions, ie as in a diffusion system, can give rise to complex patterns which are similar to those found in viscous fingering, aggregation and electrochemical deposition. The patterns that form can be grouped into a small number of typical morphologies such as faceted, dendritic, dense branching and fractal, (fig 2.2.3a). Recent research has indicated that growth patterns may be determined by the interplay between microscopic interfacial dynamics and external macroscopic thermodynamic forces determined by the diffusion field. A review of this subject is given by Ben-Jacob and Garik (1990).

The theories so far developed depend on the transfer of information from a microscopic to a macroscopic level. This is a known phenomenon, eg in a snowflake the six-fold symmetry of the ice crystal lattice manifests itself in the dendritic branches of the snowflake. In the case of a precipitating snowflake we have a system far from equilibrium in which a stable solid phase will propagate into an unstable supersaturated water/vapour phase. The growth rate of the stable phase is limited by the

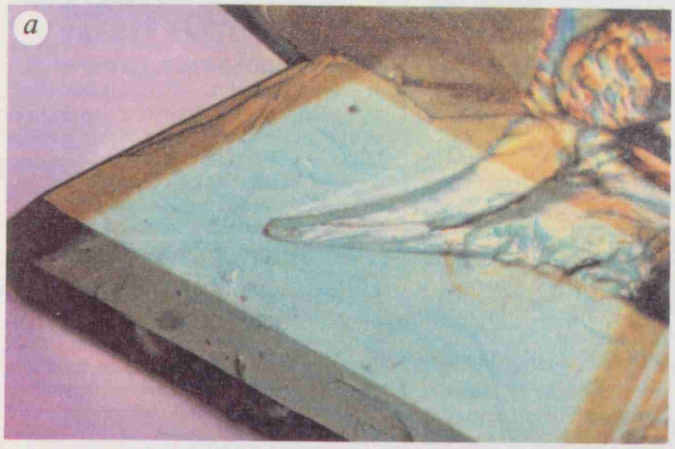

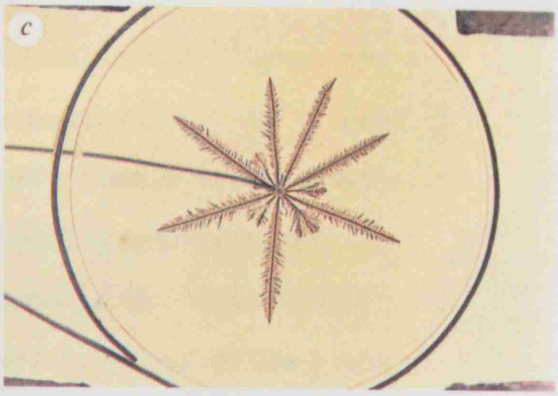

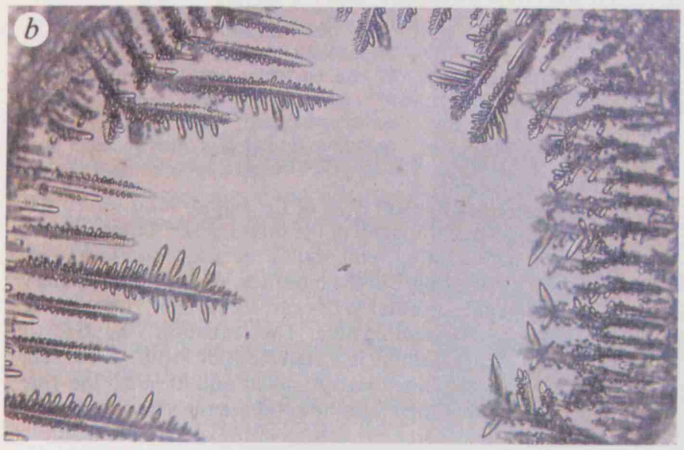

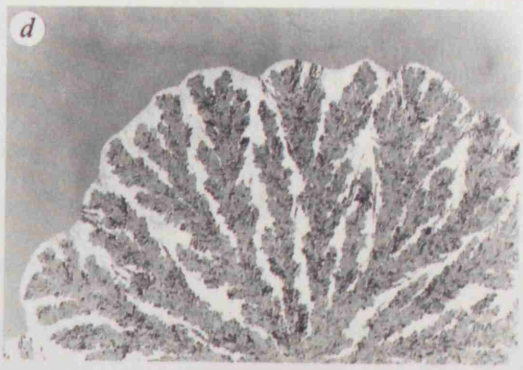

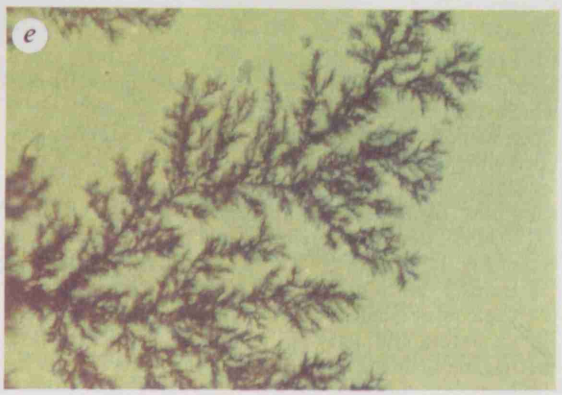

The "essential shapes" of non-equilibrium growth processes; a) faceted growth during solidification of copper sulphate, b) dendrites formed during solidification from supersaturated solution, c) dendrites grown by electrochemical deposition, d) dense branched morphology in the annealing of amorphous material, e) a fractal shape produced by electrochemical deposition.

fig 2.2.3a (from Ben-Jackob and Garik, 1990)

diffusion of water molecules from the gas phase into the crystal and the diffusion of latent heat away from the crystal. In this process the interaction of the macroscopic diffusion kinetics and the microscopic dynamics occurring at the interface (determined by surface tension, surface kinetics and the anisotropic orientation of atoms at the interface) tend to drive the system towards the formation of irregular shapes.

On the problem of how microscopic dynamics are amplified to such an extent that they control macroscopic morphologies, dentritic growth has been studied closely. Previous theories emphasized macroscopic dynamics and included microscopic dynamics only as a refinement. Ivantsov (1947) showed that for a solid forming from a melt the growing crystal front is parabolic when the process is controlled by heat diffusion alone and surface tension and kinetics are ignored. The parabolic shape of the tip and the constant velocity of growth are both consistent with observations of dendritic growth. However, Ivantsov's solution only specifies the product of the velocity of growth and the radius of curvature of the dendrites' parabolic tip; neither one alone can be predicted. It has since been demonstrated by Glicksman et al (1976) that one dendrite, ie one tip velocity and radius of curvature, is observed for a given undercooling, yet Isantsov's solution predicts a continuous family of parabolic solutions for given experimental conditions. This poses a selection problem.

Moreover, Ivantsov's solutions are linearly unstable, ie they are unable to maintain their shape during growth.

The incorporation of a microscopic term, surface tension, and the proposal by Oldfield (1973) that the selected dendrite was the one growing slowest or with maximum tip radius (stabilised by surface tension) led to a slightly more stable solution and further advanced the concept of a selection principle.

Advances in computing led to the incorporation of all microscopic dynamics which led to a better understanding of the importance of factors such as surface tension and surface kinetics. These factors may totally alter the character of solutions and must be incorporated into calculations from the start. The results from these calculations have shown the conditions for dendritic growth to be anisotropic surface kinetics and surface tension which is argued supresses heat gradients at the tip of growth and prevents splitting, in contrast to isotropic microscopic dynamics which lead to heat gradients at the point of growth, which cause splitting and a dense branched morphology.

At present much work is being carried out on the interplay of microscopic and macroscopic dynamics and their effect on pattern formation in far from equilibrium conditions.

2.3 THE GEL GROWTH METHOD

2.3.1 Introduction

Gel growth has been used for many years in the production of moderately insoluble materials (Henisch, 1973, 1988), where it has specific advantages of controlled mixing, suppressed convection currents, filtering, mechanical protection and the reduction of nucleation and aggregation (Abdullah et al, 1986). These advantages make the gel method, in some cases, an excellent way of precipitating good single crystals, on which the advancement of solid state science depends so much. Other applications of the gel growth method include the preparation of materials in the pores of gels, offering a route to intimately mixed composites (Roy and Roy, 1984) and the precipitation of material on suspended gel particles as a means of preparing supported catalysts (Geuss, 1983). Another interesting phenomenon associated with gel growth is Liesegang Rings. This is the occurrence of periodic precipitation in a gel diffusion system, first observed by R. E. Liesegang (1896) when he precipitated silver chromate by the diffusion of silver nitrate through gelatin impregnated with potassium chromate. Fig 2.3.1a illustrates Liesegang Rings in silver chromate and calcium phosphate systems. Although there is and has been much interest in periodic precipitation the phenomenon is, at present, not fully understood. Since the late 1800's many materials have

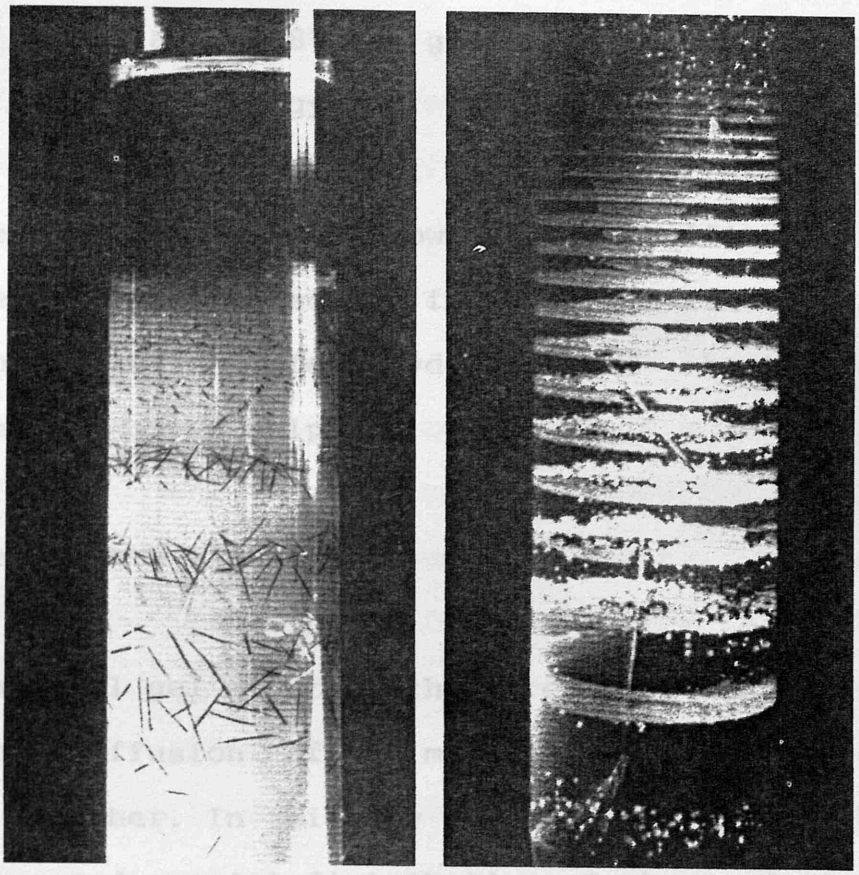

(i) (ii)

Liesgang Rings in (i) silver chromate system and (ii) calcium phosphate system.

fig 2.3.1a (from Henisch, 1988)

been precipitated in gels, far too many to be discussed in this thesis. One early worker (Hatschek, 1911), working with gelatin and agar gels reported the precipitation of well-formed and distinct barium carbonate crystals, a material which has been studied to great extent in this project. In previous work in this department (Abdullah, 1988) the gel method has been used to study the morphology of various metal oxides, carbonates and other salts. The structures and morphologies found have been shown to be specific to the material being precipitated and include hair-like bundles of iron oxyhydroxide (ferrihydrite) and bowtie-like morphologies of copper sulphate.

2.3.2 Gel Growth Procedures

In the classical gel growth method precipitation arises through the diffusion of one material through a gel containing another. In this way the rate of formation, total loading and spatial distribution of the product are controlled by diffusion. This method gives rise to non-uniform product loading due to the Liesegang Ring phenomenon and because the diffusion gradient constantly falls as material is used up.

These non-uniformities are themselves a subject of interest (Henisch 1988), but can pose major problems in the preparation of a uniform new composite material. Recent work at Glasgow (Abdullah et al, 1987) has shown

that for metal carbonates and hydroxides such problems are avoided by homogeneous reaction techniques, in which the gel is preloaded with reagents which slowly react to give the desired product uniformly throughout the pores of the gel. In this case gels were preloaded with one component of a precipitate and the precursor of the other, eg a metal salt and hexamine or urea. Subsequent heating of the gel results in the hydrolysis of urea or hexamine and the precipitation of a metal carbonate.

2.3.3 Gel Structure and Properties

It is very difficult to define exactly what a gel is as there is a great deal of overlap in the descriptions of gels, sols, colloidal suspensions and pastes. However, one definition by Alexander and Johnson (1949) is a "two component system of a semi-solid nature, rich in liquid". Although this is a grossly simplified definition it helps give a feel for a gel as a three-dimensional crosslinked polymer with liquid trapped in the pores.

The most common type of gel is silica gel usually prepared from commercial waterglass, sodium silicate solution. Others include agar, a carbohydrate polymer derived from seaweed; gelatin, with a structure similar to that of proteins; polyvinyl alcohol and tetra ethoxysilane in the presence of electrolytes and co-solvents such as methanol.

In this work the gels used were restricted to silica and agarose (a more refined agar gel). The following sections discuss these gels in turn and consider gelling mechanisms, structure and properties.

2.3.3.1 Silica Gel

Silica gel is usually prepared from diluted sodium silicate solution in which monosilicic acid is considered to exist according to the following equilibrium:

$$Na_2SiO_3 + 3H_2O \rightleftharpoons H_4SiO_4 + 2NaOH$$

Monosilicic acid is known to polymerise according to the following equation:

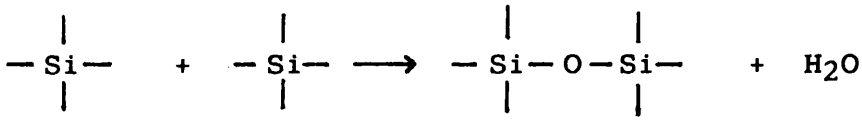

This polymerisation reaction continues until a three-dimensional particle composed of Si-O links is established. These particles in turn crosslink to form the rigid framework of the gel:

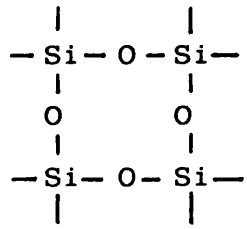

The reaction is of course, not as simple as this, nor is the crosslinked network as regular as illustrated. During

the polymerisation reaction water accumulates on top of the gel surface; this is known as syneresis and the origin of the water lies in the condensation reaction and perhaps from slight shrinkage of the gel.

The pH of the sodium silicate solution is critical to gelling time, as illustrated in fig 2.3.3.1a. It can be seen that in the absence of an ionic strength, gelling occurs quickest at around pH 6 and no gel is possible above pH 7. This is because the growing silica particles are negatively charged and repel each other preventing crosslinking. In the presence of a background ionic strength gelling occurs quickest around pH 7 and depends greatly on the concentration of the ionic strength. In this case gelling occurs up to relatively high pH values as the ionic charge on the silica particles is lowered, allowing crosslinking.

The mechanism of silica gel formation is not fully understood, but the existence of the two ions which are involved, is known: $H_3SiO_4^-$ and $H_2SiO_4^{2-}$ (Iler, 1979). The latter is favoured at high pH values and in silica gels formed in the basic pH range one would expect the existence of this ion (and perhaps similar ones) in solution as well as the silica which forms the three-dimensional network.

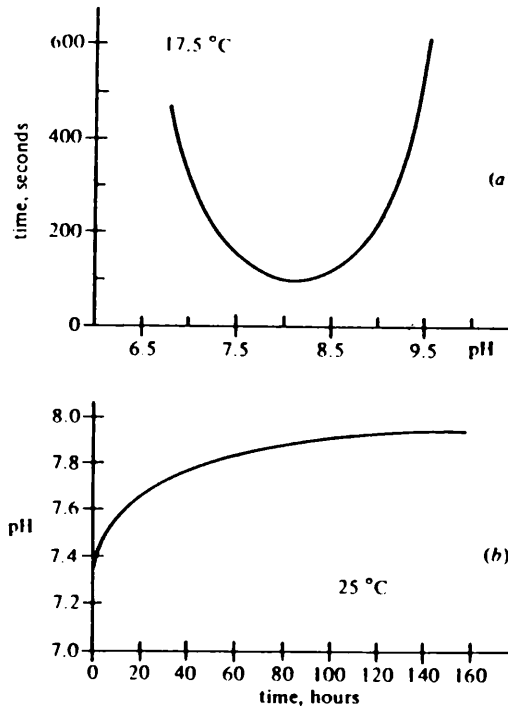

Gelling processes and pH; a) effect of pH on gelling time, b) changes in pH of an originally neutral gel during syneresis.

fig 2.3.3.1a (from Henisch, 1973)

2.3.3.2 Agarose Gel

Agar is a carbohydrate polymer derived from seaweed. Agarose is a more refined version of this. When dissoved in hot water and allowed to cool it forms a three-dimensional tangled network which acts as a rigid structure, trapping water in its pores, and forming a gel. This gel will re-soften on heating.

2.4 AIM OF PRESENT WORK

The aim of the work described in this thesis was to study factors which affect morphogenesis in inorganic precipitates in gels.

The main thrust of the work was concerned with verifying Juan Manual Garcia Ruiz's observation of "Induced Morphology Crystal Aggregates" (section 1.3) and establishing factors which affect their formation. Other materials were also examined to see if they exhibited this strange phenomenon. Finally a series of experiments was undertaken in order to characterise the membrane responsible for the induced morphologies.

EXPERIMENTAL.

3 EXPERIMENTAL: PRECIPITATION TECHNIQUES AND SAMPLE PREPARATION

3.1 PRECIPITATION BY A DIFFUSION MECHANISM IN SILICA GELS

3.1.1 Preparation of Basic Silica Gels with an Ionic Exchange Resin

3.1.2 Preparation of Basic Silica Gels with 1M HCl

3.1.3 Preparation of Acidic Silica Gels with 1M HCl

3.1.4 Preparation of Agarose Gels

3.2 PRECIPITATION BY A DIFFUSION MECHANISM IN AGAROSE GELS

3.3 HOMOGENEOUS PRECIPITATION IN SILICA GELS

3.4 REACTION VESSELS

3.5 PREPARATION OF PRECIPITATES FOR ANALYSIS

3.5.1 In-Situ Analysis : Optical Microscopy and Cross-Polarised Optical Microscopy

3.5.2 Removal of Precipitates from Silica Gel

3.5.3 Removal of Precipitates from Agarose Gel

3.5.4 Scanning Electron Microscopy (SEM)

3.5.5 Transmission Electron Microscopy (TEM)

3.5.6 X-Ray Diffraction (XRD) and Fourier Transform Infra-Red Spectoscopy (FTIR)

3 PRECIPITATION TECHNIQUES AND SAMPLE PREPARATION

This chapter describes the techniques involved in the precipitation of materials in gels, and the preparation of these materials for analysis.

3.1 PRECIPITATION BY A DIFFUSION MECHANISM IN SILICA GELS

Silica gels were the main precipitation medium used in this study. They were prepared in the following ways:

3.1.1 Preparation of Basic Silica Gels with an Ion Exchange Resin

(i) Sodium silicate solution (30% SiO_2, 12%Na_2O) supplied by BDH was diluted to 4% SiO_2 (w/v) with distilled water*. These solutions were stored in 250ml reagent bottles sealed with Nesco Film to prevent CO_2 uptake from the air.

* For gels prepared for the precipitation of materials other than carbonates de-gassed distilled water was used to dilute the sodium silicate solution. This was prepared by bubbling nitrogen gas through the water at about 90^{o}C for two hours.

(ii) The appropriate amount of solution, measured in a measuring cylinder, was transferred to a beaker and stirred with a magnetic stirrer.

(iii) The solution was then loaded with whatever materials were required in the final gel, eg reactants such as Na_2CO_3 in the precipitation of $BaCO_3$, NaCl as a source of background ionic strength and materials which can act as growth or habit modifiers.

(iv) The pH of the solution (approximately 11 to 12 depending on what materials were added at stage (iii)) was then reduced to the desired value for gelation by the addition of "Dowex" 50W-X8 (H), a cation exchange resin. The pH reduction was monitored with an EIL 7050 pH meter used in conjuction with a series of pH electrodes during the study and/or Johnson universal pH paper.

(v) When the desired pH was reached the electrode was removed, the stirrer stopped and the ion exchange resin was allowed to settle.

(vi) The solution was then transferred to the reaction vessel (see 3.4) and allowed to gel. In some cases this operation had to performed very quickly as gel setting time was as little as thirty seconds.

3.1.2 Preparation of Basic Silica Gels with 1M HCl

The procedure detailed in 3.1.1(a) was repeated with the following modifications:

In step (i) the sodium silicate solution was diluted to 6% SiO_2.

In step (iv) 1M HCl, instead of the cation exchange resin, was added dropwise from a burette to the stirred solution until the desired pH value was reached.

3.1.3 Preparation of Acidic Silica Gels with 1M HCl

The procedure detailed in 3.1.1(a) was repeated with the following modifications:
In step (i) the sodium silicate solution was diluted to 6% SiO_2.
In step (iv) instead of adding the cation exchange resin, the sodium silicate solution was added dropwise from a burette to a stirred 1M HCl solution until the desired pH was reached.

After gelling, a solution, or, more commonly, an agarose gel containing the other reactant at a higher concentration than the reactant in the silica gel, was placed in contact with the silica gel. Agarose gels were prepared in the following way:

3.1.4 Preparation of Agarose Gels

The gelling agent (Electran agarose "10" supplied by BDH) was added to distilled water, 1% w/v, in a beaker. The reactant, usually $BaCl_2$, was added at whatever strength was required. This was heated gently with magnetic stirring to about 90^{o}C until the solution was clear (a watch-glass was placed over the beaker to return condensate). This was then transferred to the reaction vessel, in contact with the silica gel and allowed to set. The vessel was then sealed or stored in conditions to prevent drying and cracking of the gel.

3.2 PRECIPITATION BY A DIFFUSION MECHANISM IN AGAROSE GELS

This was similar to precipitation in silica gels with the exception that two agarose gels were prepared in accordance with procedure 3.1.2. One was prepared loaded with one reactant at low concentration and any other materials if required. This was allowed to set and the other agarose gel containing the other reactant at higher concentration was placed in contact with it. The vessels were again sealed to prevent drying.

3.3 HOMOGENEOUS PRECIPITATION IN SILICA GELS

$BaCO_3$ was the only material precipitated homogeneously in this study. Unloaded silica gels were prepared and transferred to test tubes in accordance with procedures 3.1.1 and 3.1.3. $BaCl_2$ and urea solutions were placed in contact with the gels for one week. The solutions were then decanted, the tubes sealed and the gels heated at $90^{o}C$ for 14 hours.

3.4 REACTION VESSELS

Three types of vessel were used in this study:

(i) The 15cm test tube.

The gelling solution containing one reactant at low concentration was simply poured into the test tube to an

approximate depth of 10cm and allowed to gel. The second solution containing the second reactant at higher concentration was gently poured on top of it to an approximate depth of 2cm. The tube was then sealed with Nesco film.

Advantages: Quick and easy, little preparation needed.

Disadvantages: Curvature of glass and depth of gel made in-situ optical microscopy difficult.

(ii) The 76x26mm microscope slide.

The microscope slides were masked with teflon tape as illustrated in fig 3.4a(i). This was securely attached to the glass by pressing it firmly on and slightly stretching it with the index fingers while wearing latex gloves. This is a permanent mask which holds the liquid in place while it gels. The over-hanging areas of teflon can be tucked under as in the arrangement represented by fig 3.4a(ii). Two temporary strips of teflon were then attached as shown in fig 3.4a(iii). The gelling solution containing the reactant at low concentration was then transferred to area A with a syringe and allowed to gel. The approximate volume of gel in area A was 1ml. After gelling the strip of tape nearest area A was removed and an unloaded gelling solution was transferred to area B in fig 3.4a(iv) and allowed to gel (approximate volume 0.2ml). The purpose of this zone was to avoid irreproducible behaviour due to steep diffusion fronts. In the subsequent experiments of this study it was found unnecessary to have this zone. The final strip of tape

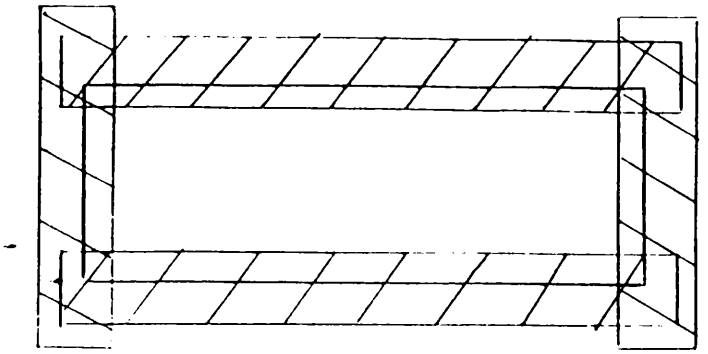

(i)

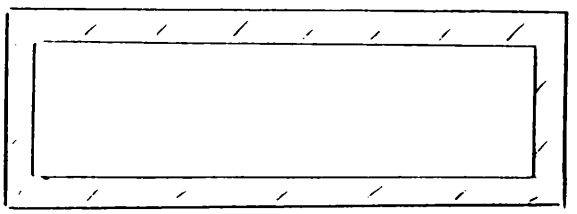

(ii)

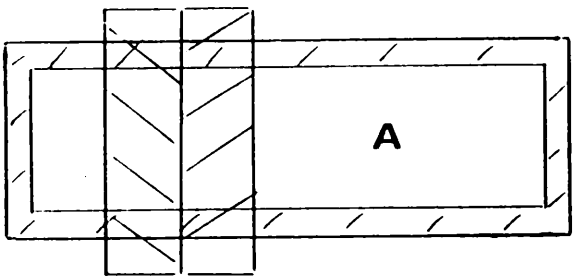

(iii)

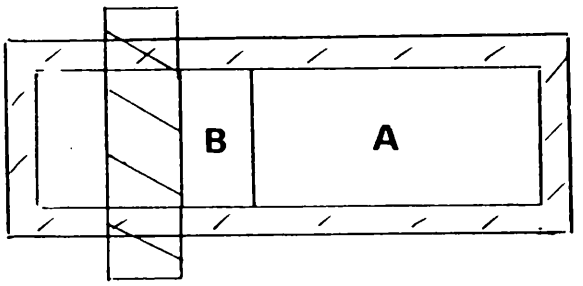

(iv)

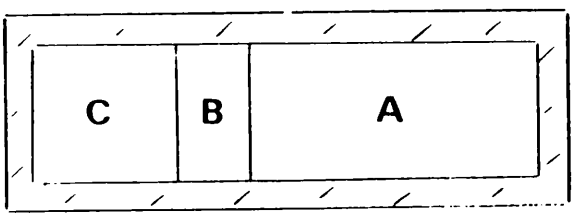

(v)

fig 3.4a (i - v)

Microscope slide Technique

was then removed and a gelling solution containing the other reactant at higher concentration was deposited on area C in fig 3.4a(v) (approximate volume 0.4ml). The slides were then transferred to a moisture chamber (a tank, filled to a few inches depth with water and lagged with filter paper to absorb the water, containing a shelf to hold the slides and a sliding glass lid) to avoid drying and cracking.

Advantages: A thin layer of gel, the absence of curved glass and the possibility of recording the coordinates of any point in the gel made this an excellent technique for in-situ optical microcopy and in particular time-lapse in-situ optical microscopy.

Disadvantages: Very tricky technique with some degree of failure and frustration common. Difficulty in keeping gels from drying out while examining under optical microscope.

(iii) The glass cassette

This was developed in collaboration with Garcia Ruiz and consisted of two sheets of glass (10x6.75cm) which sandwich a rubber mask (3mm depth) with an opening cut to allow solutions to be poured into it. This was held together with four bulldog clips. Gelling solutions were simply poured in and allowed to gel as described for the test tube technique. The cassette was then sealed with silicone sealant. Fig 3.4b is a photograph of a sealed cassette containing $BaCO_3$ precipitates in silica gel.

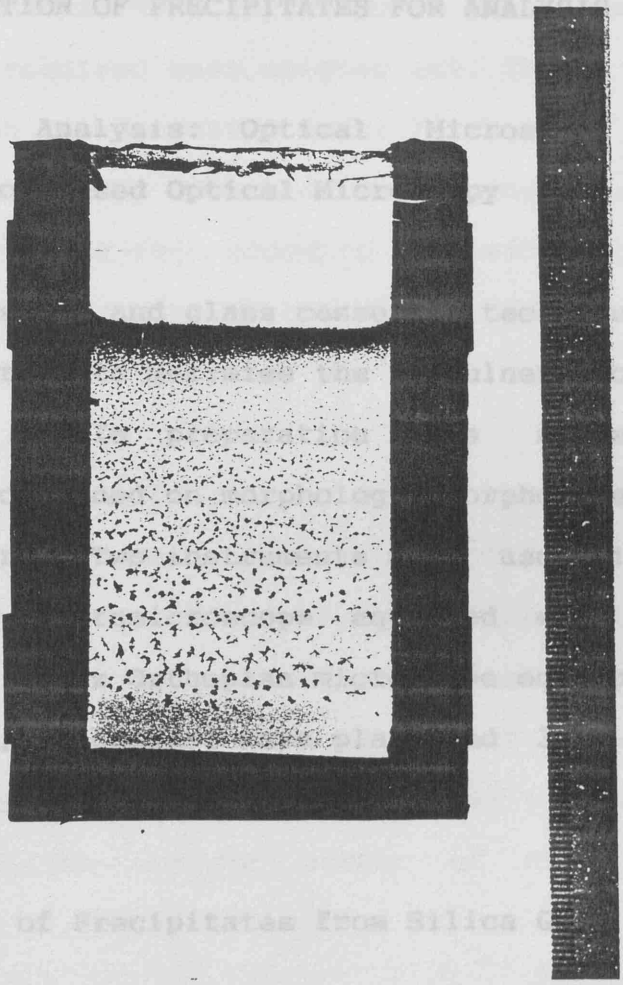

Glass cassette containing dendritic $BaCO_3$ precipitates in silica gel. Units in cm's

fig 3.4b

Advantages: This was the most extensively used vessel as it combines the advantages of both the test tube and the microscope slide with no obvious disadvantages.

3.5 PREPARATION OF PRECIPITATES FOR ANALYSIS

3.5.1 In-Situ Analysis: Optical Microscopy and Cross Polarised Optical Microscopy

The microscope slide and glass cassette technique were developed in order to maximise the usefulness of this analysis. No sample preparation was needed and information was obtained on morphology, morphogenesis and crystal structure. Two instruments were used in this study, a Zeiss photomicroscope equipped with cross-polarisers and a Leitz Orthoplan microscope equipped with cross-polarisers, a quarter wave plate and 35mm camera attachment.

3.5.2 Removal of Precipitates from Silica Gel

Most techniques of analysis used during this study require the removal of the precipitates from the gel. The following details this procedure:

(i) The area of gel containing the precipitates of interest was removed from the vessel and placed in a Petri dish containing approximately 1M NaOH* made with distilled water.

* For precipitates other than carbonates the extra precaution of trying to remove as much carbonate as possible from the NaOH solution was undertaken. The distilled water was de-gassed by bubbling oxygen free nitrogen through it at 90^{o}C for 2 hours. Twice the amount of NaOH pellets required were weighed out. These pellets were washed with the de-gassed water for a few seconds and the solution quickly decanted. The appropriate amount of de-gassed water was then added to the washed pellets. This procedure removed most of the Na_2CO_3 contaminants on the surface of the NaOH pellets.

(ii) From time to time the gel was gently manipulated to aid its dissolution. As soon as precipitated objects became free of the gel they were examined by light microscopy for adhering gel and if clean they were transferred from the NaOH with a fine paint brush, to a petri dish containing distilled water. This procedure was repeated until the desired number of objects was collected.

(iii) The precipitates were washed free of NaOH adhering by continuous dilution and solution removal with a syringe. This was monitored with pH paper and continued until the pH of the water containing the precipitates was equal to the pH of the water being added.

3.5.3 Removal of Precipitates from Agarose Gel

Agarose gels re-soften on heating and therefore the removal of precipitates avoids the use of NaOH. The following details the procedure:

(i) The section of gel containing the precipitates of interest was removed and placed in a Petri dish containing distilled water. This was then heated on a hot plate (80-90^{o}C) until the gel re-softened and dissolved in the water. This would generally take a few minutes but depended on the size of the section.

(ii) The precipitates were removed from the solution and transferred to another Petri dish containing distilled water.

(iii) The precipitates were washed by continuous dilution and solution removal.

When removed from the gel the precipitates were subject to further analysis:

3.5.4 Scanning Electron Microscopy (SEM)

Aluminium stubs, 1cm in diameter, were coated with conductive carbon paint (CCC Leit-C, 1216). As this dried the precipitates were dropped onto the stub with the use of a fine paint brush. As the paint dried the

precipitates became secured to the stub. The precipitates and stub were then made conductive by gold coating in a Polaron E5000 Sputter Coater under Argon at 0.08 Torr, 0.75kV and 25mA for 7 to 9 minutes depending on the coarseness of the precipitate texture. This gave an approximate coating thickness of 65 to 85nm according to the equation:

$$d = I \times V \times t \times k$$

where d is the coating thickness in nm.

I is the current in mA.

V is the voltage in kV.

t is the coating time in minutes.

k is a constant equal to 0.5 for Argon.

The precipitates could then be examined by SEM. The main instrument used was a Philips 500 but during studies at the University of North Texas a JEOL P300 was used. The latter was also equipped with energy dispersive spectroscopy (EDS). When this was used the precipitates were coated with carbon, instead of gold, in an Edwards High Vacuum coating unit. X-ray photoelectron spectroscopy (XPS) was also carried out at UNT.

3.5.5 Transmission Electron Microscopy (TEM)

$BaCO_3$ IMCA's were the only gel precipitated materials studied by TEM. Two sample preparations were used. An

acid wash preparation was used to determine membrane structure and a cross-section preparation was used to determine internal structure and membrane thickness.

(i) The Acid Wash Preparation: A planar aggregate was carefully placed on a 3mm carbon coated gold sample grid. A drop of dilute acetic acid was added and the carbonate part of the aggregate was seen to dissolve to leave behind the membrane. A drop of distilled water was then added to the grid and drawn away with a piece of filter paper. This was repeated several times until the membrane was free of soluble impurities. The grid was then allowed to dry and the membrane could then be examined by TEM.

(ii) The Cross-Section Preparation: Planar aggregates with braids were embedded in resin and cross sections of the planar parts and the braids in the range 650-1000nm thick were cut with a microtome using a diamond knife. The sections were placed on a 3mm copper sample grid and examined on either a Jeol 100C TEM, a Jeol 1200EX TEM or a Jeol 100C TEM equipped with EDS.

3.5.6 X-Ray Diffraction (XRD) and Fourier Transform Infra-Red Spectroscopy (FTIR)

Precipitates were ground in a mortar and pestle and dispersed in acetone on a glass slide for XRD analysis by Philips instruments using either Co K alpha 1, 2 radiation or Cu alpha 1, 2 radiation. Ground precipitates

were mixed with KBr and pressed into pellets for FTIR analysis.

4 TECHNIQUES OF ANALYSIS

4.1 LIGHT MICROSCOPY

4.1.1 History

4.1.2 Theory

4.1.2.1 The Two-Stage Image Formation of the Microscope

4.1.2.1a The First Stage of Magnification

4.1.2.1b The Second Stage of Magnification

4.1.2.2 Kohlers' Principle of Illumination

4.1.2.3 Image Formation According to the Principle of Wave Optics

4.1.2.4 Resolution According to the Theory of Wave Optics

4.1.2.5 Useful Magnification

4.2 CROSS-POLARIZED LIGHT MICROSCOPY

4.2.1 The Wave Nature of Light

4.2.2 Cross-Polarization

4.2.3 Investigations between Crossed Polarizers

4.2.3.1 Birefringence

4.3 INTRODUCTION TO ELECTRON MICROSCOPY

4.4 SCANNING ELECTRON MICROSCOPY (SEM)

4.4.1 History

4.4.2 The Principle of Scanning Electron Microscopy

4.4.3 Electron Beam and Specimen Interaction

4.4.3.1 Secondary Electrons

4.4.3.2 Backscattered Electrons

4.4.3.4 Characteristic X-Rays: Energy Dipersive Spectroscopy (EDS)

4.4.4 X-Ray Photoelectron Spectroscopy (XPS)

4.5 TRANSMISSION ELECTRON MICROSCOPY (TEM)

4.5.1 History

4.5.2 The Principle of Transmission Electron Microscopy

4.5.3 Electron Beam and Specimen Interaction

4.5.3.1 Elastic Scattering

4.5.3.2 Inelastic Scattering

4.5.3.3 Other Interactions

4.5.4 Electron Diffraction

4 TECHNIQUES OF ANALYSIS

This chapter considers the principles behind the techniques of analysis of precipitates and the instruments used in this analysis.

4.1 LIGHT MICROSCOPY

4.1.1 History

A short account of the history of light microscopy is given by Hayat (1978) in the introduction of his book on scanning electron microscopy.

In the late 13th century Roger Bacon referred to convex lenses as "an aid to old men and to those that have weak eyes". In the early 17th century Galileo or possibly Kepler devised and used the first compound microscope to examine insects. In 1673, Anthony von Leenwenhoek made a microscope with plano-convex and bi-convex lenses giving magnifications from x30 to x300. The first partially corrected lens was produced by Coddinton in 1837 and in 1870 an achromatic substage condenser was developed by Abbe, a type of condenser still in common use.

By the mid 20th century the microscope had reached its theoretical limits of resolution and only in the fields of design and utility has it improved since. Most post-war microscopes focus by means of an adjustable stage and

substage with a fixed body tube rather than the reverse. This assembly gives a smoother operation and a longer life. Automatic photomicroscopes which take good micrographs at the touch of a button have become standard. These developments have led to the microscope becoming a scientific tool that is as versatile as it is indispensable.

4.1.2 Theory

An account of the principles of light microscopy is given by Determann and Lepusch (1974).

4.1.2.1 The Two-Stage Image Formation of the Microscope

Light microscopes are generally very small and the involved optical paths are found almost exclusively in the interior of the instrument. As an aid to the understanding of image formation comparisons are drawn to a slide projector, an instrument with a very much larger involved optical path and to a large extent, external to the instrument.

4.1.2.1a The First Stage of Magnification

In a slide projector when any point on a slide is illuminated by a projector lamp a cone of rays will originate from it. These rays are deflected by a lens so that they combine at an image point at a certain distance

from the projector. If a screen is placed at this point it can be seen that the image is both inverted and magnified. This process corresponds to the first stage of magnification in a microscope and the comparison is illustrated in fig 4.1.2.1a.

4.1.2.1b The Second Stage of Magnification

The second stage of magnification is achieved by the microscope eye-piece. This contains an eye-piece lens and a field lens. The field lens is usually situated below the intermediate image and acts to deflect the rays diverging from the objective lens towards the eye-piece lens where they are magnified and made acceptable to the eye.

4.1.2.2 Kohlers' Principle of Illumination

Illumination is essential for good light microscopy. The light for illumination is collected with a condenser system situated betwwen light source and slide. According to Kohlers' principle of illumination the condenser system is so placed as to form an image of the filament of the light source in the rear focal plane of the objective. As a consequence of this the light source is fully utilized as each point of the light source illuminates the entire object field on its own. These conditions must be met in the microscope for a number of objective/eye-piece combinations and object fields of

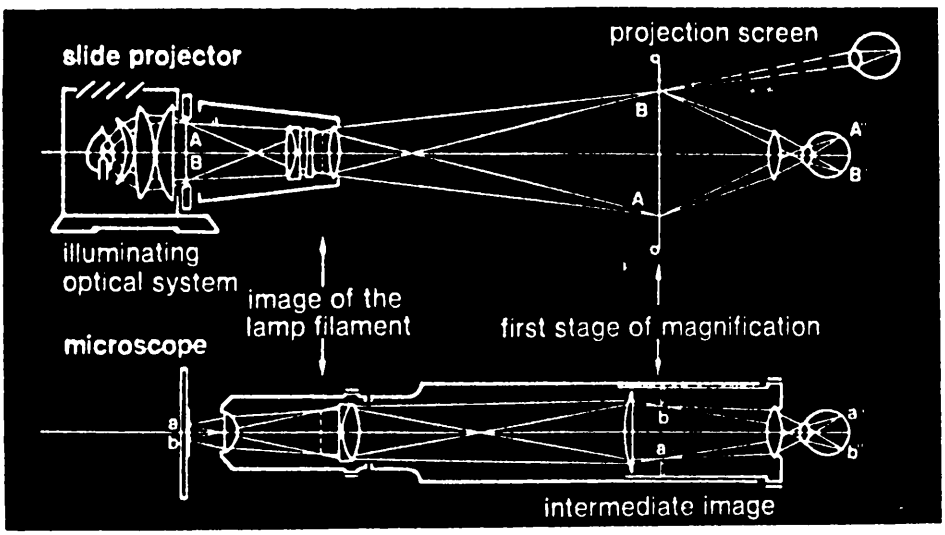

Comparison of the optical paths in a slide projector and in a microscope

fig 4.1.2.1a (from Determan, 1974)

different dimensions. The illumination system must therefore permit the variation of the cross section of the ray bundle both in the rear focal plane of the objective and in the object itself, by means of diaphragms.

Figs 4.1.2.2a and b illustrate the illumination optical path and the image forming optical path. For convenience they are drawn separately but together they are considered "the involved optical path".

Considering fig 4.1.2.2a (the illumination optical path) first, directly in front of the light source S is the lamp condenser which when combined with the light source forms the illuminator. The lamp condenser forms an image of the filament, S', of the substage condenser. The aperture diaphragm is also situated in this plane. Another image of the filament is formed by the sub-stage condenser and objective in the rear focal plane, S'', of the objective and finally the image is reproduced in the pupil of an observer's eye, S''', looking through the eye-piece. The planes S, S', S''and S''' are optically conjugated since each is the optical image of the proceeding one.

A second system of optically conjugated planes is found in the image forming optical path, fig 4.1.2.2b. The field diaphragm, L, limits the aperture of the lamp condenser. An image, L', is formed in the diaphragm in

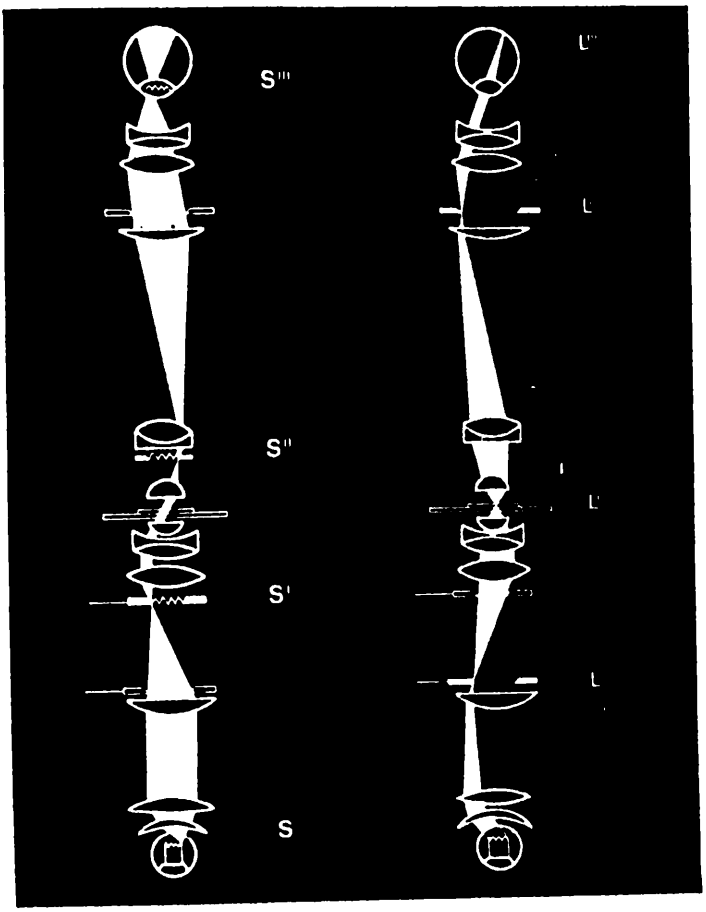

(a) (b)

The involved optical path; a) the illumination optical path and b) the image forming optical path.

fig 4.1.2.2a & b (from Determan, 1974)

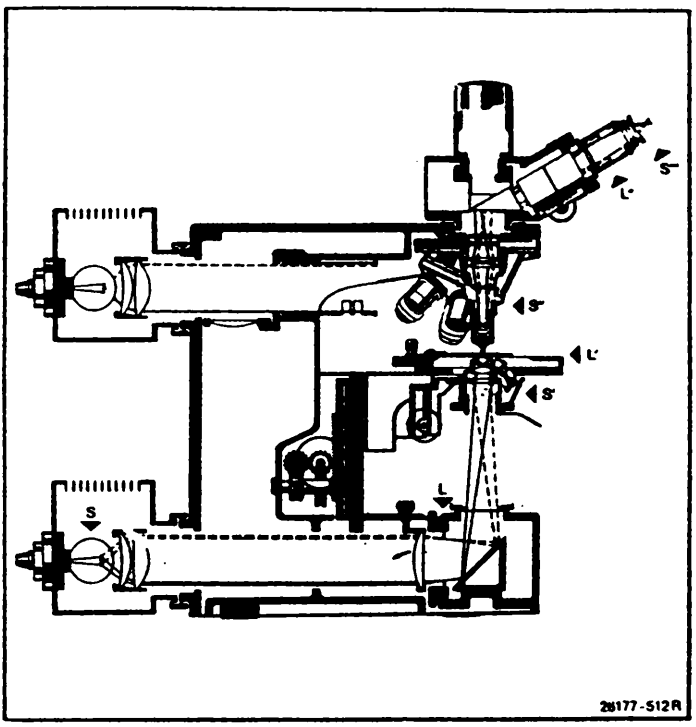

Optical path in the ORTHOPLAN microscope.
This illustration shows the involved optical path (illumination and image-forming beams) in the ORTHOPLAN microscope. The optical planes and their positions in the microscope are clearly seen here.

S = lamp filament
L = field diaphragm
S' image of the lamp filament in the plane of the aperture diaphragm
L' image of the field diaphragm in the object plane
S'' second image of the filament in the exit pupil of the objective
L'' second image of the field diaphragm in the field-of-view plane of the eyepiece
S''' third image of the filament in the exit pupil of the eyepiece
The third image of the field diaphragm is produced together with the microscopic image on the retina of the eye.

fig 4.1.2.2c (from Determan, 1974)

the object plane by the sub-stage condenser. A magnified image of the object and of the field diaphragm, L'', is then formed in the intermediate image plane by the objective. This is once again magnified when viewed through the eye-piece. The third image of the object and field diaphragm are produced on the retina of the eye. Therefore, there are two groups of optically conjugated planes which succeed each other alternately to form an involved optical path.

As mentioned earlier the cross section of the ray bundle must be variable. This is achieved through the aperture diaphragm and the field diaphragm. The aperture diaphragm permits the formation of the image of the filament. It thus produces the required ray bundle cross section in the microscope. The field diaphragm alters the cross section of the ray bundle in the object plane.

Fig 4.1.2.2c shows the progress of the optical path in a Leitz Orthoplan microscope, as used in this study.

4.1.2.3 Image Formation According to the Principle of Wave Optics

Up to now only geometrical laws have been considered in determining the optical path in a microscope. Now the wave nature of light is considered. When parallel light passes through an aperture it is diffracted. This can be clearly demonstrated in a light microscope by focussing

on a fine grating, reducing the aperture diaphragm to its smallest size, removing the eye-piece and observing the rear focal plane of the objective. In this plane can be seen the image of the aperture diaphragm which appears bright in the centre. To either side of this are partially overlapping secondary images with coloured fringes. When the grating is removed the secondary images disappear whereas the central image remains. The central image is therefore produced by geometrical laws and the secondary images are the result of the diffraction of light in the grating. The intensity and position of the diffracted images is due to interference.

Since objects examined under the microscope are likely to contain fine structures which could act as a microscope grating, diffracted images are important in the final image formation.

Fig 4.1.2.3a illustrates image formation with regard to diffraction. The lines indicate the direction of propagation of individual waves. Parallel light is incident on a grating. Waves which pass through in phase form the 0 order maximum (the image of the aperture diaphragm formed by geometrical laws) in the focal plane of the objective. Waves which arrive at this focal plane at phase differences of 1, 2, etc wavelengths, form the secondary images, the 1st, 2nd, etc order maxima. The secondary images occur through constructive interference of the out of phase waves. The dark areas separating

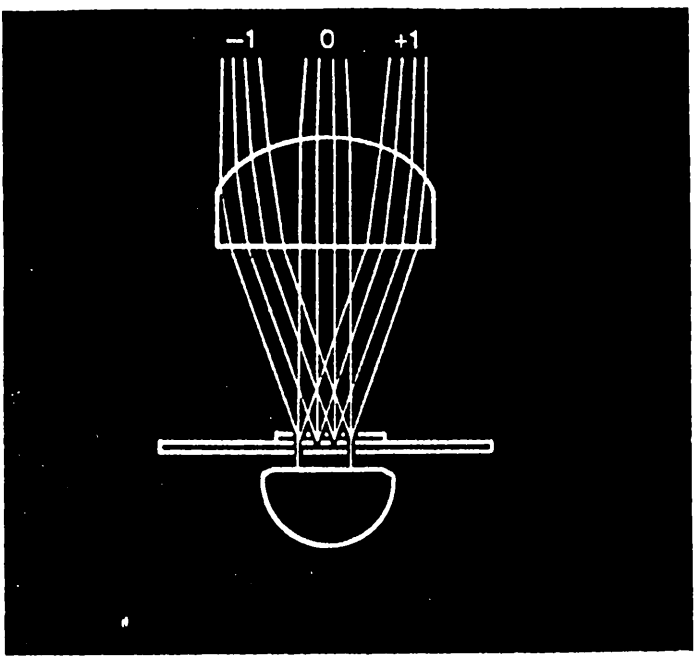

Parallel light incident on a grating produces ray bundles of the 1st, 2nd, ...nth order by diffraction. Together with the 0 order light they form the microscope image.

fig 4.1.2.3a (from Determan, 1974)

these images arise through destructive interference. Finally, new waves originate from the interference maxima which interfere with the magnified image of the object (in this case a grating) in the intermediate image plane.

4.1.2.4 Resolution According to the Theory of Wave Optics

The resolving power of an objective can be directly established by considering the wave optical approach. Resolving power is defined as the ability of an objective to make two closely spaced points appear as separate entities. Fig 4.1.2.4a shows parallel light waves incident on a grating and the resulting image on the rear focal plane of the objective. The distance d is the separation between slits in the grating. Waves at the points A and B are in phase since the incident light is parallel. Waves at the points C and B are in phase since the distance between A and C is one wavelength. The angle between AB and BC is represented as α. Thus for a first order diffracted bundle:

$$\sin\alpha = \frac{\lambda}{d}$$

For the resolution of a grating, the objective must at least accept the diffracted 1st order bundle, so that an image can be produced through interference in the intermediate image plane. This depends on the aperture, A, of the objective lens, defined as:

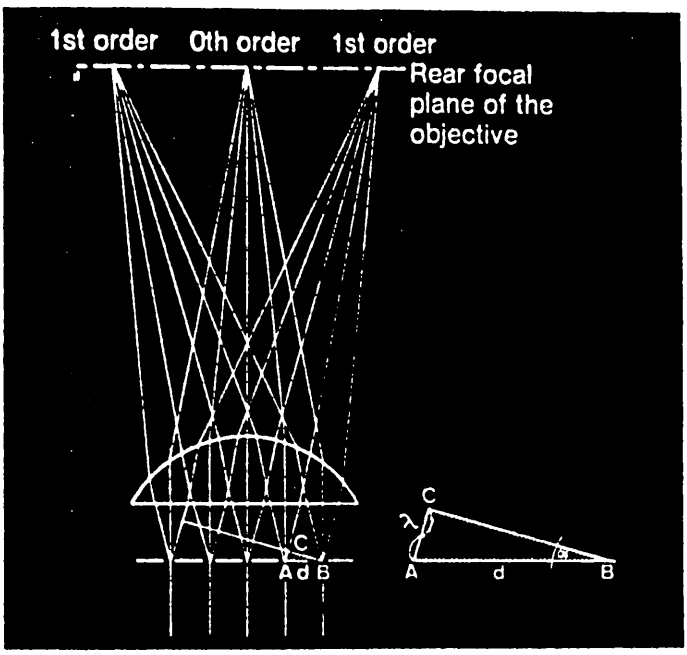

Parallel light incident upon a 5 grating slit. Part is propagated in the same direction and is collected at the focal point of the objective. The first order diffracted bundles are also shown. They are focussed on the rear focal point of the objective. The direction of the diffracted bundles is determined by the triangle ABC.

fig 4.1.2.4a (from Determan, 1974)

$$A = \sin\alpha$$

Here, α is the largest angle a ray can form with the optical axis, to be just accepted by the objective. Hence an objective resolves a grating with slit separation, d, if its aperture A (= $\sin\alpha$) is at least λ/d:

$$A = \lambda/d$$

This is a good approximation for vertical illumination. However vertical illumination is never used and furthermore the field aperture (condenser) is usually smaller than the objective aperture. Here resolution is given by:

$$d = \frac{\lambda}{A_{obj} + A_{cond}}$$

This formula is also a good approximation but is based on perfectly corrected objectives. Abberations will adversly affect resolving power.

The objective aperture also influences image brightness. Changes in image brightness vary with the square of the aperture. Reducing brightness increases depth of field, but at the same time the diffraction fringes will surround all image details reducing the resolving power.

4.1.2.5 Useful Magnification

In order to resolve an object's structure, it is not enough to use an objective of suitable numerical aperture. The image of the object's structure must be offered to the eye at a sufficiently large angle. The minimum size of this angle must be larger than the resolving power of the eye. The human eye can resolve 0.15mm at 25cm distance corresponding to an angle of $2'$. This is a physiological parameter.

Relating the limit of resolution of the eye to the wave-optically derived resolving power of an objective, we have:

$$M \cdot d = R_d$$

where; M is the magnification,

d is the distance between two points in the object ($= \lambda/2A$), at the limit of the resolving power of the objective,

R_d is the magnified resolved distance between the points.

Then:

$$M \cdot \frac{\lambda}{2A} = 0.15\text{mm}$$

For $\lambda = 550\text{nm}$, it follows, $M \approx 500A$

This approximation holds for medium contrast. For high contrast magnification of objects, it can be increased up to 1000A. The range between 500A and 1000A is known as useful magnification. Below 500A the images are brilliant and difficult for the human eye to resolve. Above 1000A the images will not appear sharp.

Greater resolution is possible in Photomicrography than for visual observation since the limiting factors are very different. For visual observation resolution is limited by the human eye whereas in photomicrography the limit of resolution is determined by the silver halide grains of the photographic emulsion. These grains have a certain size depending on the speed of the film. For a medium sized film they are about 2μm. The grains are blackened on contact with light. Including the circle of dispersion, they can resolve to 1/60mm giving a useful magnification (by analogous treatment) of 60A.

4.2 CROSS-POLARIZED LIGHT MICROSCOPY

An account of cross-polarized light microscopy is given by Patzelt (1974).

4.2.1 The Wave Nature of Light

Light is an electro-magnetic vibration. A model which aids the understanding of the phenomenon of light is the transverse vibrations of a rope fixed at one end. If

movement is imparted to the rope at the loose end a wave will progress along the length of the rope. The wave nature of each vibration can be described in terms of wavelength, λ, frequency, f, propagation direction, vibration direction, velocity of propagation and intensity, (fig 4.2.1a).

Visible light is made up of many waves, with wavelengths in the range 400 to 750nm, vibrating in all directions. The frequency of these waves is of the order 10^{-15} Hz. The frequency of an electromagnetic wave is constant, even when it enters matter, but its velocity and wavelength may vary.

4.2.2 Cross-Polarization

Light which contains only rays of the same vibration direction is called linearly polarized light. Without aid, the human eye is not able to distinguish between polarized and natural light.

The light microscopes used in this study were equiped with polarizers or Nicols (after the inventor). These are the collective names for a polarizer and an analyser. The polarizer is situated in front of the object plane and combined with the condenser. The analyser is situated behind the object plane. Fig. 4.2.2a illustrates this. The polarizers have the following effect:

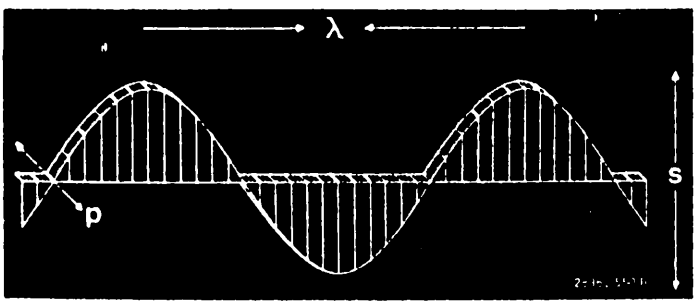

Wavelength, λ , vibration direction, s, and polarizing direction, p, of a transverse wave.

fig 4.2.1a (from Patzelt, 1974)

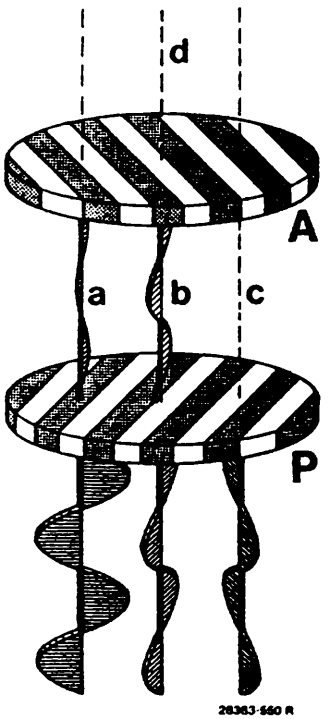

Crossed polarizers
P = Polarizer
A = Analyser

fig 4.2.2a (from Patzelt, 1974)

(i) Rays which are already travelling in the vibration direction of the polarizer are transmitted with a slight loss in intensity, (wave B).
(ii) Rays which vibrate vertically to the transmission direction are completely supressed, (C)
(iii) Waves which vibrate obliquely to the transmission direction are divided into a transmitted and an eliminated component, (wave A).
(iv) Crossed polarizers block the passage of light completely (D).

4.2.3 Investigations between Crossed-Polarizers

Precipitates analysed under crossed polarizers can immediately be categorised as either isotropic or anisotropic. Amorphous precipitates and crystals with simple cubic lattice system have the same properties in all directions and are therefore isotropic. These materials show no effect under crossed polarizers. Crystals or aggregates of crystals with a lattice system other than the cubic one are anisotropic. They have different properties in different directions. These materials exhibit the phenomenon of birefringence under crossed polarizers.

4.2.3.1 Birefringence

If an object is observed through a piece of calcite of several millimetres thickness it appears duplicated. When

the piece of calcite is rotated, one image remains stationary, whereas the second, equally bright image rotates around the stationary image in a circular orbit.

In this phenomenon, known as birefringence, each light ray is split into two part-rays. One ray passes through the object in a straight line whereas the other ray is latterly displaced. A phase difference exists between the two rays which have different refractive indices. The two rays produced also differ in their polarization direction. They vibrate perpendicular to each other. The two polarization directions can be demonstrated by observation of the double image produced when viewing an object through a piece of calcite with a polarizer. When either the calcite or the polarizer is rotated the "ordinary" and the "extraordinary" image disappear alternately after a rotation of 45^{o}.

The classical phenomenon of image duplication can practically never be observed during the microscopic examination of anisotropic structures. Instead, anisotropic materials can be recognised by another phenomenon.

When an anisotropic object is rotated between crossed polarizers, the intensity of the object's image changes periodically as illustrated in fig 4.3.2.1a. Every 90^{o} the object practically completely disappears. Between the 90^{o} rotations the object becomes light with maximum

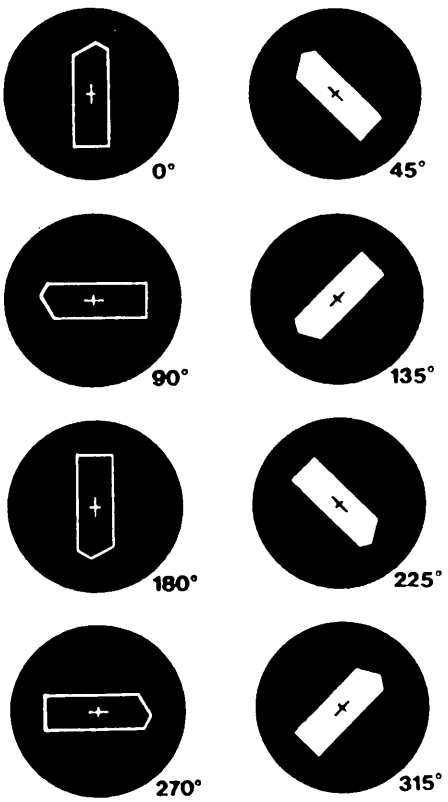

The diagonal and extinction positions of a birefringent object

fig 4.3.2.1a (from Patzelt, 1974)

intensity at 45^{o}. Interference colours can be observed in the light positions also. The four dark positions are called extinction positions and the four maximum intensity positions are called the diagonal positions.

4.3 INTRODUCTION TO ELECTRON MICROSCOPY

As discussed earlier the theoretical resolution of a light microcope is limited to around 200nm due to the wavelength of visible light. It was not until the hypothesis of wave particle duality (de Broglie, 1924) and its experimental confirmation (Davison and Germer, 1927; Thomson and Reid, 1927) that a practical method of overcoming this limit became evident. The theory predicted that an accelerated electron had a smaller wavelength than that of light and therefore a microscope employing accelerated electrons as the illuminating source would have a greater resolution than that of a light microscope.

From these predictions, two types of microscope were developed: (i) the transmission electron microscope (TEM) and (ii) the scanning electron microscope (SEM).

4.4 SCANNING ELECTRON MICROSCOPY (SEM)

The scanning electron microscope can produce a seemingly three dimensional picture of the surface of an object over a wide range of magnifications. The addition of

accessories makes it possible to determine the elemental composition of the object. An account of the history and principles of SEM is given by Hayat (1978).

4.4.1 History

In 1935 Max Knoll suggested that an electron microscope using a fine scanning beam of electrons on a specimen surface and recording the emitted current as a function of the position of the beam could be developed. Three years later Von Ardenne constructed the first SEM. In this instrument the primary beam passed through the object and exposed photographic paper behind it. It was Von Ardenne that suggested secondary electrons could be collected from the tops of opaque surfaces, amplified and used to modulate the grid of a cathode ray tube (CRT).

In 1942 Zworykin et al developed an improved version of the SEM which could examine the surfaces of opaque objects. In 1946 Brachet predicted that if a secondary electron current leaving an object could be amplified without introducing additional noise, a resolution of 10nm could be achieved.

In 1948 an intensive research project was initiated by Oatley at the University of Cambridge which led to the first commercial SEM in 1965. Since then continual improvements have been made with SEM's resolving to approximately 10nm becoming standard.

4.4.2 The Principle of Scanning Electron Microscopy

Fig 4.4.2a is a block diagram of a SEM. This illustrates the principle behind the technique. A narrow beam of electrons is produced by an electron gun at one end of the vacuum column. It is then focussed on as small a spot as possible on the surface of the object placed at the far end of the column. Along its path, the electron beam passes through several electomagnetic lenses and deflector coils. These focus the beam and make it scan. The lenses produce a small (10nm or less) electron beam which repeatedly scans and forms a raster which is viewed on a television set.

While scanning the electron beam knocks electrons out of the atoms which make up the specimen surface. These secondary electrons are collected and transferred to an amplifier. The current is then converted to a voltage signal which modulates the brightness of the spot on the CRT in synchronism with the movements of the electron beam.

The secondary electrons that emerge from each point on the specimen surface are characteristic of the surface at that point. Any changes in composition, texture or topography at the point at which electrons strike the surface will effect the current reaching the collector and in turn the brightness of the CRT spot. The image observed is a display of the received signals, built up

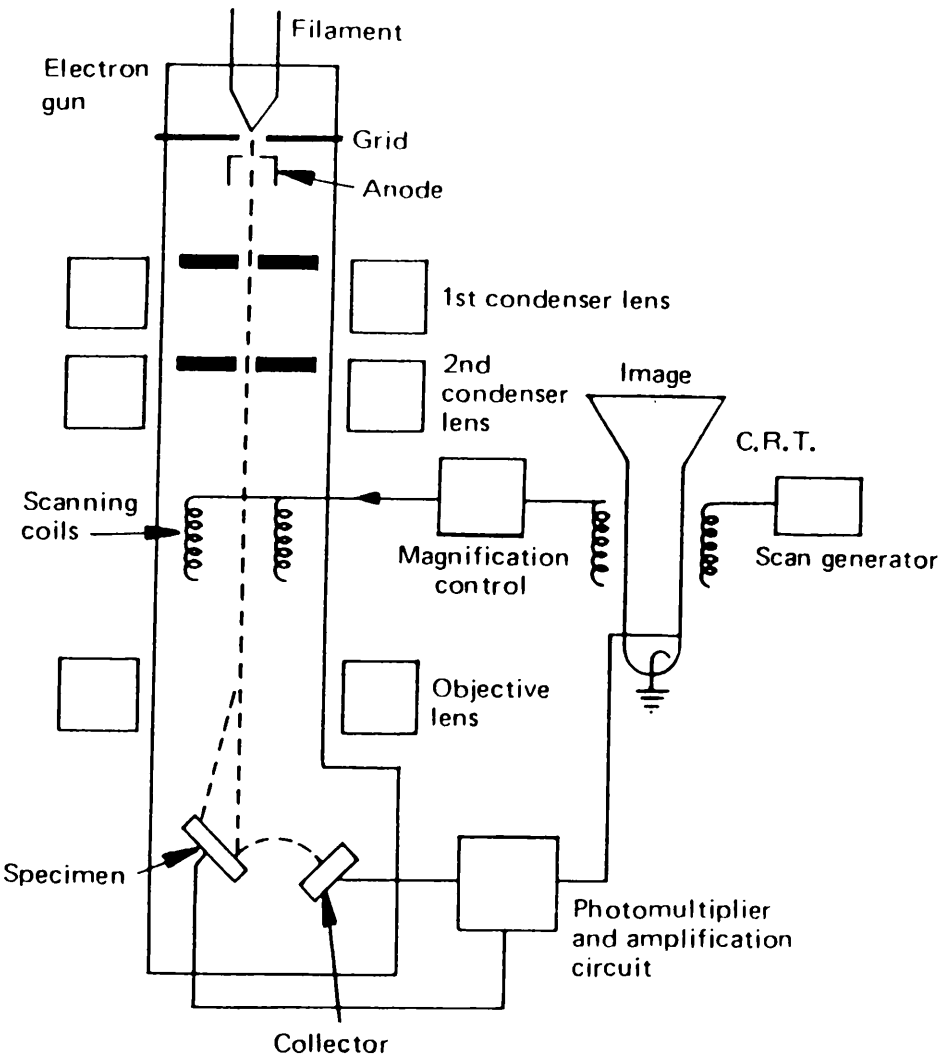

Block diagram of a scanning electron microscope.

fig 4.4.2a

point by point, to form an image of the specimens surface.

4.4.3 Electron Beam and Specimen Interaction

A primary electron beam can penetrate a specimen up to a depth of 10μm. The resultant interactions with the atoms of the specimen give rise to several different types of radiation, which include: (i) secondary electrons, (ii) backscattered electrons, (iii) Auger electrons and (iv) characteristic X-rays. Fig. 4.4.3a illustrates the origin of these electrons. The following is a brief discussion on each of these radiations and their use in SEM.

4.4.3.1 Secondary Electrons

Secondary electrons are the electrons emitted from the surface of the sample through the inelastic scattering of primary electrons with the electrons of the atoms in the target area of the specimen. The interaction is dependent on the average atomic number of the specimen:

$$\sigma_{in} \alpha Z^{1/3}$$

where: σ_{in} is inelastic scattering,

Z is average atomic number.

Only some of the secondary electrons produced reach the surface and are emitted. Others are scattered in all

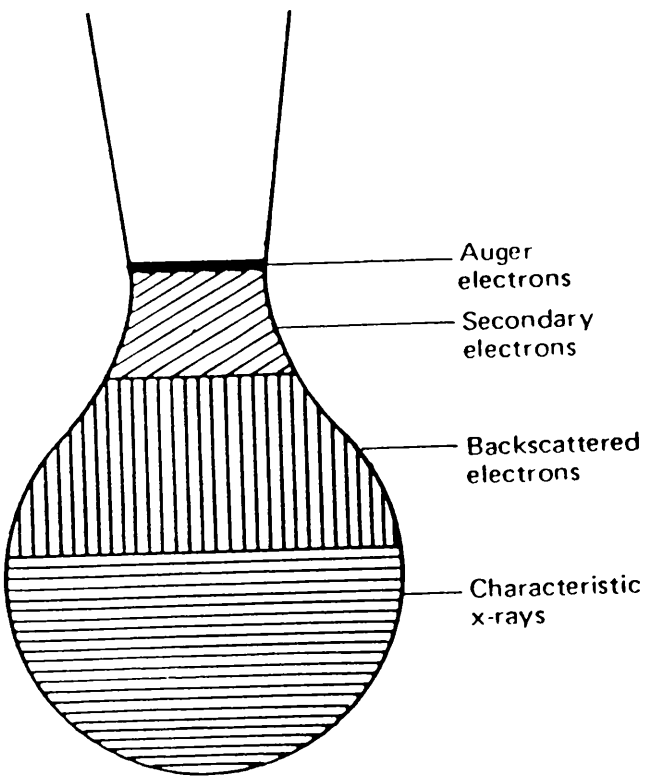

Schematic showing a pear-shaped excited volume in a bulk sample exposed to a primary electron beam. Various signals generated are indicated.

fig 4.4.3a (from Hayat, 1978)

directions. Some secondary electrons can also be produced by backscattered electrons.

Secondary electrons are of low energy, less than 50ev by convention and approximately 75% have energies less than 15ev. They are normally emitted from the top 5-10nm zone of the specimen. Secondary electrons are collected by means of a detector, which is sensitive to the energies mentioned. These electrons are capable of providing high resolution images of the specimen surface, because they are derived from a specimen area only marginally larger than the diameter of the electron probe. These are the electrons used in the normal imaging mode of a SEM.

4.4.3.2 Backscattered Electrons

Backscattered electrons arise through the interaction of the primary electron beam and the nuclei of atoms in the target area of the specimen. Many of these interactions take place and a portion of the scattered electrons are emitted from the surface. They can escape from depths up to several micrometers and have energies almost comparable with the beam energy since little energy is lost through electron-nucleus interactions (Rutherford scattering). By convention electrons leaving the surface with energies greater than 50ev are considered backscattered.

The intensity of a backscattered signal significantly influences image contrast. The intensity, in turn, depends upon the square of the atomic numbers of the atoms in the specimen and on the incident angle of the primary beam on the specimen. Differences in atomic number of the specimen give rise to appreciable contrast in the image.

The use of backscattered electrons in SEM gives rise to an image where areas of different chemical composition can be clearly distinguished.

4.4.3.3 Auger Electrons

Auger electrons are generated by electronic transitions in an atom, which occur following excitation of bound electrons. A primary electron, striking an atom in the target area, can eject a core electron from the atom. An electron from a higher level will fill the vacancy created and the atom will either emit an X-ray photon or, if a forbidden transition is involved, eject an Auger electron. The energy of the ejected Auger electron is nearly equal to the energy difference between the two electron shell levels; hence, Auger electrons are characteristic of the atom they are emitted from. Auger electrons are generally emitted from the top 1nm of the specimen.

Auger electrons are used in SEM to generate a spectrum which reveals atomic composition in the top 1nm of a target area surface.

4.4.3.4 Characteristic X-Rays : Energy Dispersive Spectroscopy (EDS)

When a primary beam of sufficient energy strikes a solid specimen, two types of interactions produce X-rays: (i) inner shell ionisation which yields characteristic X-rays and (ii) core scattering which results in continuous radiation.

Characteristic X-rays result from the interaction of the primary electron beam with the core electrons of the atoms in the target area of the specimen. If the incident electron has sufficient energy it can ionise an atom by ejecting a core electron. The atom will return to its ground state by the transition of an electron from an high energy outer L shell to the vacancy in the low energy inner K shell. This relaxation process is accompanied by a loss of energy through the emmission of a photon.

X-ray photons are usually emitted from the top 1μm of the specimens surface and have a discrete energy equal to the difference in energies between the two levels. The wavelengths of characteristic X-rays are specific to the atom from which they are emitted (wavelength decreases

with atomic number).

When electrons of sufficient energy interact with atoms, continuous radiation is emitted in addition to characteristic X-rays. The radiation arises through electron decelerating during collisions with atoms. This decelerating effect is greater for heavier atoms which have denser electron clouds.

Characteristic X-rays are utilised in SEM in the form of energy dispersive X-ray analysis (EDS), a method of obtaining a spectrum which identifies the chemical composition of the top 1μm of the target area of the specimen. Continuous radiation is a major source of unavoidable noise in EDS and is therefore a primary factor limiting its sensitivity.

4.4.4 X-Ray Photoelectron Spectroscopy (XPS)

This technique is closely associated with the surface analysis techniques previously descibed. XPS is the application of the photoelectric effect as induced by X-rays of a fixed energy interacting with a specimen. On irradiation the specimen emits photoelectrons from discrete atomic electron energy levels. By measuring the binding energy of emitted photoelectrons identification of the elements present in the specimen is possible.

4.5 TRANSMISSION ELECTRON MICROSCOPY (TEM)

The transmission electron microscope can produce structural information of thin samples over a wide range of magnifications. Resolution is much greater than in SEM and can be less than 0.1nm for lattice resolution (Fryer, 1983) and for suitable specimens atomic resolution can be achieved. The TEM can also be used in the electron diffraction mode and energy dispersive spectroscopy accessories may be added, both of which can provide additional structural information.

4.5.1 History

The first electron microscope built was a TEM. This was achieved by Knoll and Ruska in 1931 and two years later a high resolution instrument was built capable of resolving 0.05μm. Since then the development of the TEM has been well documented (Ruska, 1980; Cosslett, 1981a & 1981b) In recognition of the importance of electron microscopy in many fields of science Ruska gained the Nobel prize for physics in 1986.

4.5.2 The Principle of Transmission Electron Microscopy

The principles of TEM are similar to those of light microscopy. In both the illuminating agent is focussed on the sample, interacts with it and passes through. The wave exciting from the sample is then magnified to give

an image which can be studied.

In the TEM magnetic or electrostatic lenses alter the path of an electron in the same way glass lenses alter the path of light in a light microscope. As the electron beam is not visible, it is projected onto a fluorescent screen for examination. Since electrons have a low penetrating power and can only travel significant distances in vacuum, it is necessary to have thin samples and the column of the microscope must be kept under a vacuum of 10^{-3} Pa or less.

The main features of a TEM are illustrated schematically in fig. 4.5.2a and the optical path in transmission mode is depicted in fig. 4.5.2b. A fine beam of electrons is produced by the electron gun (either a hairpin filament, a tungsten filament or a lanthanum hexaboride cathode). The beam is then accelerated by the potential difference between the filament and the anode plate kept at earth potential. It is then focused onto the sample by the condenser lens system. After the beam emerges from the specimen the image is magnified and projected onto a fluorescent screen by a system comprising objective, intermediate and projector lenses. The excitation of the intermediate lens determines magnification, the brightness is controlled by the excitation of the condenser lens and the focus is controlled by the objective lens.

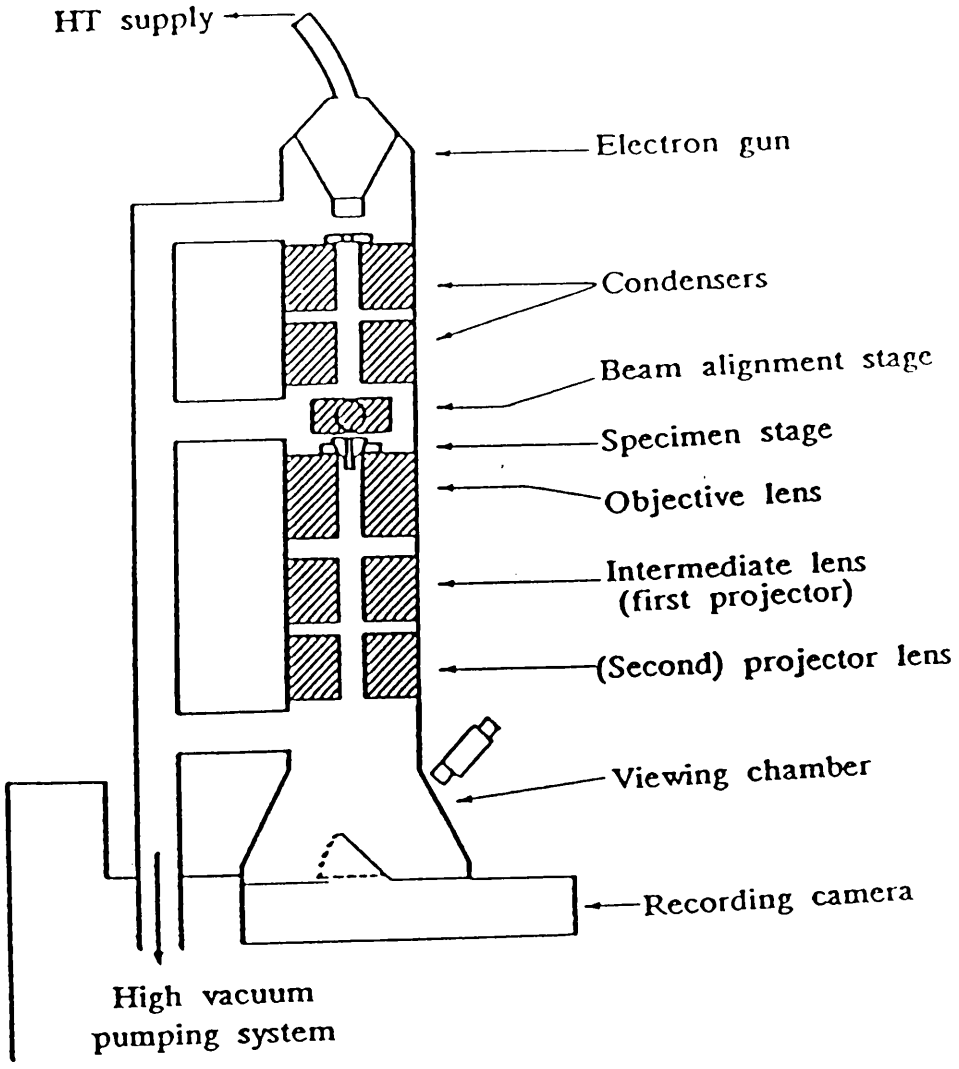

Schematic diagram of a transmission electron microscope.

fig 4.5.2a

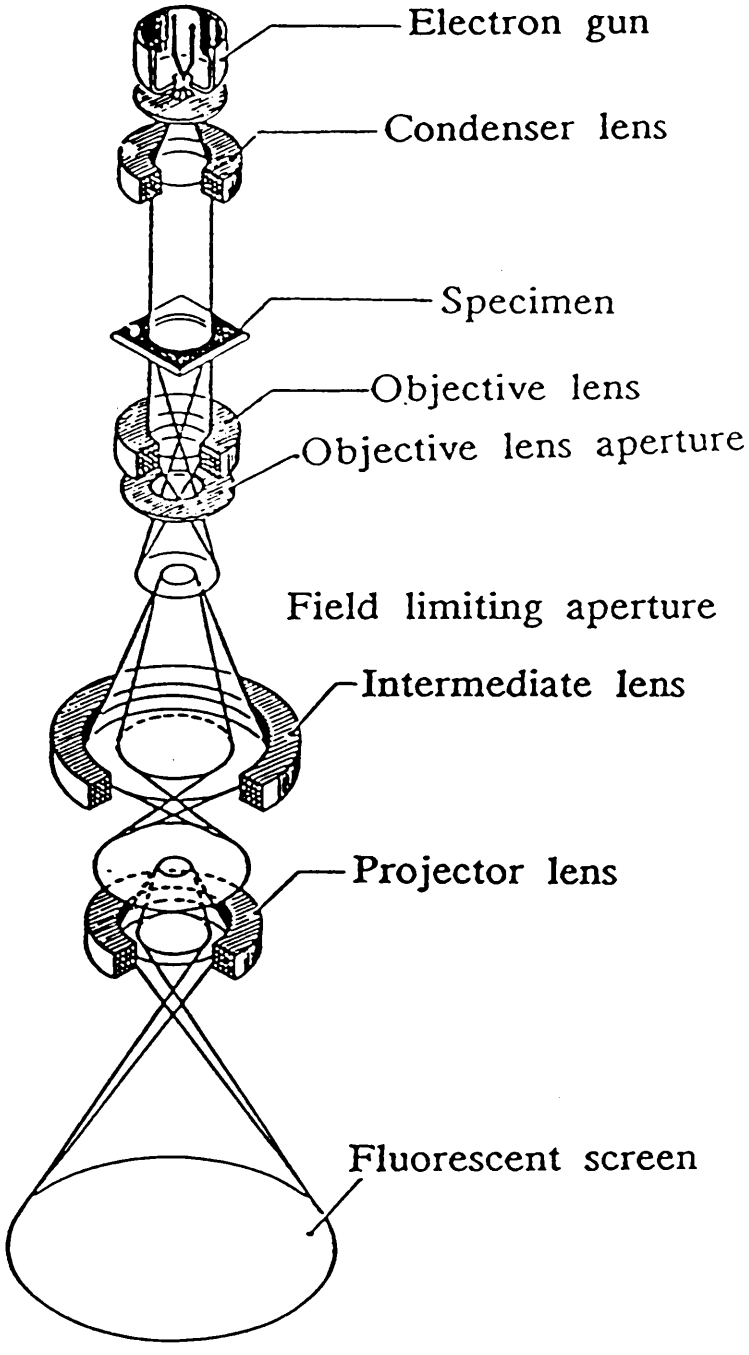

ELECTRON MICROSCOPE IMAGE

Operation of the TEM in the transmission mode.

fig 4.5.2b

The performance of a TEM depends on the quality of the objective lens as it detects, transmits and magnifies the modified electron beam. Light microscopes employ a series of converging and diverging lenses to compensate for individual lens defects. However, electromagnetic and electrostatic lenses are always converging and as such lens defects cannot be compensated for in the same manner as in light microscopes.

The information which can be recovered from TEM is contained in the electrons scattered during the passage through the sample. The information is in the form of perturbations of electron waves. Electron optical defects can cause similar perturbations. However, if these are suppresed to a lower level than the specimen perturbations then meaningful information will be obtained, although lens aberations can make interpretation difficult.

4.5.3 Electron Beam and Specimen Interaction

Image formation, in the transmission mode, arises through the recombination of scattered and undeviated electron waves, or by physical exclusion of scattered electrons after passage through the sample. Electrons which interact with the specimen can either be elastically scattered or inelastically scattered.

4.5.3.1 Elastic Scattering

Elastic scattering occurs when a primary electron interacts with the nucleus of a atom in the specimen and is deflected without loss of energy. For crystalline samples, the scattering angles are related to the crystal lattice geometry and the electron wavelength, by the Bragg law.

4.5.3.2 Inelastic Scattering

Inelastic scattering occurs when a primary electron interacts with the orbital electrons of an atom of the specimen and is deflected with a loss of energy.

Both elastically and inelastically scattered electrons contribute to the image observed in a TEM. Inelastically scattered electrons are of particular importance in high resolution TEM.

4.5.3.3 Other Interactions

All the beam specimen interactions previously described for SEM will occur in TEM as well. These interactions will not be involved in any image information processes but characteristic X-ray energies can be detected and measured to provide information on elemental composition, (energy dispersive spectroscopy, EDS).

4.5.4 Electron Diffraction

Specimens with crystal planes parallel to the electron beam diffract electrons in accordance with the Bragg Law. The resulting diffraction pattern can be focussed onto the image plane and subsequent analysis can reveal structural detail such as lattice spacings and misorientations.

RESULTS.

5 $BaCO_3$ PRECIPITATED BY A DIFFUSION MECHANISM IN SILICA GEL ON GLASS MICROSCOPE SLIDES AND BY HOMOGENEOUS METHODS

5.1 $BaCO_3$ PRECIPITATED BY A DIFFUSION MECHANISM IN SILICA GEL ON GLASS MICROSCOPE SLIDES

5.1.1 EXPERIMENTAL

5.1.2 RESULTS

5.1.2.1 Light Microscopy

5.1.2.2 Acid-Dissolution L.M Experiment

5.1.2.3 Routine Chemical Analysis

5.1.3 DISCUSSION

5.2 HOMOGENEOUS PRECIPITATION OF $BACO_3$ IN SILICA GEL

5.2.1 EXPERIMENTAL

5.2.2 RESULTS

5.2.3 DISCUSSION

5.1 $BaCO_3$ PRECIPITATED BY A DIFFUSION MECHANISM IN SILICA GEL ON GLASS MICROSCOPE SLIDES

These were the first "precipitation in gels" experiments carried out in this study. They were intended to be a repeat of Garcia Ruiz's "induced morphology crystal aggregate" experiments, with a few modifications, as follows; (i) the precipitation reaction was carried out on a glass microscope slide instead of a test-tube or U-tube. This made good in-situ light microscopy possible since there was no curved glass to distort images and allowed for the possibility of time-lapse in-situ light microscopy on growing precipitates by recording the coordinates of a particular point in the gel. (ii) an ion exchange resin was used as the acidifying agent, instead of HCl, in the preparation of the silica gel as this gave a clear NaCl-free gel and allowed for better light microscopy; finally (iii) a small unloaded silica gel buffer zone was placed between the reactants. This was to avoid the irreproducibilities of behaviour corresponding to the mathematical consequences of extremely steep diffusion fronts.

5.1.1 EXPERIMENTAL

Glass microscope slides were masked with teflon tape and pre-gelled solutions were transferred to the slides according to procedure 3.4(ii) in the order (i) unloaded silica gel buffer, (ii) Na_2CO_3 loaded silica gel and

(iii) $BaCl_2$ loaded silica gel. The pH of pre-gelled silica solutions was monitored with pH paper. Each solution was allowed to gel before proceeding with the other solutions. The unloaded silica gel and the Na_2CO_3 loaded silica gel were prepared according to procedure 3.1.1 with no furher additives. The $BaCl_2$ loaded agarose gel was prepared according to procedure 3.1.4 with no further additives.

Preliminary experiments using this set-up yielded very different results from those obtained by Garcia Ruiz. The morphologies observed were that of spikes growing from a nucleus followed by dendritic growth from the spikes as opposed to IMCA's. These preliminary results prompted a series of experiments devised to determine the effects of precipitating ion concentrations, concentration gradients and pH on morphology.

Table 5.1.1a describes the successful experimental parameters studied (part of a more comprehensive series) such as $BaCl_2$ concentration and volume, the buffer gel pH and volume and the Na_2CO_3 loaded gel concentration, pH and volume. The $BaCl_2$ concentration was always set at a higher level than the Na_2CO_3 which resulted in a concentration gradient and precipitation of $BaCO_3$ in the silica gel.

1% Agarose Gel (0.4 ml)		3% Silica Gel (1 ml)	
	[$BaCl_2$] (M)	[Na_2CO_3] (M)	pH
Sample			
BC01	1.0	0.1	9-10
BC02	1.0	0.1	9-10
BC03	1.5	0.1	9-10
BC04	1.0	0.1	9-10
BC05	0.75	0.1	9-10
BC06	0.5	0.1	9-10
BC07	0.75	0.1	9-10
BC10	0.75	0.1	8-9
BC11	0.5	0.1	8-9
BC13	0.2	0.05	9-10
BC16	0.2	0.05	8-9
BC17	0.1	0.05	8-9
BC18	0.075	0.05	8-9

Each slide contained 3% silica gel buffer zone, pH 6 - 7 and volume 0.2 ml

table 5.1.1a

5.1.2 RESULTS

5.1.2.1 In-Situ Light Microscopy (LM)

The experiments BC01 and BC02 are essentially the same and act as a test for reproducibility. In both cases the first precipitates, arising where the diffusion gradient is steepest, resemble cauliflowers. Plate 5.1.2.1a illustrates this morphology. It arises through nucleation of a spherical centre followed by growth of spikes in all directions from specific faces of the nucleus and finally dense branched growth at the end of the spikes to give roughly circular objects of size 0.2 mm. Generally growth is restricted to two dimensions by the volume constraint imposed by a thin layer of gel.

As the diffusion gradient falls the precipitated objects become larger and there is a crossover to more elongated morphologies. Plates 5.1.2.1b and 5.1.2.1c illustrate typical objects and how they grow. The two plates are of the same area during and when growth is completed (micrographs taken twelve hours apart). These objects arise through the growth of two spikes in the opposite direction from each other. At various stages along these spikes outgrowths of further spikes occur in various directions. All spikes end with dense branched growth. There appears to be no preferential alignment of these objects (eg with the diffusion gradient) as random orientations of the objects are observed.

The two morphologies described, ie the cauliflower and the two-spiked growth constitute the majority of objects observed in these experiments, however some variations on these morphologies were also seen. In some cases an intermediate number of spikes grew from the nucleus and in a few cases growth stopped without dense branching.

Some strange aspects of growth were also observed, eg the long object on the right of plate 5.1.2.1c exhibits dense branched growth at the join between the main spike and one of the outgrowing spikes and a high magnification view of one of these objects reveals a cell-like structure (plate 5.1.2.1d).

The length of time an object takes to grow depends on the concentration gradient but is generally less than twenty hours.

Experiments BC03, BC04, BC05 and BC06 were designed to test the effect of varying $BaCl_2$ concentration, keeping all other factors constant. BC03 (1.5M $BaCl_2$) yielded mainly a two-spiked morphology with outgrowths and dense branching at the ends of spikes. BC04 which was a repeat of BC01 and BC02 (1M $BaCl_2$) produced different results from BC01 and BC02. Plate 5.1.2.1e illustrates typical morphologies obtained. There is a greater degree of spike outgrowth from the point of nucleation than in the two-spiked morphologies of BC01 and BC02. These spikes then split towards the end of growth to form a more solid

more solid branched growth than in BC01 and BC02. Reducing the $BaCl_2$ concentration further to 0.75 and 0.5M as in BC05 and BC06 produces similar but perhaps intermediate morphologies to those already described. Plate 5.1.2.1f illustrates a typical morphology from BC05. A high degree of branching, both solid, and near the ends of growth, sometimes dense, produced objects of irregular shape. Further strange aspects of growth can be observed clearly in BC06. In plate 5.1.2.1g, during their growth, spikes are seen to enlarge suddenly and then taper off to an end.

Experiment BC07 was a repeat of BC05 and yielded similar results. BC10 and BC11 were repeats of BC05 and BC06 but using silica gel of lower pH (8-9). The results obtained in both were similar. Growth appeared to be restricted and a globular morphology with small spikey outgrowths was obtained (plate 5.1.2.1h).

In the remaining successful experiments Na_2CO_3 concentration was reduced to 0.05M and a range of lower $BaCl_2$ concentrations was used. In BC13 (silica gel pH 9-10) small globular morphologies with spikey outgrowths were obtained as the first precipitates. As the diffusion gradient fell a variety of morphologies were obtained including the two-spiked morphology with outgrowths and multispiked objects, in some cases, exhibiting the "suddenly enlarging spike" aspect of growth (plate 5.1.2.1i).

In BC16, BC17 and BC18 a silica gel of pH 8-9 was used. Similar morphologies were obtained in all three cases. The number of spikes growing from the central nucleus was restricted in comparison to earlier morphologies. Plate 5.1.2.1j illustrates a typical object.

When observed under cross-polarized light none of the precipitates so-far described showed any maltese cross effect previously reported as indicative of the formation of induced morpholgy crystal aggregates, IMCA's (Garcia-Ruiz, 1985 and section 1.3 of this thesis).

5.1.2.2 Acid-Dissolution L.M. Experiment

When any of the precipitates so-far described were placed on a glass microscope slide and observed when a drop of dilute acetic acid was placed on top of them (procedure 3.6.5i), the entire aggregates were seen to dissolve leaving no trace of any membrane.

5.2.2 Routine Chemical Analysis

Precipitates were removed from gels by dissolving the gel in NaOH in accordance with procedure 3.5.2. Fourier transform infra-red spectroscopy (FTIR) and X-ray diffraction (XRD) were carried out in accordance with procedure 3.5.6. Data were obtained identical to that shown and described in chapter 6 for sample BC[0.05]9. Both techniques identified the presence of $BaCO_3$ with XRD

further identifying the phase analogous to $CaCO_3$ aragonite.

5.1.3 DISCUSSION

From the results described in the next chapter it is clearly shown that the pH of the silica gel has a critical effect on $BaCO_3$ precipitate morphology. This is also suggested in the results described in this chapter. Since the pH was monitored only with pH paper it can be assumed that the irreproducibilities observed, eg BC04 yielding different results from BC01 and BC02, arose through inaccurate pH measurements. These inaccurate pH measurements also make it difficult to interpret the effects on morpholgy caused by different diffusion gradients and precipitating ion concentrations.

It is also clear that none of the precipitates so-far described are induced morphology crystal aggregates (IMCA's); they do not look like aggregates described and reported by Garcia-Ruiz (1985), they are normal dendritic precipitates rather than induced morphologies. They do not exhibit the maltese cross effect and there is no trace of a membrane after dissolution in acid.

The main difference between Garcia-Ruiz's silica gels and the silica gels so-far prepared in this study is the presence of NaCl in the former. Thus it would appear that NaCl also has a critical effect on $BaCO_3$ precipitate

morphology. This is borne out by results discussed in the next chapter which is an account of the effect of pH and NaCl presence on $BaCO_3$ precipitate morphology.

5.2 HOMOGENEOUS PRECIPITATION OF $BaCO_3$ IN SILICA GEL

The precipitation of metal carbonates by homogeneous methods has been previously studied at Glasgow (Braterman, 1987 and section 2.3.2 in this thesis).

As a comparison to results obtained for $BaCO_3$ precipitated by a diffusion mechanism , a homogeneous series of experiments involving the the hydrolysis of urea as the source of carbonate and alkalinity was devised.

5.2.1 EXPERIMENTAL

A silica gel (pH 5.5) was prepared by the addition of sodium silicate solution to 1M HCl in accordance with procedure 3.1.3. The pre-gelled solution was transferred to four test tubes each containing 10 ml . Two of these test tubes contained a few drops of pH universal indicator solution. The gels set in approximately 2 minutes.

To two tubes (one without and one with indicator) 10ml of

a solution containing 0.1M $BaCl_2$ and 0.3M urea was added. To the other two tubes a solution containing 0.2M $BaCl_2$ and 0.6M urea was added. The $BaCl_2$ and urea were allowed to diffuse into the gels for 1 week.The test tubes were then placed in a water bath at 85^{o}C for 14 hours.

This procedure was repeated with the exception that Dowex ion exchange resin was added to the sodium silicate solution (procedure 3.1.1, no additives) instead of adding sodium silicate solution to HCl. This produced gels free of NaCl which has been shown (chapter 6) to have a great effect on precipitate morphology in the diffusion experiments. A gel of pH 4 was prepared and split among 4 test tubes, two of which contained indicator solution.

The weak and strong top solutions were added as before and allowed to diffuse through the gels for a week. This was then followed by heating in a water bath for 14 hours.

This whole procedure was repeated with silica gel of pH 6.5 also.

5.2.2 RESULTS

The gel prepared to pH 5.5 by 1M HCl and containing the high concentration of reactants rose in pH to approximately 8 and produced large dendritic crystals up

to 1cm long. Plate 5.2.2a is a SEM view of part of a typical precipitate. Noteworthy is the very precise hexagonal crystal symmetry. The same gel but with the lower concentration of reactants produced a similar result but with fewer precipitates and less branching. The gels prepared with Dowex returned to solution at edges and made observation of precipitates difficult. The one prepared at pH 4 with the lower concentration of reactants rose to approximately pH 7 and contained large (1cm) thin precipitates similar to those shown in plate 5.2.2a.

5.2.3 DISCUSSION

It is clear that these dendritic precipitates formed under homogeneous conditions are not IMCA's. A major reason for the failure to form IMCA's is that the pH does not reach a high enough value. As the urea is hydrolysed the pH increases with the formation of NH_4^+. As it reaches the value of 8 - 8.5 the carbonate is almost entirely in the form of HCO_3^-. As this reacts with barium H^+ is released which buffers the rise in pH.

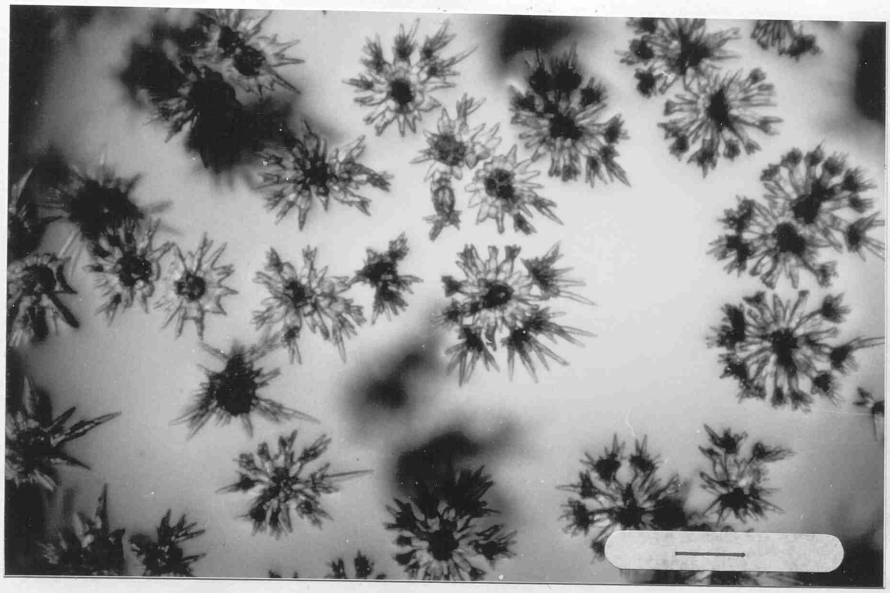

Plate 5.1.2.1a. BC01/02. Scale bar 0.1 mm.

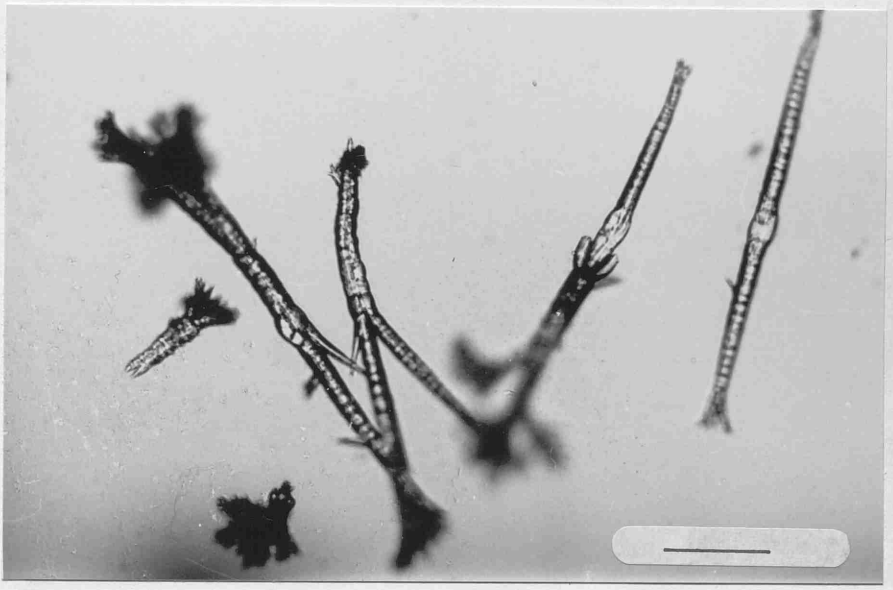

Plate 5.1.2.1b. BC01/02. Scale bar 0.1 mm.

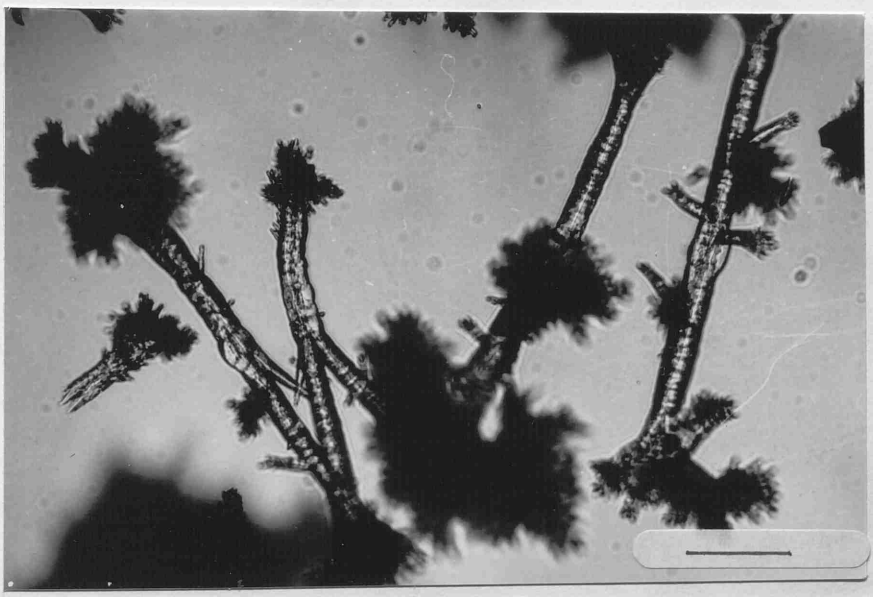

Plate 5.1.2.1c. BC01/02. Scale bar 0.1 mm.

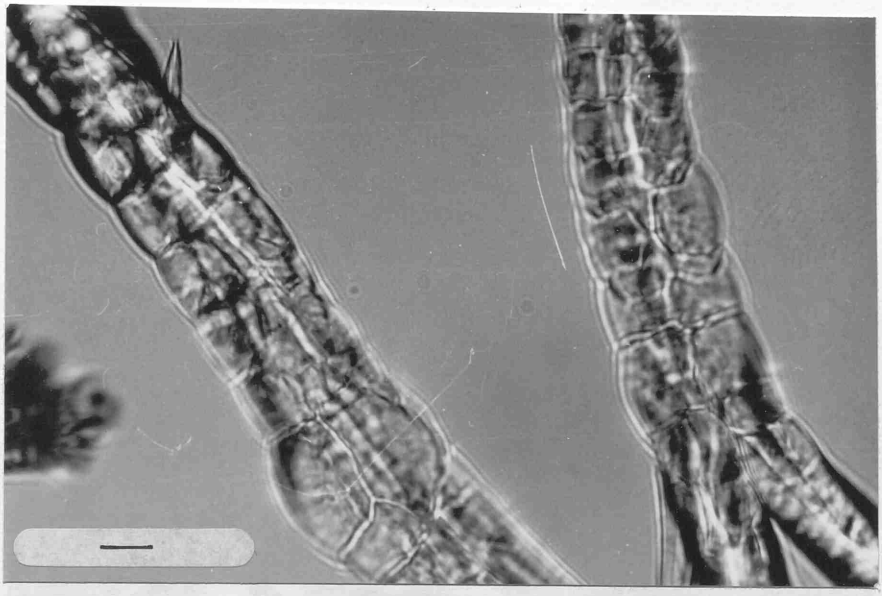

Plate 5.1.2.1d. BC01/02. Scale bar 10 µm.

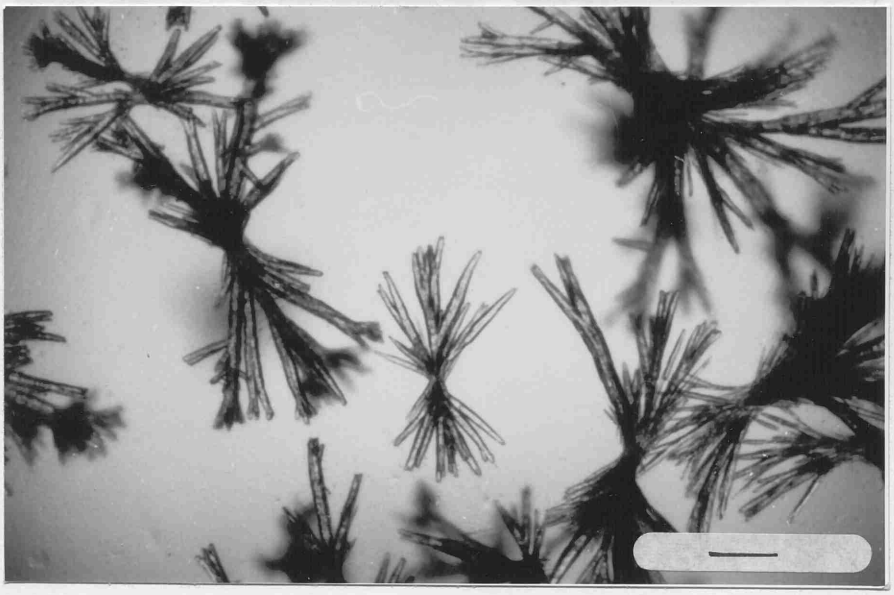

Plate 5.1.2.1e. BC04. Scale bar 0.1 mm.

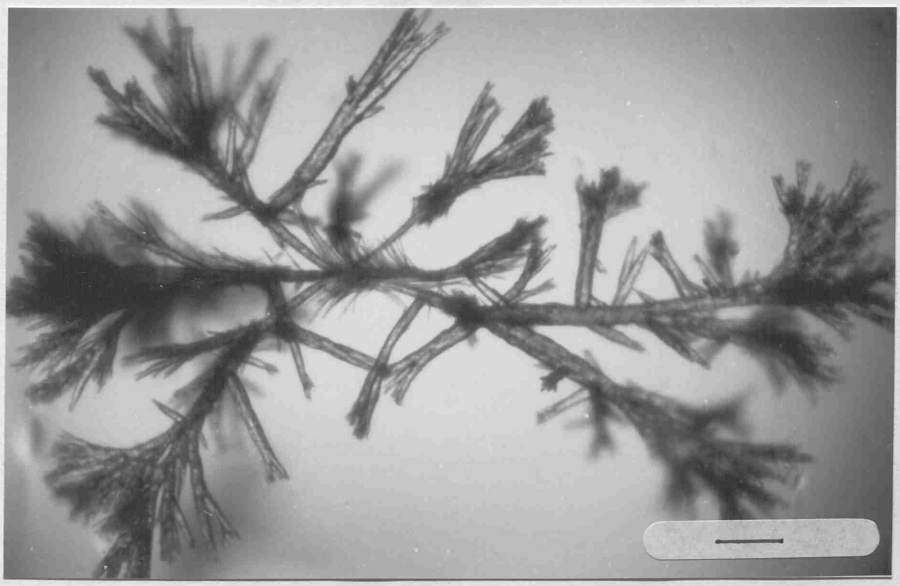

Plate 5.1.2.1f. BC05. Scale bar 0.1 mm.

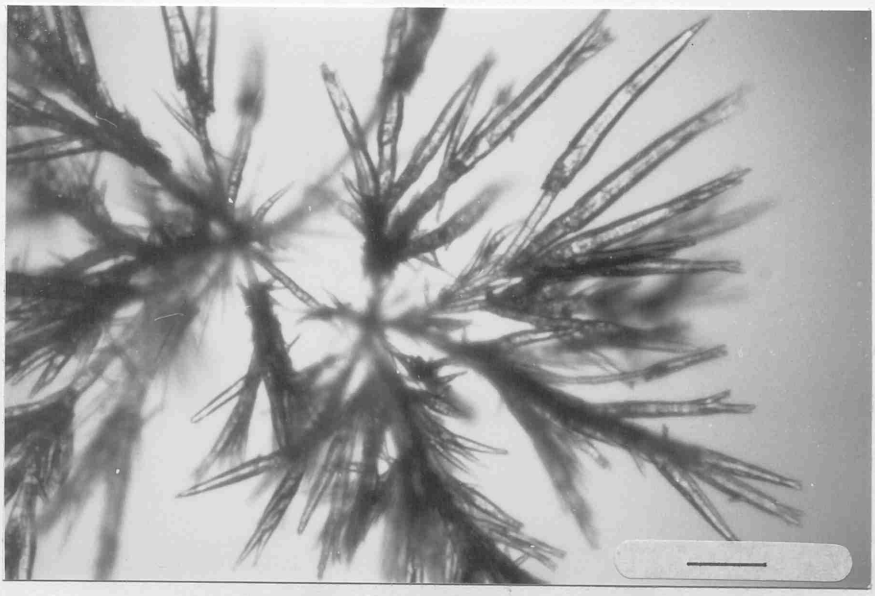

Plate 5.1.2.1g. BC06. Scale bar 0.1 mm.

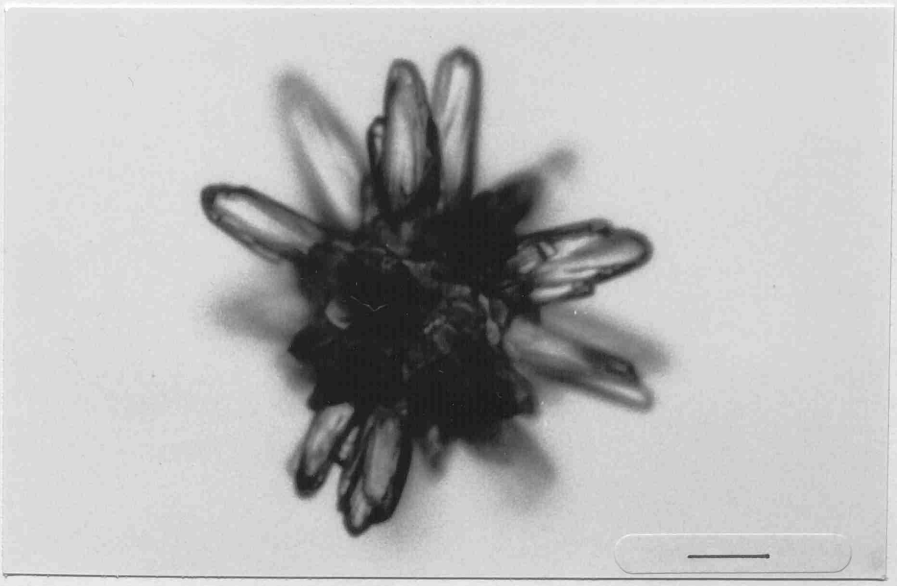

Plate 5.1.2.1h. BC10/11. Scale bar 25 µm.

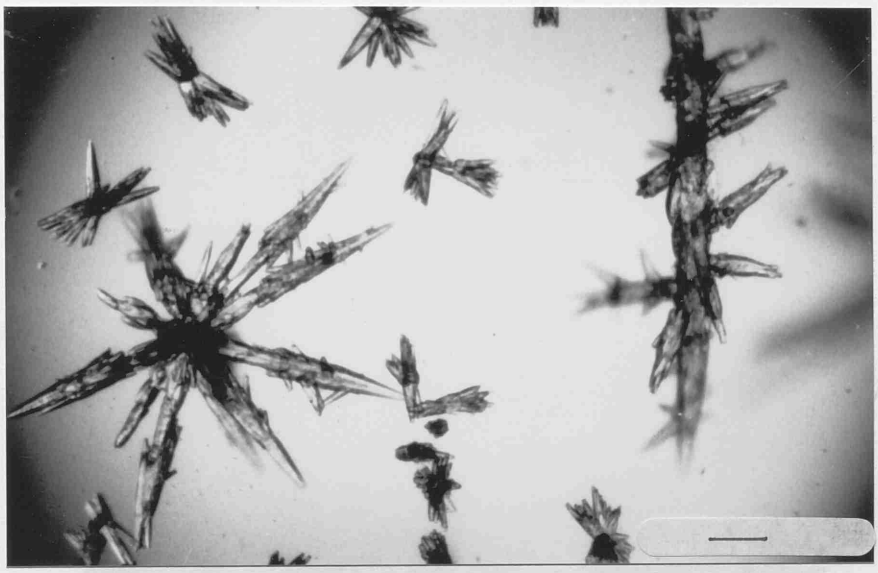

Plate 5.1.2.1i. BC13. Scale bar 0.1 mm.

Plate 5.1.2.1j. BC16/17/18. Scale bar 0.1 mm.

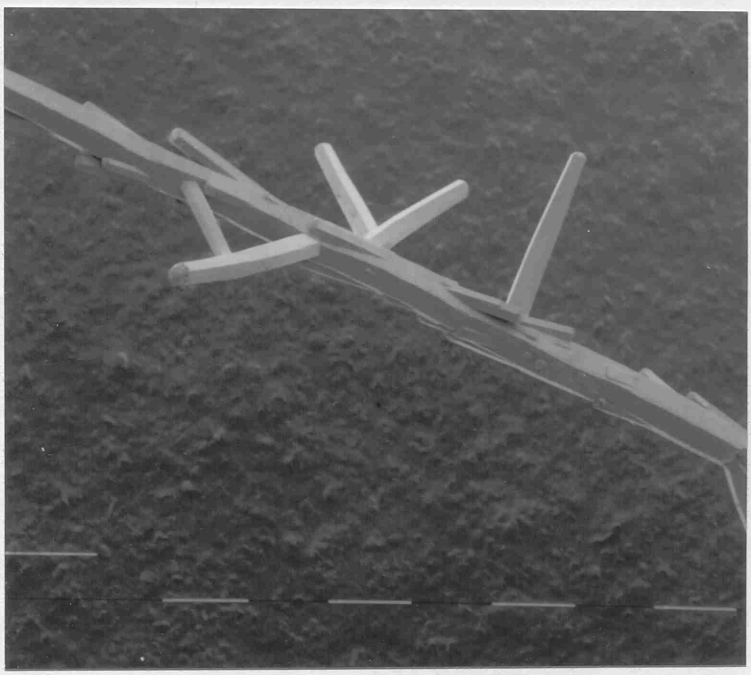

Plate 5.2.2a. SEM of homogeneously precipitated $BaCO_3$. Scale bar 0.1 mm.

6 $BaCO_3$ PRECIPITATED BY A DIFFUSION MECHANISM IN SILICA GEL IN GLASS CASSETTES

6.1 EXPERIMENTAL

6.1.1 NaCl-Free Experiments

6.1.2 NaCl-Containing Experiments

6.1.3 Control Experiments

6.2 RESULTS

6.2.1 In-Situ Light Microscopy

(i) NaCl-Free Experiments

(ii) NaCl-Containing Experiments

(iii) Control Experiments

6.2.2 Routine Chemical Analysis

6.2.2.1 Fourier Transform Infra-Red Spectroscopy (FTIR)

6.2.2.2 X-Ray Diffraction (XRD)

6.2.3 The Acid Dissolution LM Experiment

6.2.4 Scanning Electron Microscopy (SEM)

(i) Precipitates From Silica Gel

(ii) Precipitates From Agarose Gel

6.2.5 Scanning Electron Microscopy (SEM) Equipped with Energy Dispersive Spectroscopy (EDS)

6.2.6 Transmission Electron Microscopy (TEM) Equipped with Energy Dispersive Spectroscopy (EDS)

6.2.6.1 The Acid Dissolution TEM Experiment

6.2.6.2 The Thin Section TEM Experiment

6.2.7 X-Ray Photoelectron Spectroscopy (XPS)

6.2.8 Rutherford Backscattered Image

6.3 DISCUSSION

6 $BaCO_3$ PRECIPITATED BY A DIFFUSION MECHANISM IN SILICA GEL IN GLASS CASSETTES

From the previously described experiments, carried out on microscope slides, it was clear that the pH of the silica gel was a critical aspect of the precipitate morphology. It was also clear that IMCA's were not obtained in these experiments and that the main difference between Garcia Ruiz's silica gels and the silica gels prepared in this study was the presence of NaCl in the former. Therefore it would appear that this was also critical to aggregate morphology.

Thus, a series of experiments was devised in order to study the effects of pH of "NaCl-free" silica gel on precipitate morphology with particular attention paid to measuring pH accurately. The effects of adding NaCl to these systems was also studied and as a control experiment the precipitation of $BaCO_3$ was studied in agarose gels. Finally an experiment was performed in basic silica gel in which ethylene glycol was added instead of NaCl in order to examine any osmotic effects.

6.1 EXPERIMENTAL

6.1.1 NaCl-Free Experiments

These experiments were carried out in glass cassettes (section 3.4(iii)). No buffer zones were used in these

experiments. Pre-gelled silica solutions containing Na_2CO_3 were prepared according to procedure 3.1.1. The pH was monitored to less than one tenth of a unit using a pH meter and glass electrode. The solutions were poured into the glass cassettes and allowed to gel. Agarose gels loaded with 0.5M $BaCl_2$ were prepared according to procedure 3.1.4 with no further additives. These pre-gelled $BaCl_2$/agarose solutions were poured gently on top of the silica gels and the cassettes sealed. Table 6.1.1a lists the experiments performed and a key to understanding the nomenclature. Each experiment was carried out in duplicate and repeated at least once.

6.1.2 NaCl-Containing Experiments

The NaCl-containing experiments were performed by the method described above but with either one or two of the following exceptions.

(i) NaCl was added prior to the addition of the ion exchange resin.

(ii) Experiments were performed without the addition of Na_2CO_3.

(iii) Experiments were performed with 1M HCl used as the acidifying agent rather than the ion exchange resin (procedure 3.1.2).

Table 6.1.2a lists the experiments performed and a key to understanding the nomenclature.

NaCl-Free Experiments

BC[0.05]8.5

BC[0.05]9

BC[0.1]9

BC[0.05]9.5

BC[0.1]9.5

BC[0.1]10

BC[0.1]10.5

Key:

BC : barium carbonate

First square bracket : molar concentration of added Na_2CO_3

Final figure : pH

table 6.1.1a

NaCl-Containing Experiments

BC[0.05][0.2]8.5

BC[0.05]0.2]9

BC[0.05][0.2]9.5

BC[0.05][0.2]10

BC[0.05][0.1]9.5

BC[0.05][0.33]9.5

BC[0][0.33]9.5

BC[0.05][HCl]9

BC[0][HCl]9

Key:

BC : barium carbonate

First square bracket : molar concentration of added Na_2CO_3

Second square bracket : molar concentration of added NaCl
or indicates acidified with 1M HCl

Final figure : pH

table 6.1.2a

6.1.3 Control Experiments

Both agarose and ethylene glycol experiments were performed in test tubes. A neutral agarose gel loaded with 0.05M Na_2CO_3 was prepared according to procedure 3.1.4 and 0.05M $BaCl_2$ in agarose diffused through. This experiment was repeated with the the addition of a pH 9.2 buffer mixture (prior to gelling) to produce alkalinity and repeated once again with the buffer mixture and 0.2M NaCl.

The ethylene glycol experiment was a repeat of BC[0.05]9 but with the addition of 0.3M ethylene glycol prior to the addition of the ion exchange resin.

6.2 RESULTS

6.2.1 In-Situ Light Microscopy

(i) NaCl-Free Experiments

In BC[0.05]8.5 the typical aggregate morphology was that of a central nucleus with dentritic spikes growing in all directions. Branching along these spikes was limited. The longest spikes grew in the direction of the diffusion gradient resulting in precipitates of regular orientation. Aggregate size increased up to around 4 mm as the diffusion gradient fell. Plate 6.2.1a illustrates a typical morphology.

In BC[0.1]9 the greater concentration of Na_2CO_3 in the silica gel resulted in a more dense branched morphology as illustrated in plate 6.2.1b. This made observation of growth features difficult. Precipitate size also increased with the falling diffusion gradient.

In BC[0.05]9 the typical morphology is somewhat similar to that of BC[0.05]8.5. There is growth of dendritic spikes in all directions from the nucleus. In this case there is a far greater degree of branching as illustrated in plate 6.2.1c. Again, growth of spikes is longest in the direction of the diffusion gradient resulting in precipitates of specific orientation. As in BC[0.05]8.5 precipitates increase in size up to around 3 mm long.

In BC[0.1]9.5 typical aggregates are similar to those found in BC[0.1]9. Dense branched morphologies increase in size with falling diffusion gradients. In a small band of growth, about 1 cm long and three quarters of the way through the system a peculiar aspect of growth occurs seen previously in experiment BC06, plate 5.1.2.1g where growing spikes suddenly enlarge. Plate 6.2.1d illustrates this more clearly.

In BC[0.05]9.5 precipitates of the type illustrated in the top left corner of plate 6.2.1e increase in size up to a maximum of ~0.75 mm. The proceeding precipitates then appear to have their growth restricted (middle and bottom right objects in 6.2.1e) and eventually the final

precipitates in this experiment have a globular appearance as illustrated in plate 6.2.1f.

BC[0.1]10 follows a similar pattern to BC[0.05]9.5 but with an additional stage of developement in the final precipitates . Wavy, sometimes slightly twisted, ribbon-like outgrowths occur from the globular morphologies as illustrated in 6.2.1g.

In BC[0.1]10.5 the morphologies obtained were best observed using cross-polarized light microscopy. In the latter stages of growth thin sheet-like morphologies predominated and figs 6.2.1h, i and j illustrate the effectiveness of cross-polarized light microscopy and in particular, with a lambda wave plate, over conventional light microscopy.

A very clear morphogenetical transition, from the first precipitates to last, occurs in BC[0.1]10.5. Illustrating this transition is a series of cross-polarized (lambda wave plate) light micrographs, figs 6.2.1l to v. The first micrograph in the series has its centre 2 mm from the interface between the agarose and silica gels. The following micrographs have their centre 4 mm from their predecessor. Each micrograph illustrates 3.75 mm of growth. Hence, this series illustrates, in almost its entirety, the morphogenetical transition from the first precipitates to the last precipitates. All micrographs were taken when growth was completed.

The first precipitates observed (plate 6.2.11) were globular with spikey outgrowths. Advancing through the cassette the precipitates become larger and the outgrowths can be more clearly seen to exhibit the induced morphology effect of spirals (plate 6.2.1m,n & o). In 6.2.1n & o colours other than the pink background can be observed. This is due to induced sheet morphologies exhibiting birefringence and interference colours in the cross-polarized light. This is particularly clear along with the spiral morphology in plates 6.2.1p & q. In plates 6.2.1r & s it can be seen that a mass of induced sheet morphologies grow in all directions from the initial globular stage and at points these sheets give rise to very tightly wound spiral morphologies. Plate 6.2.1t is an example of this. In the latter stages of growth the tightly wound spiral morphologies predominate and grow roughly in the direction of the diffusion gradient up to several mm's in length. Plates 6.2.1u & v illustrate this.

Plate 6.2.1w is a good example of the sheet morphology observed near the end of growth. The point of nucleation is at the centre of the sheet part, where the pink Maltese cross originates. Precipitates growing at this stage of the experiment when the $BaCl_2$ supply is almost exhausted do not usually have a globular centre, or if they do, it is very small. A flat sheet morphology usually results. This is illustrated in plate 6.2.1k. From the sheet objects, tightly wound spirals can grow.

Many can be seen in plate 6.2.1k and an out of focus one in 6.2.1w. The tightly wound spiral morphologies observed in 6.2.2u & v probably originated from such sheet objects although it is difficult to tell because of the length and complexity of the objects.

(ii) NaCl-Containing Experiments

Plate 6.2.1x is an example of an aggregate from BC[0.05][0.2]9.5. As can be clearly seen it is an IMCA exhibiting a central bulk part with sheet like growths and a loosely wound spiral part growing from a sheet. This type of precipitate was commonplace in experiments BC[0.05][0.2]8.5, BC[0.05][0.2]9, BC[0.05][0.1]9.5 and also in examples BC[0][0.33]9.5 and BC[0][HCl]9 even though no added carbonate was present in these experiments. Plate 6.2.1y is an example of an aggregate from BC[0][HCl]9. One difference between experiments with added Na_2CO_3 and experiments without was that in the latter there was significantly less precipitates in total.

In the experiments with added Na_2CO_3 and high amounts of NaCl and/or a high pH value: BC[0.05][0.33]9.5, BC[0.05][HCl]9 and BC[0.05][0.2]10 the aggregates were again similar but the spirals were tighter wound. Plate 6.2.1z is an example from BC[0.05][0.33]9.5

(iii) Control Experiments

The control experiments were performed in test tubes and therefore in-situ photo-microscopy was difficult. The following is an account of the morphologies observed under the light microscope. The morpholgies described are shown in the SEM section (6.2.4).

In the neutral agarose control experiment the initial precipitates were of irregular morphology and up to around 300 μm in size. The later precipitates became smaller (down to around 150 μm) and more regular and had a spherical globular/raspberry-like appearance. In the basic agarose gel experiment the initial precipitates were also of a globular/raspberry-like appearance and were around 250 μm in size. The later and final precipitates appeared spherical and of a similar size. In the basic NaCl agarose experiment spherical particles around 100 μm formed throughout.

Adding ethylene glycol to basic silica gels appeared to have no effect on morphology.

6.2.2 Routine Chemical Analysis

Precipitates were removed from experiments BC[0.05]9 (dendrites) and BC[0.1]10.5 (IMCA's) by dissolving the gel in NaOH in accordance with procedure 3.5.2.

6.2.2.1 Fourier Transform Infra-Red Spectroscopy (FTIR)

FTIR spectrocopy was carried out in accordance with procedure 3.5.6. Figure 6.2.2.1a is the FTIR spectrum of BC[0.1]10.5 which was identical to that of BC[0.05]9. Peaks due to $BaCO_3$ were observed at 1751, 1451, 1060, 858, and 694 cm^{-1}. Fig 6.2.2.1b is the FTIR spectra of AnalaR $BaCO_3$. The $BaCO_3$ identifying peaks in the AnalaR sample can be seen to be identical to that of the precipitated sample. All other peaks in both spectra can be assigned to water (~3500 cm^{-1}), coatings on the instrument detector (2800 - 3000 cm^{-1}) and carbon dioxide (2300 - 2500 cm^{-1}). Therefore the FTIR spectrum would seem to contain no bands which can be assigned to a barium silicate structure.

6.2.2.2 X-Ray Diffraction (XRD)

XRD analysis was carried out in accordance with procedure 3.5.6 (Cu alpha 1, 2 radiation). Figure 6.2.2.2a (i) is the XRD pattern of BC[0.05]9 and printed below is the reference $BaCO_3$ pattern from the powder diffraction files (5-378). Table 6.2.2.2a (ii) lists the measured peak angles, calculated d-spacings and intensities. Figure 6.2.2.2b (i) and table 6.2.2.2b(ii) are the corresponding XRD pattern of BC[0.1]10.5 (and reference pattern) and the list of peak angles, d-spacings and intensities. Table 6.2.2.2c lists the reference unit cell parameters, d-spacings intensities and Miller indices of $BaCO_3$ from

the powder diffraction files (5-378).

In both samples it can be seen that the patterns show the presence of $BaCO_3$ with orthorhombic symmetry analogous to $CaCO_3$ aragonite. However (in both cases) there are a few differences from the reference pattern.

(i) A few low intensity peaks are missing or are not resolved from adjacent peaks, eg the 1.133 Å spacing is missing in both cases.

(ii) Relative peak intensities differ from the reference pattern, eg in BC[0.05]9 the 2.590 Å peak is significantly more intense than the reference pattern.

(iii) A few additional (unassigned) low intensity peaks are also present. These peaks are asterixed in tables 6.2.2.2a (ii) and 6.2.2.2b (ii)

The differences outlined in (i) and (ii) may be due to orientational effects either inherent in the sample or caused by the XRD sample preparation procedure. The difference outlined in (iii) is due to the presence of materials other than $BaCO_3$ in the sample either incorporated during the precipitation or in the sample preparation for XRD, such as NaOH, Na_2CO_3 and $BaCl_2$. The small number of peaks and low intensities made assignment difficult, but there is the possibility that these unassigned small intensity peaks may be due to a barium

silicate structure, particularly in the case of BC[0.1]10.5.

Ignoring additional peaks and by matching measured reflections to the reference reflections, unit cell parameters were computer-calculated for both samples.

For BC[0.05]9 they are:

a = 5.311 b = 8.900 c = 6.441

For BC[0.1]10.5 they are:

a = 5.314 b = 8.903 c = 6.441

in comparison to the reference values:

a = 5.314 b = 8.904 c = 6.430

6.2.3 The Acid Dissolution LM Experiment

An IMCA exhibiting sheet-like parts (removed from gel) was placed on a glass microscope slide and a drop of dilute acetic acid was placed on top of it in accordance with procedure 3.5.5 (i). Plate 6.2.3a shows the intact aggregate under cross-polarizers, Plate 6.2.3b shows the aggregate slowly dissolving (loss of colour from the planar parts and bubbles of CO_2 forming) to leave behind the membrane in exactly the same shape as the original aggregate. Plate 6.2.3c shows the $BaCO_3$ part of the aggregate almost completely dissolved apart from a spherical centre part. It is clear that the membrane left

behind is the same shape as the original aggregate (rotated slightly due to it floating in the acetic acid). If the spherical centre part is crushed with a fine needle further dissolution of the interior occurs.

6.2.4 Scanning Electron Microscopy SEM

Precipitates were removed from the silica gel in accordance with procedure 3.6.2 and from agarose gel in accordance with procedure 3.5.3. They were prepared for SEM in accordance with procedure 3.6.4.

(i) Precipitates From Silica Gel

At low magnification the dendritic-type precipitates removed from BC[0.05]9 had an appearance illustrated by 6.2.4a. At higher magnification some other growth characteristics could be observed. At the tips of spikes "normal" hexagonal symmetry could be seen (plate 6.2.4b). This arises through the orthorhombic symmetry of $BaCO_3$. Nearer the core of the precipitate a very different surface texture is observed as illustrated in plate 6.2.4c. Combining these growth procedures is the area of precipitate detailed in plate 6.2.4d. Here the normal hexagonal crystal symmetry can be seen to be growing from the course-textured part.

Plate 6.2.4e is an example of the "enlarging spike" morphology observed in BC[0.1]9.5. Normal hexagonal symmetry can also be observed in this example.

Plate 6.2.4f is an example of the restricted growth globular morphology which appears towards the end of growth in BC[0.05]9.5. This appears to have a similar if not rougher texture than the area of precipitate observed near the core of the dendritic-type morpholgy (plate 6.2.4c).

Plate 6.2.4g is an example of the globular morphology with outgrowths obtained from BC[0.1]10. The micrograph quality is rather poor in this case due to charging effects caused by the difficulty in coating all the surface area in gold. Plate 6.2.4h is a higher magnification detail showing the rough surface texture.

Plate 6.2.4i is an example of the sheet-like type IMCA morphology obtained from BC[0.1]10.5 (this object would most likely have contained spiral parts which have been broken off in the gel dissolution process) and plate 6.2.4j is an IMCA morphology obtained at lower pH, but with the addition of 0.33M NaCl, detailing the twisted ribbon morphology. Plates 6.2.4k & l are higher magnification details illustrating the complexity of similar type morphologies.

Plate 6.2.4m is an unusual view of the cross-section of a broken tightly wound spiral part of an IMCA. On the outside can be seen a porous looking ring of approximately 1μm thickness. This would appear to be the membrane. On the inside can be seen a radial, slightly spiraling pattern of crystal growth.

(ii) Precipitates From Agarose Gel

Plate 6.2.4n is an example of the irregular-type objects which form initially in the neutral agarose control experiment. The image is poor due to charging caused by the difficulty in succesfully gold coating irregular and coarse-textured objects. Plate 6.2.4o is an example of a more regular globular/raspberry-like precipitate formed a little later in the same experiment (charging is still a problem). Plate 6.2.4p is an example of an even more regular precipitate formed in the final stages of growth in the same experiment.

In the basic agarose control experiment the initial precipitates formed are globular and raspberry-like identical to that shown in plate 6.2.4p. Later precipitates formed become spherulitic as shown in plate 6.2.4q.

In the basic NaCl agarose control experiment spherulitic precipitates form throughout, identical to that shown in plate 6.2.4q.

6.2.5 Scanning Electron Microscopy (SEM) Equipped with Energy Dispersive Spectroscopy (EDS)

The IMCA precipitates removed from BC[0.1]10.5 were subjected to EDS analysis in order to gain some structural information on the membrane.

Precipitates were removed from the gel in accordance with procedure 3.6.2 and mounted on stubs with carbon paint and coated with carbon in accordance with procedure 3.6.4.

Figure 6.2.5a is an EDS analysis of a sheet-like part of a precipitate. It clearly shows the presence of Ba and Si peaks and a subsequent computer generated semi-quantitative analysis gave a Ba : Si atomic ratio of 94 : 6. Since EDS electrons are emitted from a depth of usually 1 micron it would appear that the membrane was thinner than this and that a large part of the Ba signal was coming from the bulk of the sample rather than the membrane.

IMCA precipitates which were subjected to prolonged NaOH treatment (1 - 2 days) showed a reduced or no Si signal on EDS analysis.

Precipitates removed from BC[0.05]9 were also subjected to EDS analysis in the same way. Areas exhibiting "normal" hexagonal crystal symmetry showed no trace of Si

whereas the areas with the coarser texture did.

6.2.6 Transmission Electron Microscopy (TEM) Equipped with Energy Dispersive Spectroscopy (EDS)

6.2.6.1 The Acid Dissolution TEM Experiment

Since EDS used in conjunction with SEM failed to give any structural information on the membrane because of the depth of emitted X-rays from the sample an experiment was devised in which the membrane could be examined on its own by TEM.

An aggregate exhibiting sheet-like areas was dissolved of its carbonate part on a gold TEM sample grid by the action of weak acetic acid in accordance with the procedure detailed in 3.6.5(i) to leave behind the membrane.

Inspection by TEM revealed a thin film and at higher magnification the film appeared holey as in plate 6.2.6.1a. This suggested that the Ba had been leached out of the membrane by the action of the acid to leave behind a thin film of silica. This was backed up by EDS analysis which indicated only the presence of silicon as illustrated in figure 6.2.6.1a. The gold and copper peaks are due to the sample grid and the column of the microscope.

6.2.6.2 The Thin Section TEM Experiment

Some selected precipitates from BC[0.1]10.5 exhibiting sheet-like and spiral morphologies were embedded in resin and sectioned using a microtome and diamond knife as described in 3.6.5(ii). Since the resin cannot penetrate into a crystalline structure, unlike a biological specimen, sectioning was very difficult. Thin sections tended to break up and on thicker sections although there was less likelihood of the material breaking up, the sections were so thick that no structural information could be obtained.

6.2.7 X-Ray Photoelectron Spectroscopy (XPS)

This was by far the best surface analysis technique used for elucidating structural information since information is collected only from the top few nm of the sample.

A selected precipitate from BC[0.1]10.5 exhibiting both sheet-like and spiral parts was subjected to surface analysis. Both areas were identified as a barium silicate carbonate. However the spiral part had a higher Si to Ba ratio and lower Si binding energy than the sheet part as the overlaid spectra indicate (fig 6.2.7a). This indicates two different silicate structures. The presence of carbonate in the specimen is confirmed by the overlaid spectra in fig 6.2.7b

6.2.8 Rutherford Backscattered Image

The micrograph illustrated (fig 6.2.8a) was obtained by imaging the backscattered electrons from the sample using the same instrument as in the XPS analysis. Electrons backscattered from different types of atoms in the sample produce areas of different contrast in the image. The image illustrated, of a broken spiral part of a precipitate from BC[0.1]10.5, clearly shows how a spiral twists and grows and also clearly shows the presence of a membrane (<1 μm thick) as the area of different contrast on the outside of the sample.

6.3 DISCUSSION

It is clear from the results just described that the observation of the phenomenon of IMCA's, first observed and reported by Garcia Ruiz and Amoros (1981) has been verified. Crystal aggregates with the same morphological characteristics as those reported by the aforementioned authors have been successfully precipitated in this study. These precipitates exhibit a uniaxial dark cross when observed under cross-polarized light, which remains stationary when the object is rotated and when the interior of these objects is dissolved in acid an external membrane, the same shape as the original aggregate is left intact. Both these observations are in agreement with the observations of the aforementioned authors.

IR and XRD analysis both confirmed the presence of $BaCO_3$ although no categorical evidence of a barium silicate structure was present in either. However SEM equipped with EDS analysis did confirm that the surface of IMCA's contained silicon. Analysis of the membrane (after dissolution of the $BaCO_3$ interior by acid) by TEM equipped with EDS also confirmed the presence of silicon, but any barium which may have originally been present was removed in the dissolution process.

XPS analysis did, however, confirm the presence of a barium silicate carbonate membrane. It was also shown that this membrane had two different compositions and structures corresponding to the two different types of morphology it enclosed, ie sheet-like and spiral. A Rutherford back-scattered image further identified the membrane to be of the order of one micron thick.

It was also observed that pH and the presence of NaCl in the gel had major effects on the formation of IMCA's. In the absence of NaCl and in the pH range 8.5 - 10.5 a morphogenetical transition was observed from dendrites to restricted growth dendrites to globular morphologies to globular morphologies with induced outgrowths through to fully induced morphologies.

In the presence of NaCl IMCA's were formed at all pH values from 8.5 - 10 suggesting that the NaCl effect is more critical and swamps the pH effect. But even in the

NaCl experiments it could be seen that the pH, Na_2CO_3 concentration and NaCl concentration had an effect on morphology. Low carbonate concentrations (impurity levels), low NaCl levels (0.1M) and low pH favoured loose wound spirals whereas higher carbonate concentrations (0.05M) coupled with high pH (10) or high levels of NaCl favoured tighter wound spirals.

In the case of the control experiments where $BaCO_3$ was precipitated in agarose gels a morphogenetical transition was also established. This transition depended on pH and to some extent NaCl presence. In the neutral experiment the irregular precipitates which form first (6.2.4o) can be likened to the dense branched morphology (6.2.1b) obtained in BC[0.1]9. These objects quickly become more regular and the final globular precipitates (6.2.4p) are remarkably similar to the globular precipitates (6.2.4f) obtained in BC[0.05]9.5. In the basic agarose control experiment the initial precipitates are of the globular type and later precipitates are spherulitic. The tendency for spherulitic growth is caused by the basic pH increasing CO_3^{2-} concentration in the system resulting in faster growth. In the basic NaCl experiment spherulites are obtained throughout suggesting that as well as fast growth due to high CO_3^{2-} concentrations there may be "salting out" effect in which the reaction of carbonate eases the solubility of NaCl.

A full account of the IMCA phenomenon, the factors which affect it and the transition towards it is given in chapter 9.

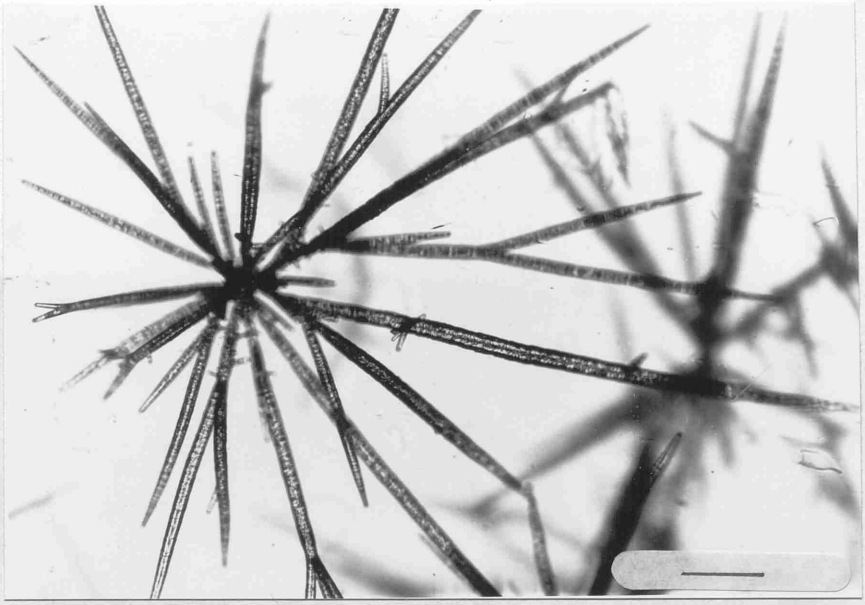

Plate 6.2.1a. BC[0.05]8.5. Scale bar 0.3 mm.

Plate 6.2.1b. BC[0.1]9. Scale bar 0.3 mm.

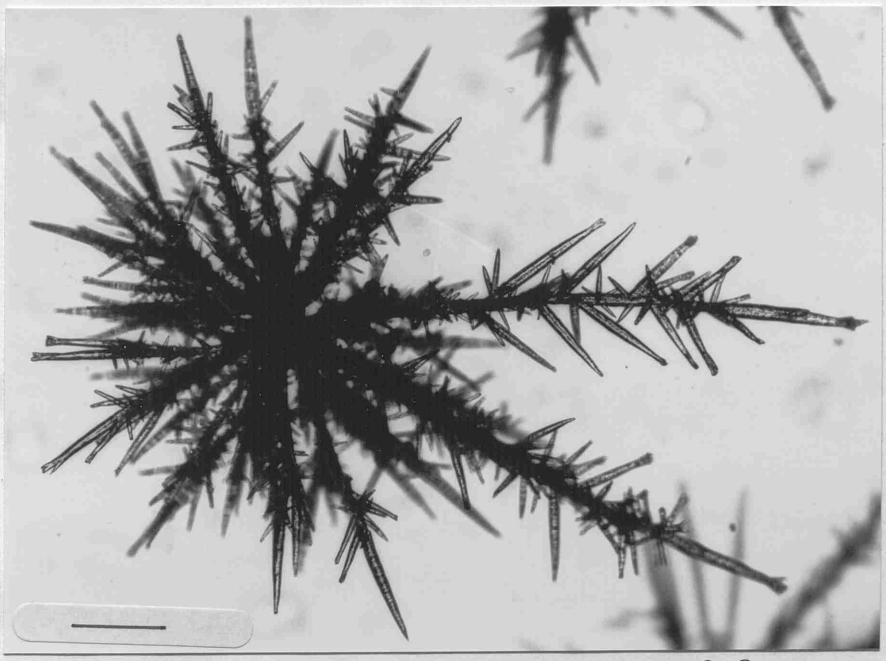

Plate 6.2.1c. BC[0.05]9. Scale bar 0.3 mm.

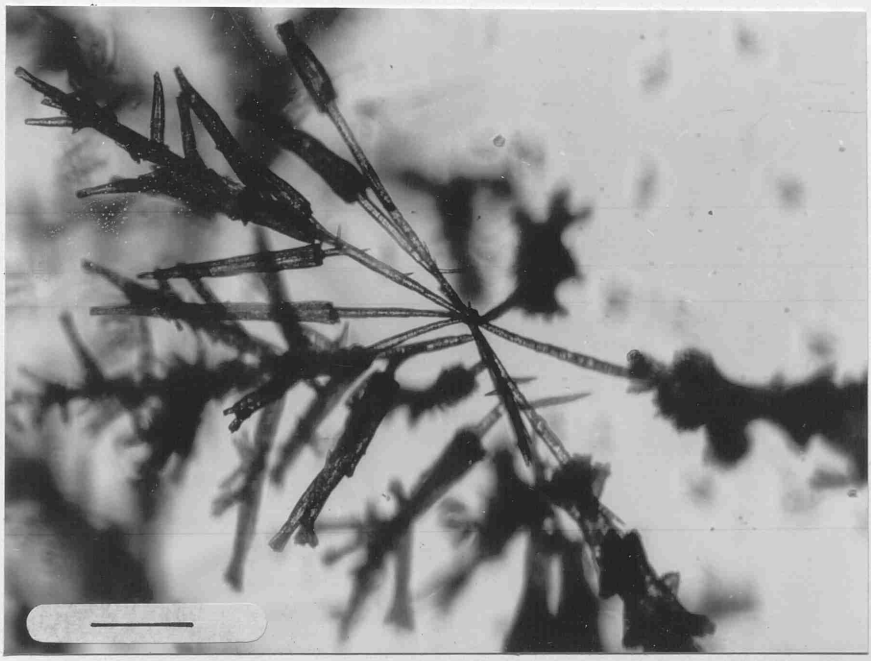

Plate 6.2.1d. BC[0.1]9.5. Scale bar 0.3 mm.

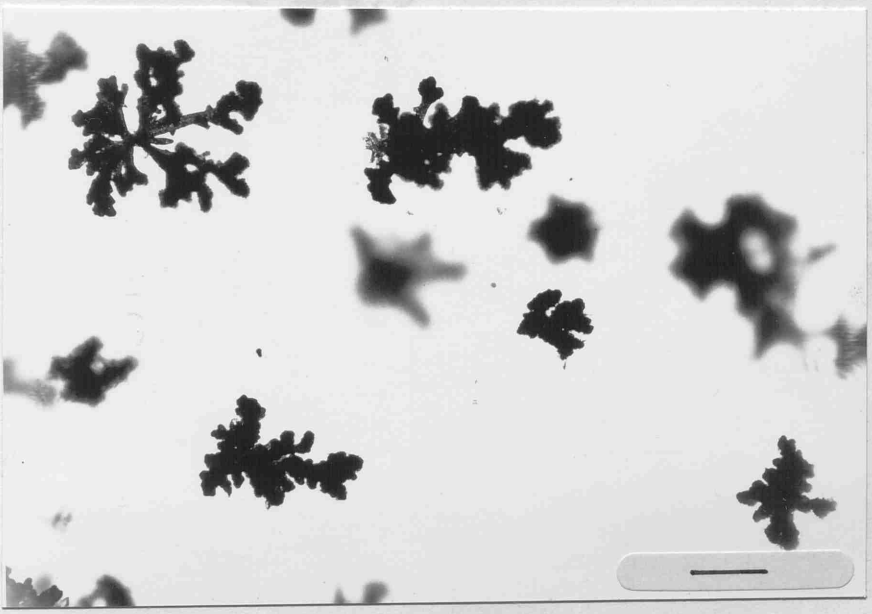

Plate 6.2.1e. BC[0.05]9.5. Scale bar 0.3mm.

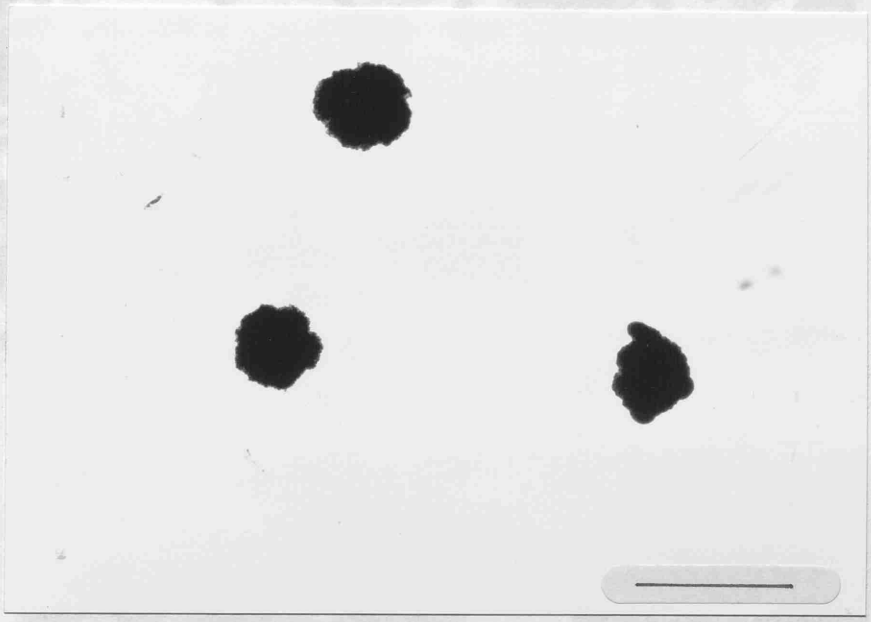

Plate 6.2.1f. BC[0.05]9.5. Scale bar 0.3 mm.

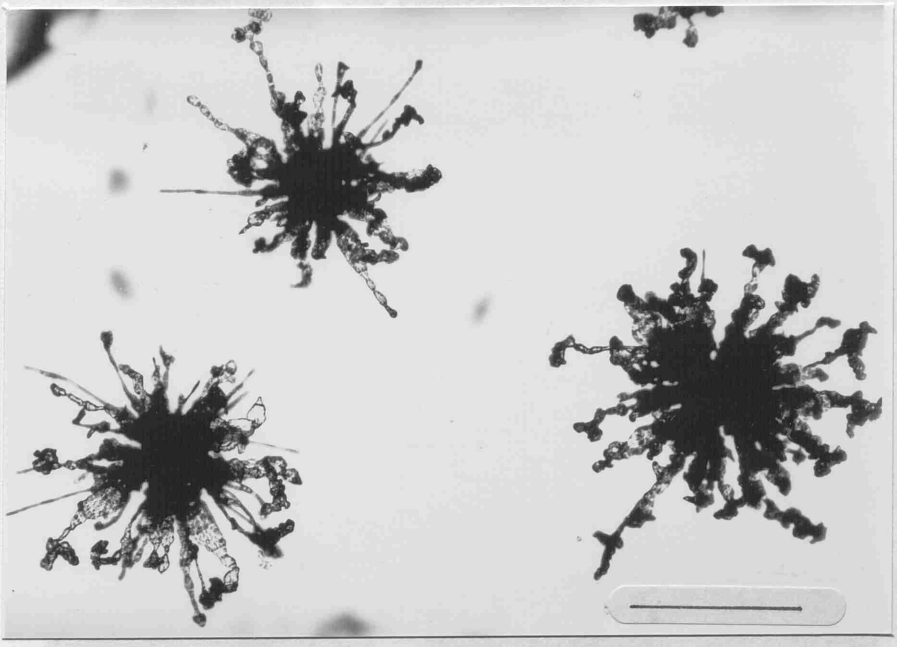

Plate 6.2.1g. BC[0.1]10. Scale bar 0.3 mm.

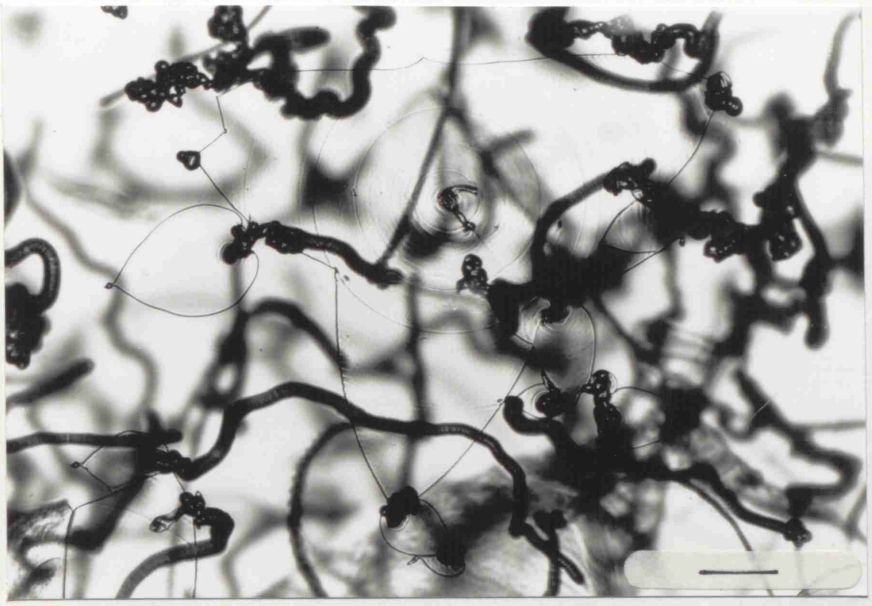

Plate 6.2.1h. BC[0.1]10.5. Scale bar 0.3 mm.

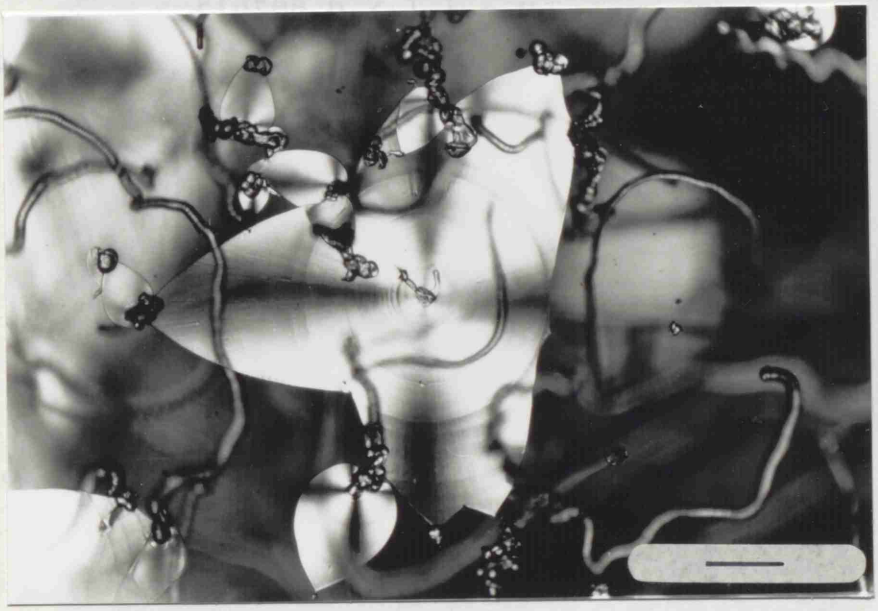

Plate 6.2.1i. BC[0.1]10.5. Scale bar 0.3 mm.

Plate 6.2.1j. BC[0.1]10.5. Scale bar 0.3 mm.

Plates 6.2.1 1 - v.

Series showing morphogenetical transition

from first precipitates to last

in BC[0.1]10.5

Plate 6.2.1w. BC[0.1]10.5

Planar IMCA

Each plate corresponds to 2.5 mm in length

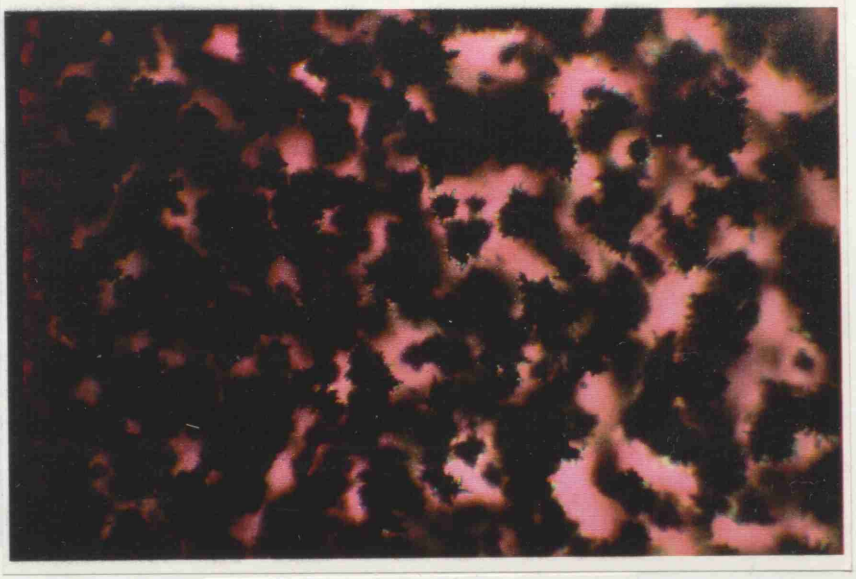

Plate 6.2.11

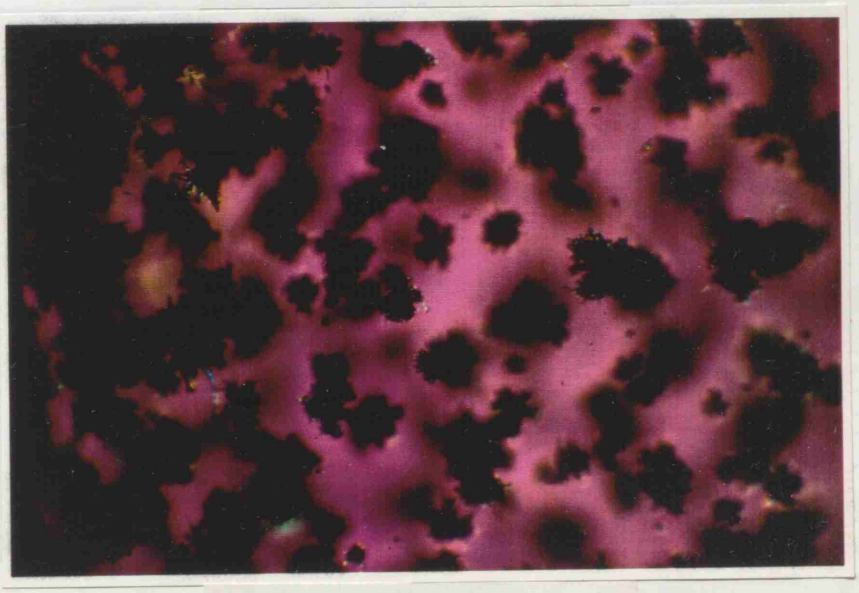

Plate 6.2.1m

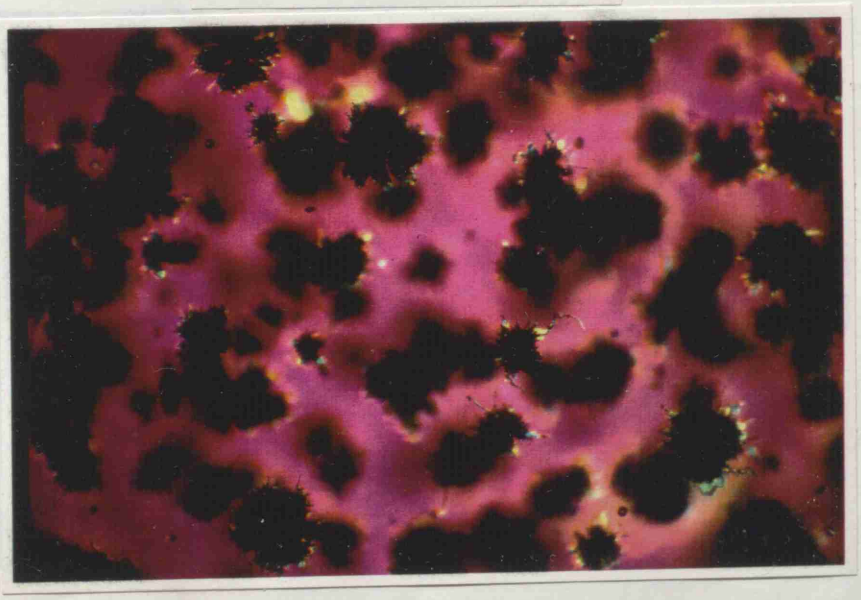

Plate 6.2.1n

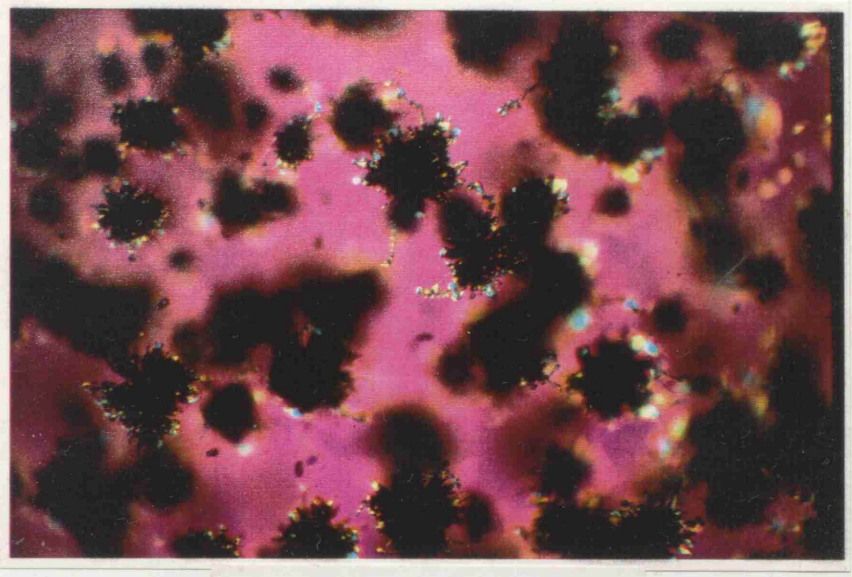

Plate 6.2.1o

Plate 6.2.1p

Plate 6.2.1q

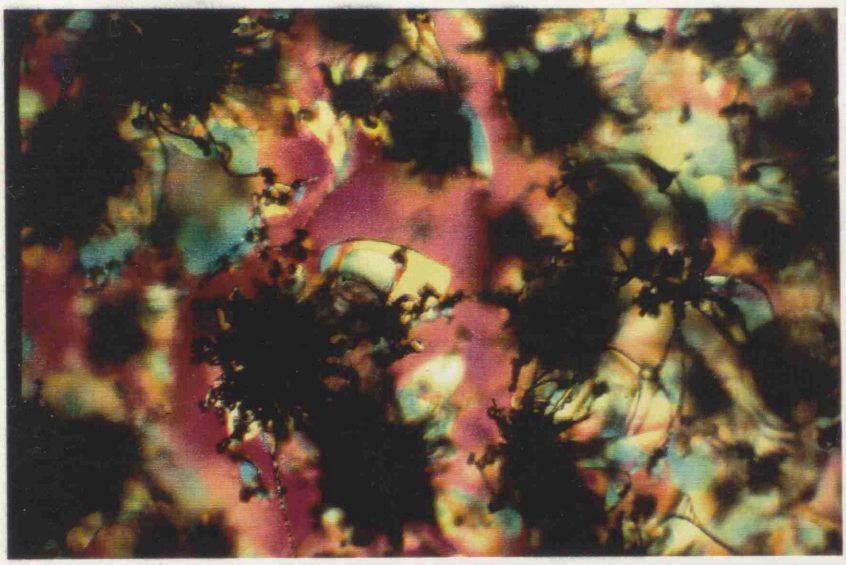

Plate 6.2.1r

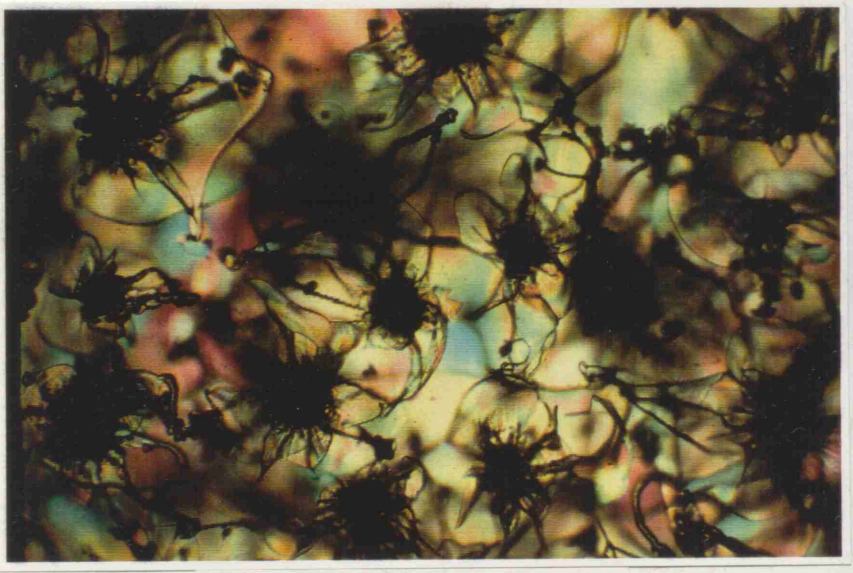

Plate 6.2.1s

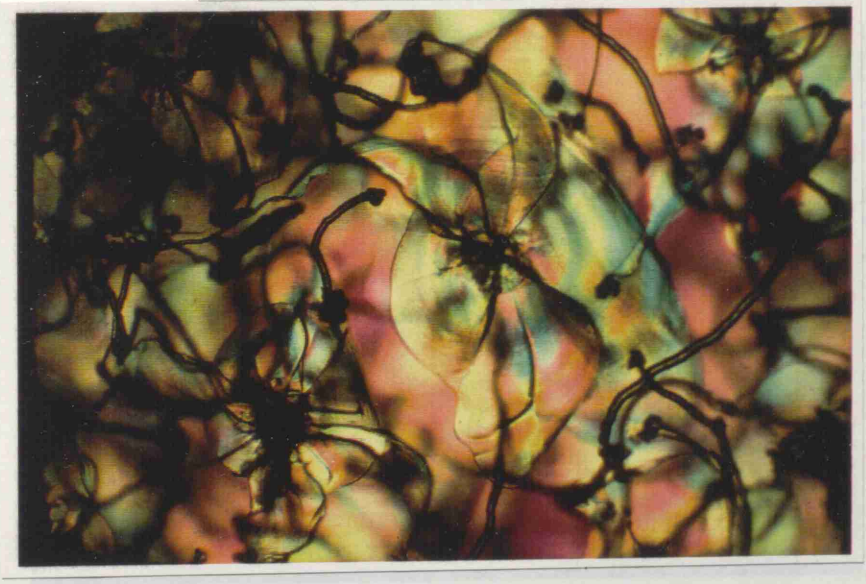

Plate 6.2.1t

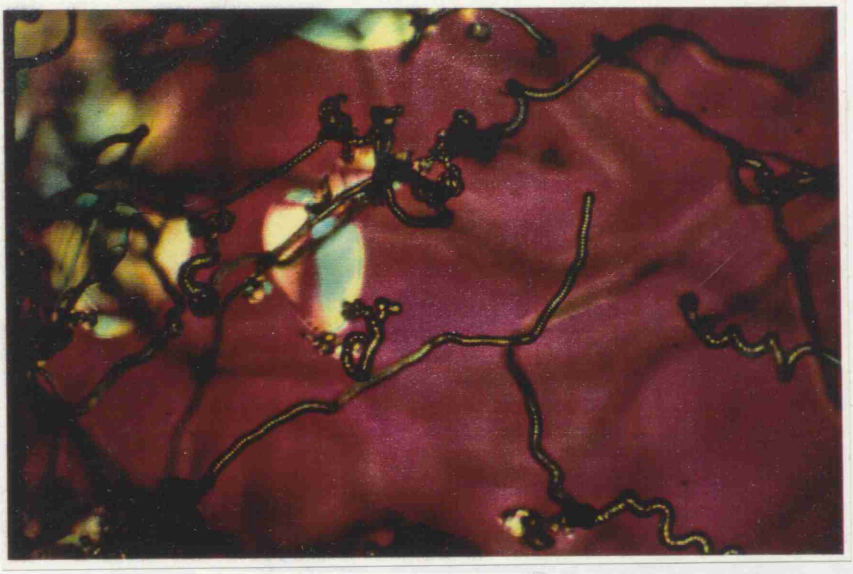

Plate 6.2.1u

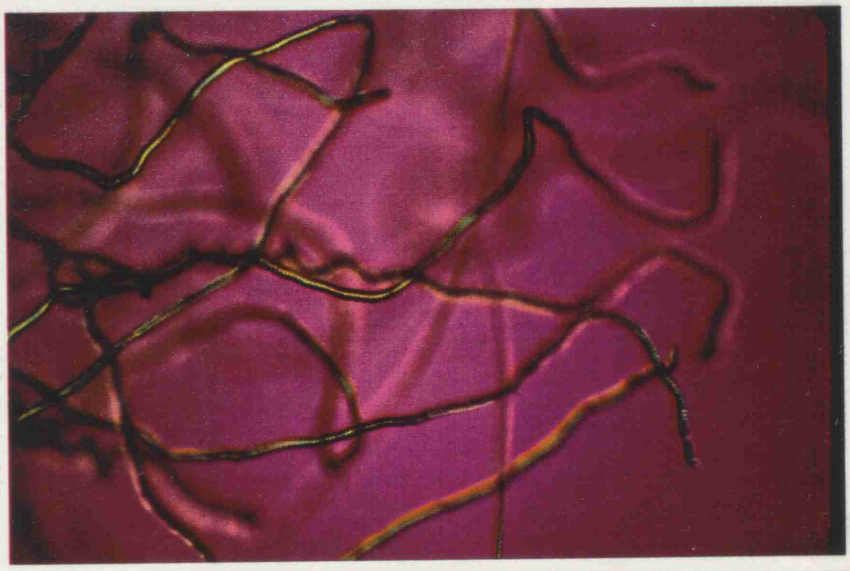

Plate 6.2.1v

Plate 6.2.1w

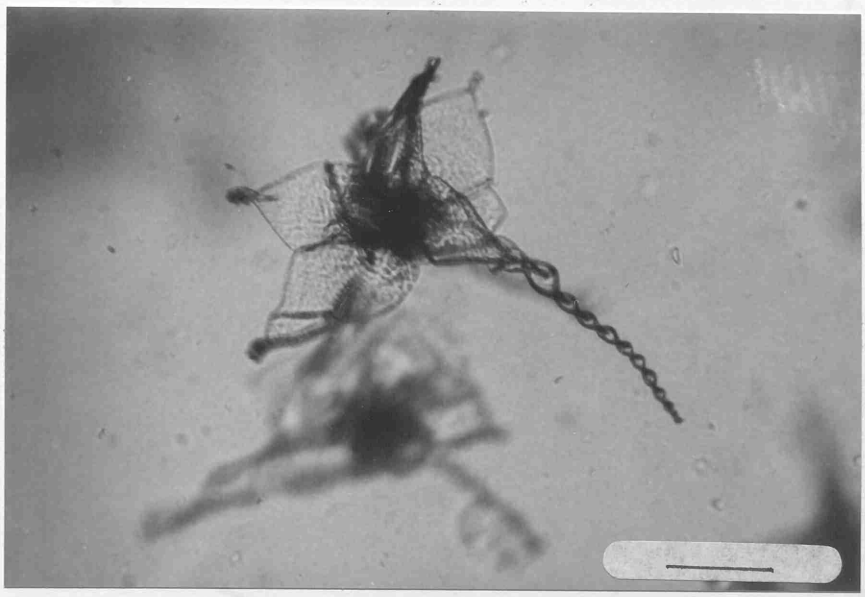

Plate 6.2.1x. BC[0.05][0.2]9.5. Scale bar 0.2 mm.

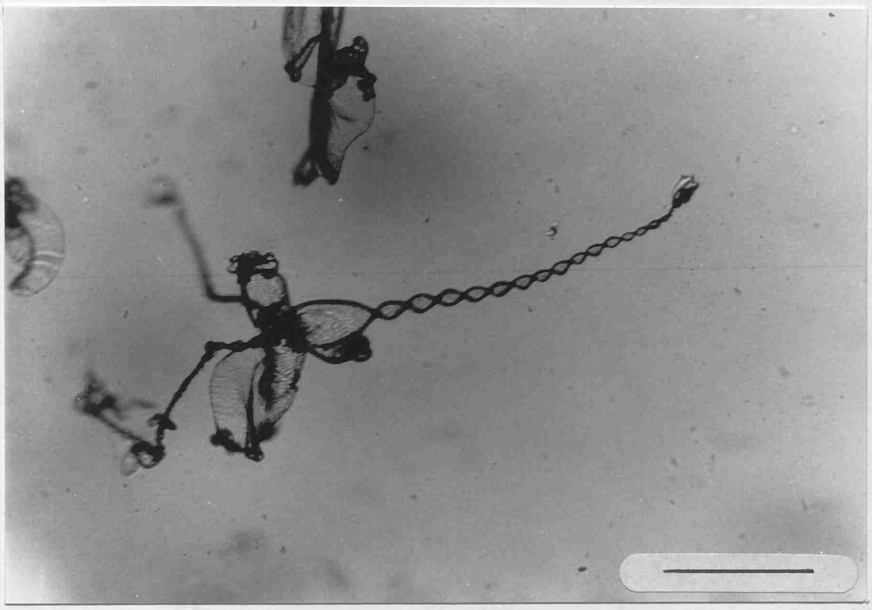

Plate 6.2.1y. BC[0][HCl]9. Scale bar 0.2 mm.

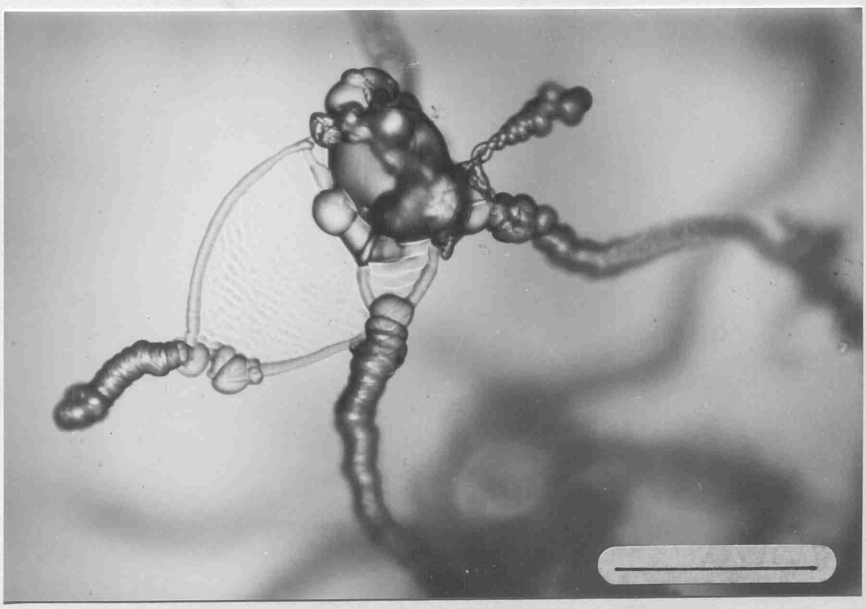

Plate 6.2.1z. BC[0.05][0.33]9.5. Scale bar 0.2 mm.

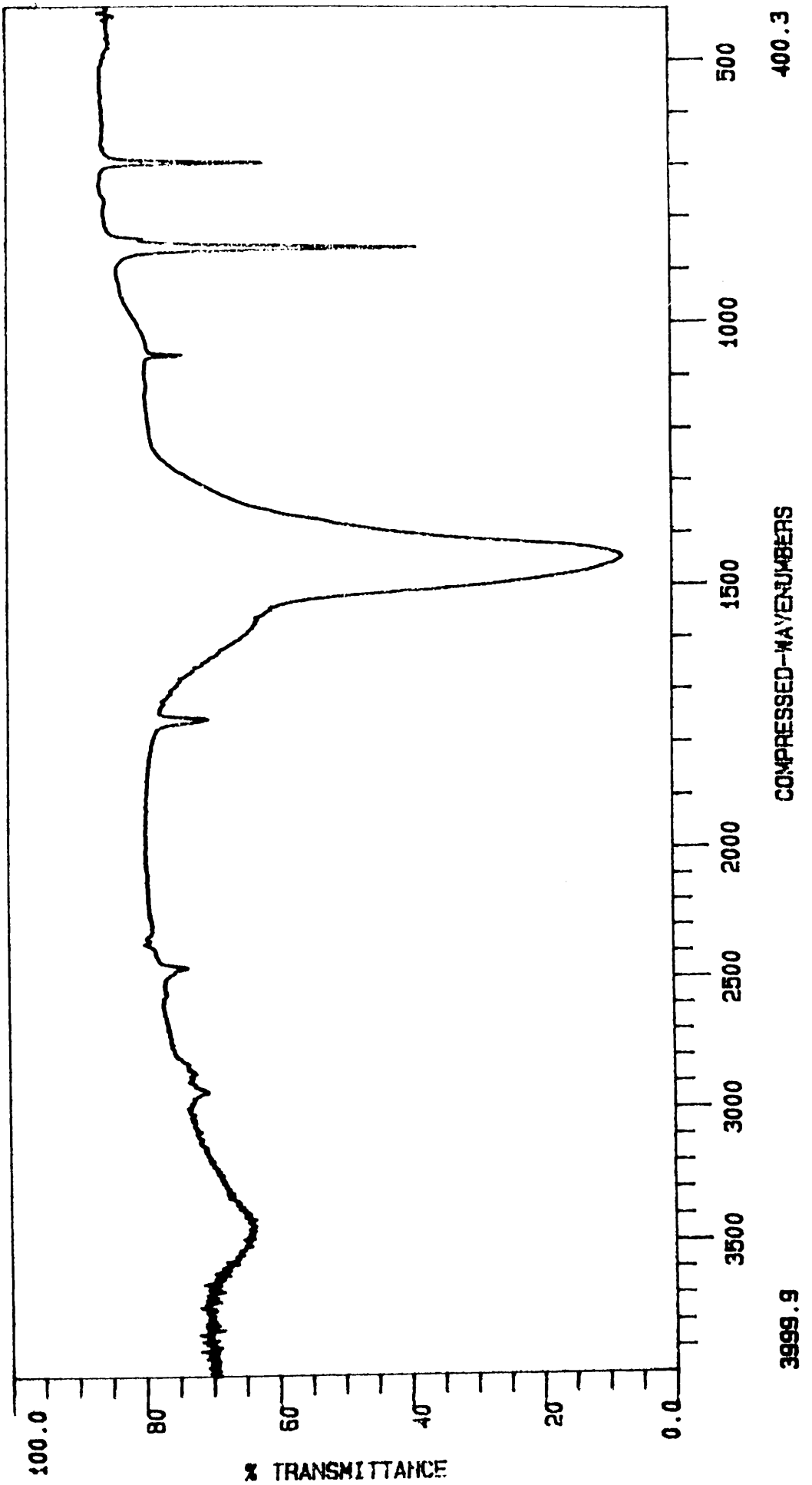

FTIR spectrum of BC[0.1]10.5

fig 6.2.2.1a

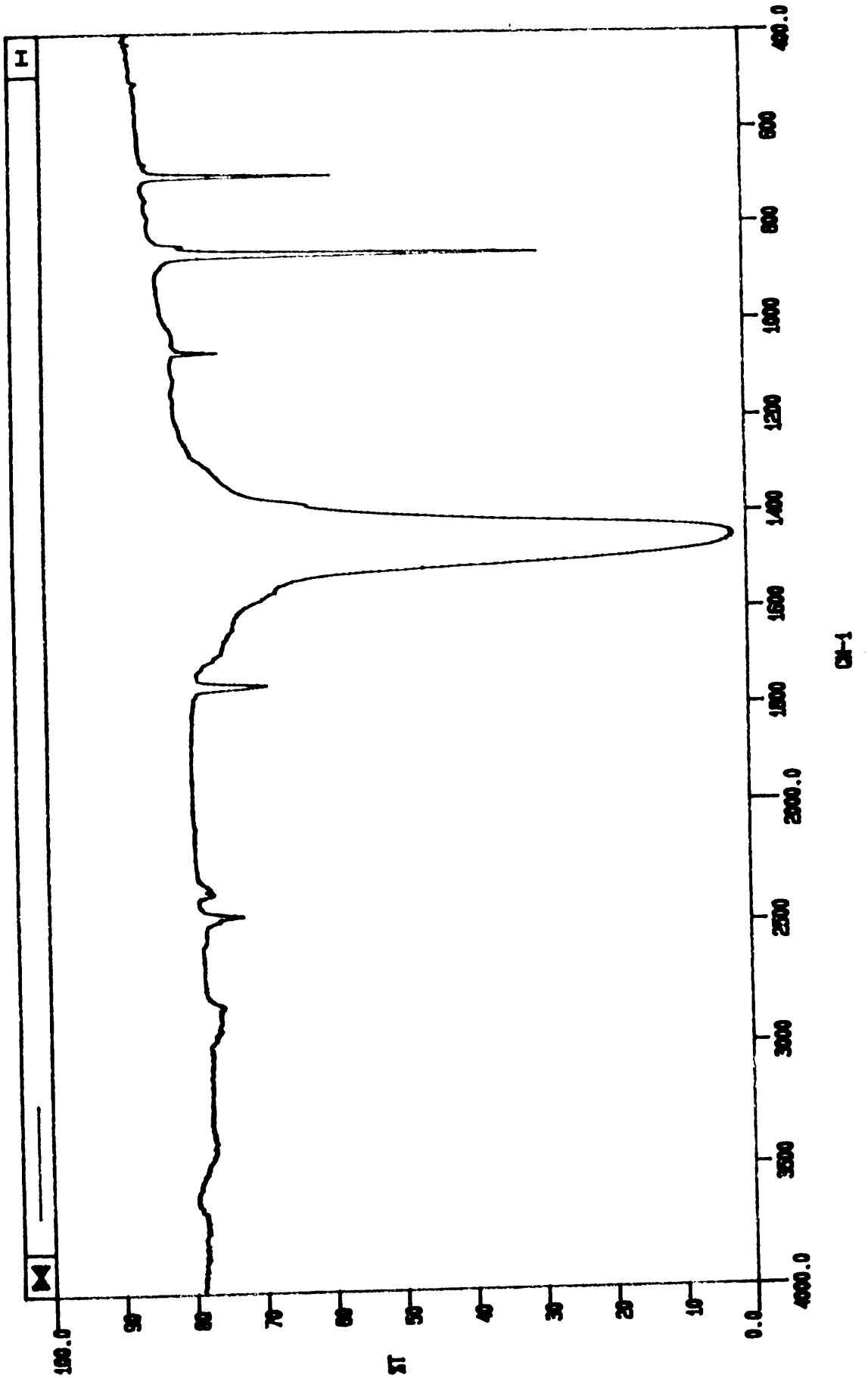

FTIR spectrum of $BaCO_3$ (AnalaR)

fig 6.2.2.1b

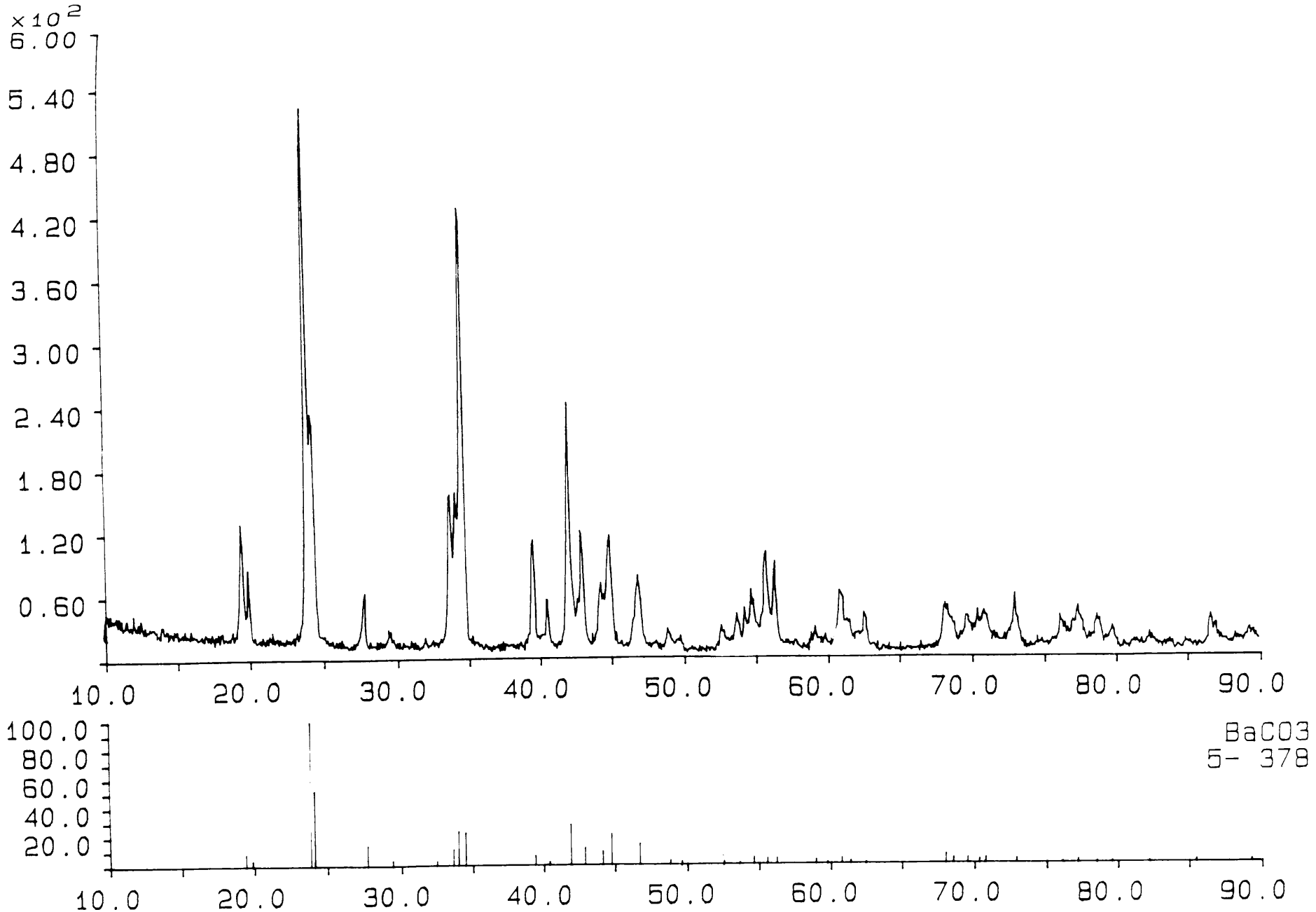

XRD of BC[0.05]9 and $BaCO_3$ reference pattern

fig 6.2.2.2a (i)

Peak no	Angle (deg)	Tip width (deg)	Peak (cts)	Backg (cts)	D spac (Ang)	I/Imax (%)
1	19.4800	0.12	71.	4.	4.5532	20.18
2	19.9400	0.12	46.	3.	4.4492	13.22
3	23.9150	0.12	350.	2.	3.7179	100.00
4	24.3225	0.14	137.	2.	3.6565	39.15
5	27.7600	0.08	31.	0.	3.2111	8.97
6	29.4950	0.40	10.	0.	3.0260	2.93
7	32.5000	0.24	10.	0.	2.7528	2.93
8	33.7500	0.10	112.	1.	2.6536	32.13
9	34.1050	0.12	83.	1.	2.6268	23.68
10	34.6400	0.12	299.	1.	2.5874	85.59
11	39.5125	0.14	76.	0.	2.2789	21.64
12	40.5375	0.16	35.	1.	2.2236	9.95
13	42.0125	0.14	169.	0.	2.1489	48.33
14	42.9825	0.12	85.	0.	2.1026	24.20
15	44.2000	0.20	30.	3.	2.0474	8.65
16	44.9000	0.12	71.	1.	2.0171	20.18
17	45.3500	0.08	10.	1.	1.9982*	2.93
18	46.8475	0.36	44.	0.	1.9377	12.46
19	48.0175	0.24	10.	0.	1.8932*	2.93
20	48.9225	0.28	14.	0.	1.8603	3.91
21	49.7825	0.08	10.	0.	1.8301	2.93
22	52.6725	0.16	16.	0.	1.7363	4.58
23	53.7200	0.16	22.	0.	1.7049	6.32
24	54.3375	0.10	24.	0.	1.6870*	6.87
25	54.7025	0.12	40.	0.	1.6766	11.35
26	55.7325	0.14	64.	1.	1.6480	18.30
27	56.3200	0.10	62.	1.	1.6322	17.85
28	59.1500	0.28	12.	0.	1.5607	3.31
29	59.4900	0.12	10.	0.	1.5526	2.93
30	60.8950	0.20	41.	0.	1.5201	11.71
31	61.4900	0.12	17.	1.	1.5068	4.81
32	62.5875	0.12	22.	2.	1.4830	6.32
33	68.1500	0.20	30.	0.	1.3749	8.65
34	69.7075	0.20	21.	0.	1.3479	6.05
35	70.4375	0.16	20.	1.	1.3357	5.79
36	70.9075	0.20	23.	1.	1.3280	6.59
37	73.0200	0.12	38.	1.	1.2947	10.99
38	74.5225	0.24	10.	1.	1.2723*	2.93
39	75.1050	0.20	10.	0.	1.2638*	2.93
40	76.2050	0.12	22.	0.	1.2483	6.32
41	77.0625	0.12	20.	0.	1.2366*	5.79
42	77.4200	0.12	27.	2.	1.2317	7.73
43	78.7850	0.08	23.	1.	1.2138	6.59
44	79.2375	0.08	10.	1.	1.2080	2.93
45	79.7625	0.16	14.	0.	1.2013	4.13
46	81.1950	0.24	10.	0.	1.1837*	2.93
47	82.2350	0.20	10.	0.	1.1714*	2.93
48	82.3200	0.16	10.	0.	1.1704	2.93
49	84.1350	0.08	10.	0.	1.1497*	2.93
50	84.9150	0.32	10.	0.	1.1411	2.93
51	86.6175	0.10	23.	0.	1.1230	6.59
52	87.6325	0.24	10.	0.	1.1126*	2.93
53	88.2825	0.24	10.	0.	1.1061*	2.93
54	89.3250	0.28	13.	0.	1.0958	3.71

BC[0.05]9 : peak angles, d-spacings and intensities

*** unnasigned peaks**

table 6.2.2.2a (ii)

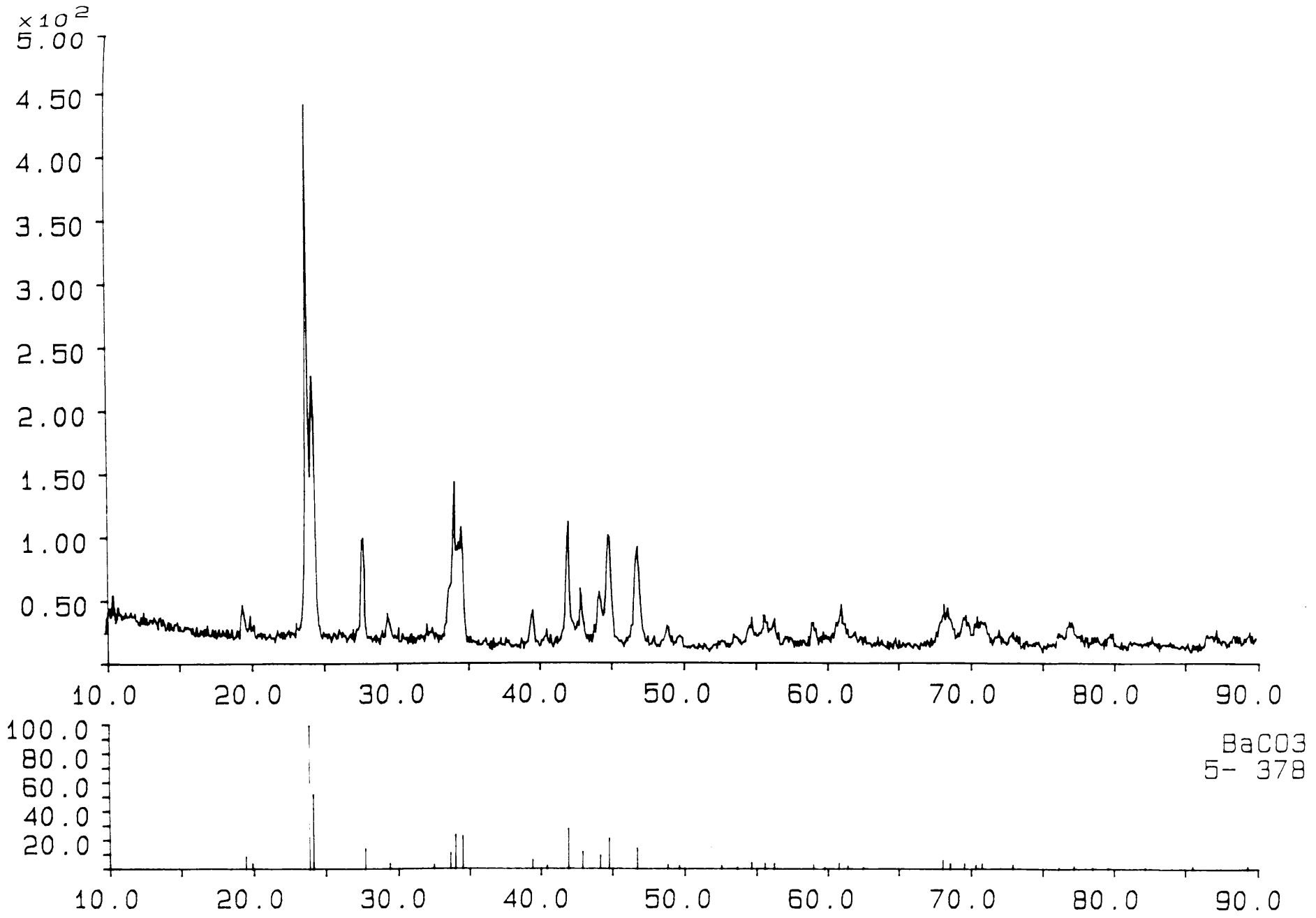

XRD of BC[0.1]10.5 and $BaCO_3$ reference pattern

fig 6.2.2.2b (i)

Peak no	Angle (deg)	Tip width (deg)	Peak (cts)	Backg (cts)	D spac (Ang)	I/Imax (%)
1	19.4025	0.16	18.	4.	4.5712	6.47
2	19.8950	0.10	13.	16.	4.4592	4.54
3	23.8725	0.10	286.	4.	3.7244	100.00
4	24.2775	0.08	146.	5.	3.6632	51.26
5	27.7000	0.08	56.	3.	3.2179	19.69
6	29.4675	0.24	16.	2.	3.0288	5.60
7	32.4800	0.10	7.	12.	2.7544	2.37
8	33.6950	0.12	27.	2.	2.6578	9.47
9	34.0800	0.10	81.	2.	2.6287	28.36
10	34.6050	0.08	62.	2.	2.5900	21.85
11	39.4775	0.24	18.	1.	2.2808	6.18
12	40.4800	0.32	10.	1.	2.2266	3.59
13	41.9575	0.12	69.	0.	2.1515	24.12
14	42.9225	0.14	36.	0.	2.1054	12.60
15	44.1675	0.12	32.	3.	2.0489	11.38
16	44.8750	0.14	67.	2.	2.0182	23.54
17	45.3525	0.10	10.	2.	1.9981 *	3.59
18	46.6925	0.12	56.	1.	1.9438	19.69
19	46.9625	0.20	38.	0.	1.9332 *	13.46
20	48.8800	0.16	15.	0.	1.8618	5.33
21	50.0250	0.16	10.	0.	1.8218	3.59
22	54.7675	0.16	16.	2.	1.6748	5.60
23	55.7025	0.12	20.	2.	1.6488	7.09
24	56.3175	0.16	18.	2.	1.6323	6.47
25	57.1675	0.24	10.	2.	1.6100 *	3.59
26	57.2725	0.10	5.	8.	1.6073 *	1.85
27	59.0475	0.16	17.	0.	1.5632	5.89
28	60.9275	0.24	17.	2.	1.5193	5.89
29	68.1125	0.16	25.	0.	1.3755	8.75
30	68.4925	0.10	14.	14.	1.3688	5.06
31	69.6075	0.32	17.	1.	1.3496	5.89
32	70.4325	0.10	13.	13.	1.3358	4.54
33	70.9350	0.24	14.	2.	1.3276	4.79
34	72.9675	0.20	10.	1.	1.2955	3.59
35	76.1600	0.16	10.	1.	1.2489	3.59
36	76.9175	0.32	14.	1.	1.2385	5.06
37	78.6775	0.10	4.	8.	1.2152	1.40
38	79.7250	0.48	10.	2.	1.2018	3.59
39	86.4200	0.24	10.	0.	1.1251	3.59
40	86.8850	0.24	12.	0.	1.1202	4.05
41	88.3750	0.40	10.	0.	1.1052 *	3.59

BC[0.1]10.5 : peak angles, d-spacings and intensities

* unnasigned peaks

table 6.2.2.2b (ii)

Ba C O3
Barium Carbonate
Witherite, syn
Hanawalt 3.72/X 3.67/5 2.15/3 2.63/2 2.59/2 2.02/2 3.22/2 1.94/2 2.10/1 2.66/1

Lambda 1.5405
Sys. Orthorhombic
SG Pmcn PS oP 20.00
a 5.314 b 8.904 c 6.430
Al Be Ga
A 0.7221 C Z 4
Dx Dm 4.308 V 304.24
F(N) 31.3 M(20) 43.1 I/Ic 4.20
d-sp
Int Diffractometer
Total d's 44
Color Colorless
Temp X-ray pattern at 26 C.

d	Int	h	k	l	d	Int	h	k	l
4.560	9	1	1	0	2.281	6	2	2	0
4.450	4	0	2	0	2.226	2	0	4	0
3.720	100	1	1	1	2.150	28	2	2	1
3.680	53	0	2	1	2.104	12	0	4	1
3.215	15	0	0	2	2.048	10	2	0	2
3.025	4	0	1	2	2.019	21	1	3	2
2.749	3	1	0	2	1.940	15	1	1	3
2.656	11	2	0	0	1.859	3	2	2	2
2.628	24	1	1	2	1.830	2	0	4	2
2.590	23	1	3	0	1.737	2	3	1	0

Reduced cell
a 5.314
b 6.430
c 8.904
Al 90.00
Be 90.00
Ga 90.00

Crystal data
a 6.430
b 8.904
c 5.314
Al 90.00
Be 90.00
Ga 90.00

d	Int	h	k	l	d	Int	h	k	l	d	Int	h	k	l
1.706	1	2	4	0	1.295	3	2	6	0					
1.677	5	3	1	1	1.248	1	2	3	4					
1.649	4	2	4	1	1.233	2	3	5	1					
1.633	4	1	5	1	1.215	1	1	7	1					
1.563	3	2	2	3	1.202	1	1	2	5					
1.543	1	0	4	3	1.202	1	2	6	2					
1.521	4	3	3	0	1.170	1	2	4	4					
1.508	2	2	4	2	1.133	2	4	3	2					
1.484	1	0	6	0	1.095	2	0	8	1					
1.375	6	3	3	2	1.095	2	4	2	3					
1.366	4	1	3	4										
1.348	4	0	6	2										
1.335	3	2	4	3										
1.328	4	4	0	2										

$BaCO_3$ reference data

unit cell parameters, d-spaces, Miller indices

table 6.2.2.2c

Plates 6.2.3a, b & c

The acid dissolution LM experiment

Plates correspond to 2.5 mm in length

Plate 6.2.3a

Plate 6.2.3b

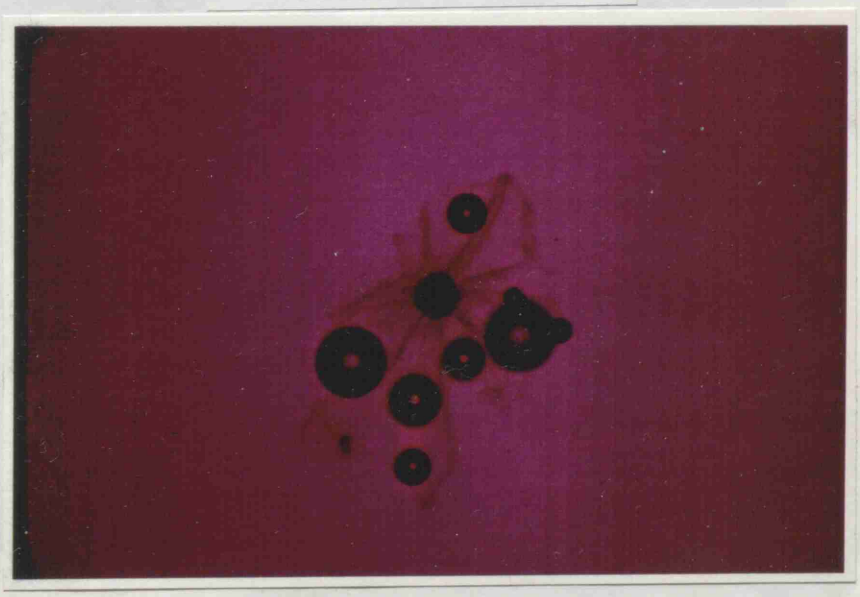

Plate 6.2.3c

Plate 6.2.4a. BC[0.05]9. Scale bar 0.1 mm.

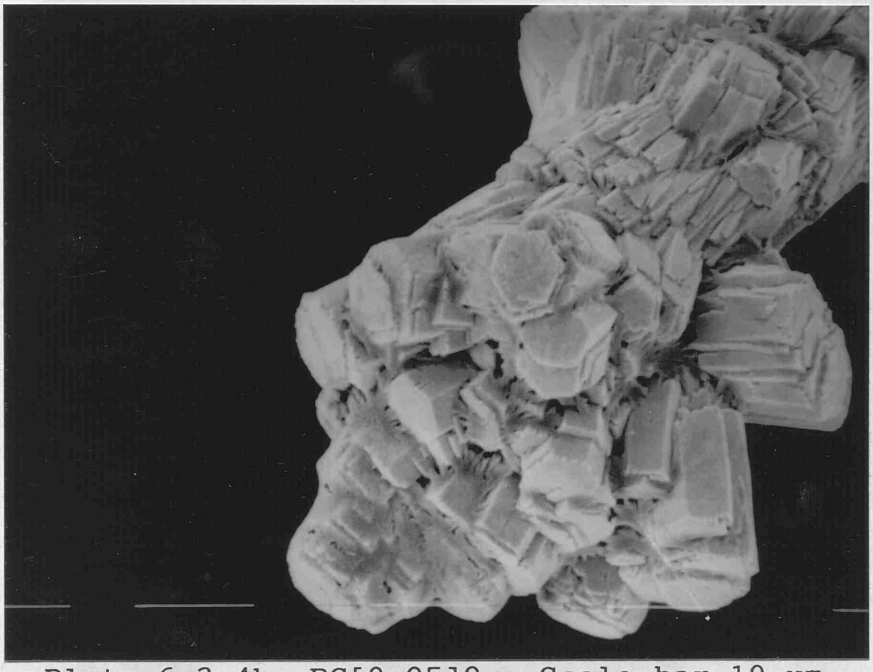

Plate 6.2.4b. BC[0.05]9. Scale bar 10 μm.

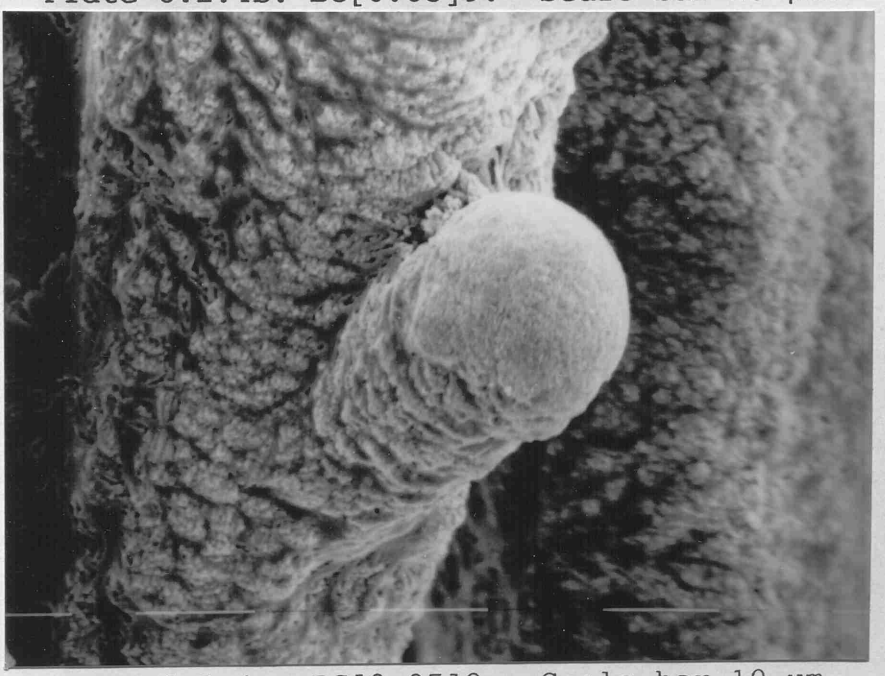

Plate 6.2.4c. BC[0.05]9. Scale bar 10 μm.

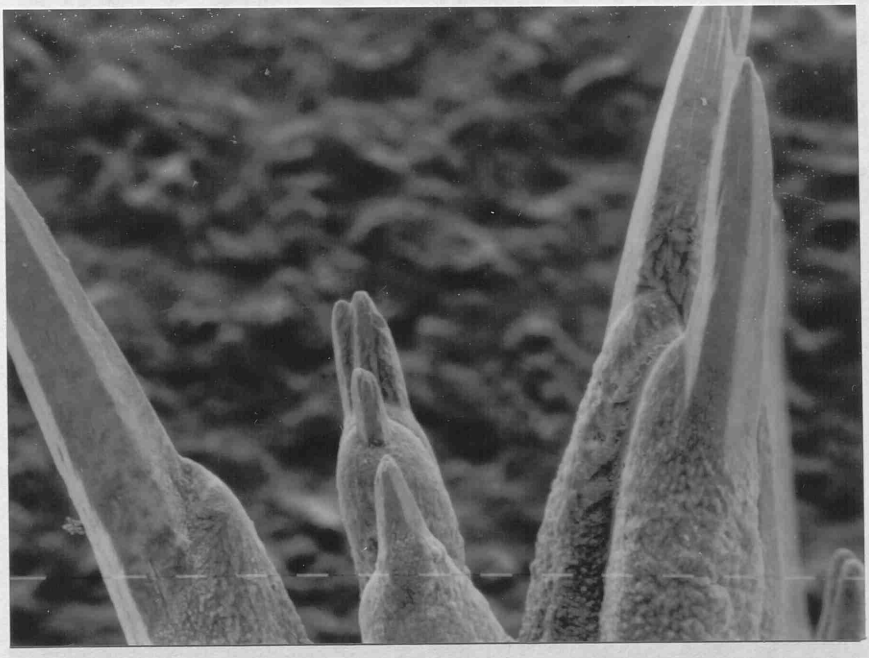

Plate 6.2.4d. BC[0.05]9. Scale bar 10 μm.

Plate 6.2.4e. BC[0.1]9.5. Scale bar 0.1 mm.

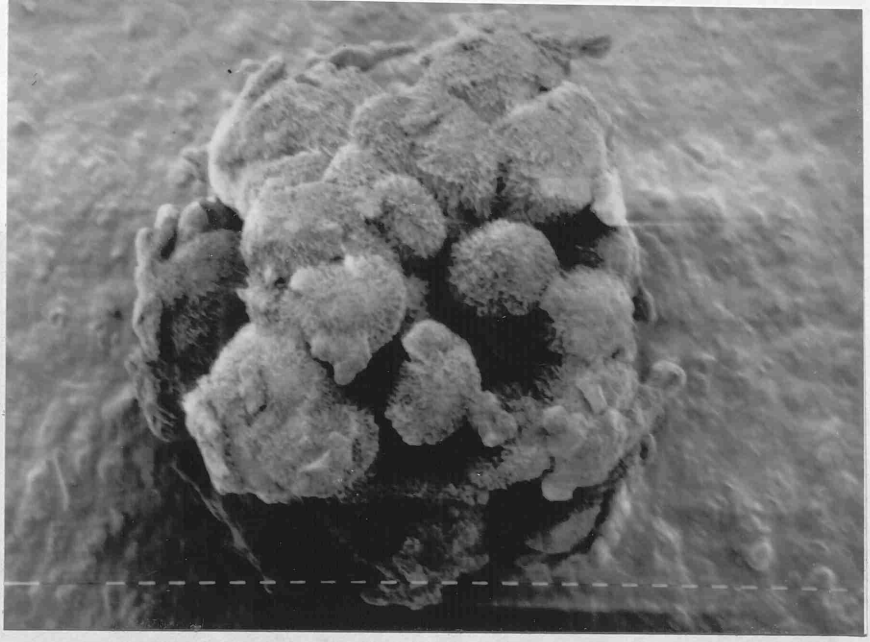

Plate 6.2.4f. BC[0.05]9.5. Scale bar 10 µm.

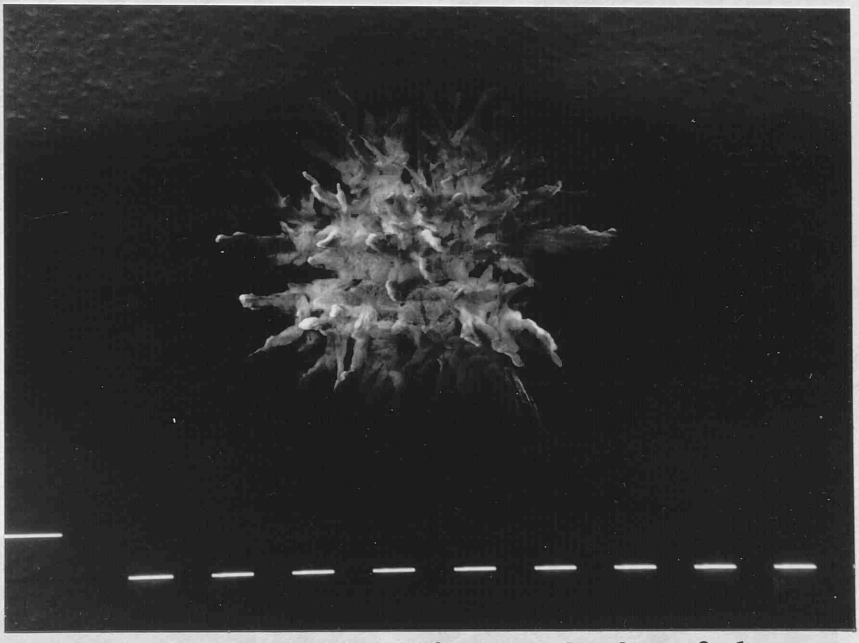

Plate 6.2.4g. BC[0.1]10. Scale bar 0.1 mm

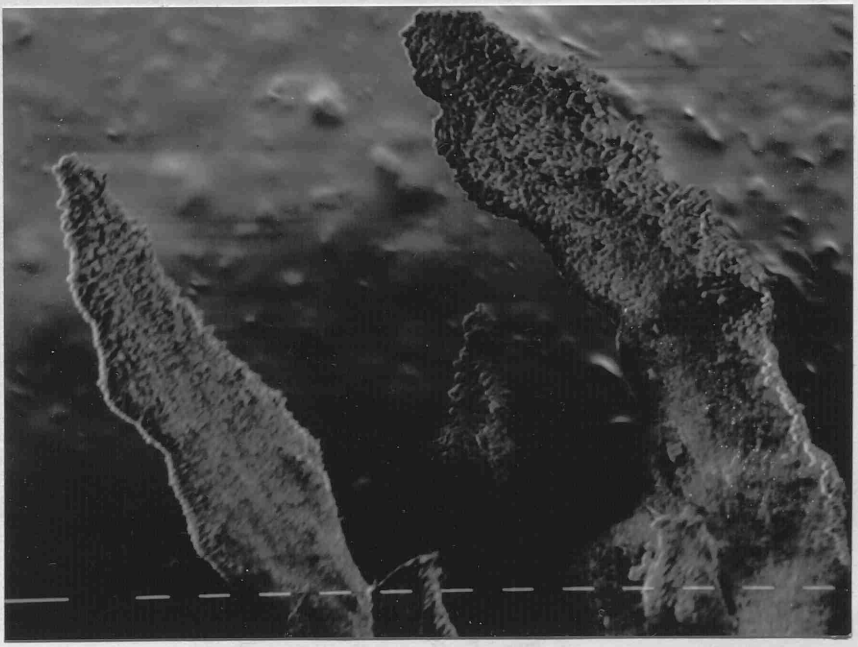

Plate 6.2.4h. BC[0.1]10. Scale bar 10 µm.

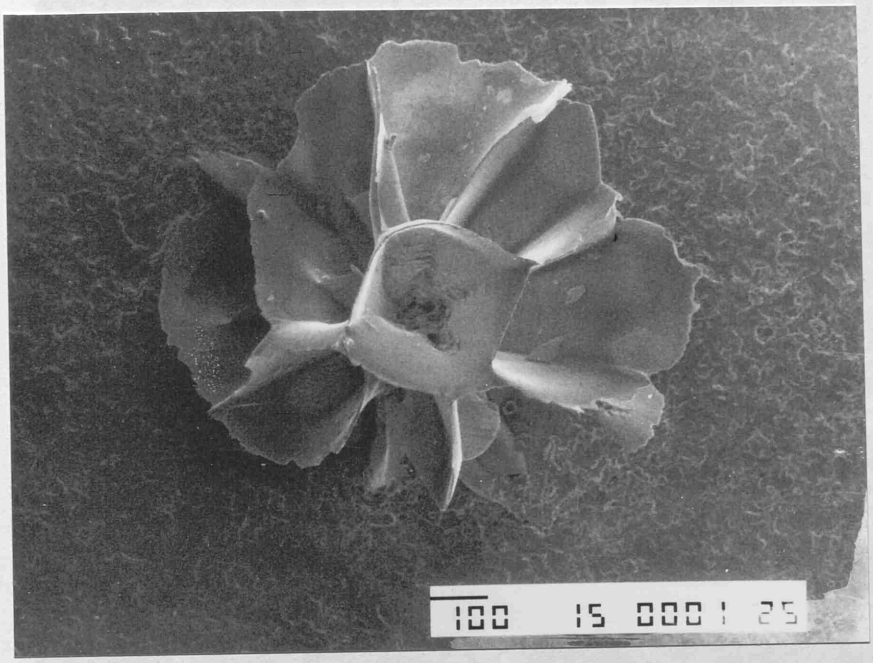

Plate 6.2.4i. BC[0.1]10.5. Scale bar 0.1 mm.

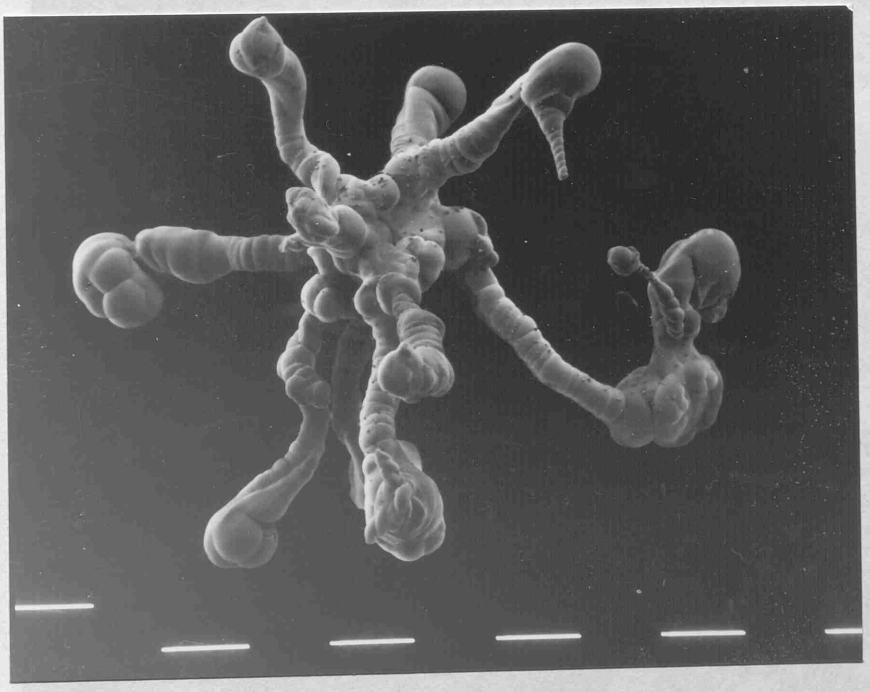

Plate 6.2.4j. Low pH, NaCl formed IMCA.
Scale bar 0.1 mm

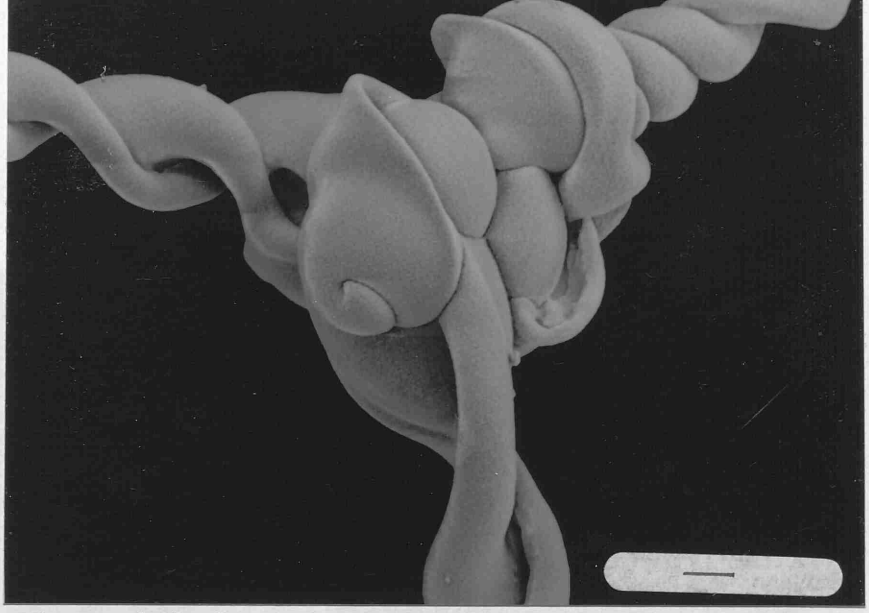

Plate 6.2.4k. IMCA detail. Scale bar 10 µm.

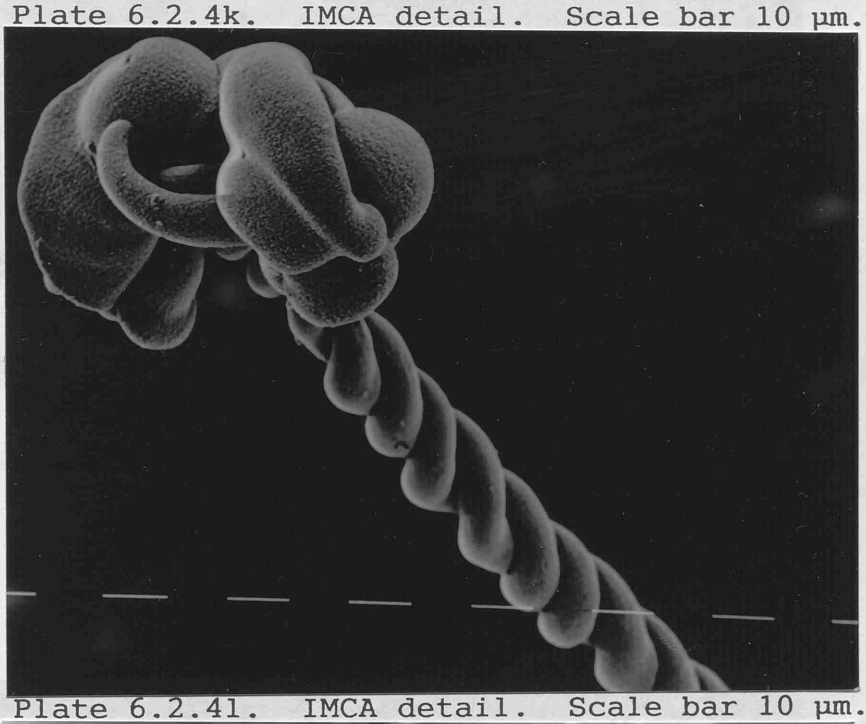

Plate 6.2.41. IMCA detail. Scale bar 10 µm.

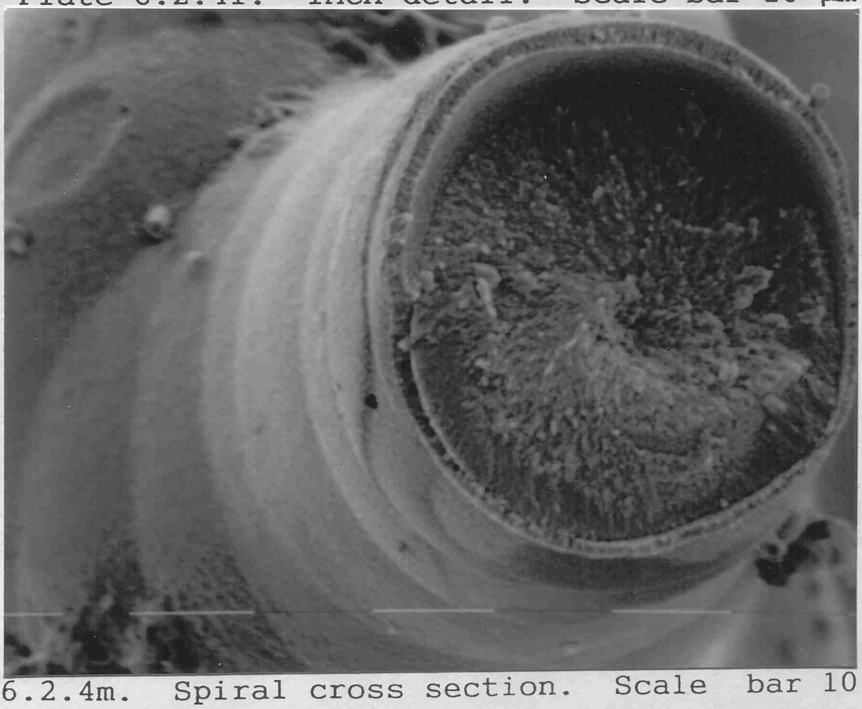

Plate 6.2.4m. Spiral cross section. Scale bar 10 µm.

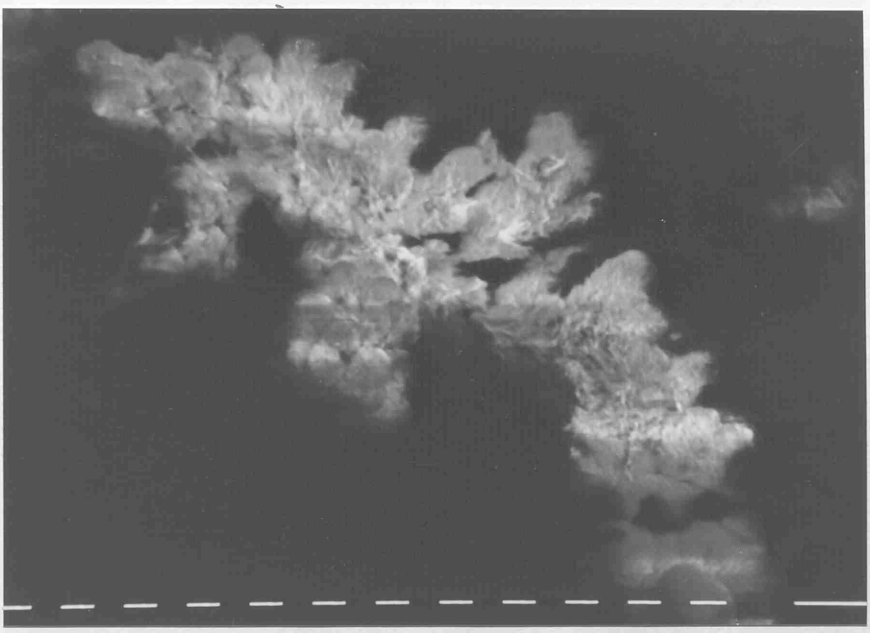

Plate 6.2.4n. Initial precipitates, neutral agarose control experiment. Scale bar 10 µm.

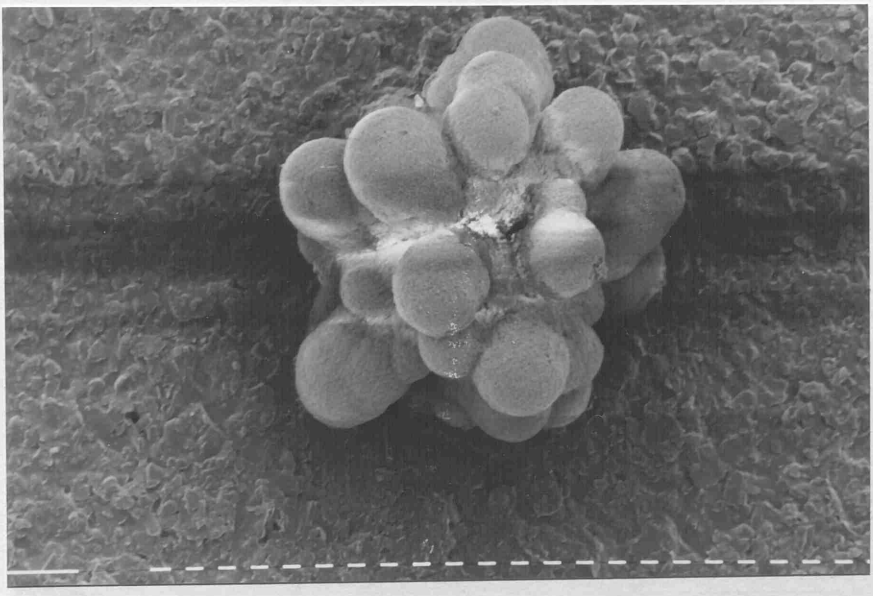

Plate 6.2.4o. Later forming precipitates, neutral agarose control experiment. Scale bar 10 µm.

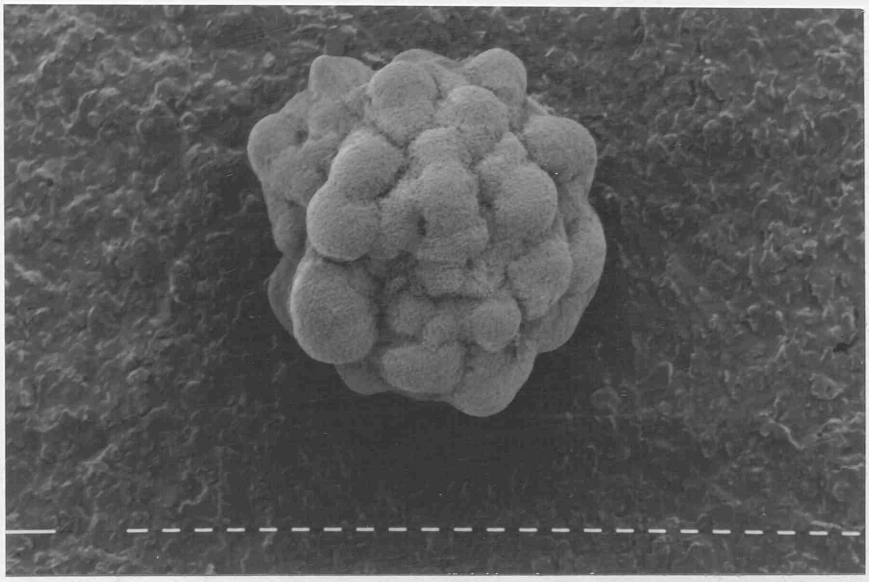

Plate 6.2.4p. Initial precipitates, basic agarose control experiment. Scale bar 10 µm.

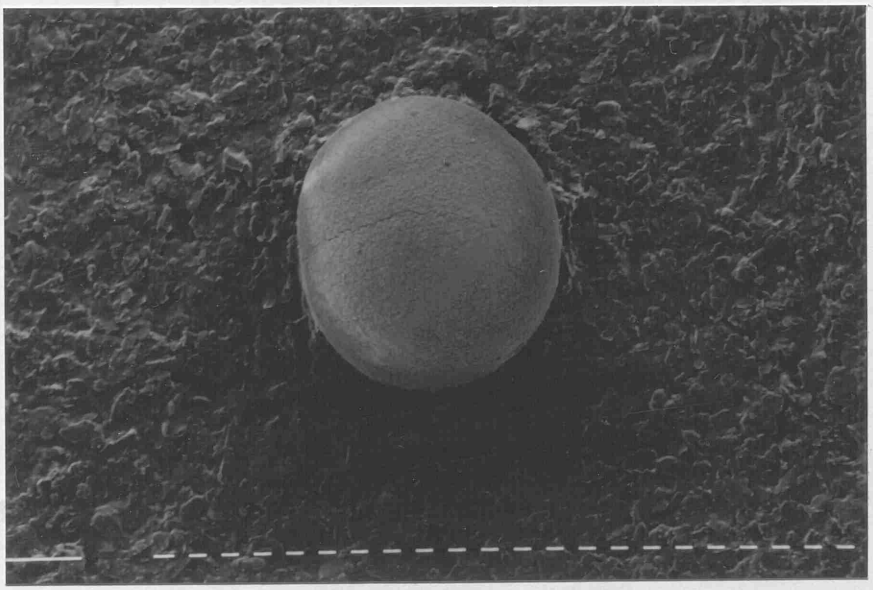

Plate 6.2.4q. Later forming precipitates, basic agarose control experiment. Scale bar 10 µm.

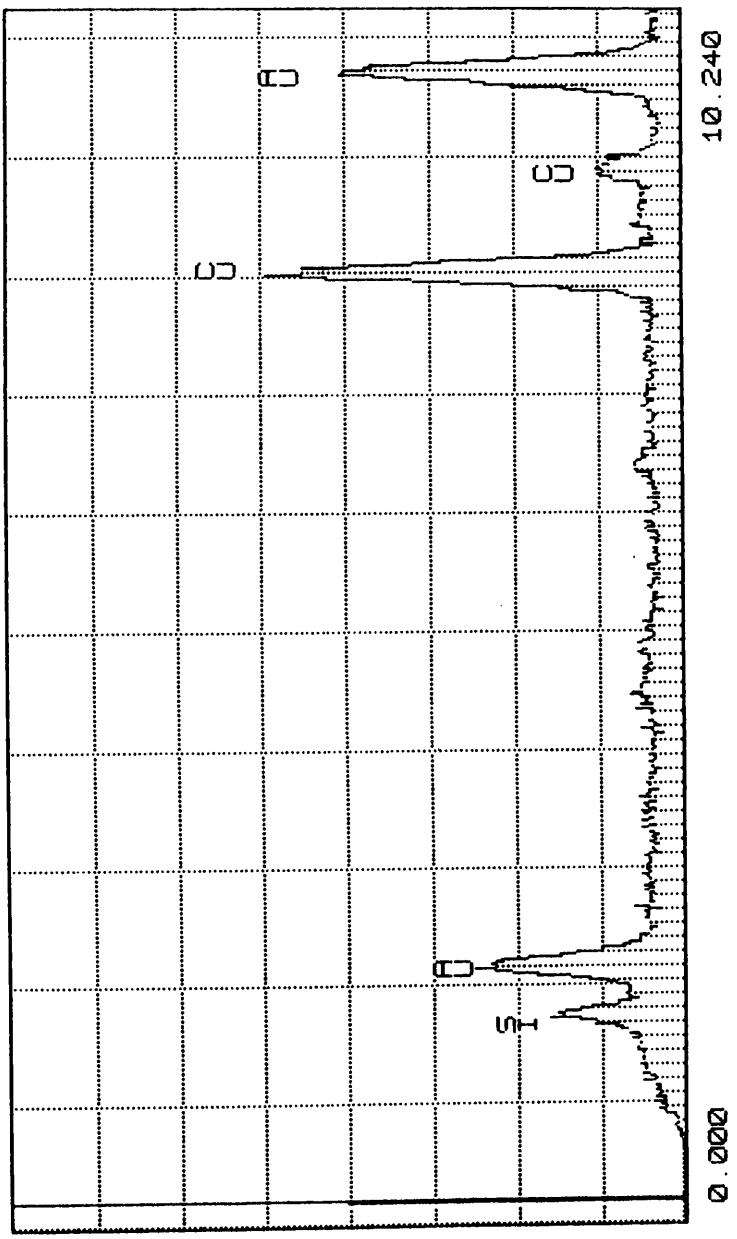

EDS analysis of membrane after acid dissolution

fig 6.2.6.1a

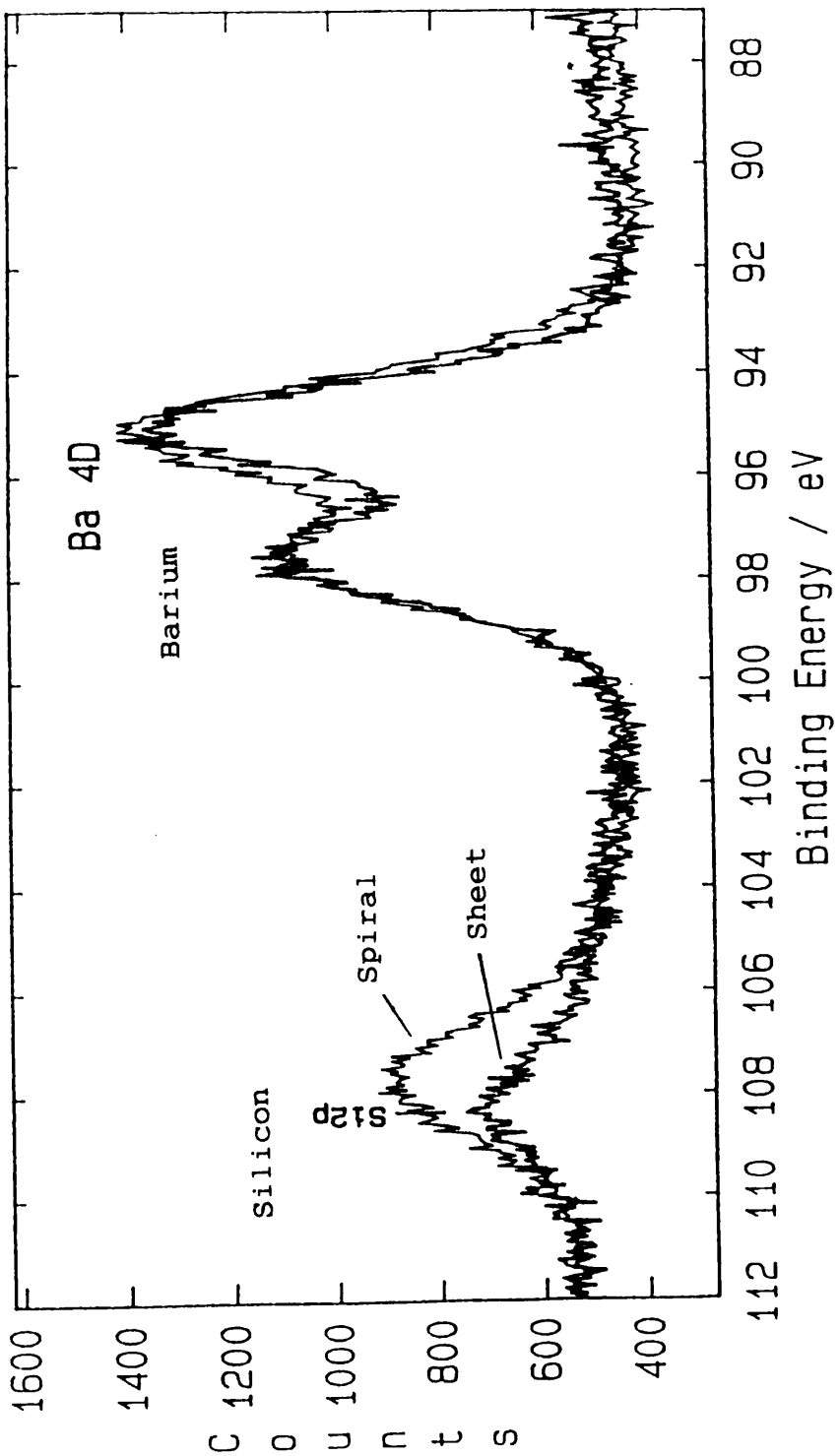

Overlaid XPS spectra showing two different silicate structures for sheet and spiral parts of an IMCA

fig 6.2.7a

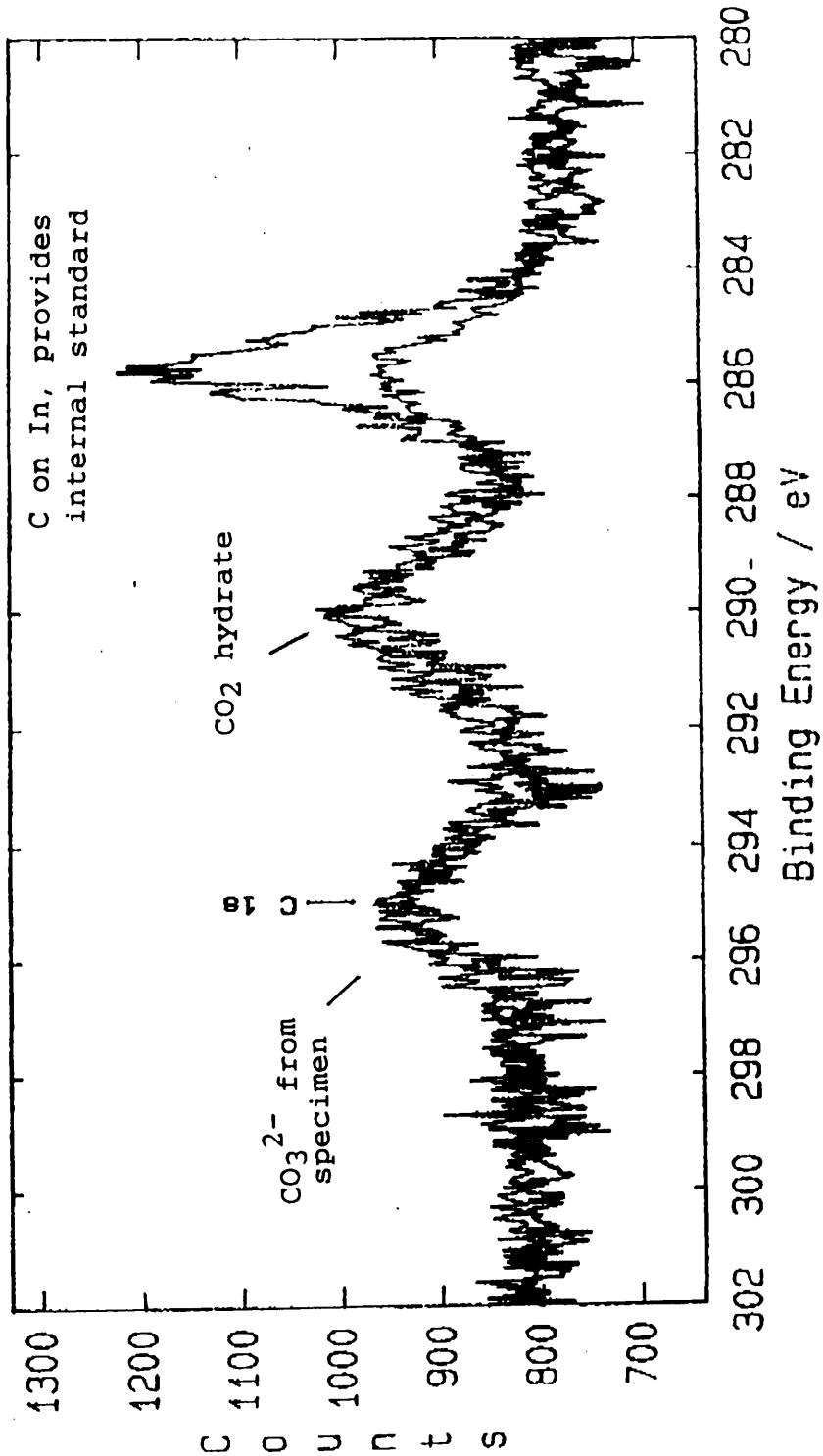

Overlaid XPS spectra showing the presence of CO_3^{2-} in the silicate structures

fig 6.2.7b

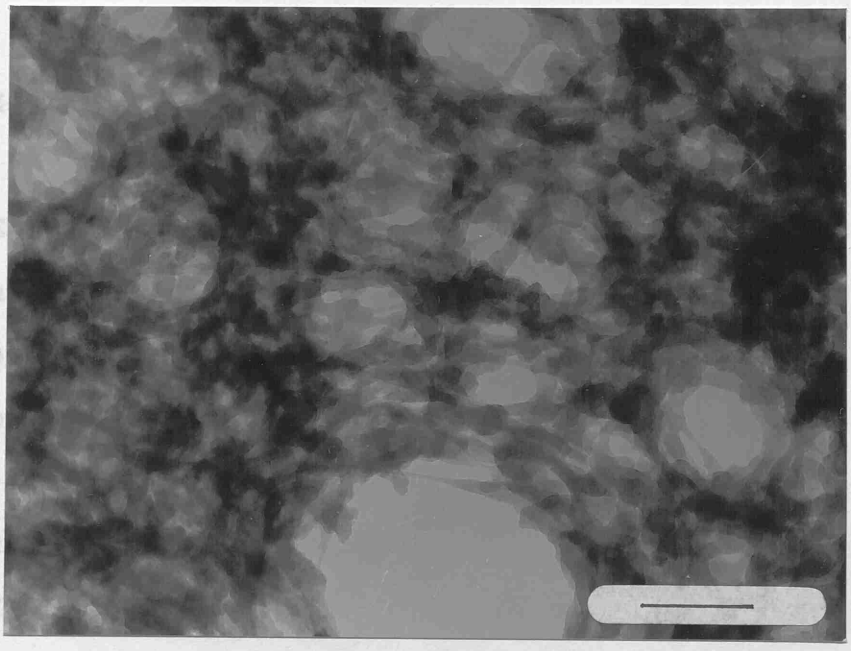

Plate 6.2.6.1a. Silica film. Scale bar 100 nm.

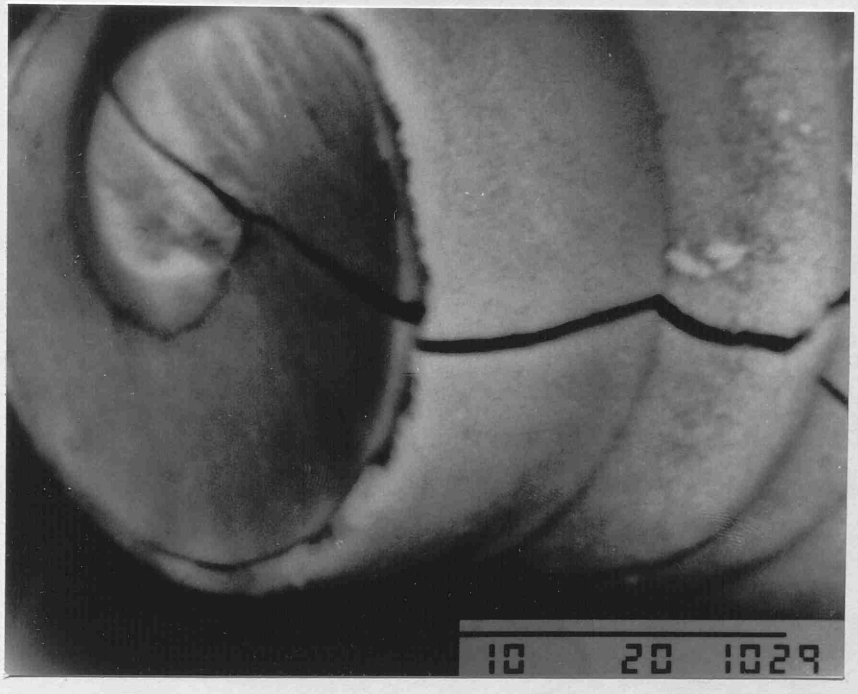

Plate 6.2.8a. Rutherford image. Scale bar 10 µm.

7 $BaSO_4$ PRECIPITATED BY A DIFFUSION MECHANISM IN SILICA GEL IN GLASS CASSETTES

7.1 EXPERIMENTAL

7.2 RESULTS

7.2.1 In-Situ Light Microscopy

7.2.2 Routine Chemical Analysis

7.2.2.1 Fourier Transform Infra-Red Spectroscopy (FTIR)

7.2.2.2 X-Ray Diffraction (XRD)

7.2.3 Scanning Electron Microscopy (SEM)

7.2.4 SEM Equipped with EDS

7.3 PRELIMINARY EXPERIMENTS ON $BaCrO_4$ AND $BaHPO_4$

7.4 DISCUSSION

7 $BaSO_4$ PRECIPITATED BY A DIFFUSION MECHANISM IN SILICA GEL IN GLASS CASSETTES

Having verified Garcia Ruiz's observations of the existence of IMCA's and establishing appropriate gel conditions for their growth, a series of experiments was devised in order to see if the effect may be quite widespread. $BaSO_4$ was chosen as an appropriate insoluble inorganic material to study.

7.1 EXPERIMENTAL

These experiments were carried out in glass cassettes (section 3.4(iii)). No buffer zones were used in these experiments. Pre-gelled silica solutions containing Na_2SO_4 were prepared according to procedure 3.1.1 including the de-gassing stage. The pH was monitored to less than one tenth of a unit using a pH meter and glass electrode. The solutions were poured into the glass cassettes and allowed to gel. The $BaCl_2$-loaded agarose gels were prepared according to procedure 3.1.4 with no further additives. The pre-gelled $BaCl_2$/agarose solutions were poured gently on top of the silica gels and the cassettes sealed. Table 7.1a lists the experiments performed and a key to understanding the nomenclature. Each experiment was carried out in duplicate and the whole procedure repeated at least once.

$BaSO_4$ Experiments

BS[0.05]8.5

BS[0.05]9

BS[0.05]10

BS[0.05][0.1]10

Key:

BS : barium sulphate

First bracket : molar concentration of Na_2SO_4

Second bracket : molar concentration of NaCl

Final figure : pH

table 7.1 a

In addition to these experiments, some agarose control experiments were carried out. These experiments were performed in test tubes. A neutral agarose gel loaded to 0.05M with Na_2SO_4 was prepared according to procedure 3.1.4. $BaCl_2$ (0.5M) in agarose was diffused through. This was repeated with a few drops of ammonia added to the gel to produce alkalinity and repeated again with ammonia and 0.2M NaCl added.

7.2 RESULTS

7.2.1 In-Situ Light Microscopy

BS[0.05]8.5 and BS[0.05]9 were very similar and produced butterfly-like objects as illustrated in plate 7.2.1a (cross polarized light view). Very often these objects would be twinned or multiple twinned. These experiments were repeated several times and depending on the exact value of pH several variations on this morphology were observed. Lower pH favoured less curved butterfly features such as in the multiple twinned example illustrated in plate 7.2.1b. Slightly higher pH values favoured induced morphology outgrowths from the butterfly-like objects, particularly at corners and edges as illustrated in 7.2.1c. In all cases the tendency for curved features and induced outgrowths increased with the later precipitates formed when the diffusion gradient was smaller.

When these butterfly-like objects are rotated under cross-polarizers with a lambda wave plate they exhibit birefringence. In the north-east diagonal position the object appears blue-green (pate 7.2.1d) and in the north-west diagonal position the object appears yellow (plate 7.2.1e). During rotation of the object to the extinction position there is no gradual colour change or loss of intensity - it is almost instantaneous, suggesting the main planar part (not the outgrowths at the centre of the object) is of the same crystal grain.

In experiment BS[0.05]10 the first precipitates to form are curved butterfly-like objects. Later-forming precipitates have induced growth at corners and edges and the final precipitates formed contain a mass of induced growths as observed as in plate 7.2.1f.

In BS[0.05][0.1]10 the early precipitates (6 mm from the interface between silica and agarose gels) are similar to the butterfly-like objects but with a great deal of induced growth as illustrated in plate 7.2.1g. In later precipitates (18 mm from interface) the induced growth influences the overall morphology to such an extent that the butterfly features are lost and irregular objects result with the beginnings of spiral structures protruding from them (plate 7.2.1h). These objects become larger and still remain very irregular up to 30 mm from the interface (plate 7.2.1i). From this point the precipitates become more regular. Very common in this

experiment were box-like or spherical centres with sheet-like and/or tightly wound spiral outgrowths as in plate 7.2.1j & k.

In the sheet-like structures a uni-axial dark cross (Maltese) cross was visible under cross-polarizers (plate 7.2.1l). This remained stationary when the objects were rotated suggesting that these objects were indeed IMCA's

In all the agarose control experiments platelet crystals formed. The curvature of the glass of the test tubes and the depth of the gel made in-situ photo-microscopy difficult. These precipitates are best observed by SEM (section 7.2.3)

7.2.2 Routine Chemical Analysis

Precipitates were removed from the latter stages of growth of experiment BS[0.05]10 (butterfly features with induced outgrowths) by dissolving the gel in NaOH (prepared with the minimum carbonate and CO_2 impurities) in accordance with procedure 3.5.2. Precipitates were also removed from the neutral agarose control experiment by dissolving the gel in warm de-gassed water in accordance with procedure 3.5.3.

Removed from their gels and observed by light microscopy under the addition of acid no precipitate dissolution was observed indicating the material was not $BaCO_3$.

7.2.2.1 Fourier Transform Infra-Red Spectroscopy (FTIR)

FTIR spectroscopy was carried out in accordance with procedure 3.5.6. Fig 7.2.2.1a is the FTIR spectrum of BS[0.05]10. Fig 7.2.2.1b is the FTIR spectrum of the material from the neutral agarose control experiment. Fig 7.2.2.1c is the FTIR spectrum of reagent grade $BaSO_4$. The Aldrich Dictionary of Inorganic FTIR spectra lists the FTIR peaks for $BaSO_4$ as 1189, 1077, 983, 638 and 610 cm^{-1}. These wavenumbers correspond to the peaks observed for the reference $BaSO_4$ spectrum (7.2.2.1c). All other peaks in the reference spectrum correspond to water, carbon dioxide and material used to coat instrument detector. The FTIR spectrum of BS[0.05]10 also contains $BaSO_4$ peaks at 1182, 1078, 983, 636 and 611 cm^{-1} in excellent agreement with the reference spectrum and the Aldrich dictionary. In addition to these there are small peaks at 858 and 694 cm^{-1} which can be attributed to $BaCO_3$ (by comparison to spectra discussed in 6.2.2.1). At 1440 and 1402 cm^{-1} there are two peaks which fall within the main carbonate stretch band (1451 cm^{-1}) for $BaCO_3$. This may be attributed to $BaCO_3$ although it is not understood why there are two peaks rather than one. The FTIR spectrum of washed and dried silica gel indicated that the peak at 444 cm^{-1} was due to silica gel adhering to the precipitates. The peaks around 1550 - 1750 cm^{-1} are unassigned and the others are due to water, carbon dioxide and instrument detector coatings.

The FTIR spectrum of the material from the agarose control experiment (fig 7.2.2.1b) contained $BaSO_4$ peaks measured at 1181, 1083, 981, 634 and 609 cm^{-1}. In this case there are no $BaCO_3$ peaks at 858 and 694 cm^{-1} although the two peaks within the main $BaCO_3$ stretch (1451 cm^{-1}) are present, this time measured at 1438 and 1402 cm^{-1} but the overall intensity of the two peaks is much lower than in the previous sample and the relative intensity of the 1438 peak is much less than the 1440 peak in comparison to the previous sample. As expected there are no peaks due to adhering silica gel although there are peaks (and more intense in this case) in the range 1550 - 1750 cm^{-1} previously unnasigned in BS[0.05]10. In this case it can be envisaged that these may be organic stretches due to agarose gel, however this would not explain there appearance in BS[0.05]10. All other peaks are due to water, carbon dioxide, and detector coatings.

Finally fig 7.2.2.1d is the FTIR spectra of BS[0.05]10 removed from the gel after prolonged soaking in NaOH. Both $BaSO_4$ and $BaCO_3$ peaks are present indicating that prolonged exposure to NaOH transforms $BaSO_4$ to $BaCO_3$. If the material is left in NaOH for 2 -3 days then a total transformation to $BaCO_3$ occurs.

In summary the FTIR analysis indicates that the main phase present in both samples is $BaSO_4$. The FTIR spectra of the material from the control experiment suggests that

a trace of $BaCO_3$ may be incorporated in the pecipitation. The FTIR spectrum of the material soaked in NaOH for a prolonged period indicated that this treatment leads to the formation of $BaCO_3$ so it is not certain how much of the $BaCO_3$ identified in BS[0.05]10 was incorporated during the precipitation or was formed during the removal from the gel.

7.2.2.2 X-Ray Diffraction (XRD)

XRD analysis was carried out in accordance with procedure 3.5.6 (Cu alpha 1, 2 radiation). Fig 7.2.2.2a (i) is the XRD pattern of BS[0.05]10 and printed below is the $BaSO_4$ reference pattern from the powder diffraction files (24-1035). Table 7.2.2.2a (ii) lists the measured peak angles, d-spacings and intensities. Fig 7.2.2.2b (i) is the XRD pattern of the material from the neutral agarose control experiment and printed below the $BaSO_4$ reference pattern. Table 7.2.2.2b (ii) lists measured peak angles, d-spacings and intensities. Table 7.2.2.2c lists the reference unit cell parameters, d-spacings, intesities and Miller indices of $BaSO_4$ from the powder diffraction files.

In BS[0.05]10 peaks below 1.3001 Å are not considered since the reference pattern has not been scanned in this range. In the material from the control experiment peaks below 1.3009 Å are not considered for the same reason.

In both samples it can be seen that the patterns show the presence of $BaSO_4$ with orthorhombic symmetry, however, as was the case for $BaCO_3$ there are a few differences from the reference pattern:

(i) Some peaks are not fully resolved from adjacent ones, eg, in BS[0.05]10 (7.2.2.2a (i)) the peak which should be due to the 2.735 Å spacing is not recorded since it is not fully resolved from the 2.7232 Å spacing (reference value 2.729 Å) and in the material from the control experiment the peak corresponding to 2.1096 Å (reference value 2.106 Å) is not fully resolved from the peak due to the 2.1203 Å spacing (reference value 2.121 Å).

(ii) Relative peak intensities differ from the reference pattern, eg in the control experiment material the 4.4448 Å peak is significantly more intense than in the reference pattern and the 4.3305 Å peak is significantly less intense than in the reference pattern.

(iii) A few additional (unassigned) low intensity peaks are also present. These peaks are asterixed in tables 7.2.2.2a (ii) and b (ii)

Since FTIR analysis suggested that a trace amount of $BaCO_3$ may have been incorporated in both samples, this may explain why a few peaks are slightly shifted and not fully resolved. The difference in relative intensities of the peaks may again be due to orientational effects. In

point (ii) the two peaks discussed correspond to Miller indices which describe crystal planes perpendicular to each other further suggesting that orientational effects may be responsible. These effects may be inherent in the sample or caused by the XRD sample preparation. The additional unassigned peaks are due to materials other than $BaSO_4$ in the sample, possibly $BaCO_3$, NaOH, Na_2SO_4, $BaCl_2$ and in the case of BS[0.05]10 perhaps a barium silicate structure.

Ignoring additional peaks and by matching measured reflections to the reference reflections unit cell parameters were calculated for the material from the agarose control experiment.

They are:

a = 7.1569 b = 8.8836 c = 5.4502

in comparison to the reference values:

a = 7.1565 b = 8.8811 c = 5.4541

An additional XRD analysis carried out on BS[0.05]10 after prolonged soaking in NaOH (3 days) gave no pattern at all, indicating an amorphous material. Since this material was identified as $BaCO_3$ by FTIR spectroscopy (fig 7.2.2.1d) it can be concluded that the transformation of $BaSO_4$ to $BaCO_3$ is the transformation of a crystalline phase to an amorphous phase.

7.2.3 Scanning Electron Microscopy (SEM)

The precipitates removed from silica gel by the method just described were prepared for SEM analysis according to procedure 3.5.4.

The butterfly-like objects obtained from BS[0.05]8.5 and BS[0.05]9 had an appearance illustrated in plate 7.2.3a. The example illustrated in plate 7.2.3b is a multiple twinned butterfly-like object. The less curved features of this example indicate it was formed at a slightly lower pH value than the previous one. Plate 7.2.3c is an example of a butterfly-like object containing induced growths at corners and edges. This precipitate was removed from BS[0.05]10.

Plate 7.2.3d is an example of an object removed from the later stages of BS[0.05][0.1]10. The box-like centre which was seen by LM can be seen to be a spherical centre with sheet-like outgrowths giving the appearance of a box. The outgrowths then developed into two conical sheet-like structures with further induced outgrowths at corners and edges.

Plate 7.2.3e is an object from the same experiment illustrating the spiral morphology which is obtained in this system and plate 7.2.3f is a more detailed view of another spherical centre (cracked) with outgrowths giving a box-like appearance.

Plate 7.2.3g is an example of the platelet morphologies observed in the agarose control experiments.

7.2.4 SEM Equipped With EDS

A $BaSO_4$ IMCA removed from BS[0.05][0.1]10 was subjected to EDS analysis (fig 7.2.4a). Peaks can be clearly seen for Ba, S and Si giving further evidence for the existence of $BaSO_4$ IMCA's.

7.3 PRELIMINARY EXPERIMENTS ON $BaCrO_4$ AND $BaHPO_4$

Preliminary experiments carried out during a stay at the University of North Texas and in collaboration with P. Chen revealed that $BaCrO_4$ and $BaHPO_4$ IMCA's could also be obtained. These materials were precipitated by an analogous method to the $BaCO_3$ and $BaSO_4$ methods and similar morphologies and trends were observed. IMCA's contained spherical centres, sheet-like structures and spiral parts. It was also observed that high pH and the presence of NaCl promoted IMCA formation. This work was continued by P. Chen and a full account will appear in his Ph.D. thesis (Chen, 1992).

7.4 DISCUSSION

From the results just described it can be concluded that $BaSO_4$ IMCA's can indeed be precipitated and from the preliminary experiments carried out on $BaCrO_4$ and $BaHPO_4$ it would appear that the effect may be quite widespread in insoluble barium salts.

It was observed from XRD and FTIR that $BaSO_4$ was the material precipitated in these experiments, however, both analyses suggested that a small amount of $BaCO_3$ may have been incorporated in the precipitation. There was no strong evidence for the presence of a barium silicate structure either, however, EDS analysis did confirm the presence of Ba, S and Si.

It was observed that $BaSO_4$ IMCA's have similar morphological characteristics to the previously described $BaCO_3$ IMCA's, eg spherical centres, sheet-like structures and spiral parts and that under cross-polarized light a uniaxial dark cross was observed which remained stationary when the object was rotated.

It was also observed that pH and the presence of NaCl in the gel had major effects on the formation of IMCA's. In the absence of NaCl and in the pH range 8.5 - 10 a morphogenetical transition was observed from butterfly-like objects to butterfly-like objects with induced growths at corners and edges through to objects with some

butterfly features and a mass of induced growths. At pH 10 and in the presence of NaCl fully induced morphologies were formed.

In the agarose control experiments platelet morphologies formed througout. NaCl presence and pH had no effect on morphology. These morphologies can be considered to be butterfly objects without the curves and the very first stage in the morphogenetical transition, free from the influence of silicates.

A full account of the IMCA phenomenon, the factors which affect it and the transition towards it is given in chapter 9.

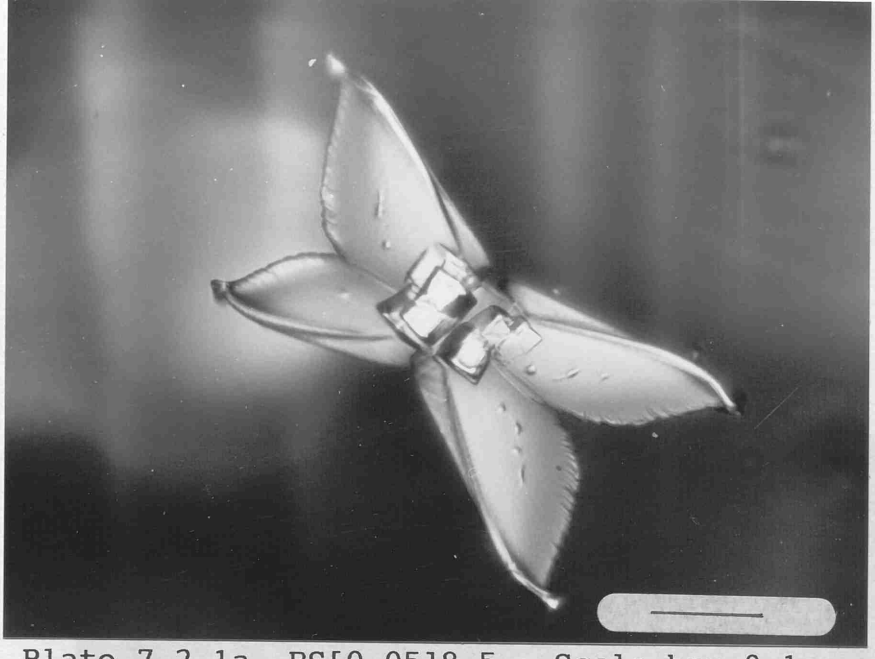

Plate 7.2.1a. BS[0.05]8.5. Scale bar 0.1mm.

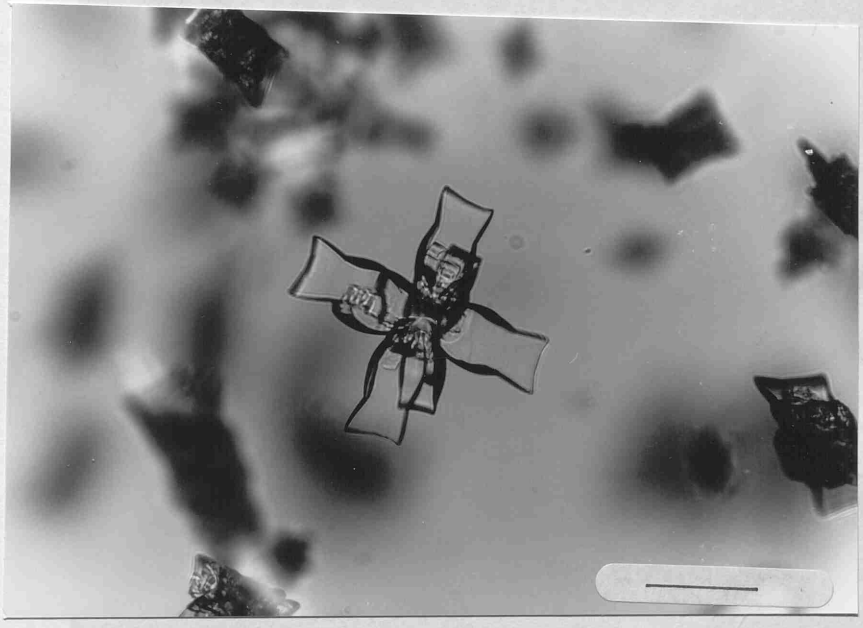

Plate 7.2.1b. BS[0.05]8.5. Scale bar 0.1mm.

Plate 7.2.1c. BS[0.05]9. Scale bar 0.1mm.

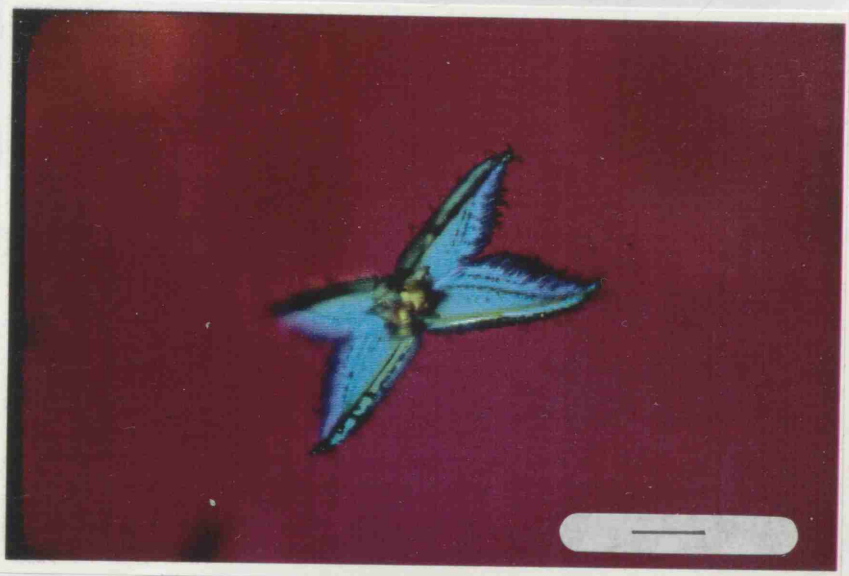

Plate 7.2.1d. Birifringence in butterfly-like objects. Scale bar 0.1mm.

Plate 7.2.1e. Birifringence in butterfly-like objects. Scale bar 0.1mm.

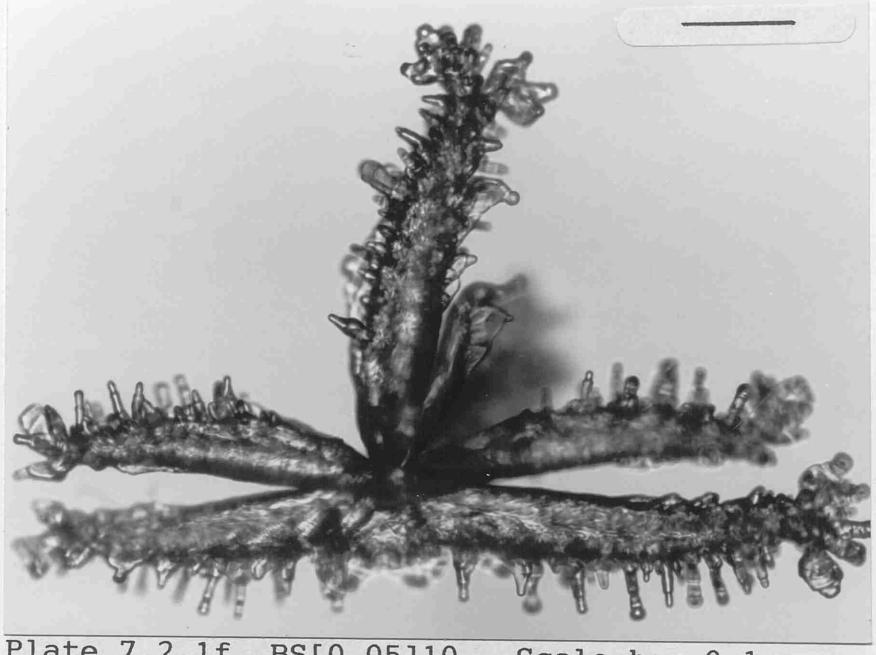

Plate 7.2.1f. BS[0.05]10. Scale bar 0.1mm.

Plate 7.2.1g. BS[0.05][0.1]10. Scale bar 0.1mm.

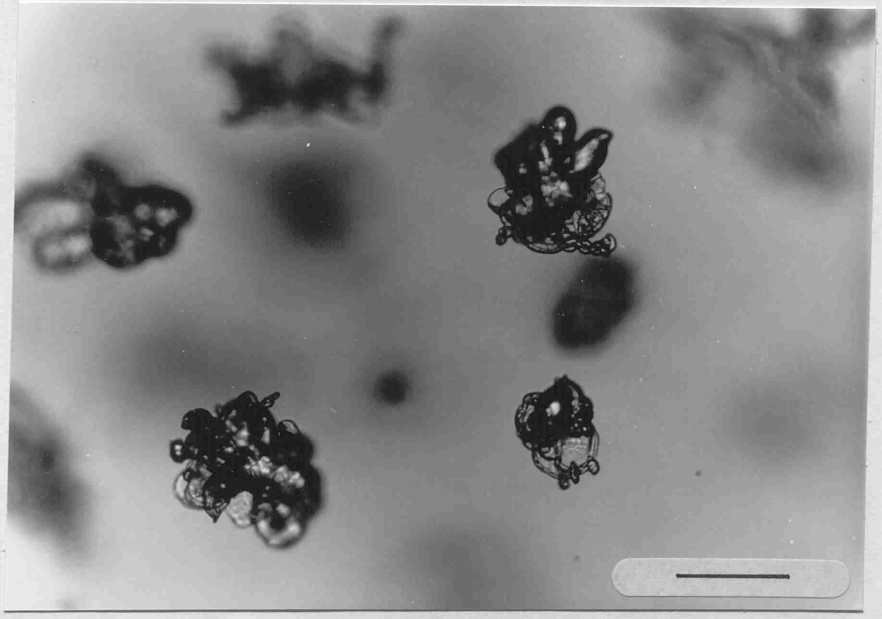

Plate 7.2.1h. BS[0.05][0.1]10. Scale bar 0.1mm.

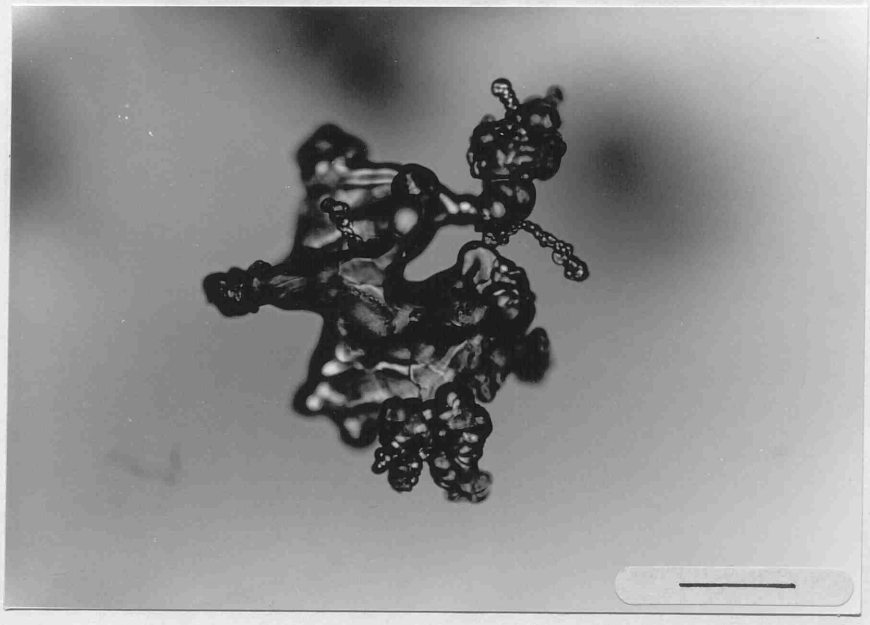

Plate 7.2.1i. BS[0.05][0.1]10. Scale bar 0.1mm.

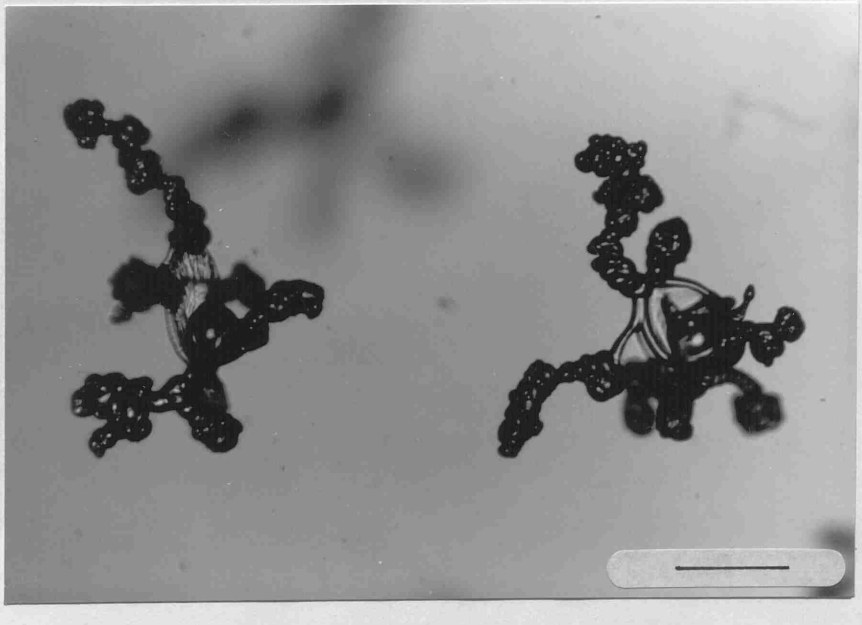

Plate 7.2.1j. BS[0.05][0.1]10. Scale bar 0.2mm.

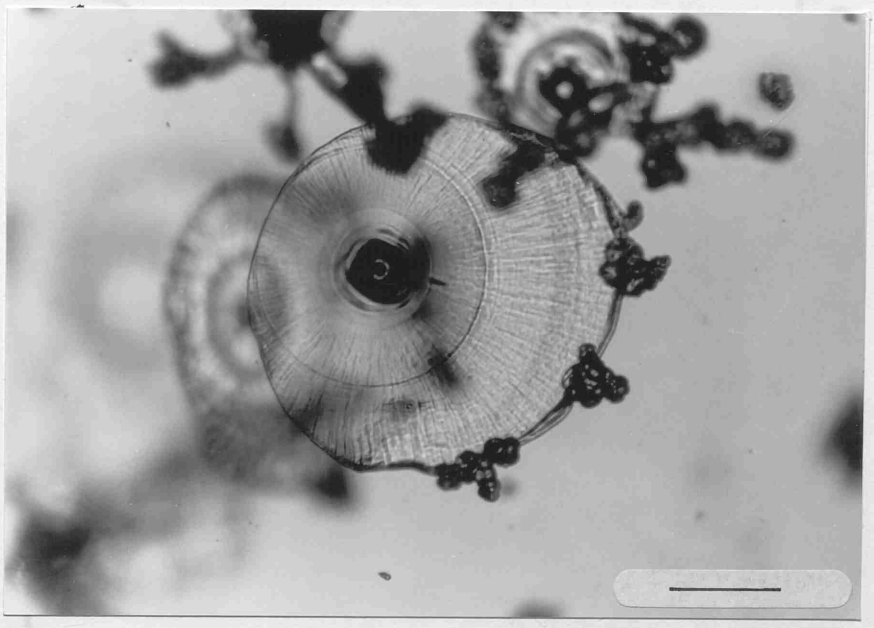

Plate 7.2.1k. BS[0.05][0.1]10. Scale bar 0.2 mm.

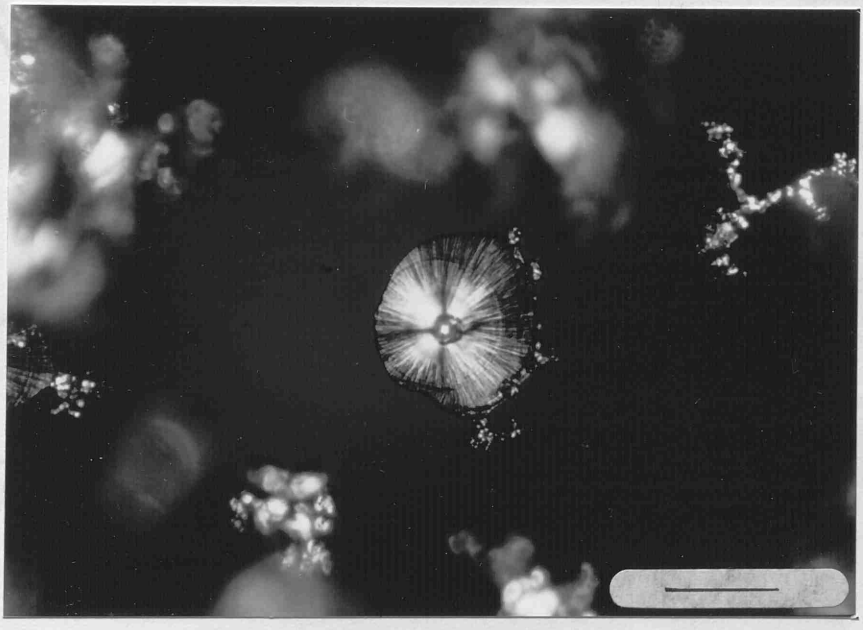

Plate 7.2.1l. BS[0.05][0.1]10. Scale bar 0.4mm.
Under cross-polarizers.

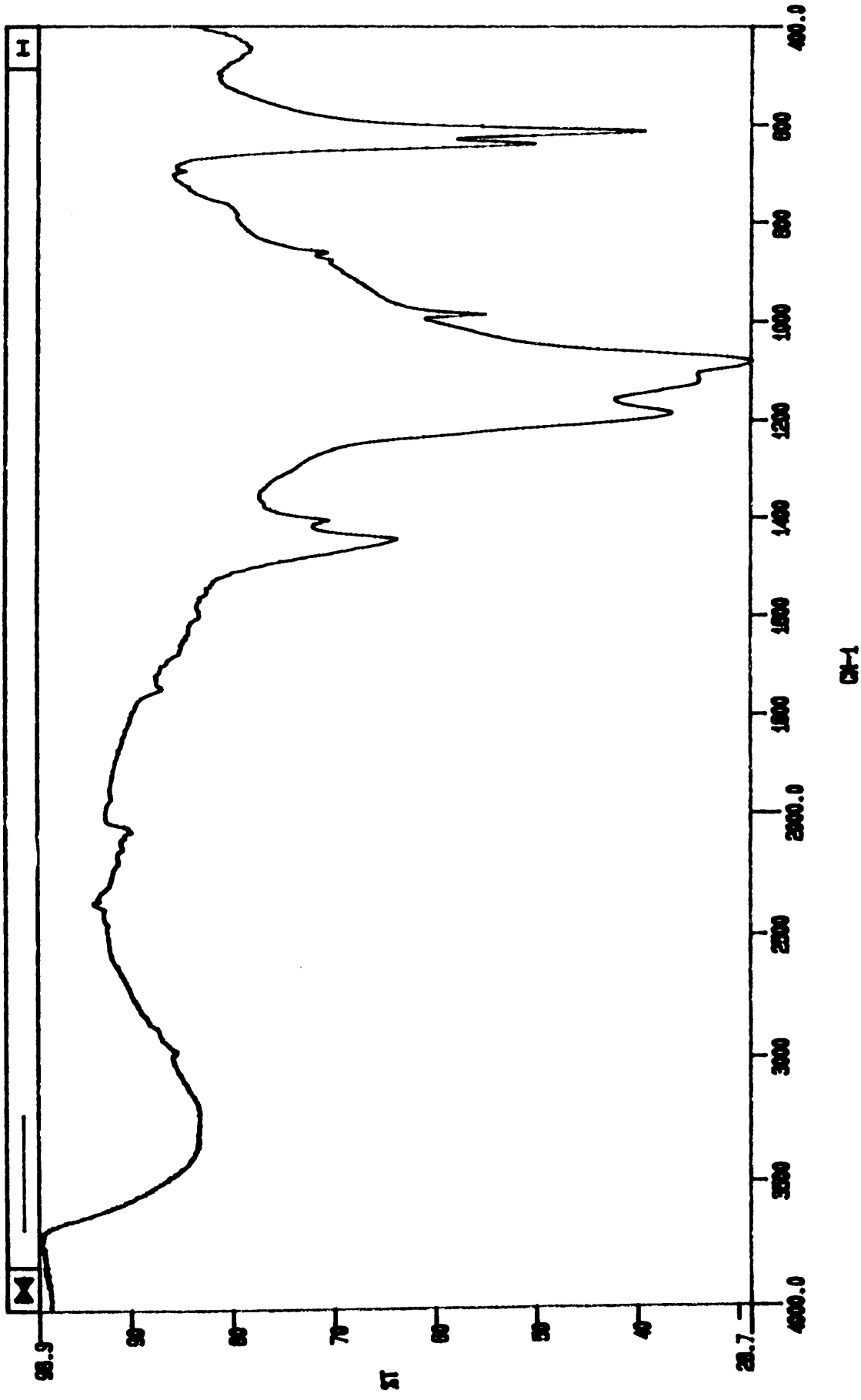

FTIR spectrum of BS[0.05]10

fig 7.2.2.1a

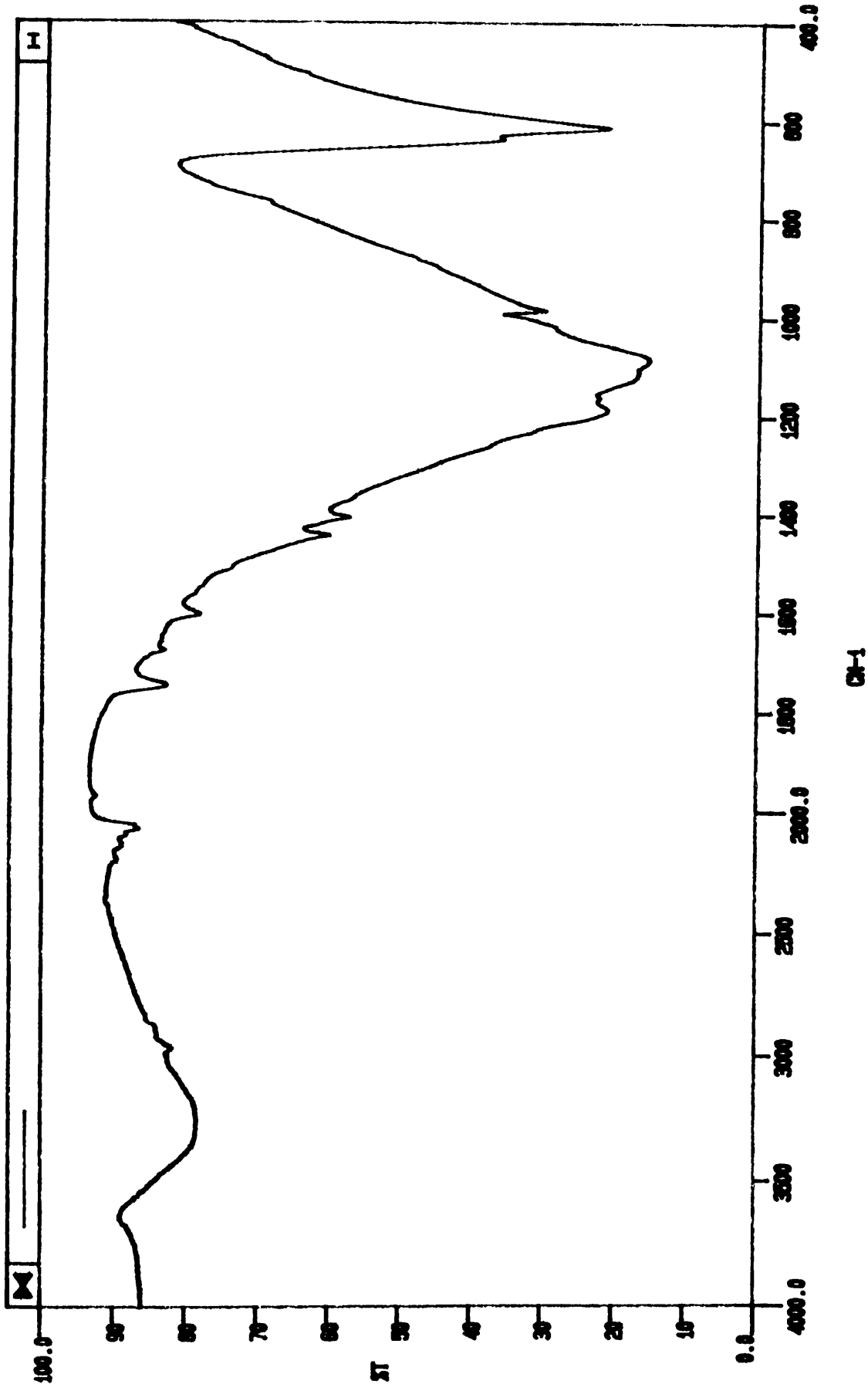

FTIR spectrum of material from neutral agarose control experiment

fig 7.2.2.1b

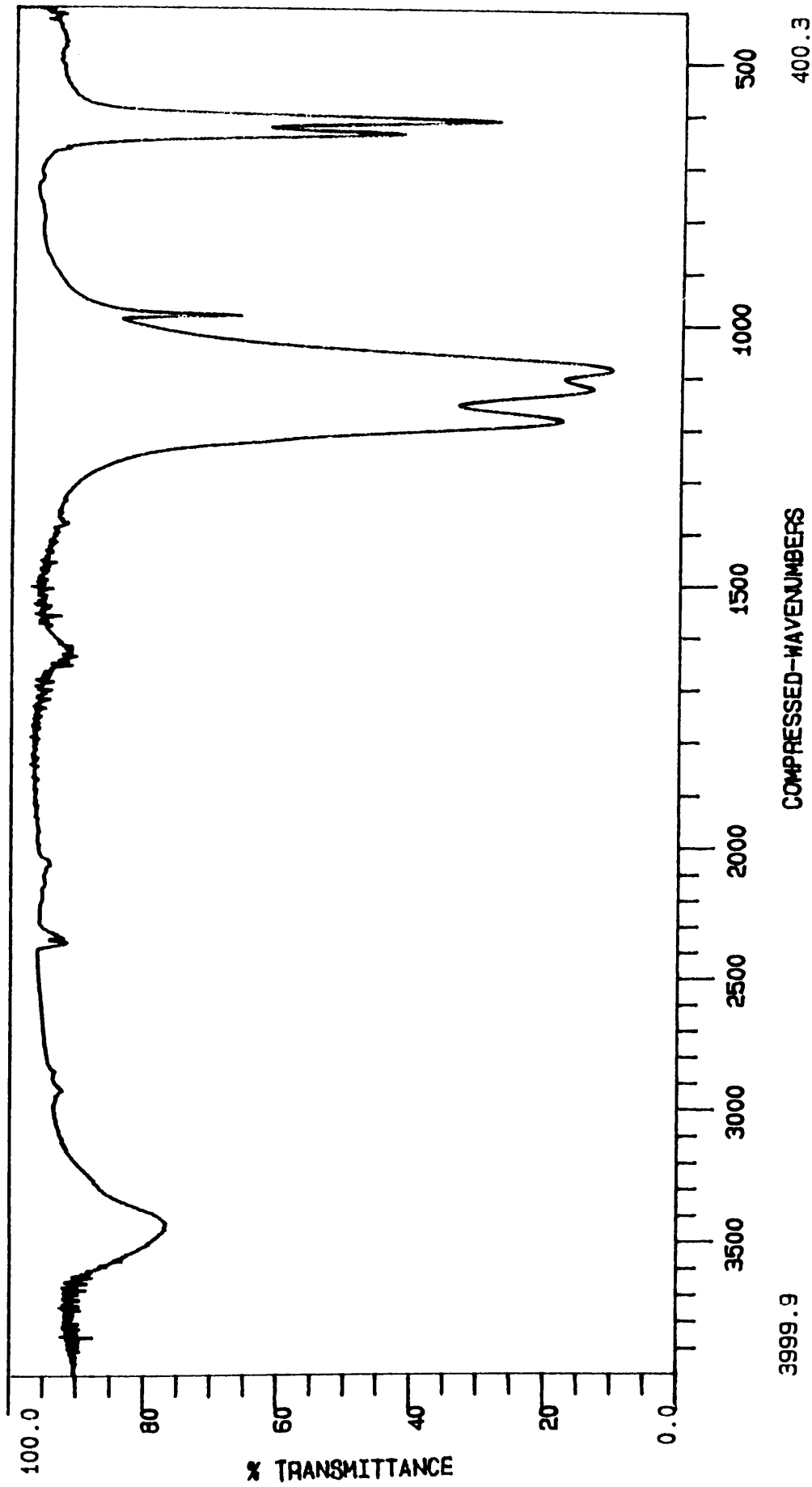

FTIR spectrum of reagent grade $BaSO_4$

fig 7.2.2.1c

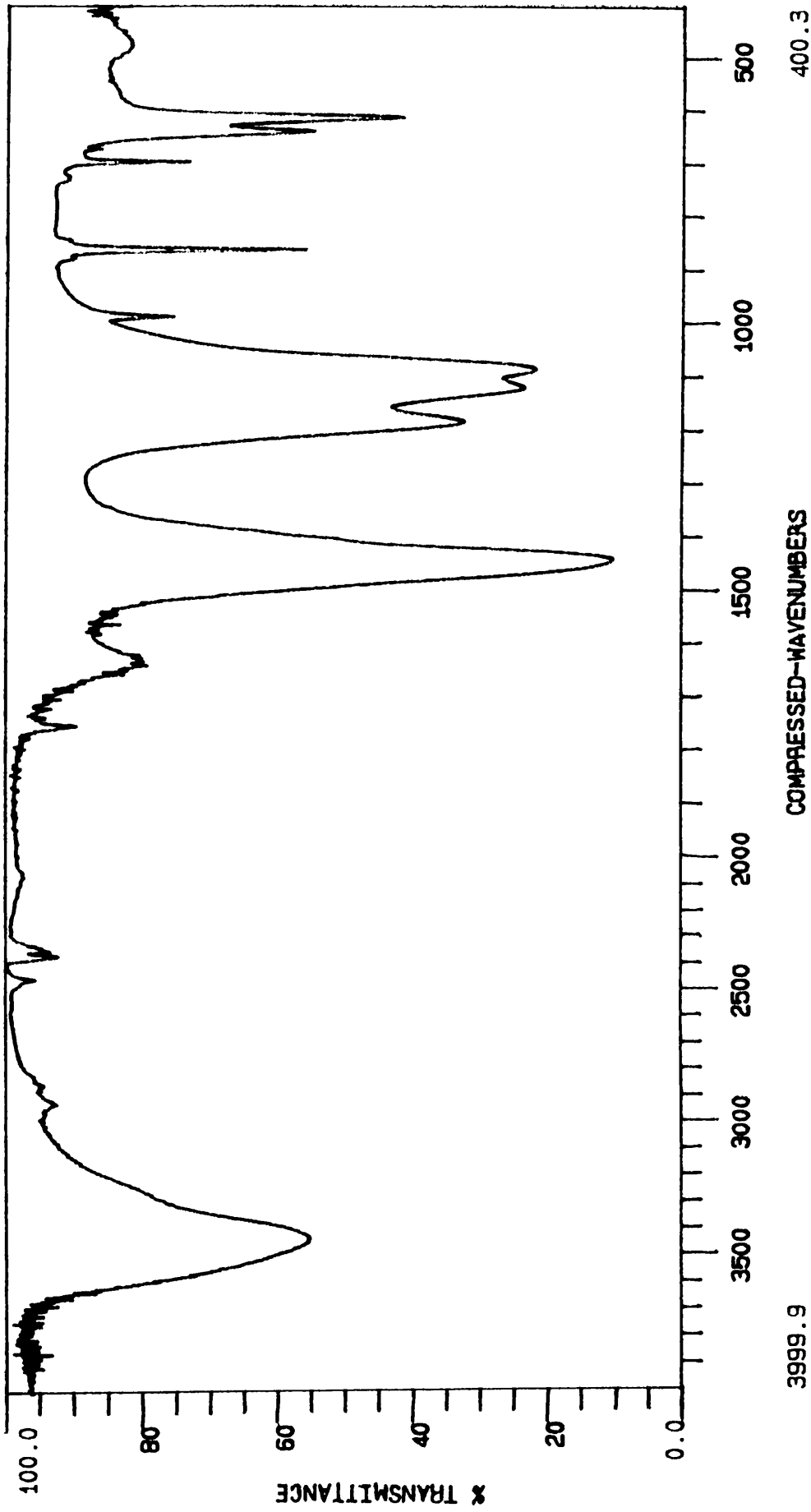

FTIR spectrum of BS[0.05]10 after prolonged soaking in NaOH

fig 7.2.2.1d

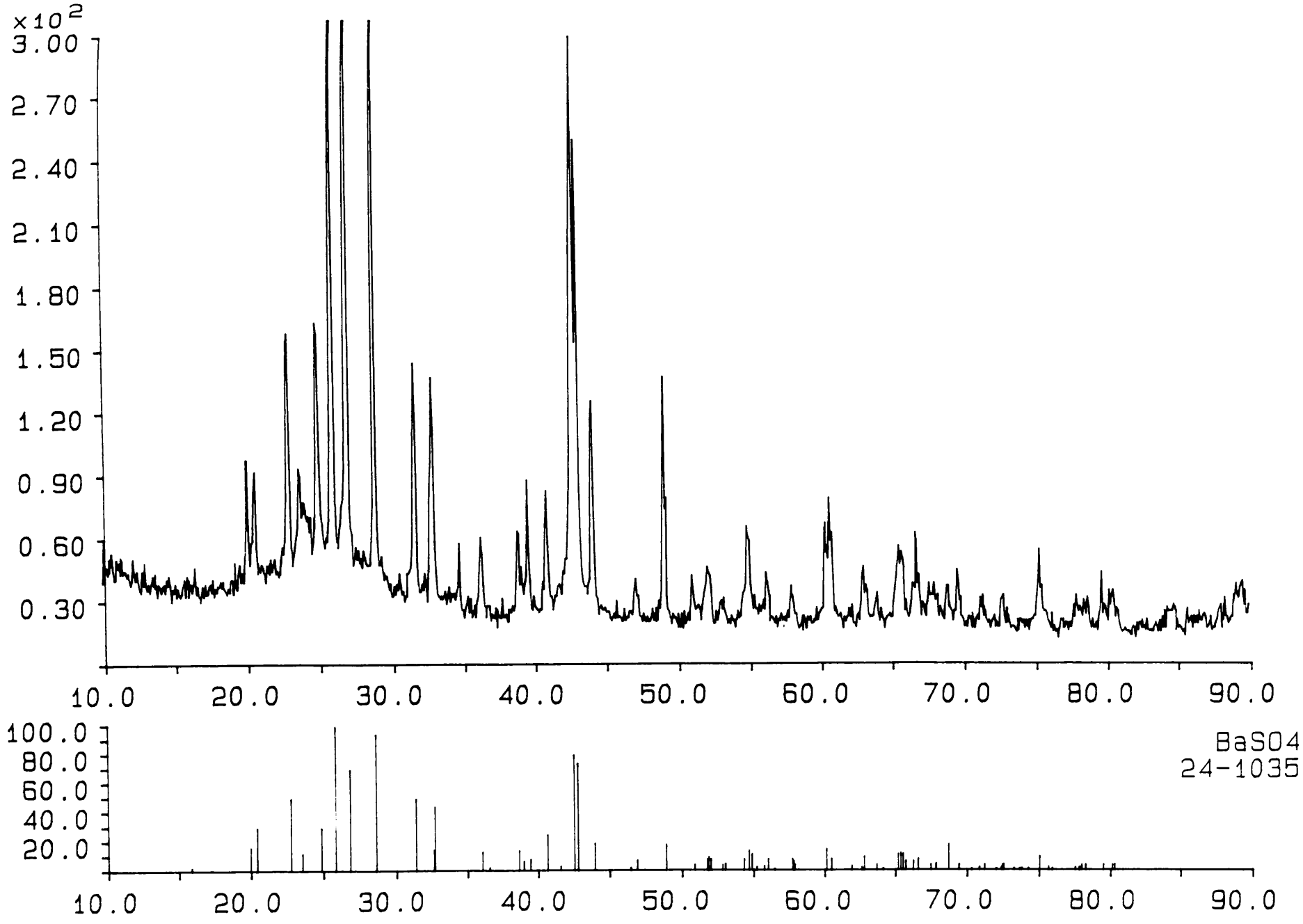

XRD of BS[0.05]10 and $BaSO_4$ reference pattern

fig 7.2.2.2a (i)

Peak no	Angle (deg)	Tip width (deg)	Peak (cts)	Backg (cts)	D spac (Ang)	I/Imax (%)
1	19.9800	0.12	42.	12.	4.4404	16.50
2	20.4550	0.12	38.	10.	4.3383	15.02
3	22.8125	0.10	85.	15.	3.8950	33.06
4	23.5550	0.10	41.	15.	3.7739	16.00
5	24.8550	0.12	64.	17.	3.5794	25.00
6	25.8600	0.08	190.	18.	3.4425	74.39
7	26.8350	0.10	240.	19.	3.3196	93.85
8	28.7600	0.08	256.	15.	3.1016	100.00
9	31.5400	0.12	71.	10.	2.8343	27.56
10	32.8625	0.08	85.	10.	2.7232	33.06
11	33.6750	0.10	14.	10.	2.6593#	5.35
12	34.5375	0.08	15.	5.	2.5949#	5.94
13	36.1825	0.08	35.	2.	2.4806	13.60
14	38.7625	0.08	35.	4.	2.3212	13.60
15	39.0625	0.08	26.	4.	2.3041	10.16
16	39.4975	0.12	35.	5.	2.2797	13.60
17	40.8200	0.08	53.	5.	2.2088	20.82
18	42.6075	0.10	216.	5.	2.1202	84.41
19	42.9500	0.10	169.	5.	2.1041	66.02
20	44.0050	0.10	85.	5.	2.0561	33.06
21	44.8375	0.20	10.	6.	2.0198#	4.00
22	46.9975	0.24	15.	2.	1.9319	5.94
23	49.0000	0.08	106.	3.	1.8575	41.44
24	49.2300	0.10	17.	3.	1.8494#	6.57
25	49.4625	0.12	10.	3.	1.8412#	4.00
26	50.9825	0.12	20.	2.	1.7898	7.91
27	52.0375	0.40	21.	2.	1.7560	8.27
28	53.1275	0.32	12.	3.	1.7225	4.52
29	54.8150	0.12	31.	4.	1.6734	12.25
30	56.1500	0.08	25.	4.	1.6368	9.77
31	57.8775	0.16	18.	3.	1.5919	7.22

BS[0.05]10 : peak angles, d-spacings, and intensities

 # unnasigned peaks

table 7.2.2.2a (ii)

continued on next page

Peak no	Angle (deg)	Tip width (deg)	Peak (cts)	Backg (cts)	D spac (Ang)	I/Imax (%)
32	60.2500	0.08	46.	1.	1.5348	18.06
33	60.6200	0.08	58.	1.	1.5263	22.56
34	62.0125	0.16	12.	2.	1.4953	4.52
35	63.0000	0.16	21.	3.	1.4743	8.27
36	63.8825	0.10	16.	2.	1.4560	6.25
37	65.4625	0.40	27.	2.	1.4246	10.56
38	66.4825	0.10	23.	1.	1.4052	9.00
39	66.7175	0.08	36.	1.	1.4009	14.06
40	67.6300	0.12	18.	4.	1.3842	6.89
41	67.9800	0.08	21.	3.	1.3779	8.27
42	68.8750	0.16	19.	2.	1.3621	7.56
43	69.6200	0.10	25.	3.	1.3494	9.77
44	71.2975	0.08	19.	2.	1.3217	7.56
45	72.6675	0.20	13.	3.	1.3001	5.06
46	73.9475	0.24	10.	2.	1.2807	4.00
47	75.2225	0.08	32.	2.	1.2622	12.69
48	77.7450	0.24	10.	4.	1.2274	4.00
49	78.4525	0.16	17.	1.	1.2181	6.57
50	79.6250	0.12	24.	0.	1.2031	9.38
51	80.1575	0.16	20.	0.	1.1964	7.91
52	80.7650	0.12	10.	1.	1.1889	4.00
53	82.3450	0.24	10.	1.	1.1701	4.00
54	84.4575	0.12	14.	1.	1.1461	5.35
55	85.7100	0.24	12.	1.	1.1326	4.52
56	86.9525	0.14	10.	1.	1.1195	4.00
57	87.3125	0.24	10.	1.	1.1158	4.00
58	87.9050	0.12	13.	0.	1.1098	5.06
59	88.3475	0.24	10.	0.	1.1054	4.00
60	88.9225	0.24	15.	1.	1.0998	5.94
61	89.4650	0.12	19.	1.	1.0945	7.56

table 7.2.2.2a (ii) continued

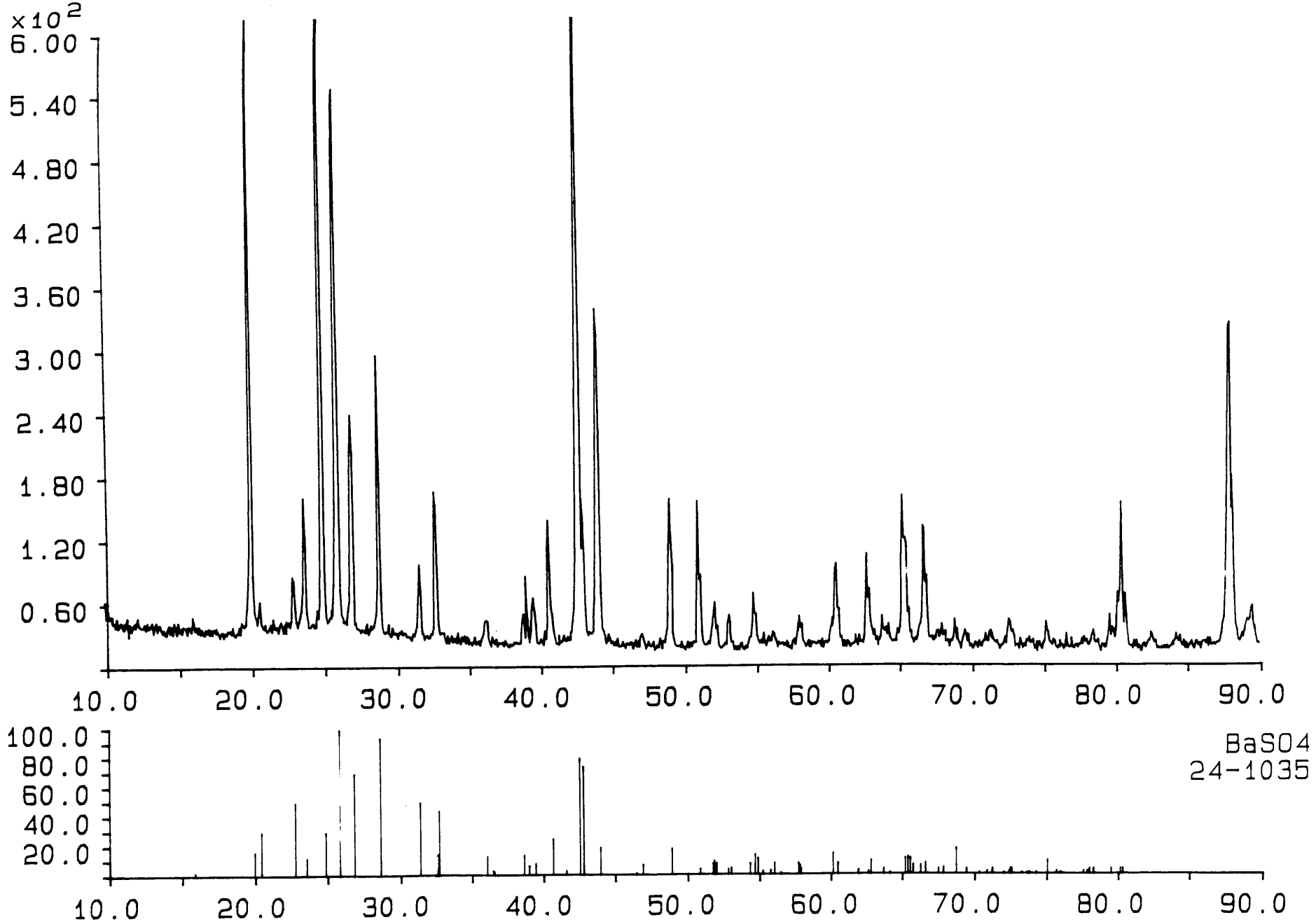

XRD of material from control experiment and $BaSO_4$ reference pattern

fig 7.2.2.2b (i)

Peak no	Angle (deg)	Tip width (deg)	Peak (cts)	Backg (cts)	D spac (Ang)	I/Imax (%)
1	19.9600	0.08	590.	10.	4.4448	100.00
2	20.4925	0.12	19.	7.	4.3305	3.28
3	22.8025	0.08	44.	11.	3.8967	7.38
4	23.5775	0.12	61.	11.	3.7704	10.30
5	24.8575	0.12	282.	12.	3.5790	47.80
6	25.8400	0.08	408.	9.	3.4451	69.10
7	26.8200	0.08	180.	9.	3.3214	30.41
8	28.7600	0.08	204.	12.	3.1016	34.63
9	31.5600	0.08	55.	10.	2.8326	9.27
10	32.7000	0.08	112.	5.	2.7364	19.03
11	36.1800	0.12	18.	7.	2.4808	3.13
12	36.6950	0.14	12.	4.	2.4471	2.07
13	38.7350	0.10	30.	3.	2.3228	5.12
14	39.0450	0.08	34.	3.	2.3051	5.70
15	39.4650	0.10	46.	3.	2.2815	7.83
16	40.5975	0.08	108.	2.	2.2204	18.32
17	40.8375	0.10	34.	1.	2.2079	5.70
18	41.0250	0.08	12.	1.	2.1983*	2.07
19	42.6050	0.10	543.	1.	2.1203	91.94
20	42.8325	0.08	67.	1.	2.1096	11.39
21	42.9400	0.12	106.	1.	2.1046	17.97
22	43.9875	0.10	292.	0.	2.0568	49.52
23	44.3825	0.10	11.	4.	2.0395*	1.84
24	44.6750	0.18	10.	4.	2.0268*	1.73
25	44.9175	0.12	10.	4.	2.0164*	1.73
26	47.0575	0.16	14.	1.	1.9296	2.45
27	49.0100	0.10	130.	1.	1.8572	22.01
28	49.2225	0.10	20.	1.	1.8496	3.43
29	49.4950	0.12	10.	1.	1.8401*	1.73
30	50.9825	0.12	76.	0.	1.7896	12.82
31	52.0975	0.08	38.	0.	1.7541	6.51
32	53.0600	0.10	34.	0.	1.7246	5.70
33	54.8100	0.10	46.	3.	1.6736	7.83

Material from control experiment : peak angles, d-spacings and intensities

* unnasigned peaks

table 7.2.2.2b (ii)

continued on next page

Peak no.	Angle (deg)	Tip width (deg)	Peak (cts)	Backg (cts)	D spac (Ang)	I/Imax (%)
34	55.8550	0.12	13.	3.	1.6447	2.19
35	56.1375	0.10	13.	3.	1.6371	2.19
36	58.0550	0.08	21.	2.	1.5875	3.58
37	60.2400	0.08	29.	0.	1.5350	4.94
38	60.5625	0.08	71.	3.	1.5276	11.95
39	60.8950	0.12	10.	3.	1.5201	1.73
40	61.2150	0.16	10.	3.	1.5129	1.73
41	62.7000	0.12	86.	0.	1.4806	14.65
42	62.9975	0.12	24.	0.	1.4743	4.07
43	63.8075	0.08	21.	1.	1.4575	3.58
44	65.2475	0.10	130.	1.	1.4288	22.01
45	65.9775	0.20	10.	3.	1.4148	1.73
46	66.7025	0.12	104.	3.	1.4011	17.62
47	67.9300	0.12	16.	2.	1.3788	2.71
48	68.8600	0.08	24.	2.	1.3624	4.07
49	69.6025	0.12	21.	2.	1.3497	3.58
50	70.9625	0.24	12.	2.	1.3271	2.07
51	71.2725	0.08	17.	3.	1.3221	2.85
52	72.6175	0.08	25.	2.	1.3009	4.23
53	73.4700	0.16	10.	2.	1.2879	1.73
54	74.0050	0.12	13.	1.	1.2799	2.19
55	75.1800	0.10	24.	0.	1.2628	4.07
56	77.6925	0.32	10.	3.	1.2281	1.73
57	78.4750	0.16	13.	1.	1.2178	2.19
58	79.6350	0.10	32.	1.	1.2029	5.50
59	80.1700	0.10	56.	1.	1.1963	9.53
60	80.4550	0.08	85.	1.	1.1927	14.33
61	82.5200	0.16	16.	0.	1.1680	2.71
62	85.7025	0.24	10.	3.	1.1326	1.73
63	87.8575	0.18	279.	1.	1.1103	47.23
64	88.3700	0.14	20.	0.	1.1052	3.43
65	88.8100	0.16	14.	0.	1.1009	2.45
66	89.4275	0.10	34.	0.	1.0949	5.70

table 7.2.2.2b (ii) continued

BaSO4 reference data

unit cell parameters, d-spacings, Miller indices

table 7.2.2.2c

24-1035 5

Ba S O4
Barium Sulfate
Barite, syn
Hanawalt 3.45/X 3.10/X 2.12/8 2.11/8 3.32/7 3.90/5 2.84/5 2.73/5 4.34/3 3.58/3

Lambda 1.54056
Sys. Orthorhombic
SG Pbnm PS oP 24.00
a 7.1565 b 8.8811 c 5.4541
Al Be Ga
A 0.8058 C Z 4
Dx 4.500 Dm 4.472 V 346.65
F(N) 69.0 M(20) 50.9 I/Ic 2.60
d-sp
Int Diffractometer
Total d's 79
Color Colorless
Temp Pattern at 25 C.

d	Int	h	k	l	d	Int	h	k	l
5.580	2	1	1	0	2.735	15	1	3	0
4.440	16	0	2	0	2.729	45	0	0	2
4.339	30	1	0	1	2.482	13	2	2	1
3.899	50	1	1	1	2.447	2	1	3	1
3.773	12	1	2	0	2.325	14	0	2	2
3.577	30	2	0	0	2.305	6	3	1	0
3.445	100	0	2	1	2.282	8	2	3	0
3.319	70	2	1	0	2.211	25	1	2	2
3.103	95	1	2	1	2.169	3	2	0	2
2.836	50	2	1	1	2.121	80	1	4	0

Reduced cell
a 5.454
b 7.156
c 8.881
Al 90.00
Be 90.00
Ga 90.00

Crystal data
a 7.156
b 8.881
c 5.454
Al 90.00
Be 90.00
Ga 90.00

d	Int	h	k	l	d	Int	h	k	l	d	Int	h	k	l
2.108	75	2	1	2	1.659	2	4	2	0	1.427	11	3	1	3
2.057	19	0	4	1	1.644	3	1	5	1	1.424	12	3	5	0
1.948	1	2	2	2	1.637	8	1	2	3	1.421	11	2	3	3
1.931	7	1	3	2	1.625	1	3	4	0	1.417	6	4	2	2
1.857	18	3	3	0	1.594	8	2	1	3	1.406	6	0	4	3
1.788	4	4	0	0	1.590	6	2	5	0	1.400	8	1	6	1
1.761	8	1	0	3	1.587	4	4	2	1	1.384	4	5	0	1
1.758	10	3	3	1	1.535	15	3	3	2	1.378	5	3	5	1
1.754	8	4	1	0	1.527	8	2	5	1	1.362	18	0	0	4
1.708	4	1	1	3	1.495	3	4	0	2	1.349	4	4	4	1
1.722	5	1	5	0	1.480	2	0	6	0	1.325	1	4	3	3
1.682	8	0	2	3	1.475	10	4	1	2	1.326	2	5	3	1
1.674	14	1	4	2	1.457	4	1	5	2	1.321	4	5	3	2
1.668	11	4	1	1	1.448	1	1	6	1	1.308	1	2	4	3

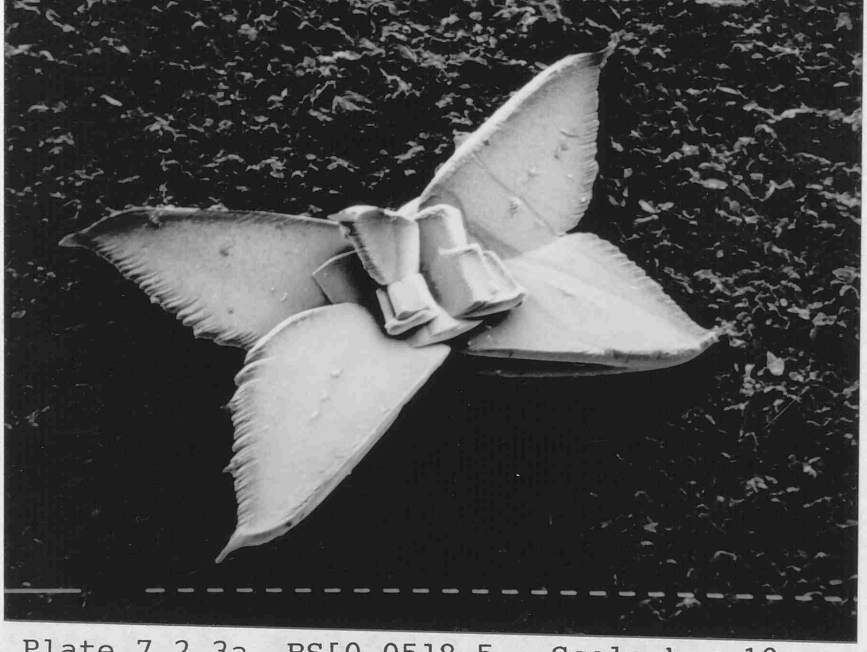

Plate 7.2.3a. BS[0.05]8.5. Scale bar 10 µm.

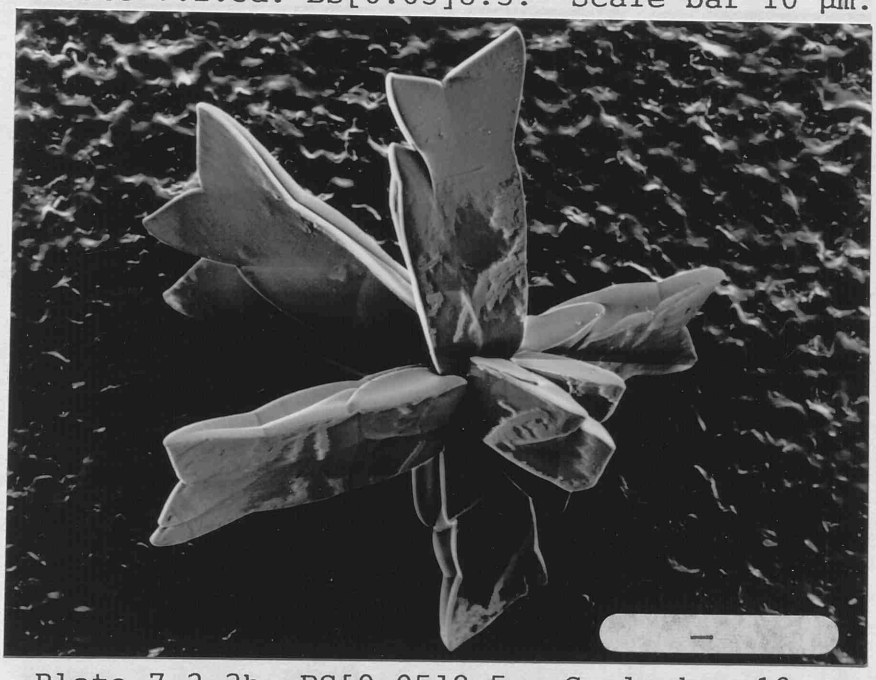

Plate 7.2.3b. BS[0.05]8.5. Scale bar 10 µm.

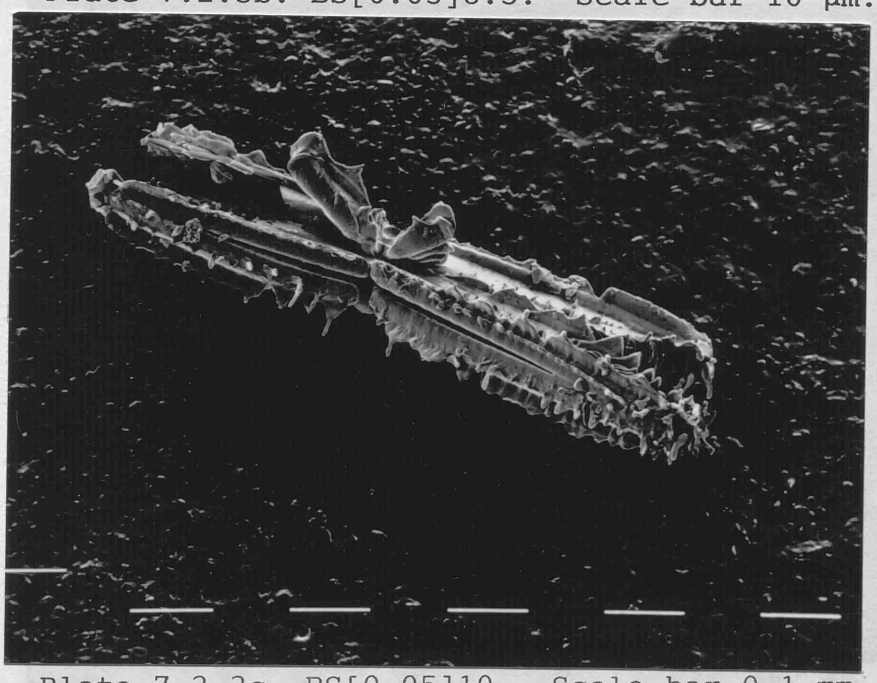

Plate 7.2.3c. BS[0.05]10. Scale bar 0.1 mm.

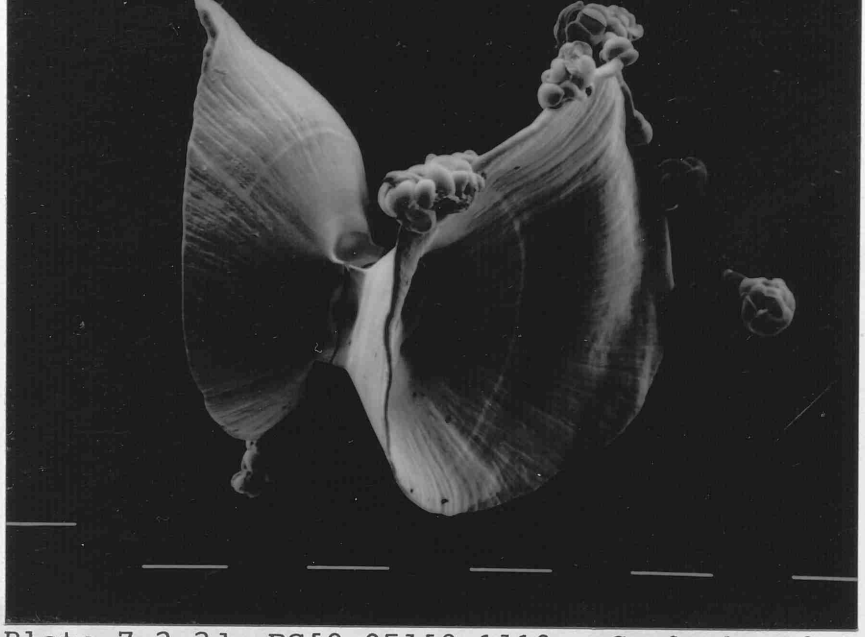

Plate 7.2.3d. BS[0.05][0.1]10. Scale bar 0.1 mm.

Plate 7.2.3e. BS[0.05][0.1]10. Scale bar 10 μm.

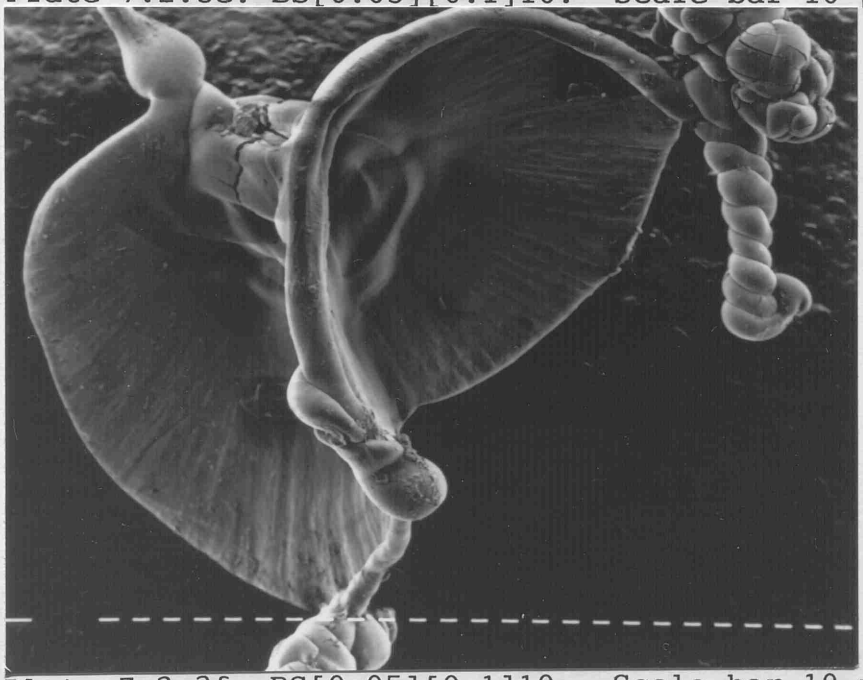

Plate 7.2.3f. BS[0.05][0.1]10. Scale bar 10 μm.

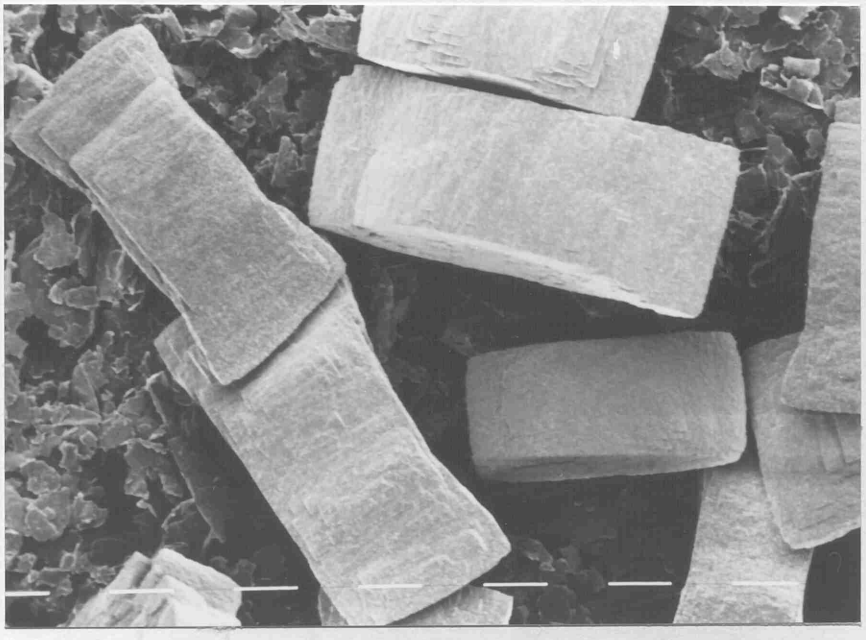

Plate 7.2.3g. Platelet precipitates from agarose control experiments. Scale bar 10 µm.

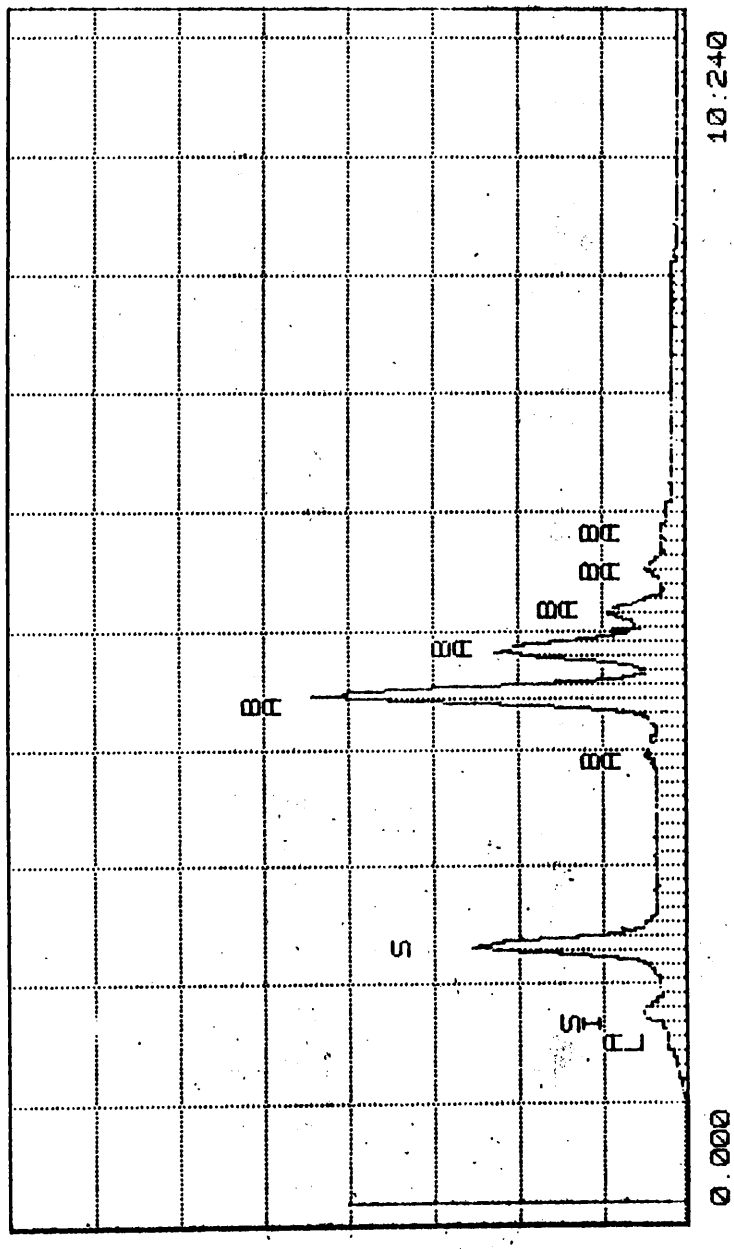

EDS analysis of a $BaSO_4$ IMCA

fig 7.2.4a

8 PRECIPITATION OF FERROUS MATERIALS BY A DIFFUSION MECHANISM IN SILICA GEL

8.1 PRECIPITATION OF $FeCO_3$

8.1.1 EXPERIMENTAL

8.1.2 RESULTS

8.1.2.1 In-Situ Light Microscopy

8.2 PRECIPITATION OF FeS

8.2.1 EXPERIMENTAL

8.2.2 RESULTS

8.2.2.1 X-Ray Diffraction (XRD)

8.2.2.2 SEM Equipped with EDS

8.3 DISCUSSION

8 PRECIPITATION OF FERROUS MATERIALS BY A DIFFUSION MECHANISM IN SILICA GEL

The IMCA phenomenon had now been shown to work for alkaline earth metal sulphates as well as carbonates. To test how widespread the phenomenon may be, a metal other than an alkaline earth one was now chosen for study. Ferrous materials and in particular $FeCO_3$ and FeS were chosen as appropriate materials for study.

$FeCO_3$ seemed like an appropriate material to study for the following reasons. In nature it precipitates as part of the Fe (II/III) compounds, along with silica, in banded iron formations (Garrels, 1987). These layers of iron and silica compounds are thought to arise through periodical evaporation from water basins. $FeCO_3$ has also been shown to exhibit interesting photochemistry. It can trap photons and produce organic molecules and Fe_2O_3 (Arrhenius, 1986). This of course has origin of life implications.

Iron suphide can occur in nature in the form of spheroidal aggregates composed of thousands of internally organised crystallites. These framboids (already discussed in 1.5) are usually in the form of pyrite (FeS_2) but also known are magnetite, greigite and limonite.

Framboids are found in sediments, lavas and hydrothermal vents and are usually less than 100 μm in diameter (Rickard, 1970). The spheroidal form is thought to be due to the infilling of organic globules and gaseous vacuoles. The internal organisation of the crystallites is thought to be due to the formation processes of pyrite itself.

Because of the similarity in shape between naturally-occurring framboids and the globular morphology obtained for $BaCO_3$ precipitated under the influence of silica (fig 6.2.1f & 6.2.4f), iron sulphide was chosen for study.

8.1 PRECIPITATION OF $FeCO_3$

8.1.1 EXPERIMENTAL

A full range of parameters was studied including basic and acidic silica gels, the presence and absence of NaCl in the silica gel, the presence and absence of an oxygen scavenger (to minimise Fe (II) oxidation) and the effect of different sources of Fe.

The most interesting experiment was almost analagous to the $BaCO_3$ and $BaSO_4$ arrangements. The experiments were carried out in glass cassettes. A silica gel of pH 10 loaded with $NaCO_3$ to 0.05M was prepared by the addition of 1M HCl to sodium silicate solution according to procedure 3.1.2 . A top solution containing 1M

$Fe(NH_4)_2(SO_4)_2$ almost saturated in $Na_2S_2O_5$ (oxygen scavenger to prevent oxidation of Fe(II) to Fe(III)) was placed in contact with the gel and the cassette sealed. A slight variation on this where $Fe(NH_4)_2(SO_4)_2$ was substituted for $FeSO_4.7H_2O$ was also studied.

8.1.2 RESULTS

8.1.2.1 In-Situ Light Microscopy

Plate 8.1.2.1a is an example of the spherical type of precipitate formed when $Fe(NH_4)_2(SO_4)_2$ is used as the source of iron. Although the precipitate appears spherical it also gives the impression of being hollow. When some of these precipitates are viewed from a certain angle they appear not to be completely spherical as in the case of the cup-shaped object in plate 8.1.2.1b. From studying a great number of these objects under the light microscope their morphologies fall under three descriptions: (i) perfectly spherical, (ii) hollow spherical and (iii) cup-shaped, although it is very likely they are all the same type of object viewed from a different angle. Twinned examples of the above were also observed.

When $FeSO_4.7H_2O$ was used as the source of iron less regular spherical particles formed suggesting that perhaps ammonia incorporation into the precipitate was involved. In both cases it was found that the presence of

$Na_2S_2O_5$ was essential for the precipitation of spherical objects.

When the objects were removed from the gel for further analysis (section 3.6.2) oxidation occurred very quickly destroying morphogenetical and structural features. No further analysis was carried out.

8.2 PRECIPITATION OF FeS

8.2.1 EXPERIMENTAL

The initial experiment carried out was analogous to the $FeCO_3$ experiment. Pre-gelled silica solutions containing Na_2S (0.05M) and NaCl (0.2M) were prepared according to procedure 3.1.1. The pH was adjusted to 9.5 by the addition of Dowex acidic ion exchange resin. The solution was poured into test tubes and allowed to gel. A top solution containing 0.5M $FeSO_4.7H_2O$ almost saturated in $Na_2S_2O_5$ (Oxygen scavenger to prevent oxidation of Fe(II) to Fe(III)) was placed in contact with the gel and the tube sealed.

Three control experiments were also carried out. Agarose gel was used instead of silica. This was prepared according to procedure 3.1.4. with the addition of 0.05M Na_2S. The same top solution was used. The experiment was also repeated without $Na_2S_2O_5$ and under vacuum.

8.2.2 RESULTS

After a few days spherical black objects, around 1 mm in diameter could be seen with the naked eye in the initial experiment. After another few days some light coloured irregular objects were visible and finally after one to two weeks more spherical black objects and a thick black band were observed. In all of the control experiments a thick black band was all that could be seen.

8.2.2.1 X-Ray diffraction

The black spherical objects were removed from the gel by picking them out with a spatula and washing with distilled water and a fine paint brush. After drying, a few black objects were ground in a mortar and pestle and XRD analysis, carried out in accordance with procedure 3.5.6, (Co K alpha 1, 2 radiation) gave the pattern shown in fig 8.2.2.1a (i). Hand measured peak angles, estimated intensities and calculated d-spacings are listed in table 8.2.2.1a (ii). These d-spacings failed to match any iron or sulphur compounds in the powder diffraction files. If the test tube, from which these black objects were removed, was re-sealed then any remaining black objects near to the surface decomposed. These decomposed objects were removed and ground up in a mortar and pestle. XRD analysis (Co K alpha 1, 2 radiation) gave the pattern shown in fig 8.2.2.1b (i). Table 8.2.2.1b (ii) lists hand measured peak angles, estimated intensites and calculated

d-spacings. This material was positively identified as monoclinic $FeSO_3.3H_2O$. Table 8.2.2.1c lists unit cell parameters, d-spacings, intensities and Miller indices of of $FeSO_3.3H_2O$ from the powder diffraction files (22-1017).

8.2.2.2 SEM Equipped With EDS

The black objects removed from the silica gel by the method just described were prepared for SEM in accordance with procedure 3.5.4. Plate 8.2.2.2a is a typical black spherical object and for comparison plate 8.2.2.2b is a framboid. There is a great deal of similarity apart from the size and perhaps the number and shape of crystallites which make up the object.

EDS analysis (fig 8.2.2.2c) identified the presence of Fe, S, O and Si and computer-generated semi-quantitative analysis gave the following atomic ratios:

Fe	:	1
S	:	1
O	:	4
Si	:	0.06

This suggested the material present to be FeS hydrate. Further evidence that this is indeed a hydrated structure can be seen by observing closely the crystals which make up the aggregate. They appear to be layered as in plate 8.2.2.2d (very common for hydrated crystal structures).

One week after the black objects had been removed from the gel, a decomposing object was removed from the same tube (by the same method). It was embedded in resin and polished down to reveal the cross-section through the object. Plate 8.2.2.2e illustrates this cross-section. In the centre can be seen the original crystallites which made up the black object. On the outside can be seen the decomposed area. The outside area gave an EDS analysis (fig 8.2.2.2f) which identified Fe, S, O and Si and computer-generated semi-quantitative analysis gave the following atomic ratios:

Fe	:	1
S	:	1
O	:	3
Si	:	0.06

Oxygen analysis by EDS is innacurate, therefore it is suggested that this material is $FeSO_3.3H_2O$, already positively identified as the decomposed material by XRD. The centre part gave an EDS analysis identical to the one previously recorded for the intact black object including identical atomic ratios.

8.3 DISCUSSION

In the case of the iron sulphide experiments it is clear that there is a striking similarity between the black precipitated objects and naturally-occurring framboids. The precipitation of these objects was dependent on the presence of sodium metabisulphite in order to maintain

iron in the ferrous oxidation state. It was also clear from EDS analysis that silicon was homogeneously distributed within the objects to the value of 1.2% (atom percent). This value remained constant whether the exterior or interior was probed suggesting that silicate adsorption onto precipitating FeS may be part of the growth mechanism and in part, responsible for the observed morphology.

In the case of iron carbonate the presence of sodium metabisulphite was also found necessary in order to precipitate spherical-type objects. No structural analysis was carried out in this case although the unusual morphologies may suggest that silicate adsorption is involved.

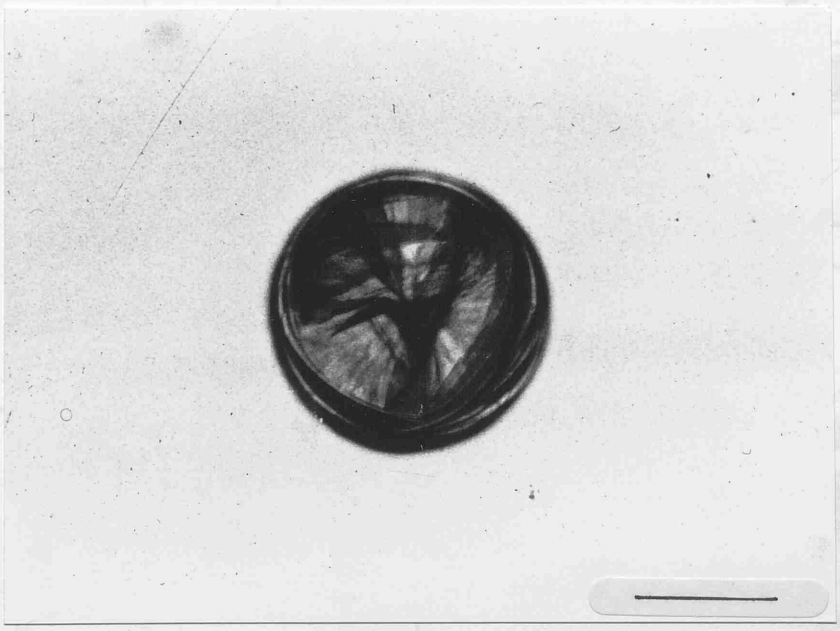

Plate 8.2.1a. $FeCO_3$ spherical type precipitate.

Scale bar 0.5 mm.

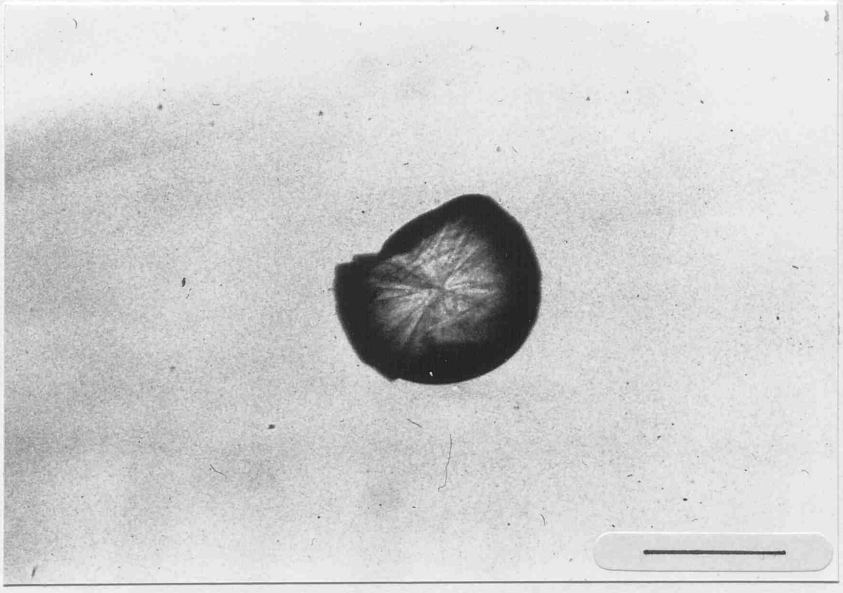

Plate 8.1.2.1b. $FeCO_3$ cup shaped precipitate.

Scale bar 0.5 mm.

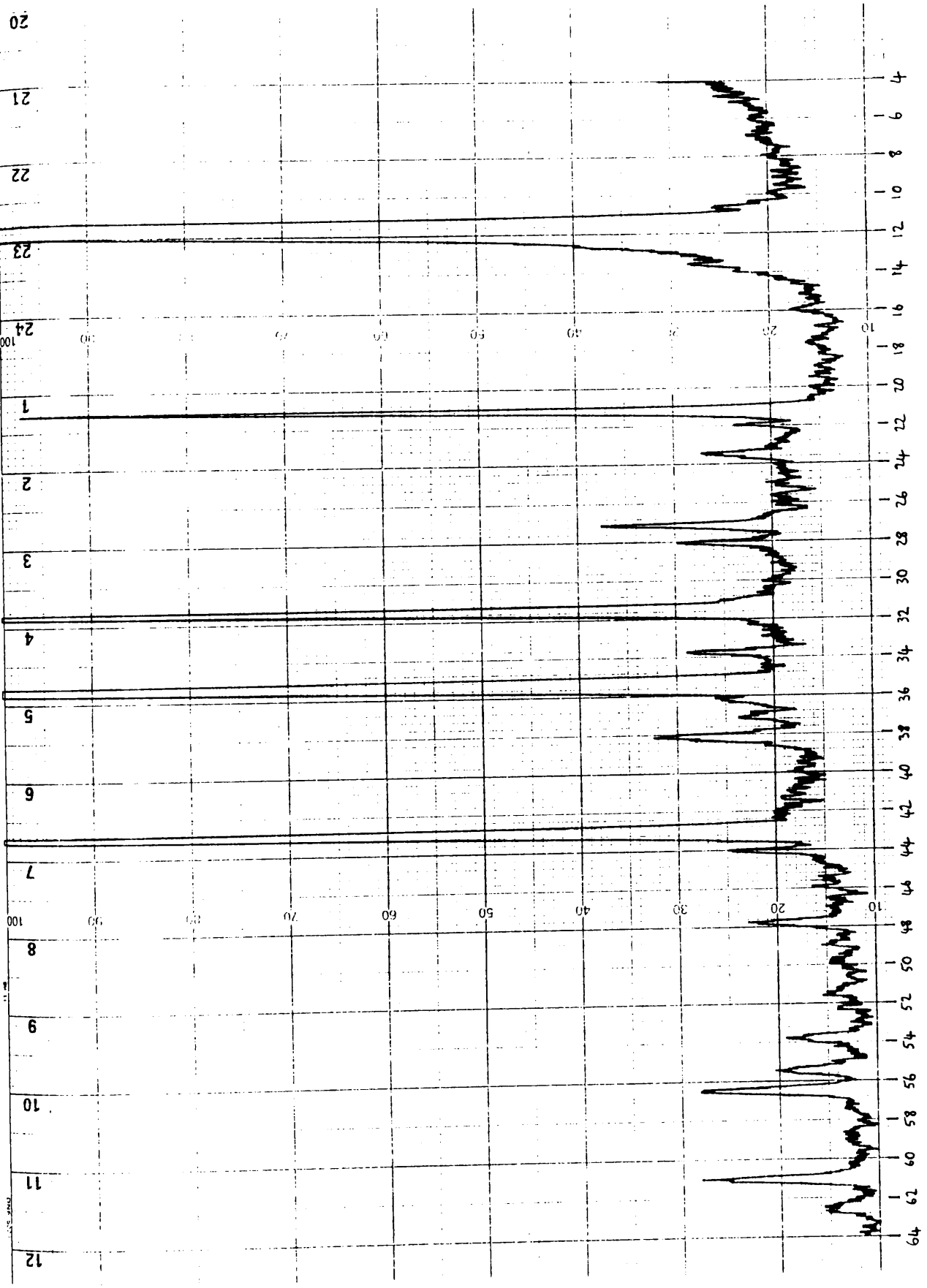

XRD of black spherical objects

fig 8.2.2.1a

Peak Angle	Intensity	d-spacing
11.7	100	8.782
12.6	5	8.157
15.9	2	6.472
21.1	30	4.866
22.0	3	4.691
23.4	4	4.414
27.2	8	3.807
28.1	5	3.687
31.5	50	3.298
33.8	5	3.079
35.4	60	2.944
36.1	3	2.889
37.0	2	2.821
38.2	6	2.736
43.0	50	2.442
44.1	3	2.384
45.8	3	2.300
53.8	3	1.978
56.5	6	1.891
61.0	6	1.764
62.5	2	1.725

Black spherical object : hand measured peak angles, estimated intensities and calculated d-spacings.

table 8.2.2.1a (ii)

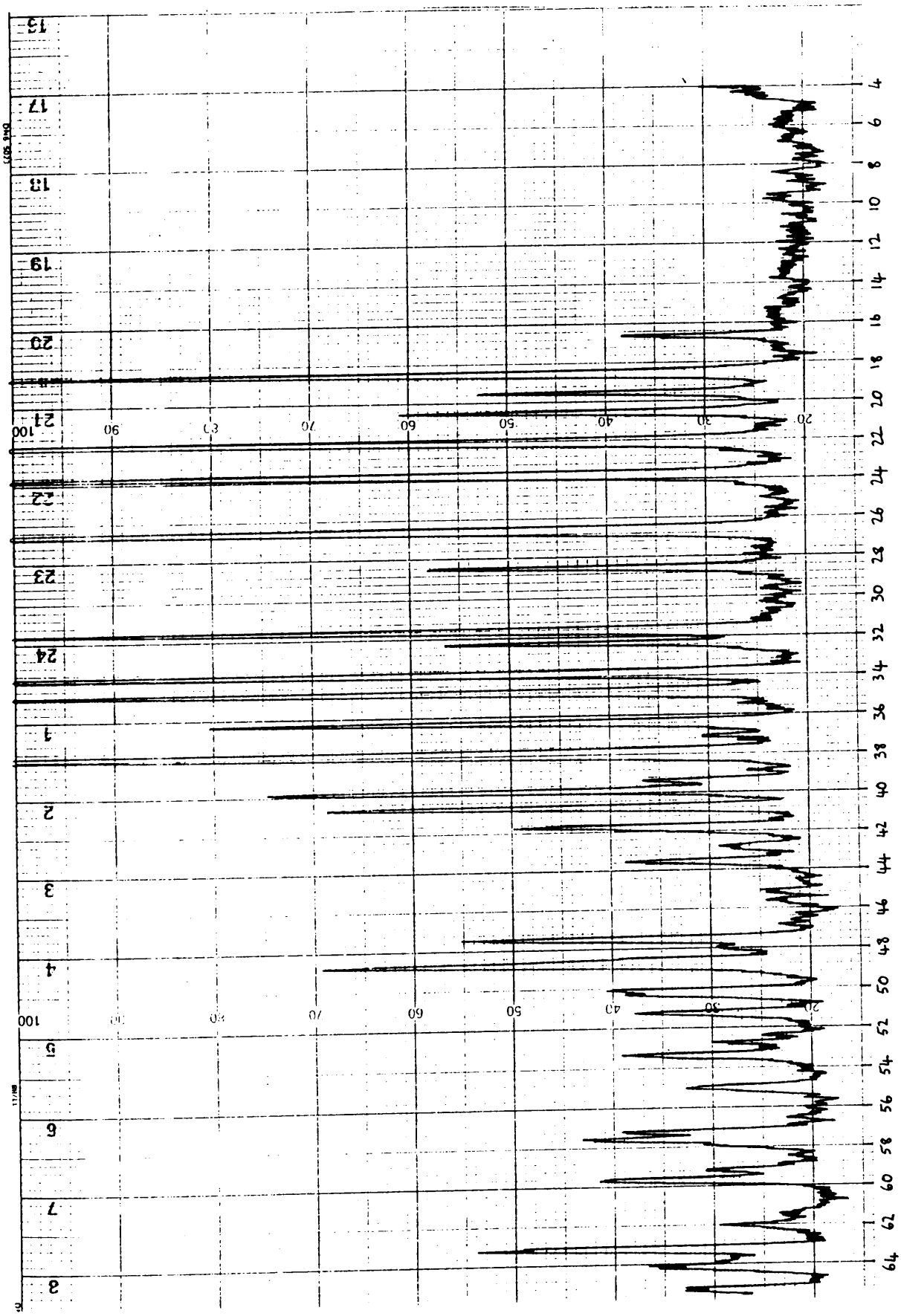

XRD of decomposed objects

fig 8.2.2.1b

Peak Angle	Intensity	d-spacing
16.6	10	6.201
18.6	60	5.539
19.6	30	5.259
20.7	40	4.982
22.1	90	4.670
23.8	80	4.341
26.7	90	3.877
28.6	40	3.624
31.6	70	3.288
32.4	40	3.208
33.8	80	3.079
34.8	80	2.993
36.3	50	2.874
37.2	3	2.806
37.9	100	2.756
39.4	10	2.655
39.9	60	2.623
40.7	60	2.574
41.7	40	2.515
42.6	5	2.464
43.5	20	2.416
45.1	2	2.334
45.6	2	2.310
47.5	50	2.223
48.8	60	2.167
50.2	30	2.110
51.2	20	2.072
52.7	5	2.017
53.3	20	1.196

Decomposed objects : hand measured d-spacings, estimated intensities and calculated d spacings

table 8.2.2.1b (ii)

22-1017

d	3.27	4.66	2.75	6.13	$FeSO_3 \cdot 3H_2O$
I/I_1	100	90	90	20	Iron Sulfite Hydrate

Rad. FeKa λ 1.9373 Filter Mn Dia. 114.6mm
Cut off I/I_1 Visual
Ref. Bugli and Pannetier, Bull. Soc. Chim. France, 2355-56 (1968)

Sys. Monoclinic S.G. $P2_1/n$ (14)
a_0 6.591 b_0 8.691 c_0 8.709 A C
α β 96.00° γ Z 4 Dx 2.54
Ref. Ibid.

$\epsilon\alpha$ $n\omega\beta$ $\epsilon\gamma$ Sign
2V D 2.55 mp Color
Ref. Ibid.

d A	I/I_1	hkl	d A	I/I_1	hkl
6.13	20	011	2.565	50	$22\bar{1}$,13$\bar{1}$
5.51	45	$10\bar{1}$	2.504	40	131
5.24	25	110	2.490	10	202
4.98	45	101	2.449	10	221
4.66	90	$11\bar{1}$	2.442	10	113
4.35	35	020	2.407	30	032,023
4.33	60	002	2.394	5	212
3.88	75	021	2.324	5	$12\bar{3}$
3.87	60	012	2.303	5	$13\bar{2}$
3.62	40	120	2.218	40	132
3.27	100	121	2.196	10	123
3.21	50	112	2.173	15	301,040
3.07	70	022,210	2.165	40	$00\bar{4}$
2.985	60	$21\bar{1}$	2.142	5	$23\bar{1}$
2.861	60	$12\bar{2}$	2.109	15	$31\bar{1}$
2.805	10	$21\bar{1}$	2.100	15	014
2.750	90	$10\bar{3}$	2.068	10	301
2.739	40	013	2.025	<5	$22\bar{3}$
2.649	20	130	2.012	<5	311
2.616	40	220	1.991	30	141

$FeSO_3 \cdot 3H_2O$ reference data

unit cell parameters, d-spacings, intensities

and Miller indices

table 8.2.2.1c

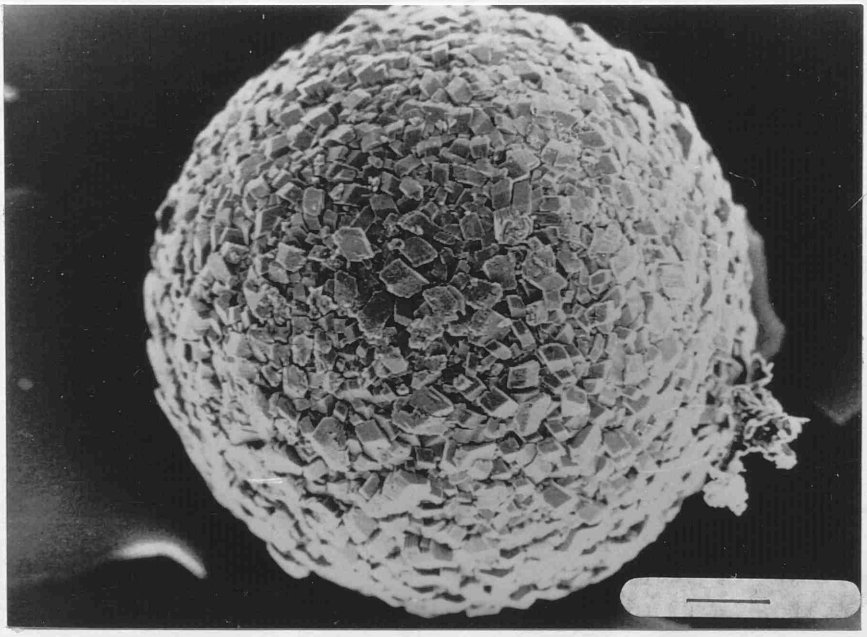

Plate 8.2.2.2a. FeS spherical precipitate.

Scale bar 0.1 mm.

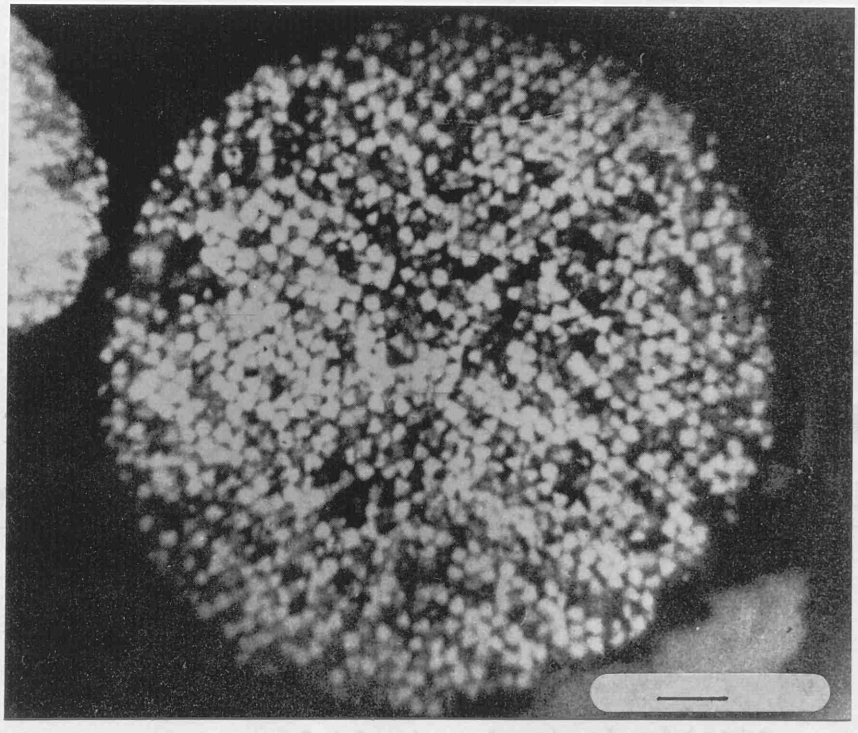

Plate 8.2.2.2b. Framboid. Scale bar 0.5 µm.

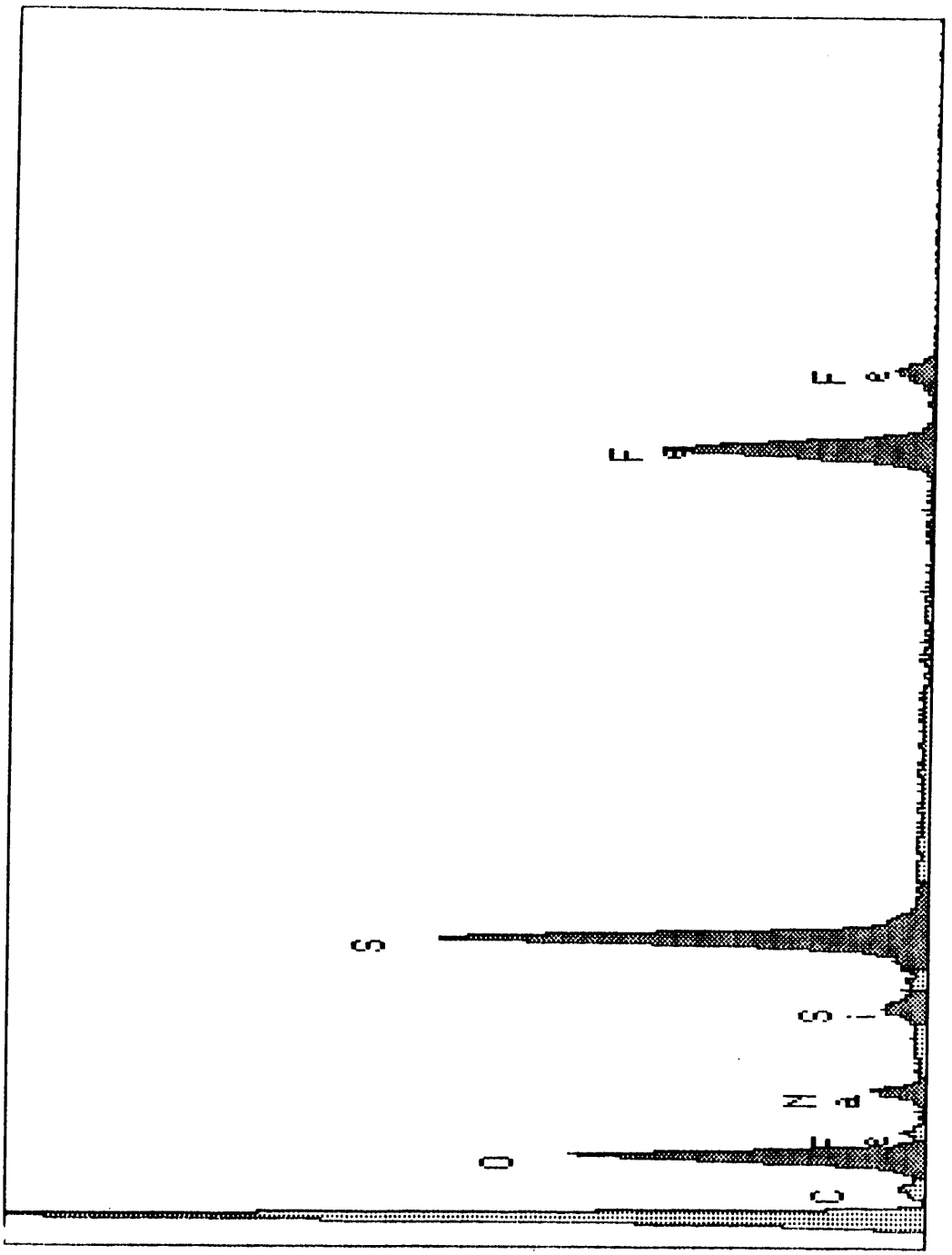

EDS analysis of black spherical objects

fig 8.2.2.2c

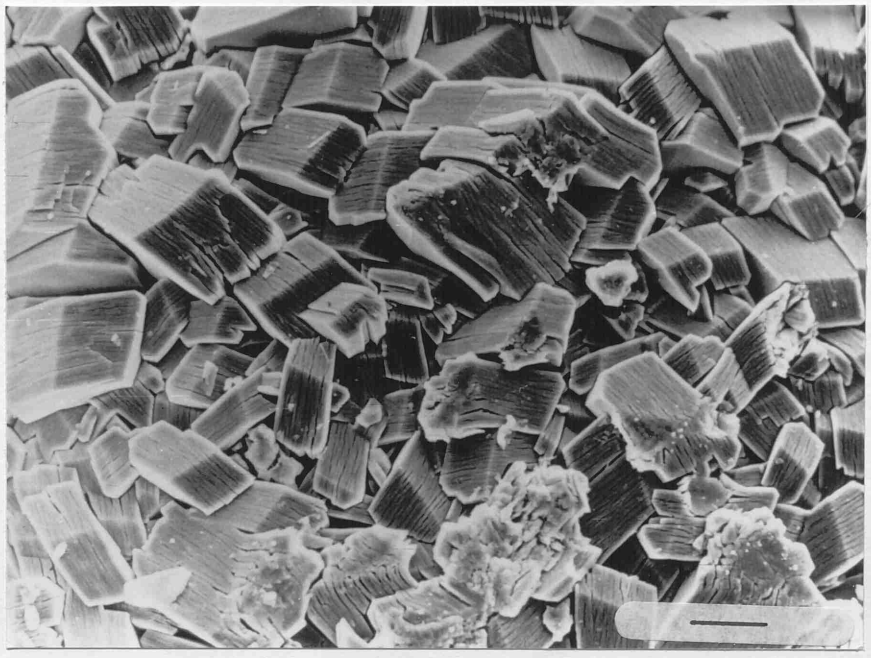

Plate 8.2.2.2d. FeS spherical precipitate, enlarged view. Scale bar 25 µm.

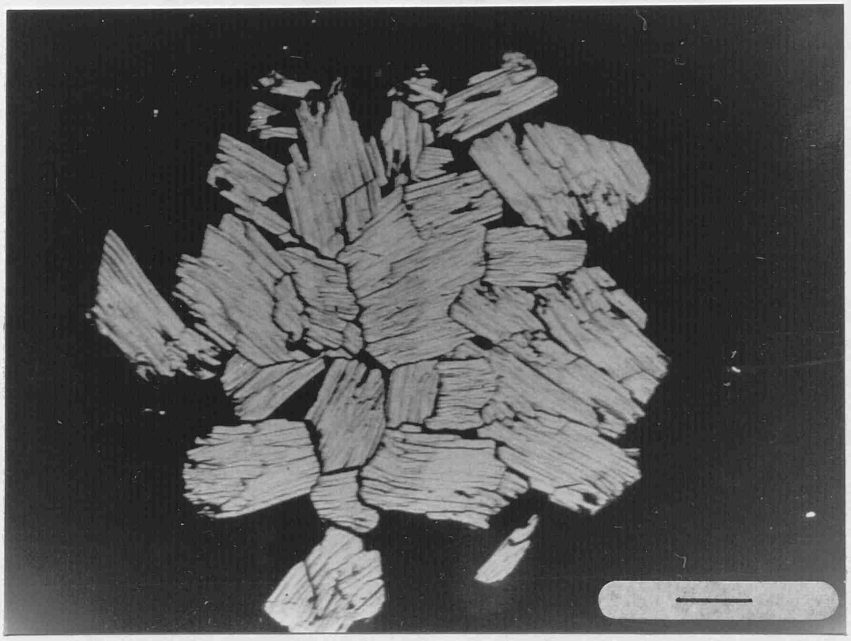

Plate 8.2.2.2e. FeS spherical precipitate, polished section. Scale bar 5µm

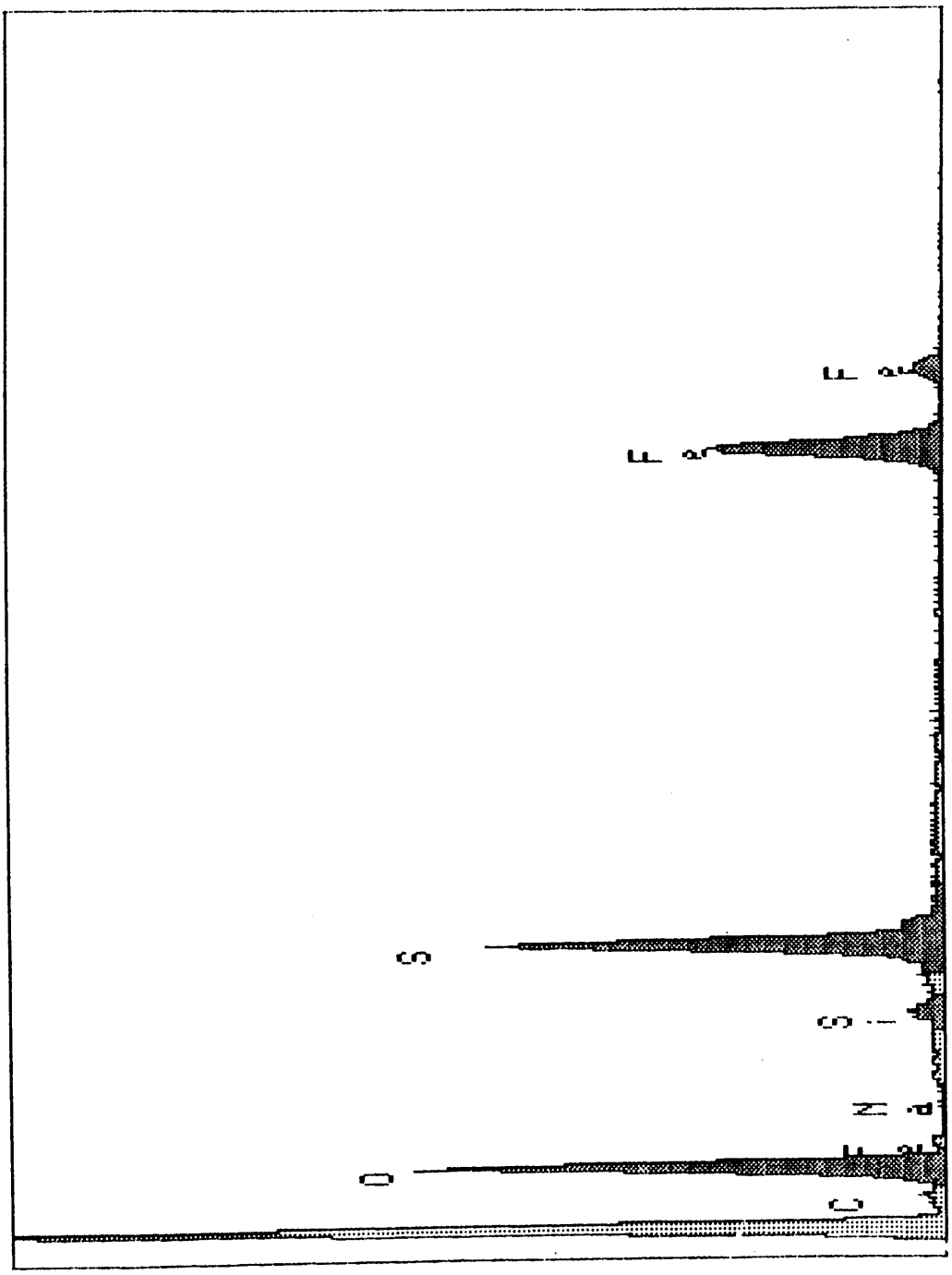

EDS analysis of decomposed area

fig 8.2.2.2f

DISCUSSION.

9 DISCUSSION

9.1 ON THE NATURE OF THE IMCA PHENOMENON

9.2 GROWTH MECHANISM OF IMCA's

9.3 MORPHOGENETICAL TRANSITIONS IN IMCA's

9.4 THE TRANSITION FROM NORMAL CRYSTAL GROWTH TO INDUCED CRYSTAL GROWTH

9.5 THE INFLUENCE OF SILICA ON OTHER PRECIPITATING SYSTEMS

9.6 CONCLUSIONS

9.7 FUTURE WORK

9 DISCUSSION

9.1 ON THE NATURE OF THE IMCA PHENOMENON

Chapters six and seven detailed experiments which established conditions necessary for the formation of IMCA's of $BaCO_3$ and $BaSO_4$. Preliminary experiments also led to the formation of $BaCrO_4$ and $BaHPO_4$ IMCA's (section 7.3 and Chen, 1992). These materials had certain similarities such as globular or spherical centres (in most cases), sheet-like structures and spiral parts.

The conditions necessary for the formation of $BaCO_3$ IMCA's in a 4% silica gel are pH > 8.5 in the presence of NaCl or a minimum pH of 10.5 in the absence of NaCl. In the case of $BaSO_4$ it is not as clear-cut but the same trend certainly exists. Non-IMCA's form in gels up to around pH 10 in the absence of NaCl, however the introduction of NaCl produces IMCA's in the pH 10 silica gel. The preliminary experiments carried out on $BaCrO_4$ and $BaHPO_4$ followed the same trend: non-IMCA's in the absence of NaCl and IMCA's in the presence of NaCl.

The formation of a barium-salt IMCA depends on the formation of a barium silicate membrane or sheath which acts to control the crystal-to-crystal relations of the growing precipitate and therefore its overall morphology.

The acid dissolution experiment carried out on a $BaCO_3$ IMCA under a light microscopical observation (6.2.3) and under an electron microscopical observation (6.2.6.1) confirmed the presence of an external membrane, the LM experiment showed the membrane to be exactly the same shape as the original aggregate.

XPS (6.2.7) and a Rutherford backscattered image (6.2.8) identified this membrane to be a barium silicate carbonate structure approximately 1 μm in thickness. It was surprising that FTIR analysis (6.2.2.1) on $BaCO_3$ IMCA's failed to show any peaks apart from the carbonate ones, in contradiction to Garcia Ruiz's observations (et al 1981). XRD did show some additional low intensity peaks although these could not be catagorically assigned to a barium silicate structure. It was observed during EDS analysis (6.2.5) that prolonged soaking in NaOH (which ensures that no silica gel adheres to the precipitates) seemed to destroy any membrane present. This may have contributed to the difficulty in identifying a barium silicate phase.

Despite the failure of XRD and FTIR analysis in categorically identifying a barium silicate phase, the IMCA phenomenon has been verified by the following observations.

i) Garcia Ruiz's experiments (et al 1981, 1985) were repeated and the same morphological observations made.

ii) The acid dissolution experiment on $BaCO_3$ IMCA's (6.2.3) clearly shows the presence of a membrane.

iii) XPS analysis (6.2.7) identified the membrane as a barium silicate carbonate structure and a Rutherford backscattered image (6.2.8) indicated it was approximately 1 micron thick.

iv) A uniaxial dark cross (Maltese) was observed in sheet-like aggregates (6.2.1, 7.2.1) which remained stationary when the object was rotated indicating an ordered arrangement of crystallites.

v) The phenomenon of IMCA formation was found to occur in materials other than alkaline earth metal carbonates. Barium sulphate (chapter 7), barium chromate and barium hydrogen phosphate (section 7.3 and Chen, 1992) all produced IMCA's suggesting that most, if not all, alkaline earth precipitates may exhibit the phenomenon.

The observations that high pH and the presence of NaCl are critical to IMCA formation is interpreted in the following way. IMCA formation is dependent on the formation of the metal silicate carbonate membrane. Factors which affect this are pH and presence of NaCl in the gel. Increasing the pH of the silica gel increases the amount of silicate ions in the solution part of the gel. The ion $H_2SiO_4^{2-}$ is known to exist in basic silica gel (Henisch, 1973, 1988) and similar ions to this one

will also be present. These are the ions which react with the metal to form the membrane. The greater the concentration of these ions, then the greater is the chance of forming a membrane.

The NaCl effect is not as straightforward. The importance of NaCl is a new observation and has not been considered by Garcia Ruiz. However, some similarities may exist between the effect of CO_3^{2-} groups on the formation of the membrane and on the effect of NaCl on the formation of the membrane. Garcia Ruiz (1985) observed the differences in IMCA structures caused by different concentrations of CO_3^{2-} in the gel; in particular the tightly wound long spirals which form in the presence of a high concentration of CO_3^{2-} and the looser wound shorter spirals which form at lower concentrations of CO_3^{2-}. Experiments described in chapter 6 produced results in agreement with this observation although NaCl and pH were also shown to have an effect on spiral pitch. In the knowledge that carbon dioxide accelerates the hydration of calcium silicate in cement pastes (Berger, 1972) Garcia Ruiz postulated (1985) that CO_3^{2-} groups could be one of the components forming the matrix. Since morphology is almost certainly related to the growth mechanism and structure of the membrane, different morphologies would be obtained for different CO_3^{2-} concentrations. Garcia Ruiz's postulateon was shown to be correct with the observation of carbonate peaks in the XPS spectrum of the surface of a $BaCO_3$ IMCA (6.2.7b).

NaCl is known to catalyse the hydration of calcium silicate in Portland cement pastes (Lea, 1970)) due to catalytic effects. Hence, by analogy it may catalyse the hydration of metal silicate carbonate particles to form a membrane. Solvated Na^+ and Cl^- ions may have a stabilising effect by lowering the charge on a precipitating IMCA membrane. Very often the sheet-like structures in IMCA's are curved or folded. If this curvature is a consequence of bending to aleviate any strain due to a mismatch in the interaction between bulk phase and membrane, the presence of Na^+ ions in solution will prevent silicate ions in the membrane from repelling each other as the membrane folds back on itself, therefore stabilising growth. Solvated Cl^- ions will have the same effect on Ba^{2+} ions present in the membrane. If the observed curves and folds in sheet-like IMCA's do not arise through any mismatch in the interaction between bulk phase and membrane, they may arise through the interaction between the membrane and solvated NaCl alone. It can be envisaged that in order to geometrically optimise charge balance stability, the precipitating membrane will "wrap" itself around solvated ions resulting in curved features. There is the possibility that both these mechanisms work in unison. Ion pairing or ionic strength effects, which increase the solubility of silicate in alkali, may also be active. Osmotic effects could also be important though the failure of ethylene glycol to influence morphology makes this seem less likely (6.2.1 (iii). On a simpler level,

perhaps the NaCl is preferentially more solvated in the gel, forcing the silicate particles to react and come out of solution.

9.2 GROWTH MECHANISM OF IMCA's

The following is a model for the growth mechanism of $BaCO_3$ and $BaSO_4$ IMCA's. The initial stage of formation is the growth of a spherulite of the bulk precipitating material. The size and order of the spherulite will depend on supersaturation levels (section 2.1). In most cases the spherulite will form under very high levels of supersaturation and will therefore be disordered (amorphous) - classically, a critical nucleus smaller than the unit cell. Depending on the initial supersaturation level and the degree to which it falls, there will be a change to a more crystallographically ordered material. At some point during this process silicate will adsorb onto, or co-precipitate with, the bulk phase. Evidence for this exists from the acid dissolution experiment (6.2.3) where a central spherulite enclosed in a silicate membrane was observed. The silicate may adhere selectively to one crystal face of the bulk material, lowering its surface energy and hence promoting growth in certain directions while inhibiting it in others.

The structural relations which may exist between the two phases need not involve epitaxis. In biomineralisation processes (1.4) crystallite size, structure and orientation are thought to be controlled by, in most cases, the interaction between opposite charges on the membrane and crystallite, or the interaction between the surface geometry of the membrane and the crystallite. The observation that IMCA's are obtained in $BaCO_3$ (chapter 6), $BaSO_4$ (chapter 7), $BaCrO_4$ and $BaHPO_4$ (section 7.3 & Chen, 1992) systems and that they all contain similar morphological features such as sheets and spirals, suggests that there is some degree of specificity between bulk phase and membrane and that the relationship may be of a physical nature rather than structural, ie it may be a charge interaction or a surface geometry interaction or both.

Returning to the growth mechanism, the situation is now one of a spherulite of the bulk crystalline phase enclosed by a silicate membrane. The ease of formation and possibly the thickness of the silicate layer increases with pH and with ionic strength. As mentioned earlier, direct experimental evidence exists supporting this situation. Plate 6.2.3c shows the result of IMCA dissolution by acid. The spherulite at the centre does not dissolve unless the surface is cracked by a needle. This confirms that it is enclosed in a protective coat - the silicate membrane, eg consider the following schematic

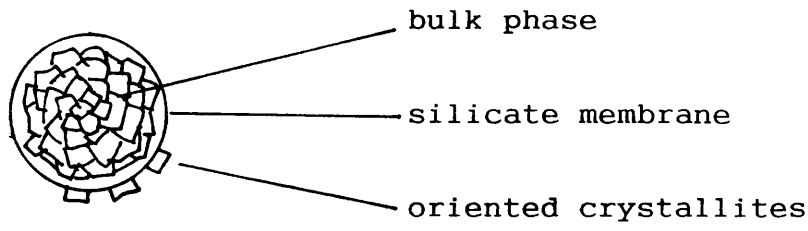

Probably at the same time as the centre bulk material is precipitating with the silicate overcoat, there will be further precipitation of bulk phase crystallites on the overcoat coupled with more silicate formation on the surface of those growing crystallites. Supersaturation levels will have decreased with the local depletion of reactants. Crystallites of various orientations will form. The nucleus will now present faces that can grow in all directions.

In the absence of any silicate effect, and at suitable growth rates, acicular growth of crystallites would occur and by a simple geometrical selection process spherical outward radiation of growing needles would occur. This is what happens in the low pH, NaCl-free experiments (6.2.1 (i)). No central nucleus enclosed in silicate is necessary, as long as the nucleus presents faces which can grow in all directions.

However, in the formation of IMCA's there is a silicate effect and the silicate will co-precipitate or be adsorbed onto crystal faces. The fact that all IMCA's have similar morphological characteristics suggests, as previously discussed, that the interaction between the

silicate membrane and the crystallites may be specific to certain crystal faces.The result of this interaction will be to retard growth in certain directions and promote it in others. It can be envisaged that through silicate adsorption, growth in the direction of the needles is retarded, while growth perpendicular to the direction of the needles is promoted resulting in sheet-like or flower morphologies (plate 6.2.1j) fully enclosed by the silicate membrane. Consider the following schematic, restricted to two dimensions for simplicity.

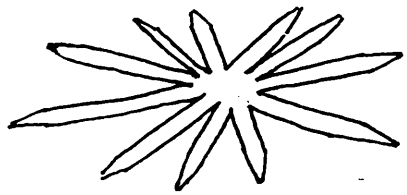

acicular growth

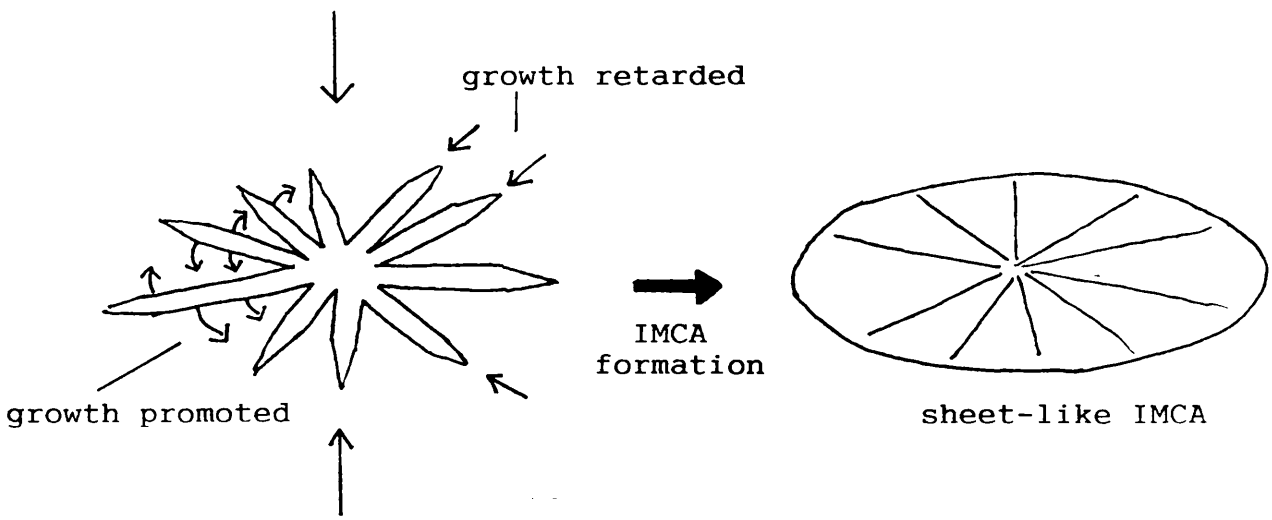

Osmotic effects may be incorporated into this model also. The existence of membranes and NaCl will produce osmotic pressures which may rupture membranes altering growth directions and the orientations of precipitating crystallites.

In many cases sheet-like structures grow towards points where spiral structures take over. The spiral propagates because silicate is not adsorbed on the growing edge. The spiral structure itself probably arises through bending and twisting to aleviate strain caused by a slight mismatch between the interacting features of the membrane and the bulk crystalline phase. The membrane surrounding spiral parts was shown to have a higher silicon to barium ratio than the membrane surrounding the sheet-like parts, by XPS analysis (6.2.7). This is as expected since different membrane structures and therefore different interactions with the bulk phase should result in different morphologies. The reason the membranes are different may be because local supersaturation levels have been depleted by the time spirals begin to form. A membrane with some degree of order (perhaps long range) may form and the interactions with the bulk crystalline phase will be different than the interactions of the less well-ordered membrane with the bulk crystalline phase.

Different types of spirals are observed in IMCA's. Loose-wound spirals form at moderate pH and tightly-wound spirals form at higher pH or in the presence of a higher concentration of Na_2CO_3 (6.2.1 (i) & (ii)). This will also be due to different membrane structures (since CO_3^{2-} is incorporated into the membrane) interacting differently with the bulk phase to give different morphologies. If the membrane precipitates with long range order then the interaction may be epitaxial in

nature.

In summary, the model for the growth mechanism of $BaCO_3$ and $BaSO_4$ IMCA's is as follows.

(i) Growth of a bulk phase spherulite.

(ii) Encapsulation of the spherulite by adsorption of silicate.

(iii) Further precipitation of crystallites of bulk phase on silicate overcoat.

(iv) Further adsorption of silicate onto specific faces of growing crystallites causing growth to be retarded in certain directions and promoted in others. This results in sheet-like and spiral morphologies.

9.3 MORPHOGENETICAL TRANSITIONS IN IMCA's

The previous section detailed how local changes in supersaturation levels may have led to changes in the degree of order of the precipitating membrane during the formation of an IMCA. It was argued that membranes with different degrees of order would have different interactions with the precipitating bulk crystalline phase, resulting in the different morphological features associated with an IMCA, eg spherical core, sheet-like

structures and spiral parts. Not only is there a local drop in supersaturation during the precipitation of one IMCA, there is also a great deal of difference in the supersaturation levels during the precipitation of the first IMCA's formed in a closed system compared with the last IMCA's formed in a system.

In the series of colour cross-polarized light micrographs, which record the complete morphogenetical transition of first precipitates to last precipitates in the IMCA forming system BC[0.1]10.5, (figs 6.2.1 l-v), one observes a similar transition to that which Garcia Ruiz observed (1985, and section 1.3.5 of this thesis) and has explained in terms of the falling level of supersaturation as the diffusing reactant is depleted, it is a explanation with which the present author is in full agreement. In the series of micrographs 6.2.1 l-v the initial precipitates are globular and irregular (l,m & n). As these precipitates increase in size with falling diffusion gradient - and hence lower supersaturation levels - spiral and sheet-like out-growths become clearer, (o,p & q). From this point the membrane has enough order to interact fully with the bulk phase and produce these fantastic sheet-like and spiral structures (r,s & t). As the diffusion of $BaCl_2$ through the system finally draws to completion very tightly wound spirals, all originating from objects with globular and/or sheet-like parts, are all that is precipitated, (u & v). When the final precipitates are forming in a closed system the

ratio of carbonate and silicate ion concentrations to the barium ion concentration will be relatively higher than when earlier precipitates formed due to the depletion of barium ions. This may influence the structure of the precipitating membrane and is in agreement with XPS results (6.2.7) which indicate a higher Si : Ba ratio in the membrane enclosing spiral parts, the final precipitates in BC[0.1]10.5. Objects of the type illustrated in plate 6.2.1w form towards the end of growth when the diffusion gradient is small. The spherulite centre is very small and the sheet-like part's flatness is influenced by the glass cassette.

A similar morphogenetical transition is obtained in the IMCA forming system BS[0.05][0.1]10 (figs7.2.1e-j) where irregular IMCA's become more regular with falling diffusion gradient. The same arguments can be applied in this case.

9.4 THE TRANSITION FROM NORMAL CRYSTAL GROWTH TO INDUCED CRYSTAL GROWTH

Having considered the growth mechanism of IMCA's and the morphogenetical transitions within an IMCA system, it is left to discuss the transition from normal crystal growth to fully induced morphologies. This type of transition was studied in the $BaCO_3$ and $BaSO_4$ systems.

In the case of $BaCO_3$ (chapter 6) the transition takes place in 4% silica gel, pH range 8.5 - 10.5, in the absence of NaCl. At pH 8.5 (BC[0.05]9, plate 6.2.1b) normal dendritic type crystal aggregates form. At pH 9 (BC[0.05]9, plate 6.2.1b) the precipitates appear similar but with a greater degree of branching. However an SEM observation of this type of precipitate reveals two different surface textures. Plate 6.2.4b illustrates a normal hexagonal crystal symmetry area. Plate 6.2.4c illustrates an area of different surface texture. EDS analysis (6.2.5) identified the presence of silicon on this surface texture which suggests it has been caused by silicate adsorption or co-precipitation with the bulk phase. The ease of formation of the silicate phase is not great so it does not form to such an extent that it has any great morphological control. Plate 6.2.4d shows an area with the silicate texture and normal crystal symmetry. This may have arisen through silicate adsorption onto the surface of the needle or may have been caused by the growing crystallite rupturing the enclosing silicate membrane.

Two different Na_2CO_3 concentrations were studied at pH 9. In the higher concentration one (BC[0.1]9.5, plate 6.2.1d & 6.2.4e) dendrites formed and the enlarging spike morphology was observed. It is not known if this is due to the involvement of silicate. In the lower concentration one, BC[0.05]9.5, a morphogenetical transition begins to take place. Dendrites form up to a

size of 0.75 mm, then their growth is restricted; they decrease in size and finally a globular morphology results (plate 6.2.1e & f). An SEM view of the globular morphology reveals the course texture associated with the adsorption of silicate (plate 6.2.4f). This morphology is very similar to the late-forming precipitates in the basic agarose control experiment (plate 6.2.4p) although the control experiment precipitates are a little more regular and have a slightly smoother surface texture. The transition towards the globular morphology is attributed to two processes; the formation of spherultic type precipitates due to the greater concentration of free carbonate at high pH, and silicate adsorption leading to a coarse and irregular surface texture. At pH 10 (BC[0.1]10) a similar pattern is followed with the additional stage of the development of induced morphological outgrowths from the globular centre. The ease of formation of barium silicate is now at a level where the final precipitates, formed at the lowest supersaturation levels, are almost full IMCA's. The tendency to form IMCA-like objects in the latter stages of growth of BC[0.1]10 may be enhanced by low supersaturation levels promoting the precipitation of a barium silicate structure with a higher degree of order than was possible in earlier-formed precipitates. The interaction between bulk phase and an ordered membrane may be more effective than the interaction with a disordered membrane. At pH 10.5 (BC[0.1]10.5), previously described (6.2.1) and discussed (9.3), barium silicate

forms to such an extent that IMCA's are formed. The following schematic illustrates this morphogenetical transition.

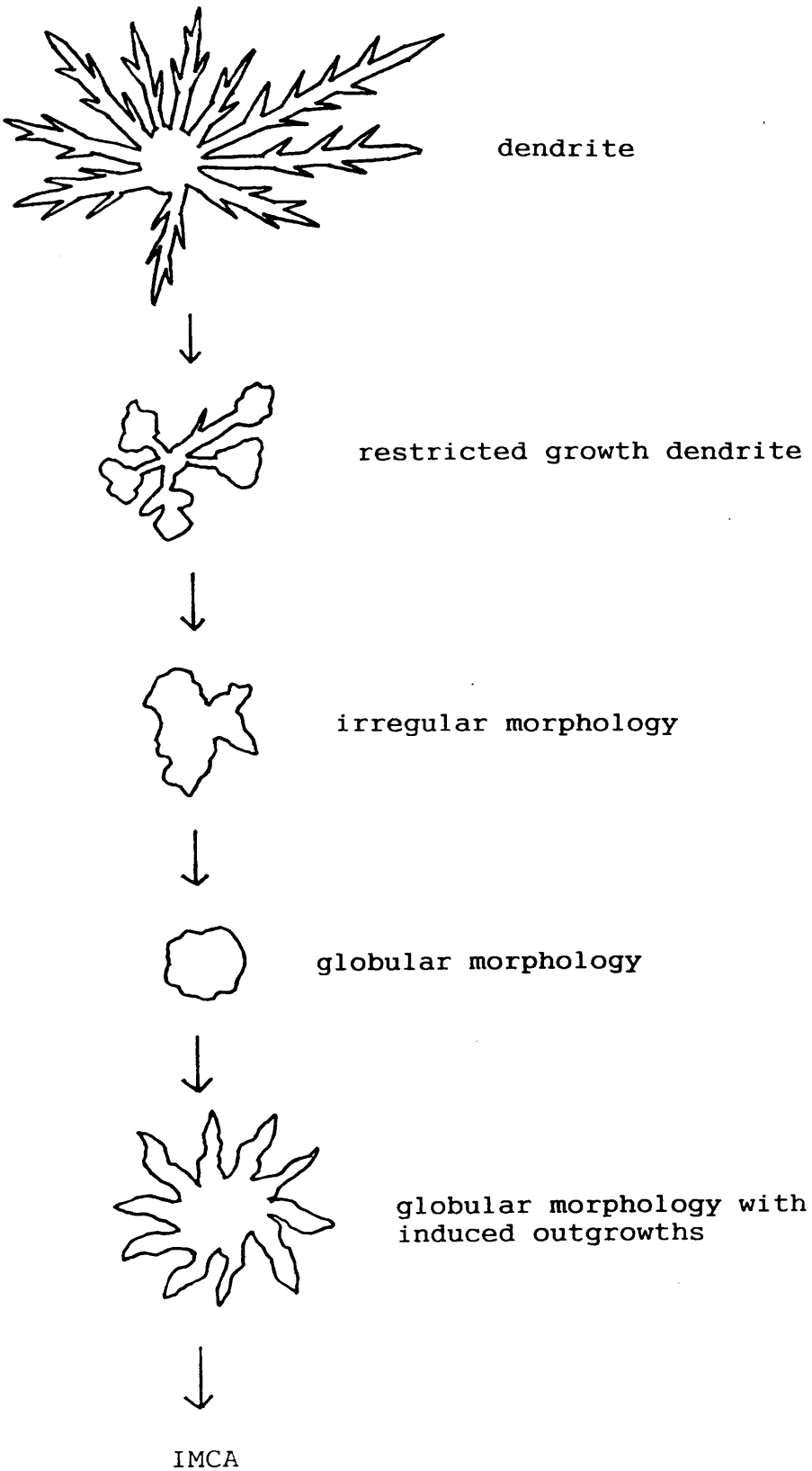

The continuity in this morphogenetical series is clearly seen by observing similar morphologies in different systems, eg the early precipitates in BC[0.1]10.5 are very similar to the final precipitates in BC[0.1]10 and the globular morphologies obtained three quarters of the way through BC[0.1]10 are similar to the globular morphologies obtained as final precipitates in BC[0.05]9.5.

The experiments carried out on the glass microscope slides (chapter 5) did not yield any IMCA's since the gels were free of NaCl and did not have a pH greater than around 9.5. In all cases dendritic type precipitates formed. Any difference in morphology between these precipitates and the dendritic type precipitates formed in experiments described in chapter 6 can be attributed to the different diffusion gradients, different initial concentration of reactants and perhaps the volume constraint of a thin layer of gel.

In the $BaCO_3$ neutral agarose control experiment, irregular objects were the first precipitates obtained (plate 6.2.4n) which can be likened to a dense branched morphology and in some ways similar to precipitates from BC[0.1]9 (plate 6.2.1b), formed under the minimal influence of silicate. Later-forming precipitates become more regular and raspberry-like (plate 6.2.4n). In the basic agarose experiment, globular-type morphologies were obtained (plate 6.2.4o) which have previously been

likened to the globular morphology obtained in the silica gel experiment BC[0.05]9.5 (plate 6.2.4f). This spherulitic habit arises through the increase in free carbonate at high pH, as previously described. In the basic NaCl agarose experiments, spherulitic precipitates form throughout (plate 6.2.4q) which as previosly described in 6.3 may be due to a combination of high free carbonate concentration and a "salting out" effect increasing growth rate.

In the case of homogeneous precipitation of $BaCO_3$ no IMCA's are formed. This is because the pH does not reach a high enough value. As the urea is hydrolysed the pH will increase with the formation of NH_4^+. As it reaches 8 -8.5 the carbonate is almost entirely in the form of HCO_3^-. As this reacts with barium, H^+ is released which buffers the rise in pH.

In the $BaSO_4$ experiments (chapter 7) the morphogenetical transition takes place in 4% silica gel in the pH range 8.5 - 10 in the absence of NaCl, and in silica gel at pH 10 in the presence of NaCl.

At pH 8.5 (BS[0.05]8.5, plates 7.2.1a & b and plates 7.2.3a & b) butterfly objects are formed. The curvature of these objects increases with pH and is probably due to silicate adsorption onto specific crystal faces. At pH 9 (BS[0.05]9, plate 7.2.1c) the greater tendency for the precipitation of barium silicate results in the formation

of induced morphological outgrowths at corners and edges of the precipitate. At pH 10 the number of these outgrowths increases (BS[0.05]10, plate 7.2.1d and 7.2.3c) until the butterfly features begin to be lost. Finally at pH 10 and in the presence of NaCl (BS[0.05][0.1]10, plates 7.2.1e - j and 7.2.3d, e & f) the amount of barium silicate which precipitates influences crystal growth to such an extent that the butterfly features are lost and full IMCA's are formed. The following schematic illustrates this morphogenetical transition.

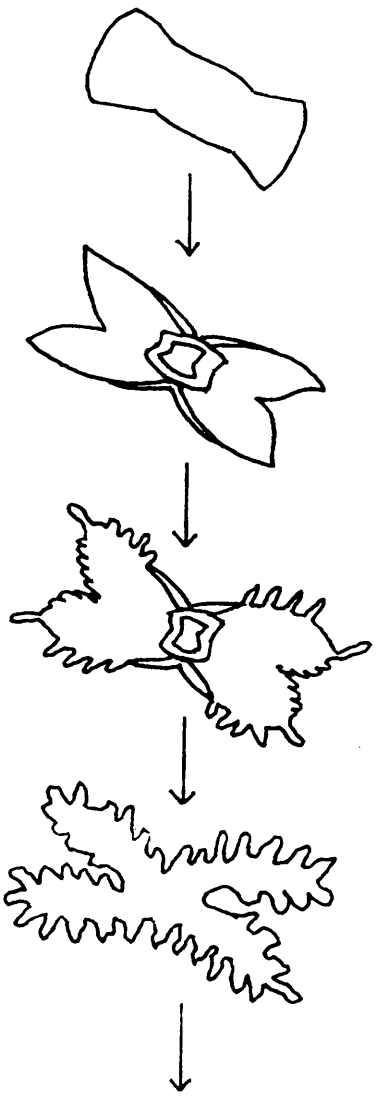

Continuity also exists in this morphogenetical series as similar morphologies are observed at different places in different systems, eg the early precipitates in BS[0.05]10 are similar to the later ones in BS[0.05]9.

In the $BaSO_4$ agarose control experiments platelet morphologies were observed, ie butterfly morphologies without the curves. This can be considered the very first morphology in the series, completely free from the influence of silica.

9.5 THE INFLUENCE OF SILICA ON OTHER PRECIPITATING SYSTEMS

Chapter 8 detailed experiments carried out on the precipitation of iron sulphide in silica gel. It was found necessary to have sodium metabisulphite present during the reaction, in order to scavenge any oxygen and maintain the iron in the ferrous oxidation state, if framboid-like objects were to be precipitated. An EDS analysis of these objects suggested that they were $FeS.xH_2O$ and that 1.2% silicon had been incorporated into the structure. The silicon peak remained constant whether the surface or the centre of a polished section was probed.

From this data the following growth mechanism can be envisaged: A nucleus of FeS forms which presents crystal faces which can grow in all directions. Silicate ions

will adsorb onto the crystal faces and inhibit growth. New crystallites will form on the surface of the adsorbed silicate and grow until their growth is inhibited by further silicate adsorption. The process will repeat itself until spherical aggregates composed of many crystallites result.

A lack of structural analysis in the iron carbonate (chapter 8) case prevents any growth mechanism being offered but the unusual morphology observed suggests that silicate adsorption may be involved.

9.6 CONCLUSIONS

The following conclusions can be drawn from this study:

(i) Experiments performed on $BaCO_3$ precipitated in basic silica gel verified the existence of the IMCA phenomenon, first reported by Garcia Ruiz and Amoros. $BaSO_4$ was also shown to exhibit the IMCA phenomenon.

(ii) Preliminary experiments on $BaCrO_4$ and $BaHPO_4$ (carried out at the University of North Texas in collaboration with P. Chen (1992)) indicated that these materials also exhibited the phenomenon suggesting the effect may be quite widespread in insoluble barium salts.

(iii) As Garcia Ruiz claimed, barium carbonate IMCA formation is controlled by a relationship between a barium carbonate core and a barium silicate carbonate overlay. Since IMCA's have been shown to form in four different barium-containing materials the relationship may be physical rather than structural, ie it may involve charge interactions or surface geometry interactions.

(iv) The form of IMCA's is extremely sensitive to pH. This is attributed to high pH increasing silicate ion concentration and favouring the formation of barium silicate.

(v) NaCl promotes IMCA formation. This may be due to charge effects stabilising the barium silicate membrane. Adding ethylene glycol is without effect making an osmotic influence on IMCA formation unlikely.

(vi) In silica gel, at moderate pH and in the absence of NaCl, growth of $BaCO_3$ is dendritic. At higher pH, whether silica is present or not, the tendency is for spherulitic growth. This is attributed to the increased concentration of free carbonate at higher pH.

(vii) In the precipitation of $BaCO_3$, increasing pH in the presence of silica leads progressively to the formation of a barium silicate membrane which encloses an initially spherulitic growth. Further growth and specific

interactions between the two phases occur, resulting in induced outgrowths, sheets and spirals. Supersaturation levels and the changing Ba : Si ratio during experiments may be key factors influencing morphology.

(viii) In the precipitation of $BaSO_4$, platelet morphologies form in the absence of silica. In the presence of silica and with increasing pH a transition occurs from butterfly objects through to objects with some butterfly-like feature and a mass of induced growths. Addition of NaCl promotes full IMCA growth.

(iv) IMCA formation is a special case of interaction between a growing precipitate and a polymeric adsorbate; in this case, the adsorbate self-assembles on the precipitate.

(x) The adsorption of silicate was shown to have an effect on the precipitation of FeS and possibly on $FeCO_3$.

9.7 FUTURE WORK

Future work should concentrate on the characterisation of the membrane, responsible for the IMCA phenomenon. Through an understanding of its structure, more can be learned of its interactions with the bulk phase. Further XPS anaysis and perhaps solid state nmr may reveal new information. There is also the possibility that further TEM analysis, this time on broken or crudely ground

IMCA's may reveal information on the interaction of the two phases.

The degree of order and self-organisation of IMCA's may be studied by XRD analysis of a single flat sheet-like IMCA. This may reveal information on the orientation of individual crystallites making up the aggregate.

Other insoluble inorganic precipitates could also be examined to see how widespread the phenomenon is, and NaCl could be replaced with LiCl or NaI in order to test if any 1 : 1 electrolyte would promote the effect.

REFERENCES

Abdullah J., Baird T., Braterman P.S., J. Chem. Soc. Chem Commun, (1986), 256-257

Abdullah J., Baird T., Braterman P.S., Kaya M., J. Cryst. Growth (1987), 83, 449-452

Abdullah J., PhD Thesis, University of Glasgow, (1988)

Addadi L., Berkovitch-Yellin Z., Weissbuch I., Lahav M., Leiserwitz L., Mol. Cryst. Liq. Cryst. (1983) 96 1-17

Akermark B., Eklumd-Westlin J., Baeckstrom P., Lof R. Acta. Chem-Scand, Ser B, (1980), 34, 27

Alexander A.E., Johnson P., "Colloid Science" Vol 2, Clarenden Press (1949)

Arrhenius G., Origin of Life Conference, Berkley, (1986)

Belyakov V.N., Soltiuski N.N., Strazhesko D.N., Strelko V.V., Vkr Khim, (1974), 40, 236

Becker R., Doring W., Am. Phys. (1935), 24, 719

Becker R., Doring W., Discuss. Faraday Soc., (1949), 5, 50

Ben-Jacob E., Garik P., Nature (1990), 343, 523

Berger R.L., Young J.F., Leung K., Nature, (1972), 240, 16

Berner R.A., Geochem Cosmochem Acta (1975), 39, 489

Birchall J.D., British Ceram. Trans. and Journal, (1983), 83, 6

Birchall J.D., Howard, A.J., Double D.D., Cement Concrete Res., (1980), 10, 145

Birchall J.D., Thomas N.L., J. Mat Sci., (1983), 18, 2081-2086

Braterman P.S., Cairns-Smith A.G., Sloper R.W., Traslott G., Craw M., J. Chem. Soc. Dalton Trans., (1984) 1441-1445

Brostow W., "Science of Materials", Wiley, (1979)

Burton W.K., Cabera N., Frank F.C., Phil. Trans. Roy. Soc. Lond. (1951), A243, 299

Cairns-Smith A.G., "Genetic Takeover", Cambridge Univ. P. (1982)

Cairns-Smith A.G., "Seven Clues to the Origin of Life", Cambridge Univ. P., (1985)

Chen P., University of North Texas, Ph.D. Thesis (1992)

Coslett V.E., Contemp. Phys. (1981a), 22, 3

Coslett V.E., Contemp. Phys. (1981b), 22, 147

Davison C., Germer L.H., Phys. Rev. (1927), 30, 705

de Broglie J., Philos. Mag., (1924), 47, 446

Determan H., Lepusch F., "The Microscope And Its Applications" (1974), Leitz Promotional Book

Double D.D., Hellawell A., Nature, (1976),261, 486

Falcone J.S. in "Soluble Silicates", ed J.S. Falcone, American Chemical Society, Washington DC (1982), p 133

Frank F. C., Discuss. Faraday Soc. (1949),5, 48

Fryer J.R., Mol. Cryst. Liq. Cryst., (1983) 96, 275

Garcia Ruiz J.M., Amoros J.L., J. Cryst. Growth (1981), 55, 379

Garcia Ruiz J.M., J. Cryst. Growth (1985), 73, 251-262

Garrels R.M., Amer. J. of Sci., (1987), 287, 81-106

Geuss J.W. , Stud. Surf. Sci. Catal. (1983), 16, 1-33

Glicksman M.E., Shaefer R.J., Ayers J.D., Metall. Trans. (1976), A7, 1747-1759

Hatschek E., Kolloid, (1911), 2.8, 13

Hayat M.A., "Introduction to Biological Scanning Electron Microscopy", University Park Press (1978)

Henisch H.K., "Crystal Growth in Gels", Pennsylvania State University Press, (1973)

Henisch H.K., "Crystals in Gels and Liesgang Rings" Cambridge University Press (1988)

Iler R.K., "The Chemistry of Silica" Wiley (1979)

Ivantsov G.P., Dohl Akad Nauk SSSR, (1947), 58, 567-569

Kinsman D.J.J., Holland H.D., Geochim. Cosmochim. Acta (1969), 33, 1

Kleman M., in "Dislocation of Solids" Vol.5, ed. F.R.Nabarro, North Holland, NY, (1980)

Kossel W., Ann. Phys. Chem., (1934), 21, 455

Lagaly G., Naturwissenschaften, (1981), 68, 82-88

Lea F.M., "The Chemistry of Cement and Concrete" Arnold (1970)

Liesgang R.E., Photo. Archiv. (1896) 221

Mann S., New Scientist, (10th Mar. 1990) 125 number 1707 p42

Mann S., Structure and Bonding, (1983),54, 125

Mann S., Williams R.J.P., J. Chem. Soc. Dalton Trans., (1983), 311

Mann S., Webb J., Williams R.J.P., "Biomineralization: Chemical and Biochemical Perspectives" Verlagsgesellschaft, (1989)

Mukherjee S.P., Zarzycki J., Traverse J.P., J. Mater. Sci., (1976), 11, 341

Mullin J.W., "Crystallisation", Butterworth, London, (1972)

Mullins W.W., Sekerka R.F., J. App Phys., (1964), 35, 444-451

Oldfield W., Mater. Sci. Enging. (1973), 11, 211-218

Patzelt W.J., "Polarized Light Microscopy", Leitz Promotional Book, (1974)

Posner A.S., Betts F., Blumenthal N.C., Prog. Cryst. Growth. Charact., (1980), 3, 49

Raistrik J.M., European Patent Publication, (1983), 0096522

Rickard D.T., "The Origin of Framboids", Lithos 3, 269-293

Roy R, "Proceedings of the Xl Conference on The Silicate Industry", Siliconf, Budapest, (1973), p.1005

Roy R.A., Roy R., Mater. Res. Bull., (1984), 19, 169-77

Roy R., White W.B., J. Cryst. Growth, (1972), 13/14, 78

Ruska E., Microsc. Acta Suppl.5: The Early Development of Electron Lenses and Electron Microscopy, (Mulvey T., transl.), (1980), Hirzel, Stuttgart

Russell M.J., Hall A.J., Gize A.P., Nature, (29 Mar.1990), 344, 387

Russell M.J., Boyce A.J., Larter R.C, Mineralium Deposite, (1981), 16, 309-318

Russell M.J., Coleman M.L., Boyce A.J., Nature, (1983), 396, 545-550

Schwartz R., Muller W.D., Anorg Allg. Chem., (1958), 296, 273

Shlenker B.R., "Introduction to Material Science", Wiley, Sydney, (1969)

Smith R.H., Bayliss P., Mills R.H., Cement Concrete Res., (1972), 2, 559

Stranski I.N., Phys. Chem., (1928), A136, 259

Swietloslawski W., "Microcalorimetry", Reinhold, New York, (1947)

Thomson G.P., Reid A., Nature (London), (1927), 119, 890

Wachterschauser G., System Appl. Microbiol., (1988), 10, 207-210

Wachterschauser G., Microbiol. Rev., (1988),52, 452-484

Williams R.J.P., Phil. Trans. R.Soc. Lon., (1984), B304, 411

Williamson R.B., J.Cryst. Growth , (1968), 3/4, 787